AER/AGS Open File Report 2025-09

Alberta Energy Regulator

Investigating the Critical Mineral Systems of the Canadian Shield of Northeastern Alberta: A Summary of 2023 Fieldwork in the Leland Lakes and Andrew Lake Areas

AGS
ALBERTA GEOLOGICAL SURVEY

AER/AGS Open File Report 2025-09

Investigating the Critical Mineral Systems of the Canadian Shield of Northeastern Alberta: A Summary of 2023 Fieldwork in the Leland Lakes and Andrew Lake Areas

N.O. Montenegro[1], R.P. Hartlaub[2], M.B.K. Belosevic[3], E.C. Morley[3] and D.M. Meek[4]

[1] Department of Earth Sciences, University of Regina
[2] Department of Mining and Mineral Exploration, British Columbia Institute of Technology
[3] Alberta Energy Regulator / Alberta Geological Survey
[4] Formerly of Alberta Energy Regulator / Alberta Geological Survey

February 2026

ISBN 978-1-4601-5740-4

Montenegro, N.O., Hartlaub, R.P., Belosevic, M.B.K., Morley, E.C. and Meek, D.M. (2026): Investigating the critical mineral systems of the Canadian Shield of northeastern Alberta: a summary of 2023 fieldwork in the Leland Lakes and Andrew Lake areas; Alberta Energy Regulator / Alberta Geological Survey, AER/AGS Open File Report 2025-09, 102 p.

Author addresses:

N.O. Montenegro
Department of Earth Sciences
University of Regina
3737 Wascana Parkway
Regina, SK S4S 0A2
Canada

Tel: 306.552.8842
Email: nmontenegro.geo@gmail.com

R.P. Hartlaub
Department of Mining and Mineral Exploration
British Columbia Institute of Technology
3700 Willingdon Avenue
Burnaby, BC V5G 3H2
Canada

Tel: 604.456.1094
Email: russell_hartlaub@bcit.ca

Published February 2026 by:
Alberta Energy Regulator
Alberta Geological Survey
Suite 205
4999 – 98 Avenue NW
Edmonton, AB T6B 2X3
Canada

Tel: 780.638.4491
Email: AGS-Info@aer.ca
Website: ags.aer.ca

Contents

Tables

Figures

Appendix

Acknowledgements

The authors would like to thank Colin Birnie, Matt Grobe, and Alex MacNeil from the Alberta Geological Survey for reviewing this manuscript and providing valuable feedback.

Thank you to all the individuals that contributed to a successful 2023 field season in northern Alberta and support on the many tasks afterwards, including

- Alex MacNeil, Abubakr Ally, Calla Knudson, Christopher Swoboda, Courtney Reimert, Dan Dodd, Levi Knapp, Nick Roman, Scott Kelly, Steven Pawley, Subir Chowdhury, and Vicki Easthom (Alberta Geological Survey and Alberta Energy Regulator);
- Gary Delaney (formerly of the Saskatchewan Geological Survey); and
- Connor Crook (University of Regina).

Thank you to Dan Wettlaufer for sharing his local knowledge of both the Leland Lakes and Andrew Lake areas.

Thank you to Smith's Landing First Nation for the privilege of conducting our 2023 field program on the traditional lands that you call Tthebatthı Dënésułıné in northern Alberta.

Abstract

The Leland Lakes and Andrew Lake areas of the Canadian Shield in northeastern Alberta were investigated for their critical mineral potential, with a 2023 fieldwork program that included detailed geological mapping, geochemical sampling, and geophysical surveys. The local geology includes Archean and Paleoproterozoic quartzofeldspathic gneisses of the Taltson basement complex (TBC) with locally abundant bands and intrusions of mafic amphibolite that are overlain by high-grade, deformed, metasedimentary rocks of the Paleoproterozoic Rutledge River complex. These components were intruded by voluminous ca. 1.99–1.92 Ga, I- to S-type, granitoid magmas of the Taltson magmatic zone (TMZ). Paleoproterozoic to Mesoproterozoic metasedimentary rocks of the Athabasca Group, exposed at the southeastern edge of the shield in Alberta, unconformably overlie these older basement rocks.

Field-based structural mapping and integrated geochemical analyses reveal a polyphase deformation history culminating in crustal thickening, arc magmatism, and transpressional shear zones. The earliest recognizable deformation phase (D_1; ca. 2.13–1.96 Ga) involved isoclinal folding (F_1) and development of a steeply dipping, composite fabric ($S_{1\text{-}x}$-S_1) under high-grade metamorphic conditions (M_1), facilitating anatexis of rare-earth-element (REE)–enriched metasedimentary rocks and the generation of early granitoids and pegmatites. Upper-amphibolite- to granulite-facies conditions persisted or were renewed during the primary orogenic episode (D_2; ca. 1.94–1.93 Ga), which produced doubly plunging F_2 folds and a pervasive $S_{1\text{-}2}$ gneissosity. Synchronous, voluminous magmatism emplaced granitoids that exhibit a transition from strongly arc-type signatures (e.g., Arch Lake, ca. 1.938 Ga) to more peraluminous, syncollisional compositions (e.g., Slave granitoid, ca. 1.934 Ga), reflecting increasing crustal thickness. Peak thermal conditions (M_2) supported partial melting, syntectonic pegmatite emplacement, and localized mineralization. As shortening evolved into transpression, major deep-seated shear zones nucleated along F_2 axial planes. Subsequent deformation (D_3, D_4), low-grade retrogression (M_3), and related hydrothermal activity persisted well beyond the ca. 1.93 Ga magmatic peak. These findings support an orogenic model where subduction-driven crustal shortening shaped the western margin of the Rae craton. Overall, they emphasize a subduction-to-collision continuum in the southern TMZ, with repeated high-grade metamorphism and crustal reworking playing a key role in its critical mineral potential.

Results of the lithogeochemical and petrographic analyses highlight significant potential of the TBC to host igneous REE mineralization. Pegmatites in the Andrew Lake study area exhibit strong light rare-earth-element (LREE) enrichment and are classified within the abyssal-LREE (U-Th-Ti) subclass of pegmatites. The pegmatites are similar to those at the Alces Lake area, approximately 120 km east in northwestern Saskatchewan, which host significant concentrations of REEs. Pegmatites in both study areas formed under mid- to high-grade metamorphic conditions within structurally favourable zones and are enriched in LREEs and depleted in heavy rare-earth elements. The Leland Lakes shear zone (LLSZ) is a promising target for gold and critical metals exploration, including Cu, Ni, Cr, and Co. The structural control of these occurrences, highlighted by the alignment with a magnetic break in aeromagnetic data and visible in bedrock exposures due to a recent forest fire, underscores the importance of the LLSZ as a promising target for future exploration. Assay results from sulphide-rich metasedimentary rocks, green fuchsitic veins, and mafic enclaves in this area demonstrate substantial concentrations of critical metals. To the west of the LLSZ, the voluminous Slave granitoid exhibits numerous pegmatitic phases with elevated lithium contents and key geochemical indicators such as low Mg/Li and Nb/Ta ratios that are promising for lithium-cesium-tantalum pegmatite exploration. The uranium potential in the region is confirmed by the presence of numerous historical occurrences, an abundance of radiometric anomalies identified with handheld gamma-ray spectrometers, and widespread elevated equivalent uranium radiometric values observed along shear zones. Notable uranium concentrations were found in leucogranites and pegmatites associated with shear zones in the Spider Lake and Cherry Lake areas.

This work was completed under the Mineral Grant provided by the Government of Alberta on June 22, 2021.

1 Introduction

1.1 Purpose

Precambrian basement rocks of the Canadian Shield are exposed in the northeastern corner of Alberta, where the last episode of glaciation eroded most of the Phanerozoic cover. In 2021, the Government of Alberta publicized the mineral strategy and action plan *Renewing Alberta's Mineral Future: a Strategy to Re-Energize Alberta's Minerals Sector*, which listed several actions to further develop Alberta's mineral industry (Alberta Ministry of Energy, 2021). In response to this initiative, the Alberta Geological Survey (AGS) formulated a plan to investigate the potential of Precambrian basement rocks in northeastern Alberta to host critical minerals.

The region is known to host a multitude of mineral occurrences including structure- and intrusion-associated uranium, intrusion-hosted rare-earth metals, gold-silver related to quartz-tourmaline veining, structurally controlled copper-gold, volcanoclastic rock–hosted chromium, vein-hosted molybdenum, and metasedimentary rock–hosted zinc-nickel-chromium (Lopez et al., 2020). These occurrences and mineral systems have been the target of exploration activities since the mid-20th century with companies undertaking extensive programs, including airborne geophysical surveying, prospecting, trenching, and diamond drilling (e.g., Pană et al., 2006; Pană and Olson, 2009; Rukhlov, 2011; Lopez et al., 2020). Even though a large portion of the Canadian Shield in Alberta was redesignated as the Kazan Wildland Provincial Park in 2018, this study on critical mineral systems has applications across the entire Canadian Shield. This most recent investigation builds upon previous studies and is distinguished by the use of high-quality airborne geophysical data acquired in 2022 combined with recent advances in the understanding of critical mineral systems, application of Earth observation techniques, and recognition that certain types of pegmatites, which had not been previously inventoried for northeastern Alberta, may be conducive to rare-earth-element mineralization. The data and interpretations presented herein provide a critical update on the mineral prospectivity of northeastern Alberta for a variety of stakeholders.

1.2 Scope of Work

A summary of the AGS 2023 field activities, including a brief geological background and field logistics description, was provided by Belosevic et al. (2024). The 33 field-day program was tasked with investigating and describing the mineral systems in the Leland Lakes and Andrew Lake study areas.

A rotating crew of AGS staff and contractors visited two main field areas during the program, namely the Leland Lakes study area and the Andrew Lake study area (Belosevic et al., 2024). Access to these remote areas was achieved via floatplane from Fort McMurray and a temporary field camp was established for the duration of the fieldwork at each location. Boat and foot traverse was the primary mode of transport from these field camps, although a floatplane was occasionally used to access more remote lakes.

Field crews collected geological information, rock samples for later lithogeochemical or petrographic analysis, and magnetic susceptibility, gamma-ray, and hyperspectral measurements from 394 stations (Belosevic et al., 2024). In total, 208 rock samples were collected from the Leland Lakes study area and 336 rock samples were collected from the Andrew Lake study area. Rock samples were subjected to several methods of digestion and analysis to obtain comprehensive elemental compositions (Belosevic et al., 2024).

A recently published AGS digital dataset (Meek et al., 2026) contains field observations, whole-rock lithogeochemical data, and a digital spectral library with field measurements.

2 Background

2.1 Regional Geology

The Canadian Shield of northeastern Alberta is the exposed surface expression of the Precambrian basement. It consists of variably metamorphosed granitoids, metasedimentary rocks, and gneisses, which range from Archean to Paleoproterozoic in age and are unconformably overlain by sedimentary rocks of Paleoproterozoic to Mesoproterozoic age. The basement rocks that are exposed in northeastern Alberta extend beneath the Phanerozoic sedimentary rocks of the Western Canada Sedimentary Basin (WCSB). The Canadian Shield of northeastern Alberta can be broadly subdivided into three major components, the Taltson basement complex (TBC), the Taltson magmatic zone (TMZ), and the Athabasca Group. See Figure 1 for a simplified regional geological map of the subdivisions.

The TMZ is a north-south-striking orogenic belt that extends from its northern boundary at the Great Slave Lake shear zone (GSLSZ) to approximately 750 km south where it is truncated by the east-northeast–west-southwest-oriented Snowbird tectonic zone (STZ; Hoffman, 1988, 1989). It is exposed at surface for approximately 350 km in the Northwest Territories and northeastern Alberta. The southern extent of the TMZ has been delineated using drillhole data and aeromagnetic mapping (Ross et al., 1991). The TMZ is bound to the west by the 2.4–2.0 Ga Buffalo Head terrane and to the east by the Archean to Paleoproterozoic Rae craton (e.g., Hoffman, 1988; Ross et al., 1991). The TMZ comprises a number of 1.99–1.92 Ga granitoids that intruded, assimilated, and reworked the western margin of the Rae craton (e.g., Berman and Bostock, 1997; Chacko et al., 2000; McDonough et al., 2000e).

In Alberta, the TBC is an older curvilinear package of high-grade gneisses that generally separates the western, granitic plutons of the late TMZ from eastern plutonic packages of the early TMZ. The TBC is considered the farthest western expression of the relict Rae craton (e.g., Ross et al., 1991; McDonough et al., 2000e) and is composed primarily of Arrowsmith orogeny–aged (2.5–2.3 Ga) orthogneiss with somewhat rarer successions of Archean orthogneisses of 3.2, 3.1, and 2.6 Ga ages (Goff et al., 1986; McNicoll et al., 2000; McDonough et al., 2000e). Recent work on the >3 Ga components of the western Rae craton has identified that these ancient crustal signatures belong to the Perry River terrane, a 1000 km long and 100 km wide belt of heavily reworked ancient crust that stretches from the STZ to the Queen Maud block (Neil et al., 2023). Despite the voluminous Arrowsmith orogeny–aged crust in the TBC, no metamorphic ages have been obtained thus far that correspond to the 2.39–2.35 Ga peak metamorphism of the Arrowsmith orogeny found in Saskatchewan, the Northwest Territories, and Nunavut (Hartlaub, 2004; Berman et al., 2005, 2013). There are widespread enclaves of 2.13–2.09 Ga pelitic and semipelitic gneisses hosted within the TBC and TMZ, which are thought to be remnants of the Rutledge River basin (e.g., Bostock and van Breemen, 1994; McDonough et al., 2000e). More recent work on samples of the Rutledge River complex (RRC) in the Pelican Rapids area (40 km west of the Leland Lakes study area) indicates that at least part of the basin fill was deposited between 2.03 and 1.94 Ga (Thiessen et al., 2024). In addition to the paragneisses, there are also enclaves of various mafic phases, such as amphibolite and hornblendite, that occur throughout the TBC and are thought to be obducted remnants of ophiolite incorporated into the TBC (McNicoll et al., 2000). The enigmatic Waugh Lake group found in the northeastern part of the Canadian Shield in Alberta is a package of relatively low-grade sheared igneous and supracrustal rocks thought to have formed in a back-arc basin during the Taltson orogeny (Iannelli et al., 1995; McDonough and McNicoll, 1997; McDonough et al., 2000e).

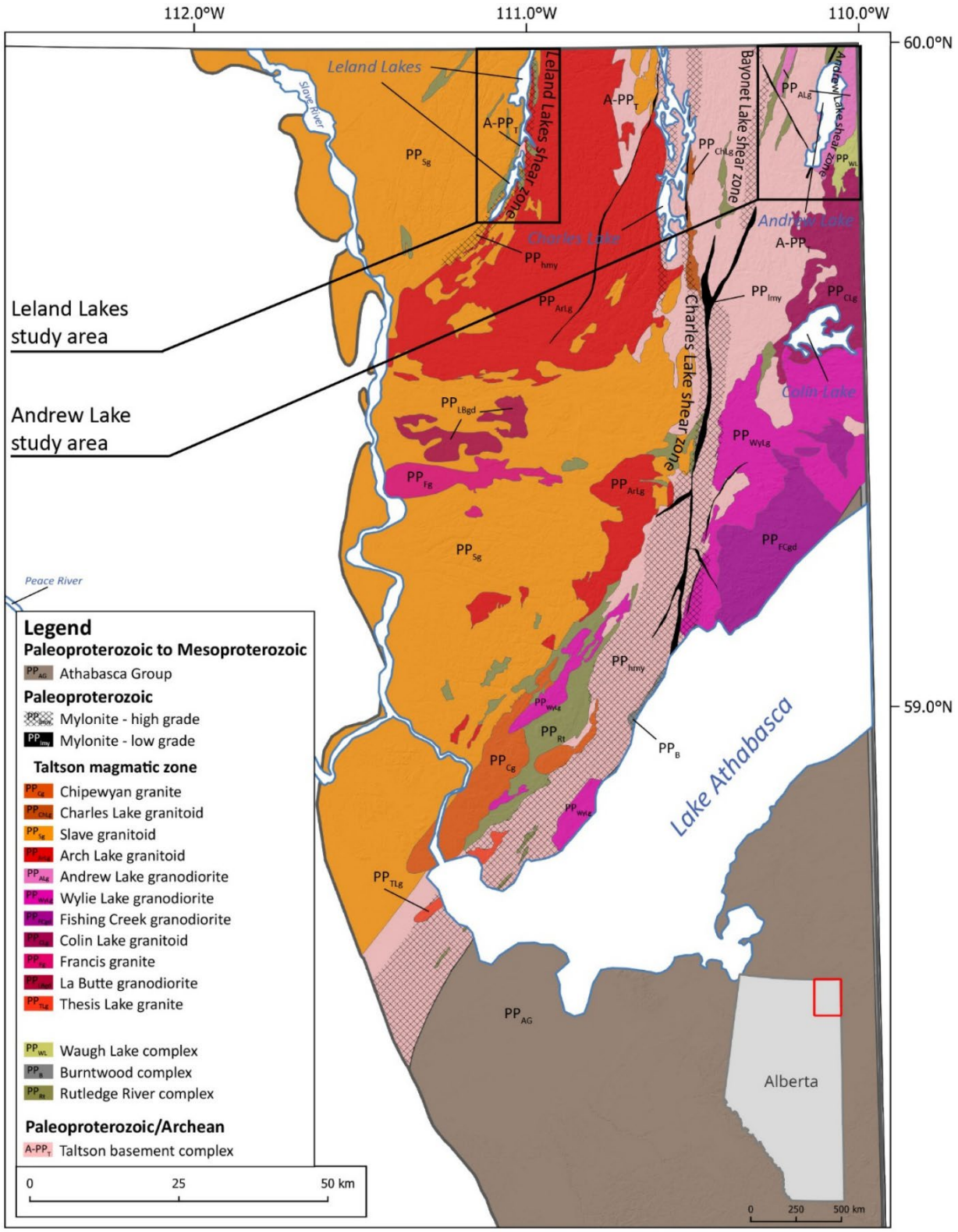

Figure 1. Simplified geological map of the Canadian Shield in northeastern Alberta, adapted from Godfrey (1986) and Prior et al. (2013). The inset map shows the location of the map area.

The variably foliated TMZ has been geochronologically and geochemically subdivided into early-stage I-type granites, which are metaluminous to weakly peraluminous, and late-stage peraluminous S-type granitoids (e.g., Bostock et al., 1991; Chacko et al., 2000; McDonough et al., 2000e). The early (1971–1959 Ma; McDonough and McNicoll, 1997; McDonough et al., 2000e; Stern et al., 2003) TMZ includes the Colin Lake granitoid, the Wylie Lake granodiorite, the Fishing Creek granodiorite, and the Andrew Lake granodiorite. The late (1960–1934 Ma; McDonough et al., 2000e) TMZ includes the Arch Lake granitoid and the polyphase Slave granitoid. In addition to these two subdivisions, there is another group of granitoids of uncertain geochemical affinity that occur in the TMZ: the Charles Lake granitoid with a minimum age of 1933 Ma (McDonough et al., 2000e), the ca. 1925 Ma Chipewyan granite (McDonough et al., 2000e), the Thesis Lake granite, the La Butte granodiorite, and the Francis granite.

There are four major shear zones trending approximately north-south in the exposed TMZ in northeastern Alberta. From west to east, they are the Leland Lakes shear zone (LLSZ), Charles Lake shear zone (CLSZ), Bayonet Lake shear zone (BLSZ), and Andrew Lake shear zone (ALSZ). The structural relationship between TMZ plutonism and the TBC is complex due to contemporaneous plutonism and deformation.

In the southern portion of the Canadian Shield in Alberta, the basement rocks of the TMZ and TBC are unconformably overlain by the Athabasca Group, a late Paleoproterozoic to early Mesoproterozoic clastic sedimentary succession that extends across the border into Saskatchewan, frequently referred to as the Athabasca Basin. Although only ~10% of the Athabasca Basin is found in Alberta, it covers ~40% of the exposed basement. In Saskatchewan, the Athabasca Basin/Group contains a number of world-class uranium deposits and is the site of advanced exploration projects.

2.2 Tectonic Setting

The origin of the TMZ is somewhat contentious, and there are three proposed models to explain the formation of the zone:

1) From 2.44 to 1.99 Ga, an Andean-type continental magmatic arc was generated on the western edge of the Rae craton during eastward subduction of oceanic crust between the Buffalo Head terrane and the Rae craton (Hoffman, 1988, 1989; Bostock et al., 1991; Ross et al., 1991; Thériault, 1992; van Breemen et al., 1992; McDonough et al., 2000e; McNicoll et al., 2000). During this collision, Rutledge River basin sedimentary rocks were accreted onto the western margin of the Rae craton, while the Waugh Lake basin sediments were deposited in a back-arc basin (McDonough and McNicoll, 1997; McDonough et al., 2000e). The early TMZ plutons, such as the Colin Lake granitoid, Wylie Lake granodiorite, and Andrew Lake granodiorite suites, formed from partial melting of the down-going oceanic slab, ca. 1.971–1.959 Ga, prior to the major continent–continent collision of the Buffalo Head terrane and the Rae craton (McDonough et al., 2000e). During the collision, crustal thickening and associated anatexis generated the Arch Lake granitoid ca. 1.938 Ga, while further anatexis of the accreted Rutledge River basin supracrustal suite generated voluminous S-type magmatism (e.g., Slave granitoid, Chipewyan granite; McDonough et al., 2000e). See Figure 2 for a cross-section configuration of this tectonic assemblage.
2) Instead of an Andean-type subduction and collision system as proposed in model 1, several authors proposed an alternative model of intraplate crustal thickening and anatexis due to a distant convergent margin (Thompson, 1989; Chacko et al., 2000; De et al., 2000). They posited that the major-element geochemical signatures and neodymium isotopic and oxygen isotopic signatures of the granitoids of the TMZ are not adequately explained by derivation from a mantle source as is the case in a convergent margin. Rather, they compare these signatures to Phanerozoic convergent-margin and intraplate granites and posit that they more closely resemble Phanerozoic intraplate granitoids. Additionally, the features of the TMZ that have been ascribed to a convergent margin also occur in intraplate settings, such as crustal thickening, extensive thrust faults and strike-slip faults, and generation of variably sized foreland basins. This model suggests that the Buffalo Head terrane, the

Slave craton, and the Rae craton amalgamated prior to 2.0 Ga (Chacko et al., 2000). Additionally, further work by Schultz et al. (2007) on the Queen Maud block in Nunavut suggests that the Slave and Rae cratons amalgamated prior to 2.0 Ga, likely during the Arrowsmith orogeny (Berman et al., 2005, 2013).

3) The third model suggests that the Thelon tectonic zone (TTZ) and the TMZ are distinct tectonic entities that separated from one another prior to 2.0 Ga via the MacDonald fault, which allowed them to develop separate geochemical signatures (Card et al., 2014; Whalen et al., 2018). Geological mapping, aeromagnetic interpretation, and geochemical and geochronological studies of the TTZ (Whalen et al., 2018; Davis et al., 2021; Berman et al., 2023, 2024) and TMZ (Card et al., 2014), which included analysis of the detrital zircon components of the basin rocks, present a somewhat complex tectonic model for the TTZ and the TMZ (Figure 3), where the Buffalo Head–Chinchaga terranes were sutured with the Queen Maud block and the Rae craton ca. 2.3 Ga. A set of rifts formed within the amalgamated Buffalo Head–Chinchaga terranes ca. 2.1 Ga, which generated contiguous sedimentary basins that evolved into the northern Ellice River and southern Rutledge River basins. Subsequent closure of these basins between 2.0 and 1.97 Ga brought together the east-verging Slave craton, Buffalo Head terrane, Chinchaga terrane, and Rae craton. The closure of these basins and subduction generated contemporaneous early-TMZ plutons from 2.0 to 1.97 Ga followed by assimilation and anatexis of the Rutledge River basin supracrustal rocks to form the late-stage TMZ plutonic assemblages younger than 1.97 Ga (Davis et al., 2021; Berman et al., 2023). Some authors have argued that portions of the TMZ may have been emplaced within crust of the Buffalo Head terrane, rather than the western margin of the Rae craton (Cutts et al., 2024). The separation of the two zones accommodates the observations by Card et al. (2014) of the differing aeromagnetic orientation of the southern TMZ distal from the GSLSZ. See Figure 3 for a plan-view model of the assembly of these terranes.

2.3 Geophysics

Geophysical data, particularly airborne data, have long provided insight into the complex lithological and structural features of the Canadian Shield in northeastern Alberta (Sprenke et al., 1986; Lyatsky and Pană, 2003).

The variations in the magnetic field result from a variety of geological features, including changes in metamorphic grade, localized shearing, brittle faulting, and granitoid masses (Sprenke et al., 1986; Lyatsky and Pană, 2003). Prominent, north- to northeast-trending, linear-type, positive anomalies mainly overlie major shear zones, including the LLSZ, the CLSZ, and the BLSZ (Sprenke et al., 1986). Conversely, mylonite zones and fault traces are sometimes associated with linear negative anomalies as magnetite was altered to hematite during mylonitization (Watanabe, 1965; Sprenke et al., 1986). When distal from major shear zones, granitoid rocks, such as the La Butte granodiorite, the Arch Lake granitoid, and to a lesser extent the Slave granitoid, are associated with circular-type, positive magnetic anomalies, which correlate to the magnetic susceptibilities and magnetite concentrations of these lithologies (Sprenke et al., 1986). In contrast, metasedimentary rocks, such as the RRC near Loutit Lake (80 km south of the study areas), often result in negative magnetic anomalies (Sprenke et al., 1986).

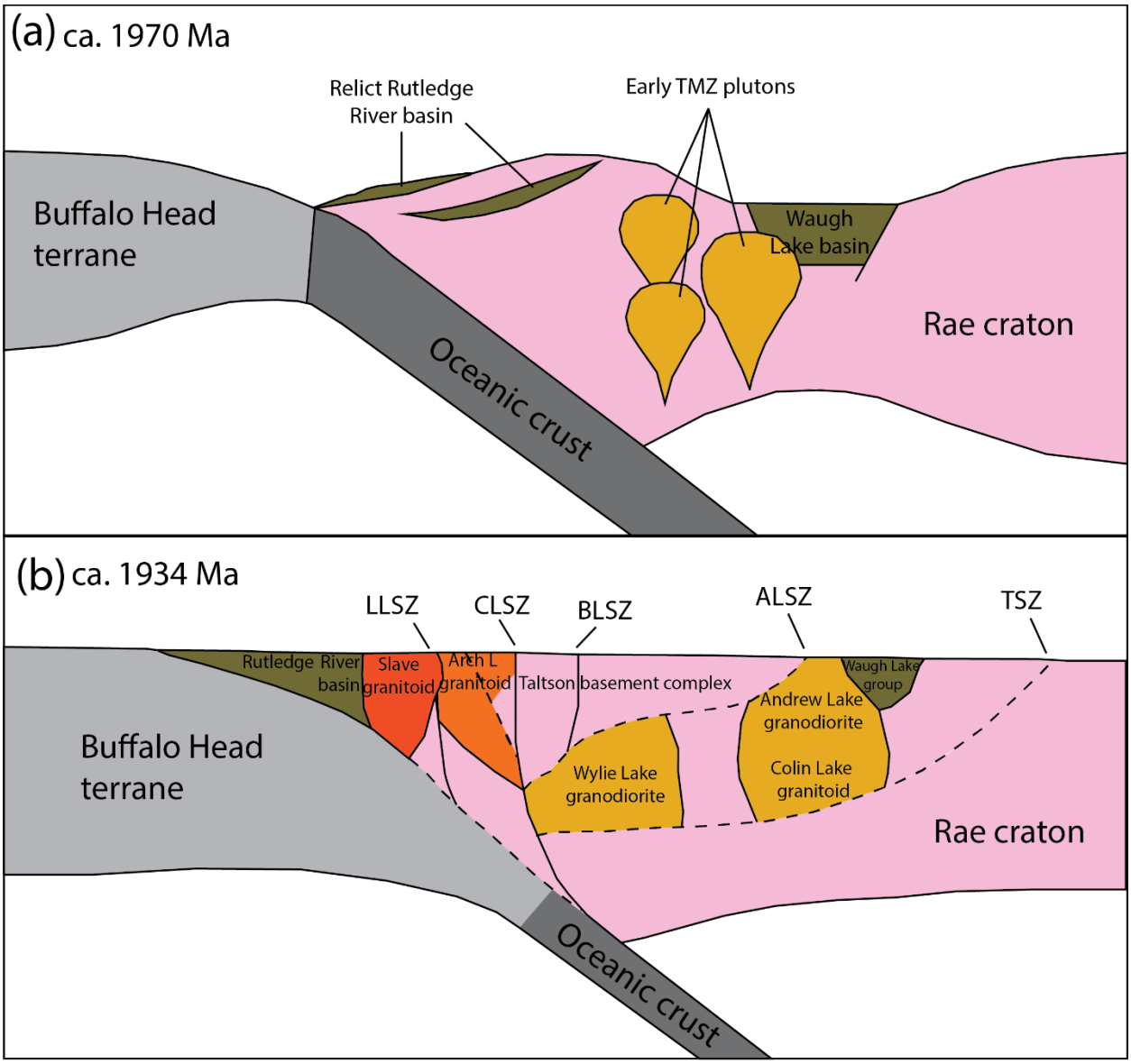

Figure 2. Tectonic assemblage cross-section of the Canadian Shield in northeastern Alberta (adapted from McDonough et al., 2000e): (a) the initial collision of the two cratons ca. 1970 Ma; (b) the end-stage of crustal thickening ca. 1934 Ma. Not to scale. Abbreviations: ALSZ, Andrew Lake shear zone; BLSZ, Bayonet Lake shear zone; CLSZ, Charles Lake shear zone; L, Lake; LLSZ, Leland Lakes shear zone; TMZ, Taltson magmatic zone; TSZ, Tazin shear zone.

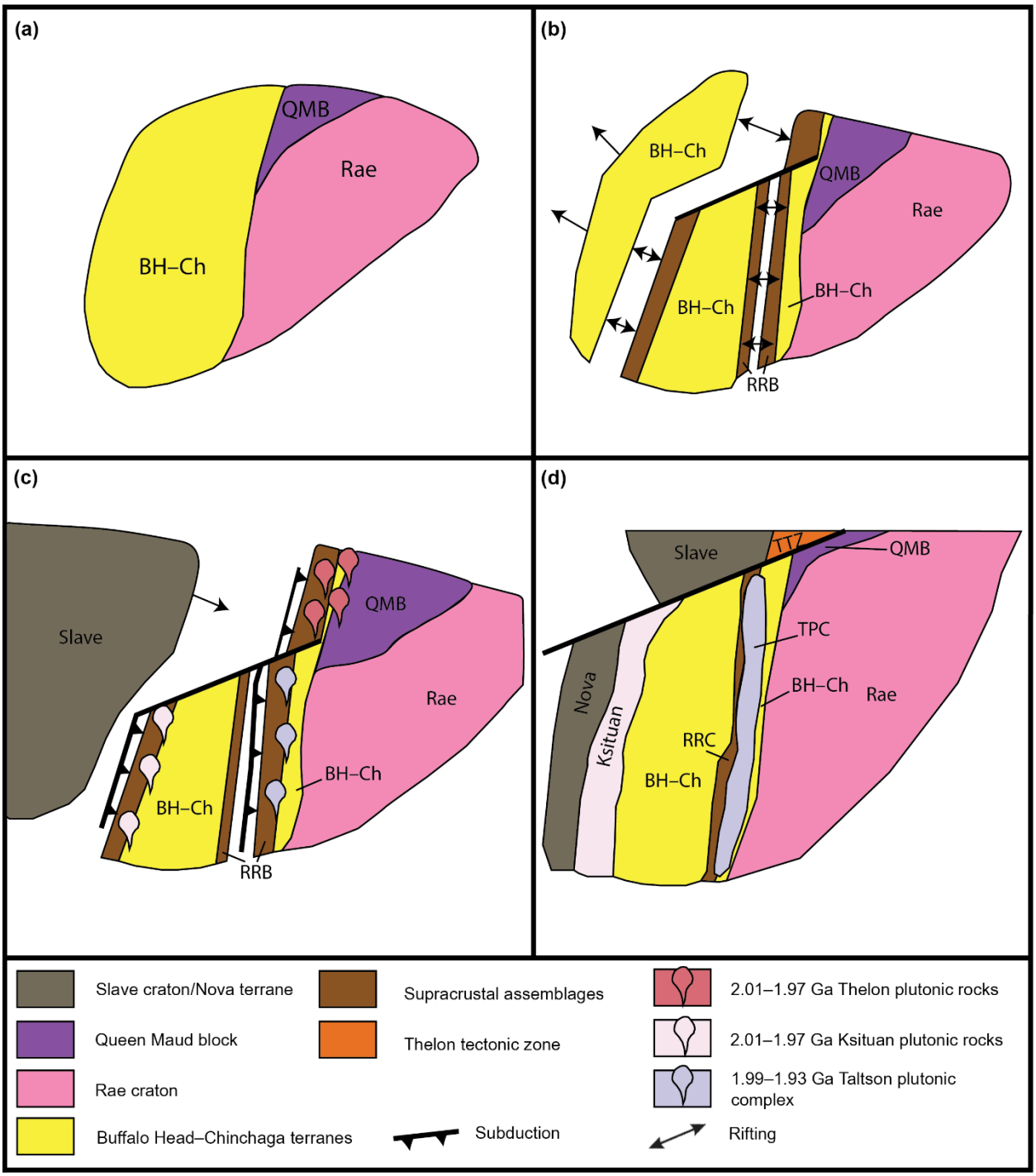

Figure 3. Modified tectonic assemblage model of the Canadian Shield in northeastern Alberta (adapted from Davis et al., 2021): (a) ca. 2.3 Ga; (b) 2.14 to 2.02 Ga, rifting and deposition of basin complexes; (c) 2.0 to 1.97 Ga, east-dipping subduction, closure of basins, and initiation of Taltson plutonism; (d) 1.97 to 1.93 Ga, collision of Slave craton and further Taltson plutonism. Not to scale. Abbreviations: BH-Ch, Buffalo Head–Chinchaga terranes; QMB, Queen Maud block; RRB, Rutledge River basin; RRC, Rutledge River complex; TPC, Taltson plutonic complex (of the Taltson magmatic zone); TTZ, Thelon tectonic zone.

Regional changes in gravity over the Canadian Shield in northeastern Alberta are interpreted to be controlled by lithological differences in rock density, as well as metamorphic facies and structural fabric (Sprenke et al., 1986). According to density measurements of rock samples collected in the Canadian Shield, metasedimentary rocks and granite gneisses are generally denser than felsic granitoids, with residual gravity maps tending to reflect this relationship (Sprenke et al., 1986). In general, granite gneisses coincide with relatively high residual gravity, whereas felsic granitoids, such as the Arch Lake granitoid and Colin Lake granitoid, coincide with low residual gravity (Sprenke et al., 1986). Exceptions include the Slave granitoid, which exhibits a moderate to high gravity response (Sprenke et al., 1986). One notable feature on gravity maps of the region is the north- to northeast-trending curvilinear Barrow-Ashton Lakes gravity high north of Lake Athabasca. Sprenke et al. (1986) interpreted the high to represent an area of high-grade (granulite facies) metamorphism unaffected by potassium metasomatism rather than representing a contrast in lithology.

Prominent radiometric anomalies occur in several locations in the region with Sprenke et al. (1986) identifying six zones north of Lake Athabasca associated with high equivalent uranium (eU) concentrations and eU to equivalent thorium (eTh) ratios, including west of Leland Lakes, north of Ryan Lake, south of Colin Lake, at Fidler Point on Lake Athabasca, near Cherry Lake, and west of Cockscomb Lake. Although regional electromagnetic data is limited to one very low frequency (VLF) survey conducted by the Geological Survey of Canada (GSC), the resultant electromagnetic anomalies appear to primarily parallel dominant foliation (Charbonneau et al., 1994). Property-scale, mineral exploration electromagnetic surveys have produced conductor anomalies that follow known faults and sulphide-bearing gossans, most notably near Waugh Lake (Stemp, 1969; Burgan, 1971; Grant and Smith, 2007).

2.4 Previous Work

2.4.1 Academic Work

The earliest geological information regarding the Canadian Shield in Alberta was published by the GSC in 1896. The GSC's Tyrrell (1896) and Alcock (1915, 1917) recorded information during their canoe-based traverses along the north shore of Lake Athabasca in the late 1890s to the early 1900s. Following this, a series of traverses were made into the Alberta Shield from the north shore of Lake Athabasca by A.E. Cameron and H.S. Hicks as part of efforts by the Scientific and Industrial Research Council of Alberta (Cameron, 1930), the Research Council of Alberta and the University of Alberta (Hicks, 1930; Cameron and Hicks, 1931), and the Research Council of Alberta and the University of Minnesota (Hicks, 1932).

Between 1957 and 1975, J.D. Godfrey of the Alberta Research Council conducted systematic district-by-district geological mapping of the Alberta Shield at a variety of scales ranging from 1:31 680 to 1:250 000 (e.g., Godfrey, 1961, 1986). Further geochronological study was performed in conjunction with, and as a result of, this mapping work (Baadsgaard and Godfrey, 1967, 1972; Kuo, 1972; Day, 1975). In addition, Godfrey (1958b) performed preliminary structural interpretations of the shield north of Lake Athabasca from airphotos. In 1959, the GSC carried out a mapping program and published a map at a 1:253 440 scale (Riley, 1960). Peikert (1961, 1963) examined the petrogenesis of granitic rocks in the Colin Lake region. Watanabe (1961, 1965) described the lithologies in the Waugh Lake area and the cataclasites of the Charles Lake area. Klewchuk (1972) conducted a petrogenetic analysis of another suite of granites from the Fort Chipewyan area. The metamorphic history of the Alberta Shield was described by Langenberg (1983) and Langenberg and Nielsen (1982). An AGS bulletin describing the geochemistry and petrology of the Canadian Shield in Alberta, with a particular emphasis on the granitoids and orthogneisses, was authored by Goff et al. (1986).

In the early 1990s, a series of reconnaissance field programs were conducted as part of the Canada–Alberta Partnership Agreement on Minerals by the AGS to investigate the mineralization systems present in Alberta. This included investigations of the mineral occurrences of the Andrew Lake–Charles Lake study area (Langenberg et al., 1993), the Selwyn Lake–Leland Lakes study area (Langenberg et al.,

1994), and the Waugh Lake complex (Salat et al., 1994). The fieldwork in the Waugh Lake area resulted in a new 1:10 000 geological map of the Waugh Lake complex, the renaming of it to the Waugh Lake group, and the subdivision of the group into formal stratigraphic sequences (Iannelli et al., 1995). As part of a large national lake sediment sampling program, the GSC conducted lake sediment sampling over the entire Canadian Shield in Alberta (Friske et al., 1994). Further Quaternary work by the GSC, including surficial mapping, was conducted in the 1990s (Bednarski, 1996, 1999). Throughout the 1990s, the GSC mapped large portions of the shield at a scale of 1:50 000, which also included geochronological, geochemical, and thermobarometric analyses of select units (Grover et al., 1993, 1997; McDonough et al., 1993a–c, 1994a–g, 1995a, b, 2000a–g; Plint and McDonough, 1995; McDonough, 1997; McDonough and McNicoll, 1997; McNicoll et al., 2000). In the late 1990s, samples from across the shield were re-evaluated by De et al. (2000) and Chacko et al. (2000) to generate an alternative tectonic model for the TMZ.

In the 2000s, several geological reconnaissance programs were carried out in northeastern Alberta, including investigation of the geological evolution and mineral potential of the Andrew Lake study area (Pană et al., 2006; Pană, 2010a; Pană and Prior, 2010) and investigation of uranium exploration along the northern rim of the Athabasca Basin (Pană and Olson, 2009). Further mapping, geochronological, and aeromagnetic interpretation work on the tectonic setting of the TMZ was completed by Card et al. (2014), though this work focused primarily on northwestern Saskatchewan. In 2022, the Waugh Lake complex was reinvestigated (J.M.K. Deane, K.M. Bethune, K.E. Ashton, N.O. Montenegro, J.L. Crowley and K.P. Larson, work in progress, 2026; N.O. Montenegro, work in progress, 2026) as part of a broader initiative to better characterize its petrogenesis and tectonic assembly. Additionally, in the early 2020s, Thiessen et al. (2024) submitted samples from the RRC in Alberta for reanalysis to better constrain their depositional history.

The geology of the Canadian Shield in Alberta has been published in several compilations, such as AGS Map 180 at a scale of 1:250 000 (Godfrey, 1986), AGS Map 537 at a scale of 1:250 000 (Pană, 2010b), and AGS Map 600 at a scale of 1:1 000 000 (Prior et al., 2013).

2.4.2 Mineral Exploration

Multiple publications have summarized the extensive mineral exploration work on the Canadian Shield near Leland Lakes and Andrew Lake in Alberta including Pană et al. (2006), Pană and Olson (2009), and Rukhlov (2011). A boom in uranium exploration in the late 1960s brought explorers to the region and subsequent activity has focused primarily, but not exclusively, on uranium potential. These early exploration programs initially relied extensively on airborne radiometric surveys and focused on occurrences described by Godfrey through his regional mapping efforts (Godfrey, 1958a, b, 1961, 1963, 1966).

The Andrew Lake region has been a focal point for uranium exploration in northeastern Alberta with significant activity from New Senator-Rouyn Ltd. and McIntyre Porcupine Mines Ltd. starting in 1967 (Hart, 1967; Lipsett and Trigg, 1968; Thorpe, 1968, 1969). In the late 1960s, these companies conducted airborne radiometric surveying, prospecting, rock trenching, and diamond drilling at Cherry Lake, Twin lakes (unofficial geographic name, lat. 59.768, long. -110.109), and Small lake (unofficial geographic name, lat. 59.771, long. -110.116), noting that anomalous uranium results were often closely related to pegmatite or granite intrusions (Thorpe, 1968, 1969). Hudson's Bay Oil and Gas Company Limited continued work south of Andrew Lake, discovering a sulphide-bearing conductor in graphitic schist at Waugh Lake and isolated veinlets of pitchblende at the informally named Carrot lake (unofficial geographic name, lat. 59.790, long. -110.121; Burgan, 1971; Pollock et al., 1971). After several years of relative quiescence, Aquarius Mines Ltd., eventually in partnership with Tachyon Venture Management Ltd., completed several large-scale exploration programs in the mid- to late 1970s centred on Spider Lake, Holmes Lake, southern Andrew Lake, and Carrot lake (Sullivan, 1974; Allan, 1976a–c, 1977).

Farther west, a host of companies, including Giant Explorations Limited, Citizens Pipeline Limited, Vestor Explorations Ltd., Slek Investments Ltd., and Souvenir Mines Ltd., completed separate airborne radiometric surveys in the Leland Lakes region and identified several anomalous zones (Gayfer, 1968; Cook, 1969a, b; Sutton et al., 1969; Greig, 1970). In the early 1970s, Vestor Explorations Ltd. focused ground exploration efforts on the southern end of Leland Lakes, near Myers Lake, and were successful in identifying several radiometric anomalies and base metal occurrences associated with north- to northeast-trending vertical faults (Williams, 1970; Babcock et al., 1971).

Since the 1980s, sporadic, small-scale exploration work has been conducted in the Leland Lakes and Andrew Lake regions with a more diverse focus, including precious metals, base metals, and rare-earth elements (Mann, 1991, 1995; Cantin, 1996; Friesen, 1998; Wiskel, 1999). These included an investigation for precious metals and lanthanides near Harker Lake (Mann, 1991), continued exploration for gold mineralization at Waugh Lake (Cantin, 1996; Wiskel, 1999), and examination of a prominent linear magnetic-high anomaly west of the Leland Lakes study area (Mann, 1995; Friesen, 1998). The most recent exploration activity on the Canadian Shield near Leland Lakes and Andrew Lake was conducted by North American Gem Inc. in 2006 and 2007 (Grant and Smith, 2007; Smith and Griffith, 2007). This regional exploration program discovered new anomalies while revisiting numerous known uranium and rare-earth-element anomalies across the region. A number of the discussed occurrences and anomalies are presented in Figure 4.

3 Methods

3.1 Sampling Methods

Sampling of the Precambrian shield in northeastern Alberta was completed by AGS staff and contractors over four weeks in June and July 2023 (Belosevic et al., 2024). The AGS staff and contractors planned traverses to evaluate critical mineral potential prior to the field season using available remote sensing data (Esri, 2023), digital elevation models (NASA JPL, 2013), geological maps (Godfrey 1961, 1963, 1966; Godfrey and Langenberg, 1986), geochemical data (Friske et al., 1994; Langenberg et al., 1994; Bednarski, 1996; Pană and Prior, 2010; Meek et al., 2023), previously recognized mineral occurrences (Lopez et al., 2020), and geophysical data (Charbonneau et al., 1994; Alberta Geological Survey, 2023). Field teams accessed planned traverses primarily via boat on both Leland Lakes and Andrew Lake. Additional planned traverses beyond the two lakes were supported by charter flights on a Cessna 180. A total of 394 stations were visited by the AGS crews, where outcrops were described and sampled to assess critical mineral potential. Sample types included representative grab samples and channel samples where glacially polished surfaces limited the ability to collect samples with a rock hammer. Additional data collection was conducted at select stations, including magnetic susceptibility measurements and background radiation measurements (Belosevic et al., 2024).

3.2 Leland Lakes Sample Localities

A total of 166 stations were visited by the AGS crews in the Leland Lakes study area. Access to stations was accomplished primarily via boat on Leland Lakes. Only two traverses were supported by chartered flights on a Cessna 180 to Myers Lake and McLelland Lake. From stations in the Leland Lakes study area, 208 samples were collected for additional analysis (Figure 5). All station observations and whole-rock lithogeochemical data from this area can be found in AER/AGS Digital Data DIG 2025-0001 (Meek et al., 2026). All petrographic descriptions completed from thin sections can be found in Appendix 1.

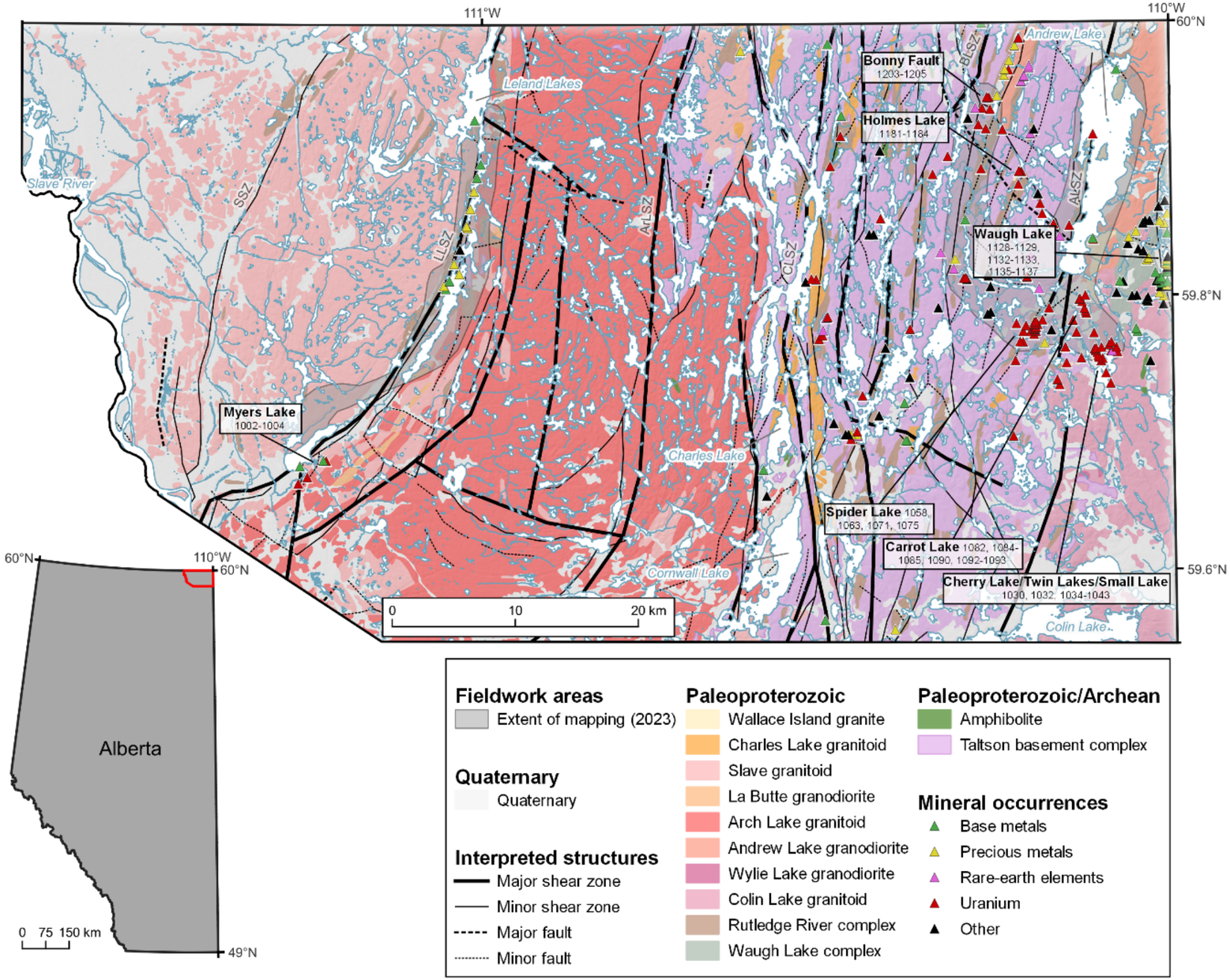

Figure 4. Simplified geology of northeastern Alberta adapted from Pană (2010b) with metallic mineral occurrences, geochemical anomalies, and showings from Lopez et al. (2020). Significant occurrences are identified on the map, with associated metallic mineral occurrences identifier, from Lopez et al. (2020). Structural interpretations from Lopez et al. (2024). Abbreviations: ALSZ, Andrew Lake shear zone; ArLSZ, Arch Lake shear zone; BLSZ, Bayonet Lake shear zone; CLSZ, Charles Lake shear zone; LLSZ, Leland Lakes shear zone; SSZ, Slave shear zone.

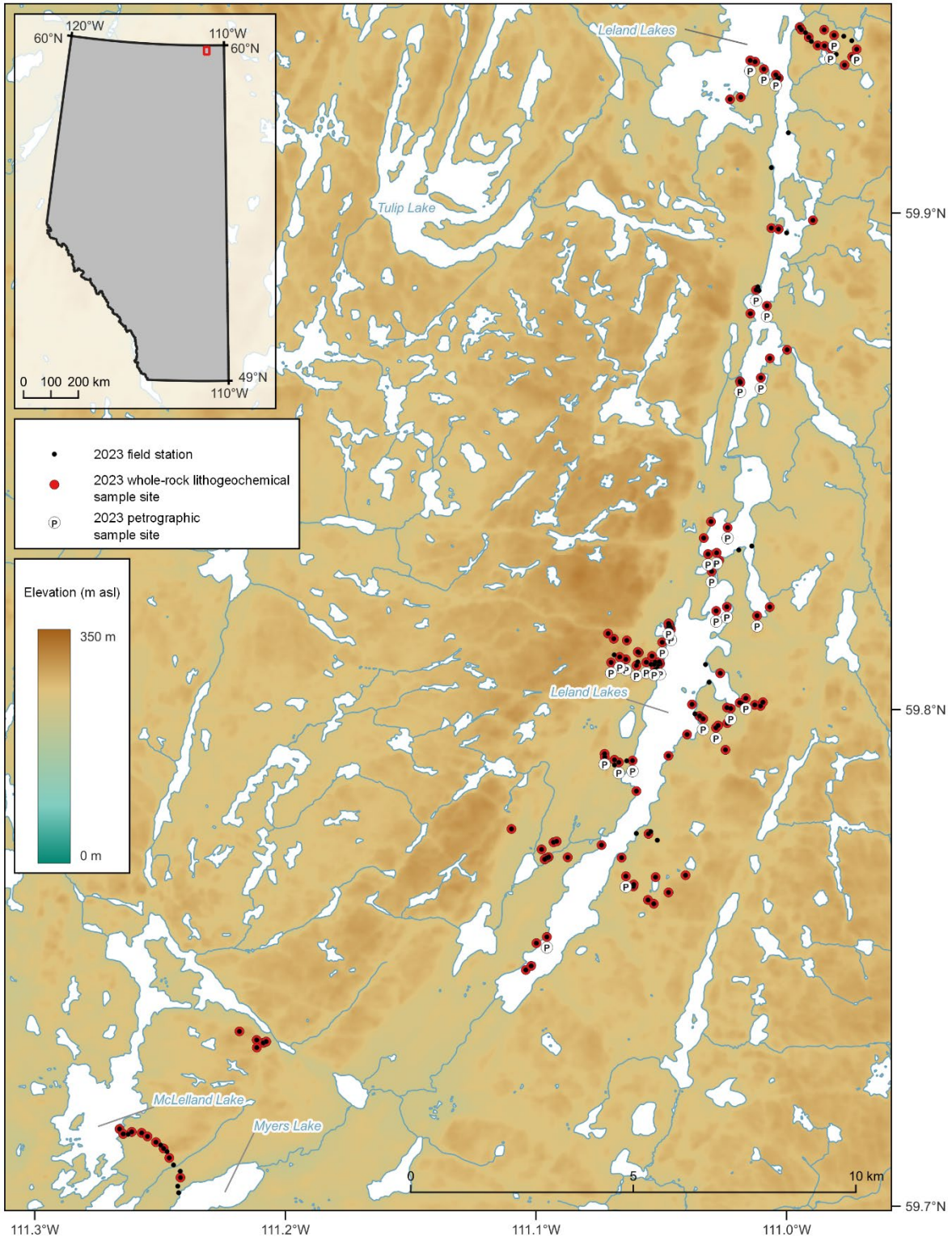

Figure 5. Leland Lakes study area in northeastern Alberta with the locations of the 2023 field stations and the whole-rock lithogeochemical and petrographic sample sites (Meek et al., 2026). Background digital elevation model from NASA JPL (2013).

3.3 Andrew Lake Sample Localities

A total of 228 stations were visited by the AGS crews in the Andrew Lake study area. Access to stations was accomplished via boat and chartered flights on a Cessna 180 in this area of interest. Boat access for traverses was possible on Andrew Lake, whereas charter flights were required for access to Bayonet Lake, Cherry Lake, Potts Lake, Sedgwick lake (unofficial geographic name, lat. 59.938, long. -110.253), and Spider Lake (Figure 6). From these stations, 336 samples were collected for additional analysis (Figure 6). All station observations and whole-rock lithogeochemical data from this area can be found in AER/AGS Digital Data DIG 2025-0001 (Meek et al., 2026). All petrographic descriptions completed from thin sections can be found in Appendix 1.

3.4 Laboratory Methods

Samples collected during the 2023 field program were returned to the AGS Mineral Core Research Facility (MCRF) in Edmonton, Alberta. Samples were checked against field inventory lists to confirm material was not lost in transit. Prior to shipment for lithogeochemical analysis or thin section preparation, samples were cleaned by removing weathered surfaces with a rock saw where necessary and photographs were taken as part of an internal quality assurance and quality control process.

3.4.1 Lithogeochemical Analysis

A total of 551 samples were submitted to Activation Laboratories Ltd. (Actlabs) in Ancaster, Ontario, for whole-rock lithogeochemical analysis. To support internal data quality control, two different certified reference materials (CRM) were used. This included 14 felsic CRMs (OREAS® 20a – barren I-Type hornblende-bearing granodiorite) and 14 mafic CRMs (OREAS 30a – olivine tholeiitic basalt) inserted at a rate of 5%, or 1 CRM included for every 20th sample.

Actlabs prepared the samples by oven drying them at 60°C, followed by crushing to ≥80% of <2 mm grain size and then pulverized in a Cr-free steel mill to ≥95% of <74 µm grain size. Three different analytical packages were completed for each sample. The 4Lithoresearch package subjected samples to lithium metaborate-tetraborate fusion within disposable graphite crucibles, with the resulting fused sample mixed in a solution of 5% nitric acid until completely dissolved. The resulting solution was analyzed for 10 major oxides (plus loss-on-ignition) and 45 trace elements using inductively coupled plasma–mass spectrometry (ICP-MS) or inductively coupled plasma–optical emission spectrometry (ICP-OES). The 4B1 package subjected samples to a four-acid digestion, starting with hydrofluoric (HF) acid and followed by a mixture of nitric (HNO_3) and perchloric ($HClO_4$) acids, which were heated using precise programmer-controlled ramping and holding cycles until samples reached dryness. After dryness was attained, samples were brought back into solution using hydrochloric acid (HCl) and ICP-OES was used to quantify seven elements, including base metals, in the resulting solution. The Ultratrace 7 package subjected samples to sodium peroxide fusion within a zirconium crucible, with the resulting fused sample acidified with HNO_3 and HCl. The resulting solution was diluted and analyzed for lithium using ICP-OES. All major oxides and trace elements included in the analytical packages described are summarized in Table 1.

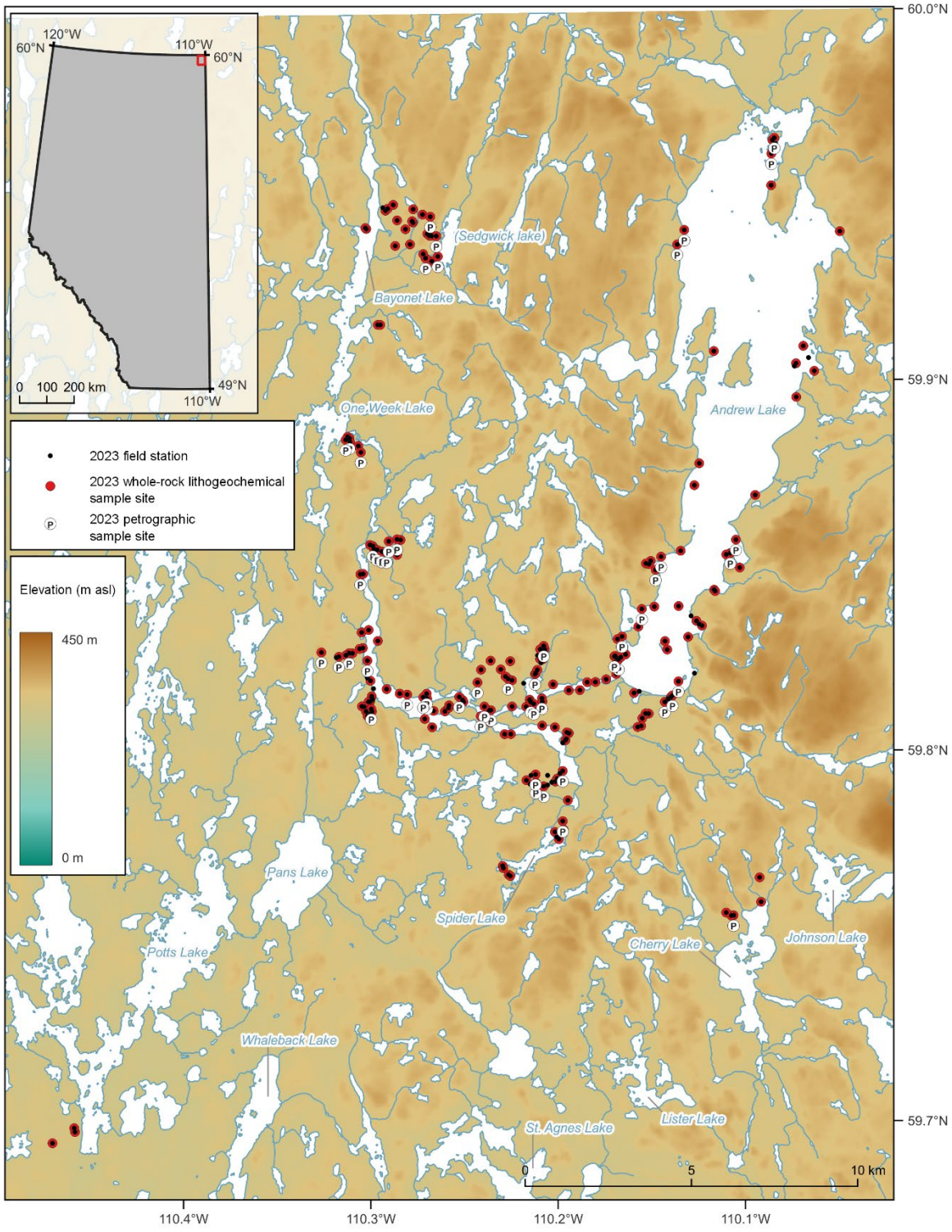

Figure 6. Andrew Lake study area in northeastern Alberta with the locations of the 2023 field stations and the whole-rock lithogeochemical and petrographic sample sites (Meek et al., 2026). Background digital elevation model from NASA JPL (2013). Lake label in parentheses indicates unofficial name.

Table 1. Analytes, associated analytical package (Pkg), units of measurement (Unit), and lower detection limit (LDL) reported from Activation Laboratories Ltd. (Ancaster, Ontario) for geochemical analysis of Leland Lakes and Andrew Lake samples, northeastern Alberta. Abbreviations: LOI, loss-on-ignition; pct, per cent.

Analyte	Analytical Pkg	Unit	LDL	Analyte	Analytical Pkg	Unit	LDL
SiO_2	4Lithoresearch	pct	0.01	Lu	4Lithoresearch	ppm	0.002
Al_2O_3	4Lithoresearch	pct	0.01	Mo	4Lithoresearch	ppm	2
Fe_2O_3	4Lithoresearch	pct	0.01	Nb	4Lithoresearch	ppm	0.2
MnO	4Lithoresearch	pct	0.001	Nd	4Lithoresearch	ppm	0.05
MgO	4Lithoresearch	pct	0.01	Pr	4Lithoresearch	ppm	0.01
CaO	4Lithoresearch	pct	0.01	Rb	4Lithoresearch	ppm	1
Na_2O	4Lithoresearch	pct	0.01	Sb	4Lithoresearch	ppm	0.2
K_2O	4Lithoresearch	pct	0.01	Sc	4Lithoresearch	ppm	1
TiO_2	4Lithoresearch	pct	0.001	Sm	4Lithoresearch	ppm	0.01
P_2O_5	4Lithoresearch	pct	0.01	Sn	4Lithoresearch	ppm	1
LOI	4Lithoresearch	pct	0.01	Sr	4Lithoresearch	ppm	2
Total	4Lithoresearch	pct	0.01	Ta	4Lithoresearch	ppm	0.01
As	4Lithoresearch	ppm	5	Tb	4Lithoresearch	ppm	0.01
Ba	4Lithoresearch	ppm	2	Th	4Lithoresearch	ppm	0.05
Be	4Lithoresearch	ppm	1	Tl	4Lithoresearch	ppm	0.05
Bi	4Lithoresearch	ppm	0.1	Tm	4Lithoresearch	ppm	0.005
Ce	4Lithoresearch	ppm	0.05	U	4Lithoresearch	ppm	0.01
Co	4Lithoresearch	ppm	1	V	4Lithoresearch	ppm	5
Cr	4Lithoresearch	ppm	20	W	4Lithoresearch	ppm	0.5
Cs	4Lithoresearch	ppm	0.1	Y	4Lithoresearch	ppm	0.5
Dy	4Lithoresearch	ppm	0.01	Yb	4Lithoresearch	ppm	0.01
Er	4Lithoresearch	ppm	0.01	Zr	4Lithoresearch	ppm	1
Eu	4Lithoresearch	ppm	0.005	Ag	4B1	ppm	0.3
Ga	4Lithoresearch	ppm	1	Cd	4B1	ppm	0.5
Gd	4Lithoresearch	ppm	0.01	Cu	4B1	ppm	1
Ge	4Lithoresearch	ppm	0.5	Ni	4B1	ppm	1
Hf	4Lithoresearch	ppm	0.1	Pb	4B1	ppm	5
Ho	4Lithoresearch	ppm	0.01	S	4B1	pct	0.001
In	4Lithoresearch	ppm	0.1	Zn	4B1	ppm	1
La	4Lithoresearch	ppm	0.05	Li	Ultratrace 7	ppm	15

3.4.2 Thin Sections

A subset of samples (199) were selected for thin section preparation. These samples were chosen to help clarify the mineralogy and petrography of selected units as well as to examine evidence of the metamorphic and structural history of the area. Thin section billets were sent to Spectrum Geosciences Ltd. (Calgary, Alberta) and AGAT Laboratories Ltd. (Calgary, Alberta) to create polished, 30 µm thick, standard-sized thin sections (25 by 45 mm). Thin sections were examined under plane-polarized–light (PPL) and cross-polarized–light (XPL) microscopy, with selected samples also examined by reflected-light microscopy. Petrographic descriptions of 108 thin sections were completed by the authors, with additional details provided in Section 4 and all descriptions included in Appendix 1.

4 Results

4.1 Local Geology and Petrographic Descriptions

Bedrock mapping was conducted with a station density consistent with 1:20 000 scale mapping and was aimed at evaluating the primary lithological units in the study areas. A summary of geological units reviewed are listed in Table 2.

4.1.1 Leland Lakes Study Area

Mapping in the Leland Lakes study area was focused along the LLSZ. Particular emphasis was placed on the RRC supracrustal units exposed along this corridor (Figure 7). A number of base and precious metal occurrences have been reported in this area by previous investigators. Geological mapping along this corridor identified a larger exposure of suspected basement gneissic rock within the well-documented Paleoproterozoic plutonic complexes than had been previously described (McNicoll et al., 2000; Pană, 2010b).

Table 2. Summary of the Leland Lakes and Andrew Lake geological units (northeastern Alberta) reviewed as part of the petrographic analysis, and the respective count of thin sections analyzed from each unit.

Area	Geological Unit	Count
Leland Lakes	Amphibolite/metagabbro	7
	Arch Lake granitoid	3
	Biotite-hornblende heterogeneous gneiss	8
	Mixed mylonite	2
	Mylonitic Arch Lake granitoid	2
	Pegmatite	1
	Metasedimentary rocks and paragneiss	10
	Slave granitoid	4
	Migmatite and spotted migmatite	5
Andrew Lake	Amphibolite/metagabbro	6
	Andrew Lake granodiorite	1
	Taltson basement gneiss	12
	Colin Lake white granite	2
	Granite gneiss	17
	Pegmatite	7
	Metasedimentary rocks and paragneiss	21

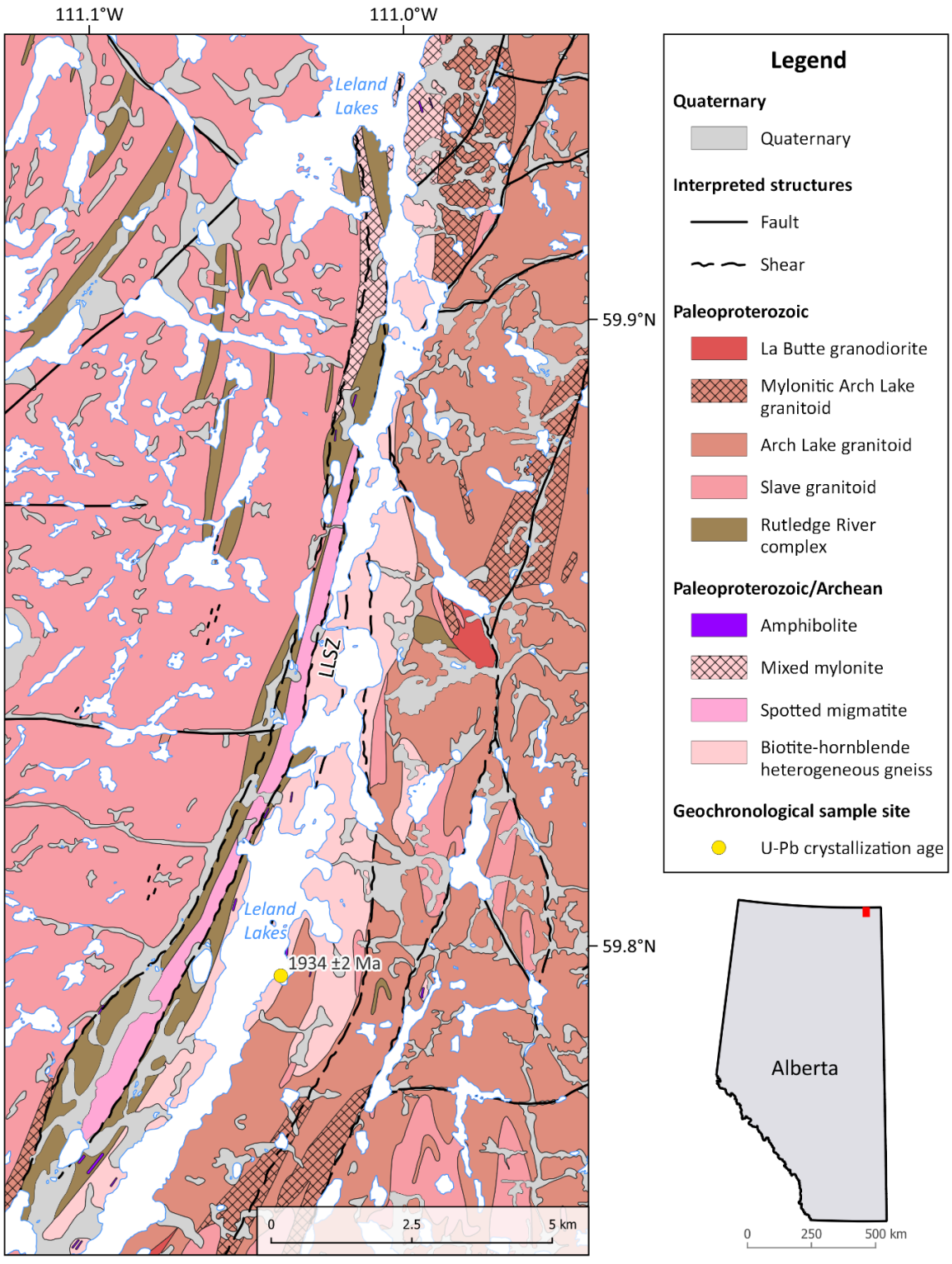

Figure 7. Bedrock geology (adapted from Godfrey and Langenberg, 1986) of the northern part of the Leland Lakes study area in northeastern Alberta with bedrock interpretations from 2023 fieldwork. The U-Pb geochronology data was sourced from McDonough et al. (2000e). Abbreviation: LLSZ, Leland Lakes shear zone. Structural interpretations are modified from Godfrey and Langenberg (1986).

4.1.1.1 Paleoproterozoic

Slave Granitoid (SG): the ca. 1934 ±2 Ma (McDonough et al., 2000e) Slave granitoid occurs as a batholithic belt exposed west of the LLSZ. Smaller bodies of this granitoid have been reported as being interspersed within the Arch Lake granitoid complex (Godfrey and Langenberg, 1986) to the east of Leland Lakes. The Slave granitoid was derived by partial melting of older granitic gneiss and metasedimentary rocks (Goff et al., 1986; Chacko et al., 2000). The area of Slave granitoid west of the LLSZ has an aeromagnetic-low signature that contrasts strongly with magnetite-rich gneisses of the Taltson basement and the Arch Lake granitoid to the east of the LLSZ.

The Slave granitoid in the study area is white to grey, leucocratic, quartz syenite to syenogranite with 1–5% biotite and trace garnet (Figures 8a and 9a). Garnet and biotite are locally retrogressed to chlorite and epidote, especially in proximity to zones of brittle-ductile deformation along the LLSZ. Biotite is locally more abundant, up to 10%, which Godfrey and Langenberg (1986) distinguished as the "Mafic Slave Granite Phase" map unit. Texturally, the granitoids are medium grained to pegmatitic and massive to weakly foliated, with localized grain-size reduction in zones of shear. Pegmatitic phases of the granitoid form abundant sheets and dikes. There is a 49 km long east-west-trending aeromagnetic anomaly termed the Dog River linear (Mann, 1996), which transects the Slave granitoid and extends across the LLSZ and Arch Lake granitoid and may either relate to the Mackenzie diabase dikes (1267 ±2 Ma, LeCheminant and Heaman, 1989) mapped in Saskatchewan and the Northwest Territories or to the Sparrow diabase dikes (1827 ±4 Ma, Bostock and van Breemen, 1992) mapped in the Northwest Territories (Lopez et al., 2024). The orientation of this aeromagnetic feature is similar to the mapped orientation of the Mackenzie dikes, however, outcrops of this feature have yet to be identified.

Arch Lake Granitoid (AR) and Mylonitic Arch Lake Granitoid (MA): the massive- to well-foliated and locally mylonitic Arch Lake granitoid is distinguished in the study area by an abundance of pink to dark grey K-feldspar megacrysts (Figure 8b). Mineralogically, this unit is composed of quartz (25–30%), K-feldspar (15–30%), and plagioclase (10–30%) with highly variable biotite content, ranging from <5 to >10% (Figure 9b). Garnet, hercynite, monazite, hypersthene, magnetite, ilmenite, and apatite are all locally present in trace to minor amounts. The Arch Lake granitoid is fairly homogeneous with little to no mafic sheets, dikes, or xenoliths. Wherever this unit is mylonitic, K-feldspar porphyroclasts lie within a fine-grained ribboned matrix. A U-Pb date of 1938 ±3 Ma was reported from the Charles Lake area for this unit (McDonough et al., 2000e).

Metasedimentary Rocks and Paragneiss (PG): this metasedimentary rocks and paragneiss unit occurs along the length of the LLSZ (Figure 8c). The rocks have compositional layering that is defined by variable amounts of garnet (1–20%), biotite (10–40%), quartz (≥30%), muscovite (≤30%), and locally sillimanite and disseminated graphite (Figure 10a and b). Cordierite is locally abundant (≥30%) and was also previously reported by Godfrey and Langenburg (1986). Although typically gneissic, the unit locally contains biotite-rich schistose interlayers as well as rare zones that appear to contain in situ migmatite. This unit has previously been ascribed to the 2.15–2.09 Ga RRC (Bostock and van Breeman, 1994), but U-Pb ages are lacking from the study area. A recent study by Thiessen et al. (2024) suggests that metasedimentary rocks at Pelican Rapids, 40 km west of the Leland Lakes study area, were likely deposited between 2.03 and 1.94 Ga. The PG unit is strongly affected by the brittle-ductile deformation of the LLSZ and its exposure appears to be controlled by this structure and the underlying Archean basement. The boundary between the PG unit and the older biotite-hornblende heterogeneous gneiss (OGN) unit appears to be tectonic.

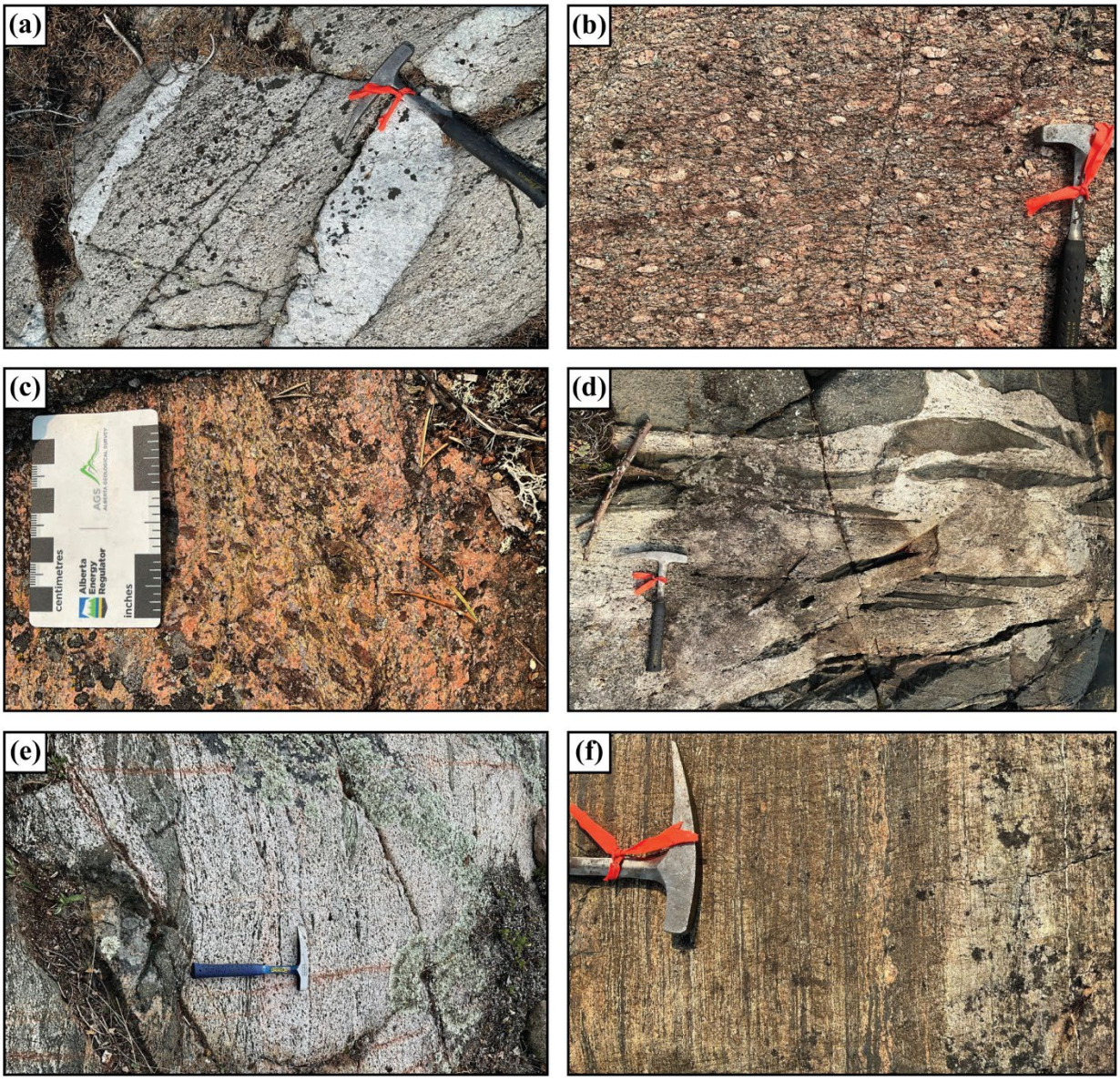

Figure 8. Representative outcrop photographs, Leland Lakes study area, northeastern Alberta: (a) ca. 1.93 Ga Slave granite cut by younger pegmatitic phases (station LL-23-1088); (b) K-feldspar megacrystic Arch Lake granite (station LL-23-1074); (c) polydeformed, garnet-bearing metasedimentary rock (station LL-23-1097); (d) biotite-hornblende heterogeneous gneiss containing dismembered and folded layers of amphibolite (station LL-23-1067); (e) spotted migmatite with numerous dismembered amphibolite bands (station LL-23-1054); (f) laminated, fine- to medium-grained mylonitic rock of intermediate composition from the Leland Lakes shear zone (station LL-23-1098).

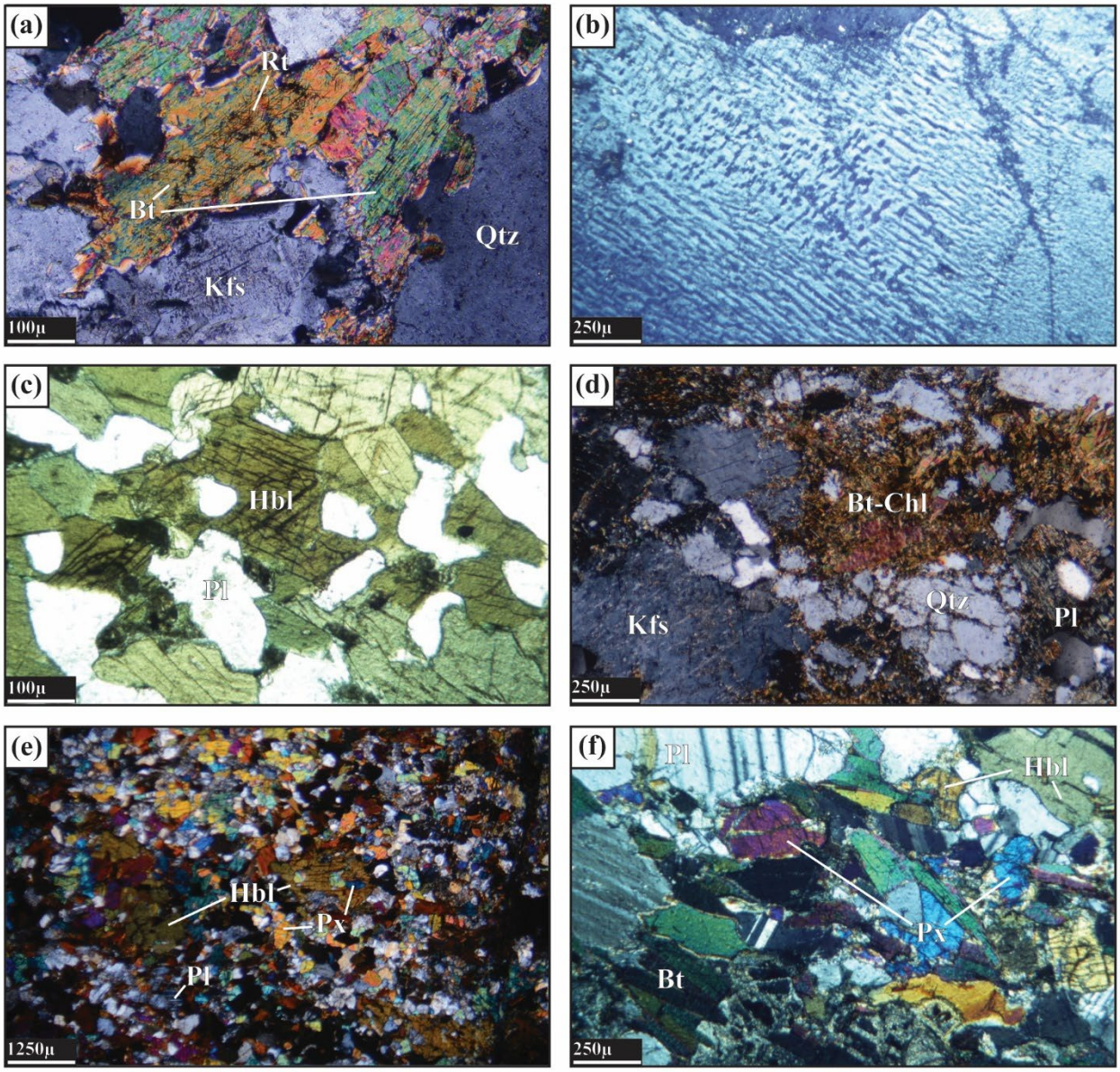

Figure 9. Representative photomicrographs of thin sections, Leland Lakes study area, northeastern Alberta: (a) Slave granite, exhibiting K-feldspar (Kfs), quartz (Qtz), and biotite (Bt) with cross-hatched needles of rutile (Rt; sample LL-23-2021-2; cross-polarized light [XPL]); (b) Arch Lake granitoid with K-feldspar (orthoclase) displaying perthitic unmixing (sample LL-23-1021-1; XPL); (c) interlocking texture of hornblende (Hbl) and plagioclase (Pl) from an amphibolite sheet; cleavage is well displayed in the hornblende (sample LL-23-1048-1; plane-polarized light [PPL]); (d) retrogressed basement gneiss (sample LL-23-2045-2; XPL); (e) gabbroic enclave within basement gneiss, exhibiting a mosaic of hornblende, pyroxene (Px), and plagioclase feldspar (sample LL-23-1002-1; XPL); (f) partially retrogressed spotted migmatite containing plagioclase and relict pyroxene overprinted by biotite and hornblende (sample LL-23-1058-1; XPL). Abbreviation: Chl, chlorite.

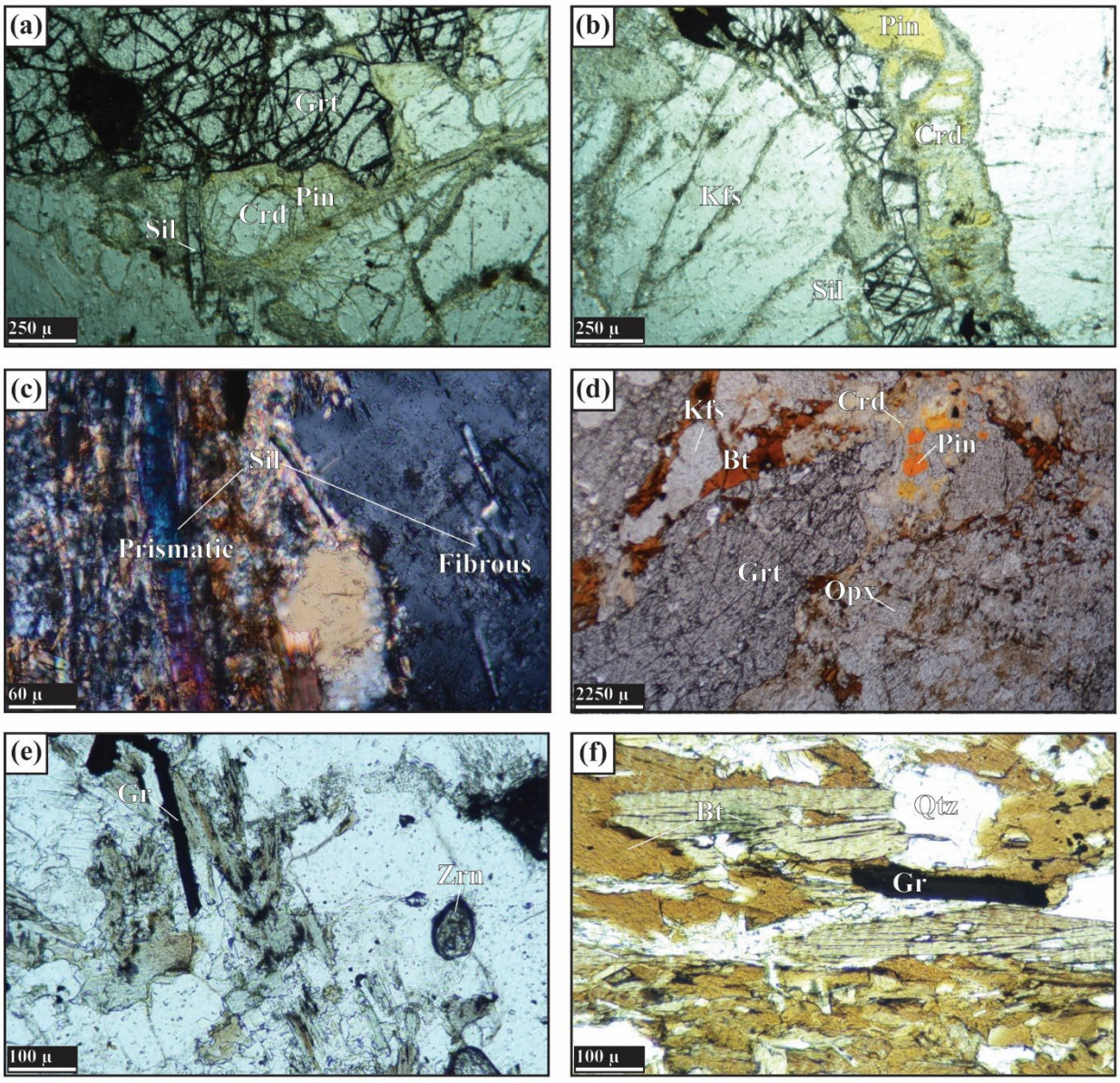

Figure 10. Representative photomicrographs of thin sections of the Rutledge River complex paragneiss, northeastern Alberta: (a) garnet (Grt)-cordierite (Crd)-sillimanite (Sil) gneiss from the Leland Lakes study area, high-relief sillimanite crystal (centre) within cordierite (sample LL-23-1071-1; plane-polarized light [PPL]); (b) high-relief sillimanite crystals in cross-section, surrounded by cordierite, from the Leland Lakes study area, cordierite displays yellow pinite (Pin) alteration (sample LL-23-1071-1; PPL); (c) paragneiss, exhibiting prismatic and fibrous sillimanite in a stable metamorphic assemblage from the Andrew Lake study area, the prismatic sillimanite crystals are elongated and well formed, whereas the fibrous sillimanite exhibits a fine, hairlike texture (sample AL-23-2172-2; cross-polarized light [XPL]); (d) biotite (Bt)-garnet-sillimanite-cordierite psammopelite from the Andrew Lake study area, cordierite displays yellow pinite alteration (sample AL-23-2078-2; PPL); (e) opaque platy graphite (Gr; top left) and rounded high-relief detrital zircon (Zrn; lower right) from a garnet-biotite-muscovite quartz metasedimentary rock in the Andrew Lake study area (sample AL-23-1168-2a; PPL); (f) opaque flake of graphite in a biotite-quartz (Qtz) matrix from a metasedimentary rock in the Andrew Lake study area (sample AL-23-1193-1a; PPL). Abbreviations: Kfs, K-feldspar; Opx, orthopyroxene.

4.1.1.2 Paleoproterozoic/Archean Basement

Mafic Rocks and Amphibolite: Mafic rocks in the Leland Lakes study area were mapped in the field and categorized lithologically as amphibolite (AMP), amphibolite enclave (AMPE), metagabbro (GB), and mafic schist (MSCH). The majority of mafic rocks were found as discontinuous layers, bands, and xenoliths within the basement OGN unit (Figure 8d). The basement mafic rocks typically have a mineralogical composition dominated by hornblende and plagioclase with relict locally abundant orthopyroxene (Figure 9c and e). Retrogression and hydration of these rocks locally replaced original pyroxene and amphibole with biotite, chlorite, and epidote. Field relationships and petrography did not identify more than one episode of mafic magmatism; mafic dikes and sills were not found in the younger Taltson plutons. The lithogeochemistry of these mafic rocks is discussed in Section 6.5.

Biotite-Hornblende Heterogeneous Gneiss (OGN): The biotite-hornblende heterogeneous gneiss unit is primarily composed of 60–90% pink quartzofeldspathic gneiss of generally granitic composition (Figure 8d). The gneiss is dominated by recrystallized quartz, plagioclase, and K-feldspar with 10–20% biotite and 0–25% hornblende (Figure 9d). Phenocrysts are generally absent and chloritic retrogression of biotite and hornblende is locally abundant. A distinctive aspect of this unit is the abundance of biotite-rich, intermediate to mafic bands, layers, and enclaves. The bands rarely exceed 2 m in thickness and commonly contain compositional layering. The compositional layering, combined with the intermediate to mafic banding and layering, is consistent with a possible supracrustal origin for parts of this unit. Younger layer-parallel intrusive leucogranite is present in most outcrops. A U-Pb age of 3.2 Ga from "Annealed mylonitic biotite-hornblende granite gneiss" is reported from the south end of Leland Lakes (McNicoll et al., 2000). This unit may be transitional to the higher grade spotted migmatite (SM) unit that is found at the western edge of the LLSZ.

Migmatite and Spotted Migmatite (SM): Spotted migmatite is a distinctive high-grade metamorphic rock exposed along the western edge of the LLSZ. This unit comprises a banded migmatite that is compositionally similar to the OGN unit but contains abundant porphyroblasts of magnetite and garnet as well as knots of partially, to fully, retrogressed hypersthene (up to 25% of the rock; Figure 8e) that give the unit a spotted appearance. Chlorite, hornblende, and biotite retrogression is locally abundant (Figure 9f). The unit locally contains coarse to pegmatitic in situ granitic leucosomes. On aeromagnetic maps, a distinct magnetic high that contrasts sharply with the low magnetic character of the SG unit to the west defines this unit. The OGN and SM units together likely represent a slice of the Archean TBC. This exposure of basement gneiss was termed the Leland Lakes block by McNicoll et al. (2000) and they reported a single U-Pb zircon age of 3186 +17/-13 Ma from the south end of Leland Lakes.

Mixed Mylonite (M): Mixed mylonite to ultramylonite is found sporadically along the LLSZ. It is a ribboned recrystallized quartzofeldspathic rock that typically contains mafic and intermediate layers, bands, and boudins, which constitute up to 20% of outcrops (Figure 8f). The unit is interpreted to be a combination of highly deformed OGN and SM units with structural slices of other units mixed within. The rock contains abundant porphyroclasts of K-feldspar and plagioclase within a quartz-rich matrix. Quartz is highly deformed and typically displays undulose extinction. Accessory minerals include hematite, pyrite, and fine-grained white mica. Late chlorite alteration is locally abundant. Heterogeneous slices and bands of highly deformed biotite- and muscovite-rich paragneiss (part of the PG unit) are common in this unit, consistent with the structural position of the PG unit along the LLSZ. These PG unit slices have abundant garnet that is typically mantled by biotite, which has been pinched to form tails and σ-type mantled porphyroclasts. The matrix of these slices is primarily muscovite and quartz. The presence of muscovite, as well as the replacement of garnet with muscovite, biotite, and chlorite, suggests that this unit underwent a late greenschist-facies, potentially metasomatic, overprint.

4.1.2 Andrew Lake Study Area

Mapping in the Andrew Lake study area was focused along a transect across the southern end of Andrew Lake and along a watercourse that extends west from the southwestern corner of Andrew Lake for

approximately 7.5 km (referred to as the E-W arm; Figures 6 and 11). This transect was chosen to examine rare-earth-element (REE) anomalies identified in the well-exposed TBC. The TBC is defined on geophysical maps as a relative aeromagnetic high in juxtaposition with the TMZ granitoids to the east along the ALSZ, a major structural boundary that runs north to south through the centre of Andrew Lake. This structure was initially interpreted by McDonough et al. (2000b) as an easterly vergent thrust, displacing the 3.2–2.3 Ga gneisses of the TBC and supracrustal gneisses of the RRC in its hanging wall over Andrew Lake granodiorite in its footwall.

4.1.2.1 Paleoproterozoic

Andrew Lake Granodiorite (AL): The Andrew Lake granodiorite is typically grey to pink, coarse grained and leucocratic (Figure 12a and b) with local variations of granitic and dioritic compositions (McDonough et al., 1994d). The unit contains large K-feldspar phenocrysts in a matrix of biotite, hornblende, quartz, and plagioclase feldspar. Trace minerals include zircon, monazite, and apatite (Figure 13a). An augen texture is locally developed where the granitoid has undergone a higher degree of strain. Xenoliths were rare in the study area. The U-Pb crystallization ages of 1959 ±3 Ma (McDonough et al., 2000e) and 1962 +16/-10 Ma (McDonough and McNicoll, 1997) have been reported from this unit.

Colin Lake White Granite (CL): the Colin Lake white granite of the Colin Lake suite in the study area is a weakly foliated to massive, leucocratic, muscovite±biotite granite (Figures 12c and 13b). To the east, it intrudes the main megacrystic phase of the Colin Lake pluton (1971 ±4 Ma; McDonough and McNicoll, 1997), forming subkilometre-scale tabular bodies widespread in the vicinity of Andrew Lake. A sample collected from the Andrew Lake shear zone was used to estimate a U-Pb crystallization age of ca. 1923–1921 Ma, with monazite growth continuing during cooling to 1913 Ma (McDonough et al., 2000e). This unit is consistently an aeromagnetic low relative to surrounding lithologies. Partial melting features are well developed within the CL unit where it has interacted with the RRC. Garnet-bearing leucosomes within the RRC exhibit both in situ and in-source morphologies (Figure 12d), with injected phases representing later, cross-cutting generations (Figure 12c). In situ leucosomes are directly associated with melanosome and occur as discontinuous veinlets, whereas in-source leucosomes, generally less common, are concentrated in structurally controlled domains, accumulating in metatexitelike layers. At the southwestern end of Andrew Lake, well-exposed outcrops show the CL unit cross-cutting metasedimentary rocks (Figure 12c). The injected leucosomes form irregular granitic veins cutting across the RRC and adjacent orthogneissic units, with cuspate to lobate contacts and truncation of earlier foliations, indicating late-stage mobilization during the waning phases of anatexis. The absence of garnet in these injections may reflect a source melt composition or crystallization conditions distinct from earlier garnet-bearing phases.

Pegmatite (PEG): granitoid (or granitic) pegmatite dikes, sills, and zones are relatively abundant within the TBC. These pegmatites are both cross-cutting and layer-parallel to the dominant gneissic fabric (Figure 14d) and are locally folded. The majority of pegmatites are suspected to be synchronous with the high-grade metamorphism evident in the basement. They are typically white to tan in colour, leucocratic, and range from syenite to monzogranite in composition (Figure 13c). Garnet, biotite, and sillimanite is locally abundant. Pegmatites are locally sheared with the basement, displaying elongation, dismembered, and porphyroclastic textures. Alteration intensity is variable, characterized by the presence of chlorite, epidote, and feldspars replaced with fine-grained white mica. Red hematite staining is common in the TBC and often overprints this unit, imparting a reddish colour.

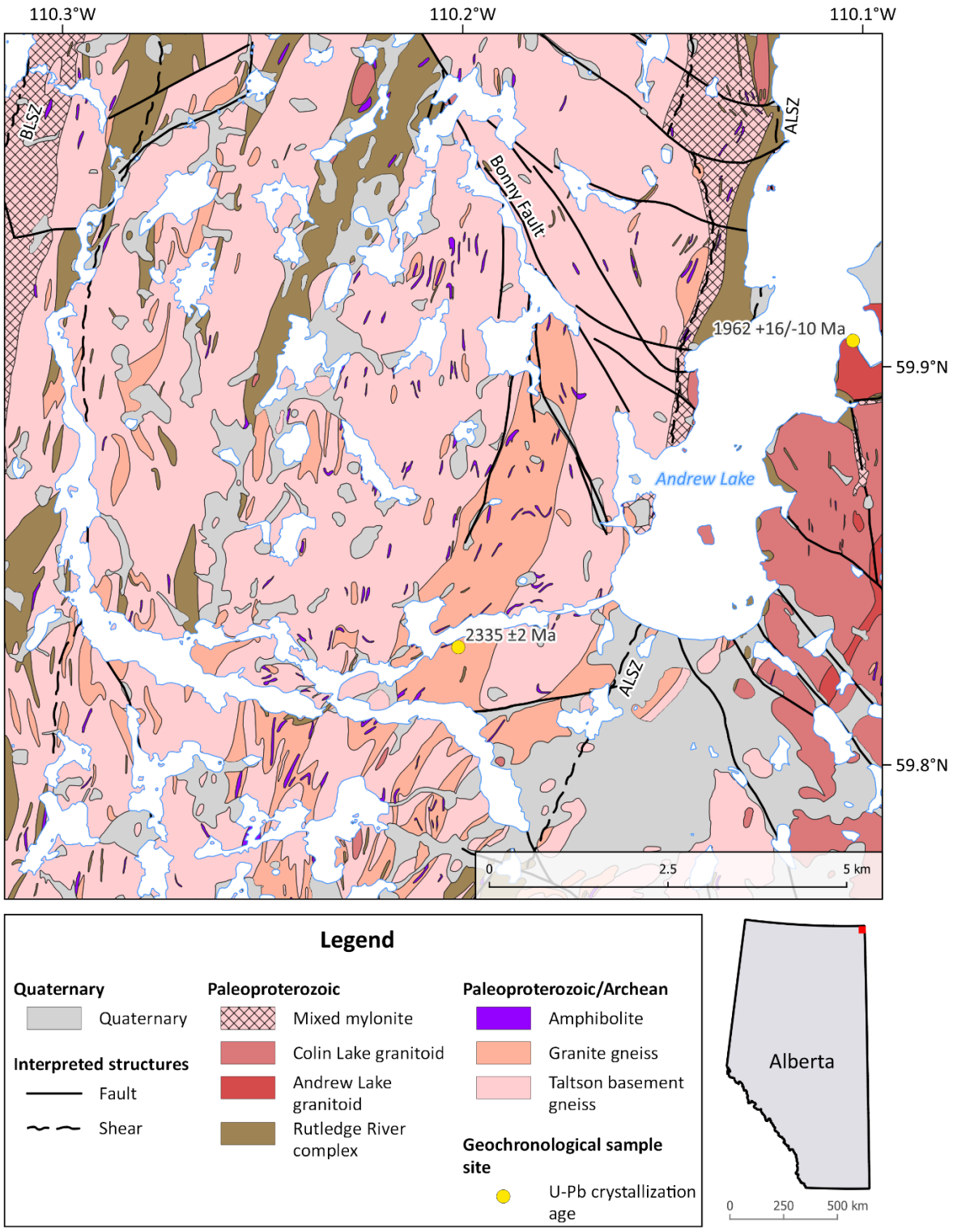

Figure 11. Bedrock geology (adapted from Godfrey, 1961, 1963, 1966) of the central part of the Andrew Lake study area in northeastern Alberta updated with bedrock interpretations from 2023 fieldwork. The U-Pb geochronology data was sourced from McNicoll et al. (2000) and McDonough et al. (2000e) and the Andrew Lake shear zone interpretation was sourced from Lopez et al. (2024). Abbreviations: ALSZ, Andrew Lake shear zone; BLSZ, Bayonet Lake shear zone.

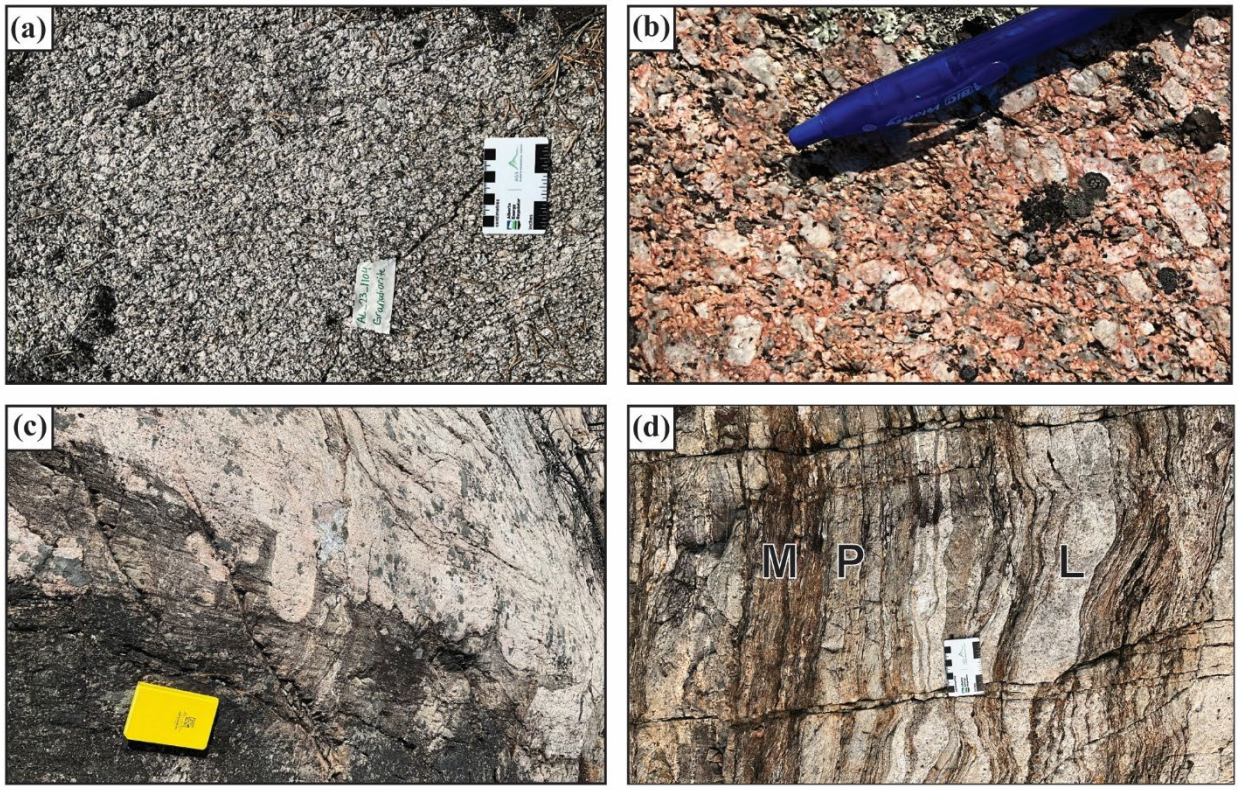

Figure 12. Representative outcrop photographs, Andrew Lake study area, northeastern Alberta: (a) grey coarse-grained Andrew Lake granodiorite (station AL-23-1104); (b) pink coarse-grained Andrew Lake granodiorite with feldspar megacrysts (station AL-23-1195); (c) intrusive, cuspate to lobate contact of Colin Lake white granite truncating Rutledge River complex (RRC) metasedimentary rocks (station AL-23-1158); (d) a component of the Colin Lake white granite forms in situ leucosome (L) interlayered with melanosome (M) and remnant metasedimentary paleosome (P) of the RRC (station AL-23-2174).

Metasedimentary Rocks and Paragneiss (PG): Metasedimentary rocks in the Andrew Lake study area have been ascribed by Bostock and van Breeman (1994) to the RRC with a suggested depositional age of 2.15–2.09 Ga. However, the recent study by Thiessen et al. (2024) suggests a younger depositional age of 2.03–1.94 Ga. This unit is composed of high-grade, deformed, quartz-rich metasedimentary rocks, including schist, gneiss, and migmatite. The rocks are typically grey and display weathering to a rusty brown with moderate to strong compositional layering (Figures 12d and 14a). Metasedimentary rocks in the Andrew Lake study area have more diverse compositions than in the Leland Lakes study area. Biotite and muscovite locally exceed 50% in some units, consistent with a typical metapelite composition. Quartzitic and psammopelitic to psammitic compositions are also common. Detrital zircon, graphite, and garnet are ubiquitous in this unit (Figure 10e and f). Fibrous and prismatic sillimanite, cordierite, orthopyroxene, microcline, and pyrite are all locally present, indicating a history of high-grade, granulite-facies metamorphism (Figure 10c and d). Amphibolite- to greenschist-facies retrogression and metasomatism is locally recorded by the presence of biotite, muscovite, 10–20% chlorite, ±epidote, and significant sericitization.

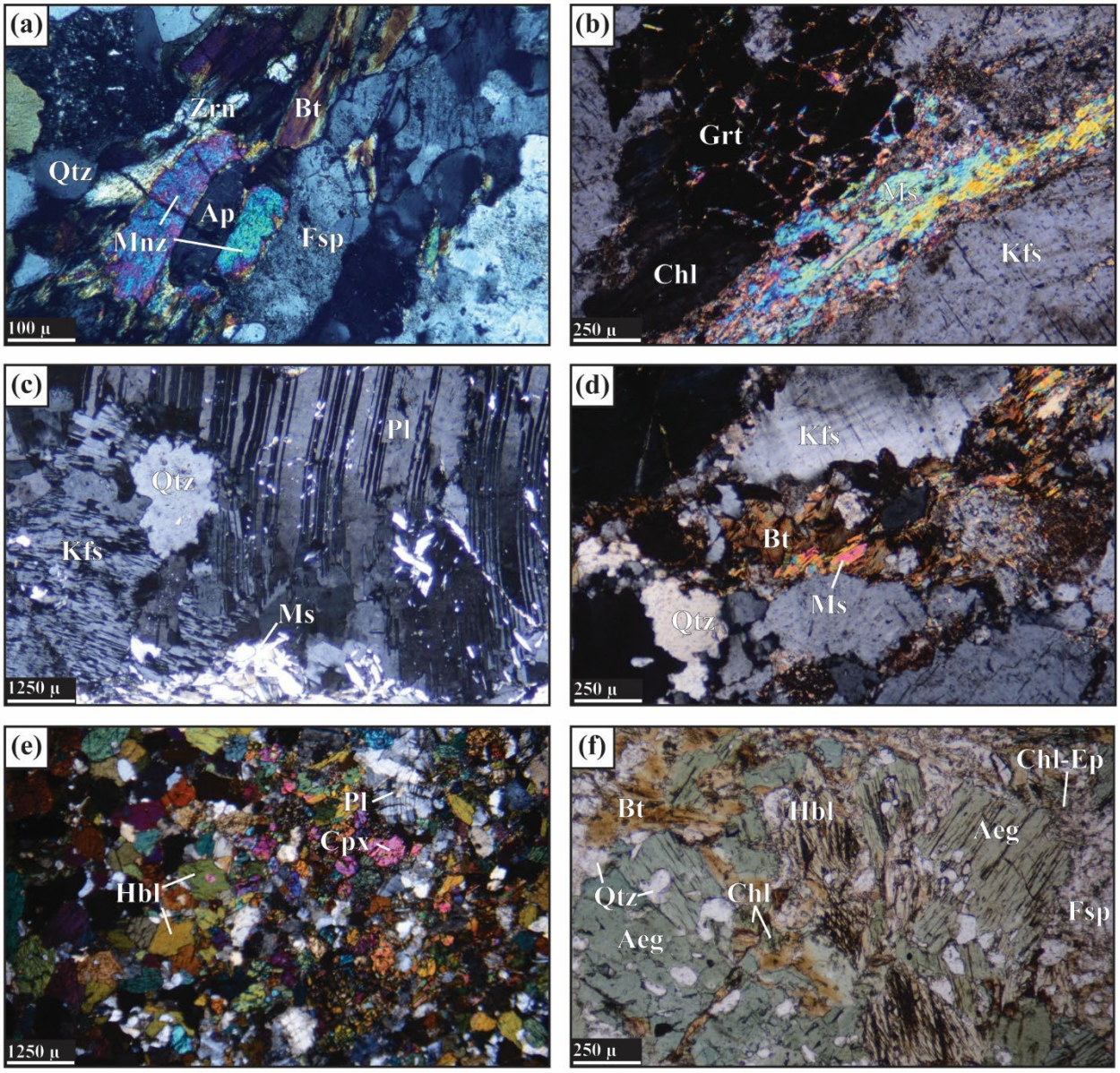

Figure 13. Representative photomicrographs of thin sections, Andrew Lake study area, northeastern Alberta: (a) Andrew Lake granodiorite, showing apatite (Ap) surrounded by monazite (Mnz; centre) with zircon (Zrn) also present (sample AL-23-1104-1; cross-polarized light [XPL]); (b) Colin Lake white granite, exhibiting garnet (Grt) replaced with chlorite (Chl), adjacent muscovite (Ms) and K-feldspar (Kfs; sample AL-23-2068-1; XPL); (c) layer-parallel, anatectic pegmatite showing plagioclase feldspar (Pl) with well-preserved growth twinning, orthoclase, quartz (Qtz), and muscovite (sample AL-23-2095-2; XPL); (d) derived granite gneiss (GG unit), exhibiting muscovite and chlorite after biotite (Bt), amidst recrystallized quartz and K-feldspar, tartan twinning characteristic of microcline is faint but present (top; sample AL-23-2128-1; XPL); (e) heterogranular mosaic of clinopyroxene (Cpx), two generations of hornblende (Hbl), recrystallized plagioclase, and minor biotite (sample AL-23-2119-2; XPL); (f) interlocking texture exhibited by hornblende and aegirine (Aeg) within Taltson basement gneiss (BG), quartz, feldspar (Fsp), biotite, chlorite, and epidote (Ep) locally present (sample AL-23-2152-1; plane-polarized light [PPL]).

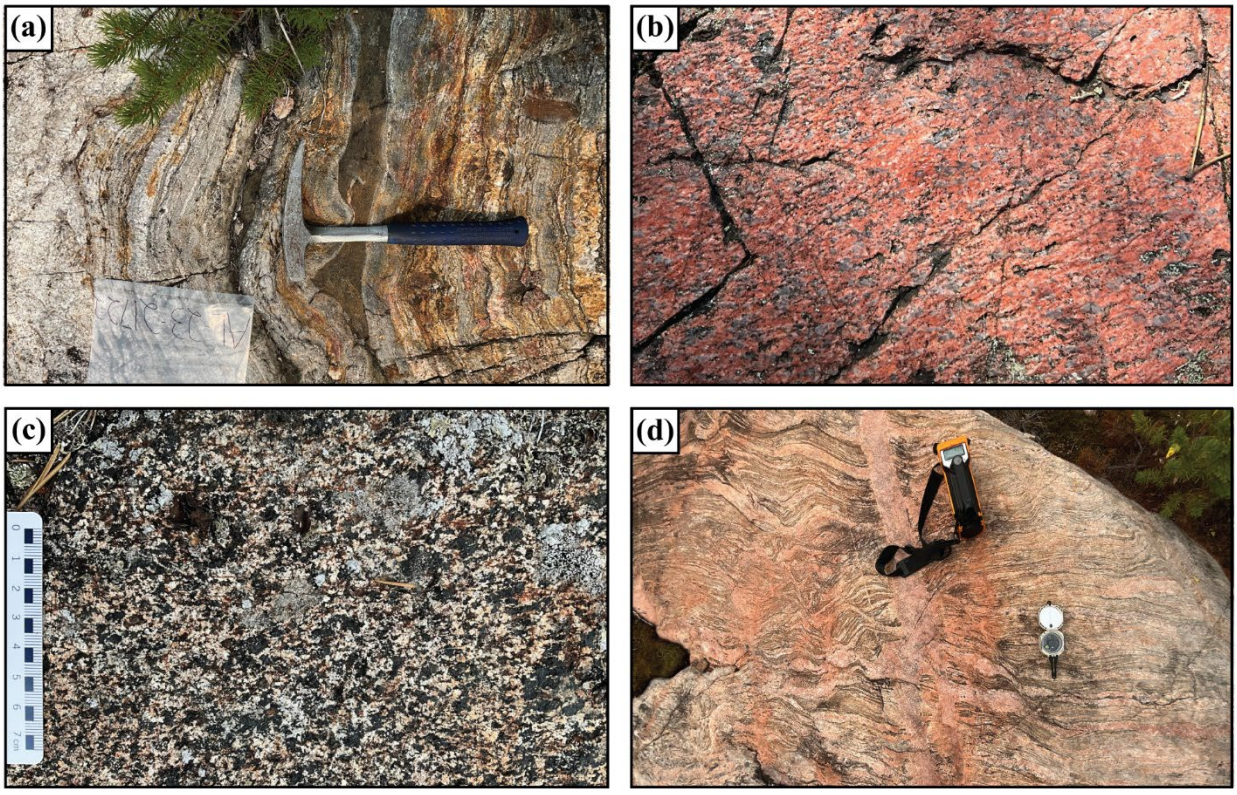

Figure 14. Representative outcrop photographs, Andrew Lake study area, northeastern Alberta: (a) quartz-rich metasedimentary rocks of the Rutledge River complex (station AL-23-2172); (b) pink, coarse-grained and strongly foliated granite displaying highly flattened grey quartz, this outcrop is close to the location of the 2335 ±2 Ma granite reported by McNicoll et al. (2000; station AL-23-1170); (c) interlocking texture of coarse-grained hornblende and plagioclase from a >500 m long amphibolite body south of Andrew Lake (station AL-23-1185); (d) pegmatitic dike cross-cutting Taltson basement gneiss southwest of Spider Lake (station AL-23-2181-1).

4.1.2.2 Paleoproterozoic/Archean Basement

Granite Gneiss (GG): Abundant, pink-weathered granite and granite gneiss occur with the shear zone–bounded block of Archean to Paleoproterozoic rocks west of the ALSZ. This unit was injected into older amphibolite and grey gneissic rocks (Taltson basement gneiss unit), which are locally present as rafts and dismembered layers in the GG unit (Figure 14b). The GG unit is composed of 10–30% quartz and variable amounts of orthoclase, microcline, and plagioclase. Feldspar typically shows alteration to fine sericite and muscovite. Biotite±hornblende, variably altered to chlorite, make up 5–20% of the unit (Figure 13d). Trace and accessory minerals include zircon, rutile, epidote, apatite, allanite, titanite, monazite, and garnet. Monazite, allanite, and zircon were observed as zoned inclusions in feldspars and as remobilized aggregates formed by metasomatic processes. Minor titanite is often disseminated throughout the matrix and intergrown with biotite. Red hematite staining is common. Locally abundant magnetite may be inherited from the basement gneisses that the GG unit intrudes. The GG unit ranges from moderately foliated, to gneissic, to locally mylonitic; undulose extinction, grain rotation, and recrystallization are typical in highly strained parts of the unit. Mylonitic zones of the GG unit may have >50% recrystalized quartz, likely related to the formation of quartz veining during deformation. Commonly, the GG unit exhibits injections of the Colin Lake white granite. A 2335 ±2 Ma U-Pb

crystallization age was reported from an area southwest of Andrew Lake that was mapped as this unit (McNicoll et al., 2000).

Amphibolite (AMP) and Metagabbro (GB): A variety of small amphibolite (AMP) bodies occur throughout the TBC in the Andrew Lake study area. These thin (<2 m typically) amphibolite bodies are parallel to the primary structure in the gneisses and are folded on a regional scale. These amphibolites lack compositional layering and likely represent dismembered dikes and sills, which formed in the basement rocks prior to high-grade metamorphism (Figure 14c). Some amphibolite bodies, however, may represent an older mafic volcanic protolith that was injected by younger igneous intrusives. Several larger (>10 m across), homogeneous, medium- to coarse-grained amphibolite bodies that lack compositional layering are referred to here as metagabbro (GB). Amphibolite and metagabbro are composed of hornblende and plagioclase with relict clinopyroxene locally present (Figure 13e). Trace minerals may include apatite, zircon, and opaque minerals, which include pyrite and magnetite. Chlorite retrogression of amphibole is common, especially in shear zones where amphibolites are commonly reduced to phyllonites. Published U-Pb crystallization ages for amphibolites are extremely rare in the region, but a large gabbroic body along the western margin of the Rae craton yielded an age of 2.330 ±0.007 Ga (van Breeman and Bostock, 1994). This age is consistent with widespread ca. 2.3 Ga magmatism of the Arrowsmith orogeny, interpreted to be postcollisional in nature (Hartlaub et al., 2007).

Taltson Basement Gneiss (BG): Taltson basement gneiss is a grey quartzofeldspathic orthogneiss that grades locally into migmatite. This unit is typically of granitic to granodioritic composition. Gneissic layering was locally replaced and overprinted by in situ partial melting, indicating a minimum metamorphic grade of upper amphibolite (Figure 14d). The gneiss is dominated by quartz, plagioclase, and K-feldspar, with 5–10% hornblende±biotite and 1–5% relict orthopyroxene (Figure 13f). Epidote and chlorite alteration and replacement of mafic minerals is typical. Zircon is generally abundant as an accessory mineral. Magnetite is abundant and ubiquitous, giving the BG a consistent aeromagnetic high relative to other units. Amphibolite layers and boudins are locally present, as are intermediate bands with a wispy relict foliation of biotite. The basement gneiss contains rare zones of dark grey diorite gneiss composed of biotite and plagioclase with minor amounts zircon, allanite, and opaque minerals dominated by magnetite. The BG unit is commonly intermixed with, and injected by, younger granite gneiss (GG unit), leucogranite, and pegmatite. The basement pegmatites tend to have much higher U and REE contents than their host gneisses. Taltson basement gneiss is deformed due to tectonic activity associated with the major ALSZ and BLSZ. The mylonitic basement gneiss is dominated by ribboned quartz and feldspar mylonite porphyroclasts and significant greenschist-facies metasomatic overprints.

5 Structure and Metamorphism

Bedrock in the study area was subjected to variable levels of deformation, shearing, alteration, high-grade metamorphism, and localized partial melting. Primary structures in supracrustal rocks were generally overprinted and original sedimentary layering (S_0) largely obliterated.

Major north- to north-northeast-trending shear zones in Alberta's portion of the Canadian Shield are primarily high-grade structures that were subsequently overprinted under low-grade metamorphic conditions. From west to east, these shear zones include the LLSZ, CLSZ, BLSZ, and ALSZ (Godfrey, 1986; McDonough et al., 2000b). Cross-cutting relationships between shear zones and granitoid bodies indicate concurrent deformation and granitoid intrusion during the ca. 2.0–1.9 Ga Taltson orogeny (e.g., McDonough et al., 2000b; Pană, 2010a). As a result of regional aeromagnetic analysis (Lopez et al., 2024), a multitude of previously unrecognized major and minor shear and fault zones were identified within Alberta's Precambrian shield (Figure 15).

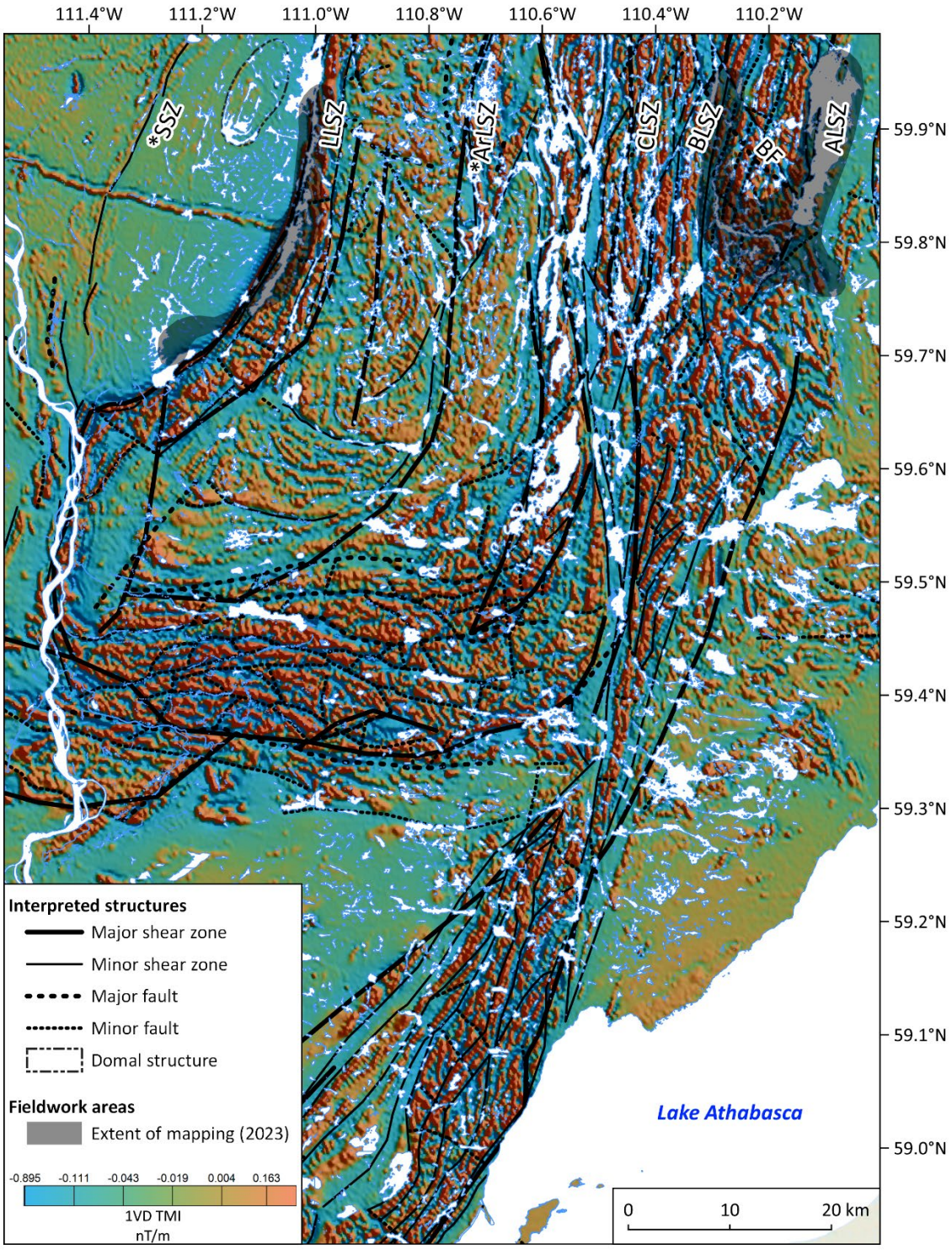

Figure 15. Regional aeromagnetic first vertical derivative (1VD) map of the Precambrian shield in northeastern Alberta, with structural interpretations after Lopez et al. (2024). Isoluminant colour range developed by Centre for Exploration Targeting (Kovesi, 2015). Asterisk denotes previously unidentified shear zones. Abbreviations: ALSZ, Andrew Lake shear zone; *ArLSZ, Arch Lake shear zone; BF, Bonny Fault; BLSZ, Bayonet Lake shear zone; CLSZ, Charles Lake shear zone; LLSZ, Leland Lakes shear zone; nT, nanoTesla; *SSZ, Slave shear zone; TMI, total magnetic intensity.

5.1 Regional Deformation

In the Leland Lakes and Andrew Lake study areas, deformation event D_1 is attributed to isoclinal folding (F_1) of a cryptic, moderately to steeply dipping foliation ($S_{1\text{-}x}$), variably defined by a preferred orientation of quartz, feldspar±hornblende, and development of a composite, north- to north-northeast-trending $S_{1\text{-}x}$-S_1 gneissosity prevalent within the TBC and the RRC (Figure 16). This fabric is lithology dependent and characterized by alternating bands of flattened and elongated quartz and feldspar, which are parallel to similarly deformed domains of hornblende and biotite±actinolite after pyroxene (Figures 17a, b and 18a, b). This early gneissic fabric established an initial structural anisotropy in TBC granitoids that subsequent deformation phases commonly exploited. Field and petrographic relationships indicate that this early folding (F_1) occurred under high-grade metamorphic conditions (M_1). Even though direct geochronological constraints for M_1 may be limited, the presence of coarse-grained feldspar, hornblende, and local relict pyroxene in alignment with this early fabric suggests temperatures were sufficiently high (upper-amphibolite to granulite facies) to allow for plastic deformation of these minerals.

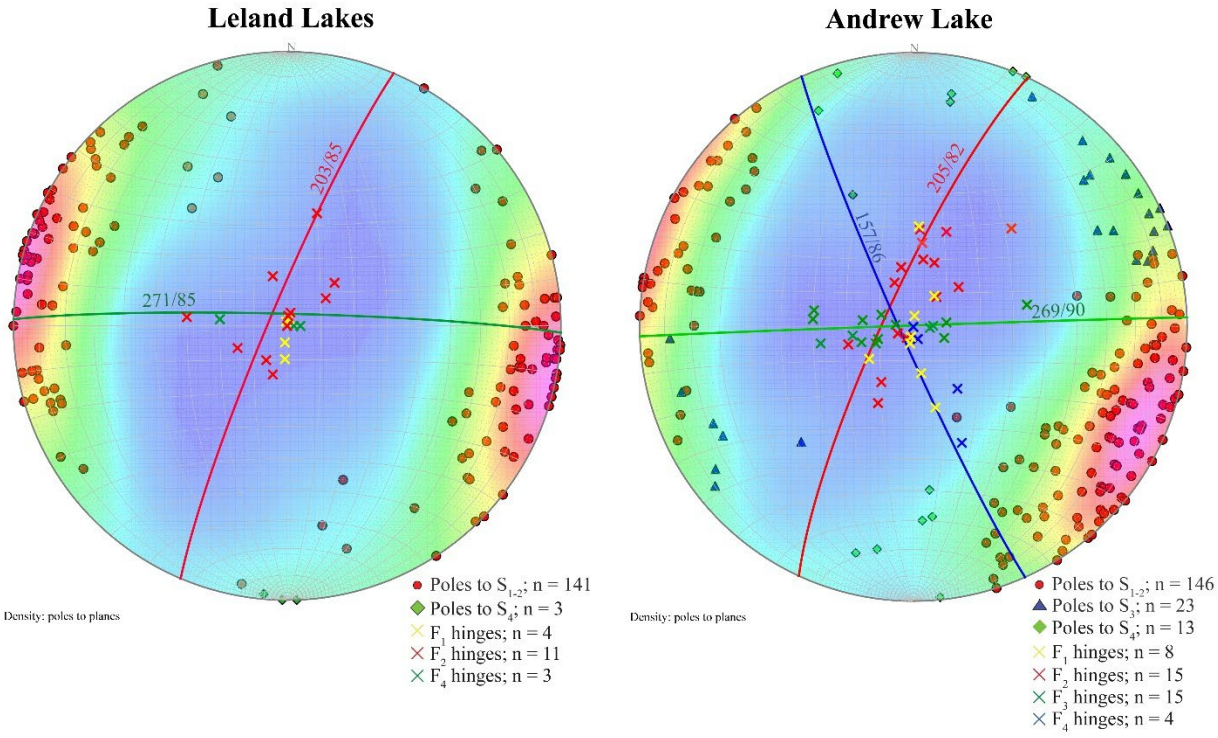

Figure 16. Stereoplots showing average trends of $S_{1\text{-}2}$ (red line), S_3 (blue line), S_4 (green line) foliations, and their related poles to planes, along with F_1 through F_4 fold hinges in the Leland Lakes and Andrew Lake study areas, northeastern Alberta. Point density and colour contours reflect the concentration of combined poles to planes in each respective study area.

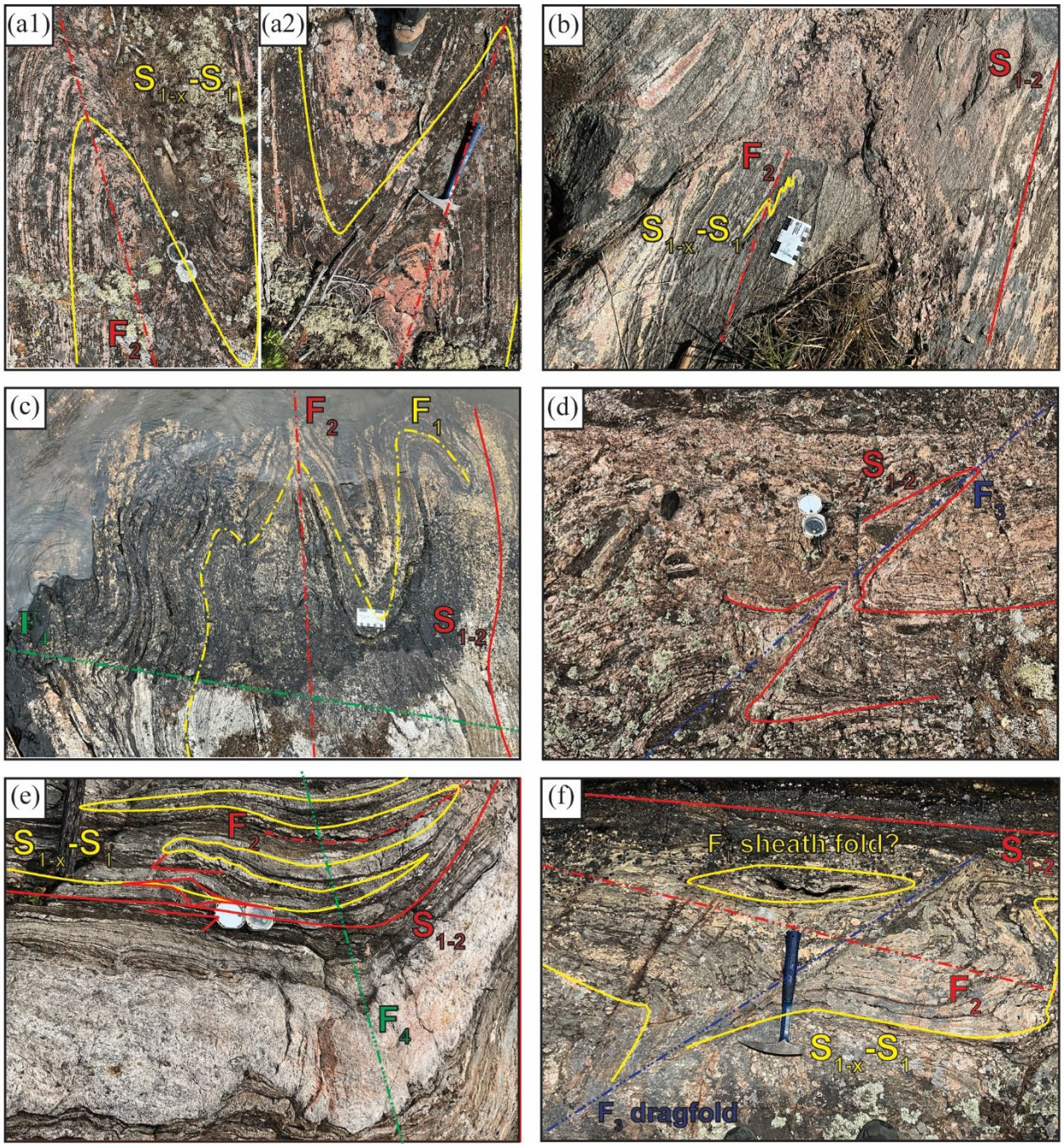

Figure 17. Representative outcrop photographs of structural features, Andrew Lake study area, northeastern Alberta: (a) tight F_2 dragfolds (opposing limbs shown in (a1) station AL-23-2149 and (a2) station AL-23-2119) refolded all early fabrics; (b) high-strain D_2 zone, where early structures were transposed by F_2 folding, leading to the development of composite S_{1-2} gneissosity (station AL-23-1135); (c) type 3 'hook'-style fold interference patterns affecting orthogneiss of the Taltson basement complex within low-strain D_2 zones (station AL-23-2087); (d) close to tight F_3 dragfolds reoriented the S_{1-2} fabric in a right-lateral sense (station AL-23-2104); (e) open, steeply west-plunging F_4 crossfolds reoriented the sheared, composite S_{1-2} foliation fabric (station AL-23-2174); (f) potential F_1 sheath fold, entrained in dominant S_{1-2} fabric, which was reoriented by F_3 dragfolds (station AL-23-2111).

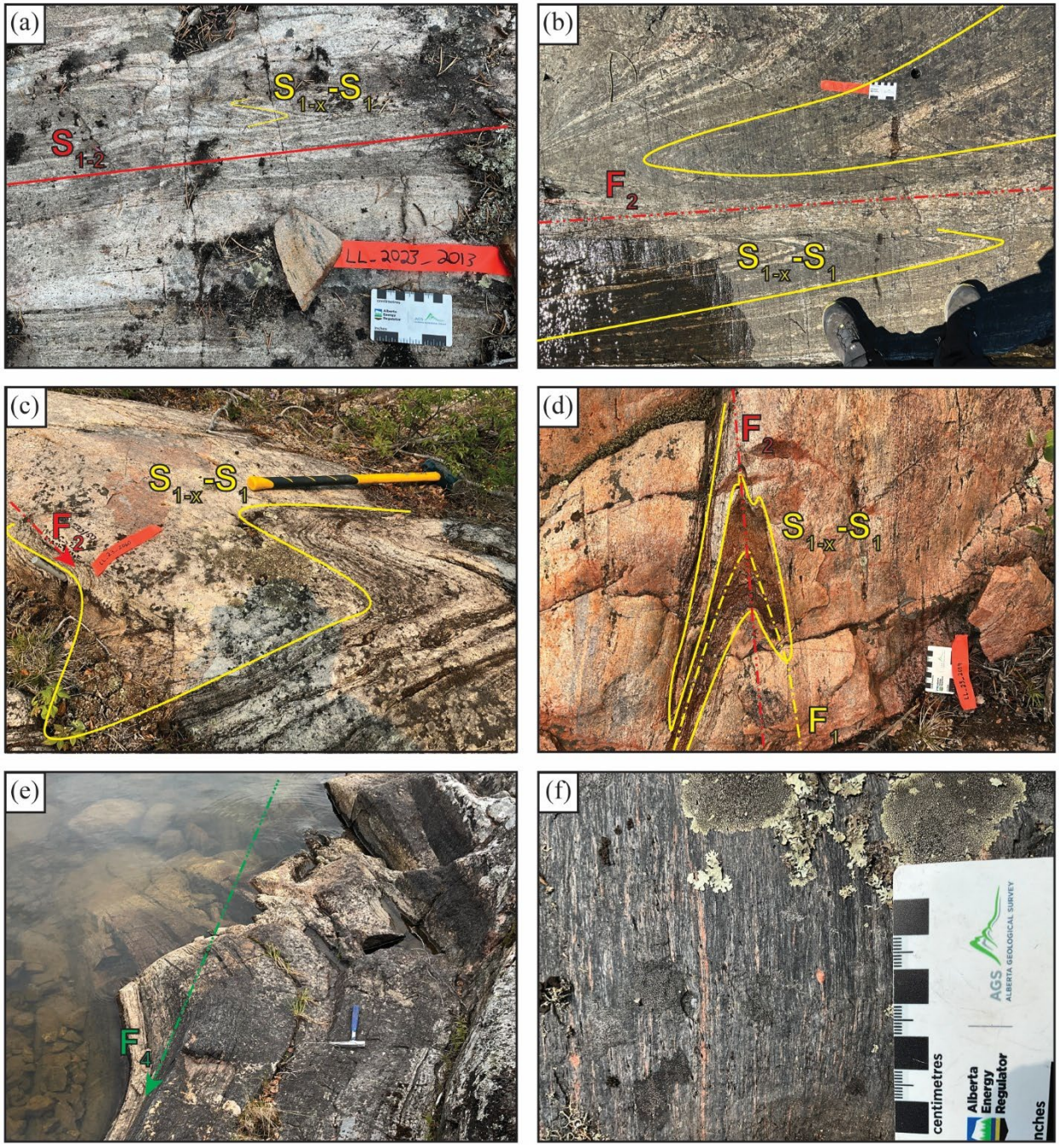

Figure 18. Representative outcrop photographs of structural features, Leland Lakes study area, northeastern Alberta: (a) highly strained orthogneiss, exhibiting tight folds of the $S_{1\text{-}x}$-S_1 fabric and development of the composite $S_{1\text{-}2}$ gneissosity (station LL-23-2013); (b) shearing along sinistral limb of F_2 dragfold, which affected the biotite-hornblende heterogeneous gneiss unit (station LL-23-2016); (c) low-strain D_2 zone exhibiting moderately northeast-plunging, southwest-striking F_2 folding (station LL-23-2060); (d) type 3 fold interference via interaction of F_2 on F_1 folds (station LL-23-2059); (e) open, upright F_4 fold affecting the Leland Lakes shear zone (station LL-23-1044); (f) vertical, dip-lineated ultramylonite exhibiting rotated dextral σ-type K-feldspar porphyroclasts, the ultramylonite divides the paragneiss of the Rutledge River complex from an ~260 m wide zone of spotted migmatite (station LL-23-2035).

As a result of subsequent deformation (D_2), earlier structures were systematically reoriented subparallel to the axial planes of regional, upright to steeply inclined, tight to isoclinal folds (F_2), with hinge lines moderately to steeply plunging to both the north-northeast and the south-southwest (Figures 17a and 18b). This resulted in the development of a heterogeneous, anastomosing, composite $S_{1\text{-}2}$ gneissosity with average orientations of 203°/85° and 205°/82° at the Leland Lakes and Andrew Lake study areas, respectively (Figures 16, 17b, and 18a). This composite foliation runs parallel to unit contacts and exhibits repeated layering, ranging from millimetre to decimetre scales, which encompasses various granitoid types and mafic to ultramafic units and lenses (Figures 17e and 18c) and establishes the dominant structural grain. Early isoclinal (F_1) folds and rare, localized sheath folds were observed transposed into parallelism with the $S_{1\text{-}2}$ composite fabric (Figure 17f), originally defined primarily by the preferential alignment of quartz, feldspar, and pyroxene.

The interaction between F_2 and F_1 folds resulted in localized type 3 fold interference patterns, via coaxial refolding, observed in both study areas (Figures 17c and 18c, d; Ramsay and Huber, 1987). Alternating F_2 Z-fold and S-fold asymmetries were observed and were particularly pronounced in high-strain mylonite zones where tightening interlimb angles, boudinage, and dragfolding were common (Figures 17a and 18b). These relationships suggest strain was first taken up by tighter F_2 folds, and subsequently by shearing along steeply, northwest- and southeast-dipping mylonite zones, tens to hundreds of metres thick, along planes of anisotropy associated with polyphase deformation. Pegmatites emplaced during this phase exploited planes of weakness along the $S_{1\text{-}2}$ fabric, indicating that partial melting and pegmatite intrusion were synchronous with, or slightly postdated, D_2 deformation (Figure 19a and b). Continual progressive deformation involved development of high-strain, upper-amphibolite- to granulite-facies shears along zones of anisotropy and emplacement of late Taltson plutons such as the Slave, Arch Lake, and Colin Lake granitoids, which bear the S_2 foliation and, based on field relationships, were emplaced during development of regional F_2 folds.

Moreover, paragneisses of the RRC contain a peak assemblage of garnet-sillimanite-microcline-orthopyroxene, with local cordierite, variably aligned to the $S_{1\text{-}2}$ foliation fabric. This mineral assemblage indicates peak metamorphic conditions (M_2, which overprinted or enhanced any earlier M_1 signatures) reached temperatures of 700°C–900°C and pressures of 5–7 Kbar before progressing through amphibolite- to greenschist-facies conditions on a retrogressive pressure-temperature-time (P-T-t) path, particularly in mylonite or shear zones. Here, pyroxene was replaced by hornblende during peak metamorphism, while hydration and cooling facilitated the crystallization of muscovite, biotite, and epidote along the foliation. Continued retrogression resulted in the formation of chlorite and actinolite, as well as partial replacement of garnet by biotite, chlorite, and epidote in localized zones. Local retention of pyroxene and garnet in $S_{1\text{-}2}$ suggests that deformation and metamorphism remained at, or returned to, upper-amphibolite- to granulite-facies conditions during the D_2–M_2 event. Geochronological evidence (e.g., Stern et al., 2003) constrains this peak event at ca. 1.94–1.93 Ga, coinciding with postulated peak tectonism and related magmatism of the TMZ (Card et al., 2014). Throughout the TBC, ca. 1.930–1.917 Ga U-Pb cooling ages were recorded in monazite, titanite, and zircon from orthogneisses (McNicoll et al., 2000).

Although M_2 represents the high-grade peak metamorphic conditions, evidence from some mylonite or shear zones indicates a localized greenschist-facies retrogression that could mark a late D_2 phase of deformation and metamorphism. In these corridors, higher grade minerals (e.g., hornblende, garnet) are partially replaced by chlorite, epidote, or muscovite, hinting at cooling or fluid infiltration during the waning stages of D_2. This retrograde signature may blend continuously into the lower grade metamorphic event(s) documented during D_3–F_3 and D_4–F_4, described below.

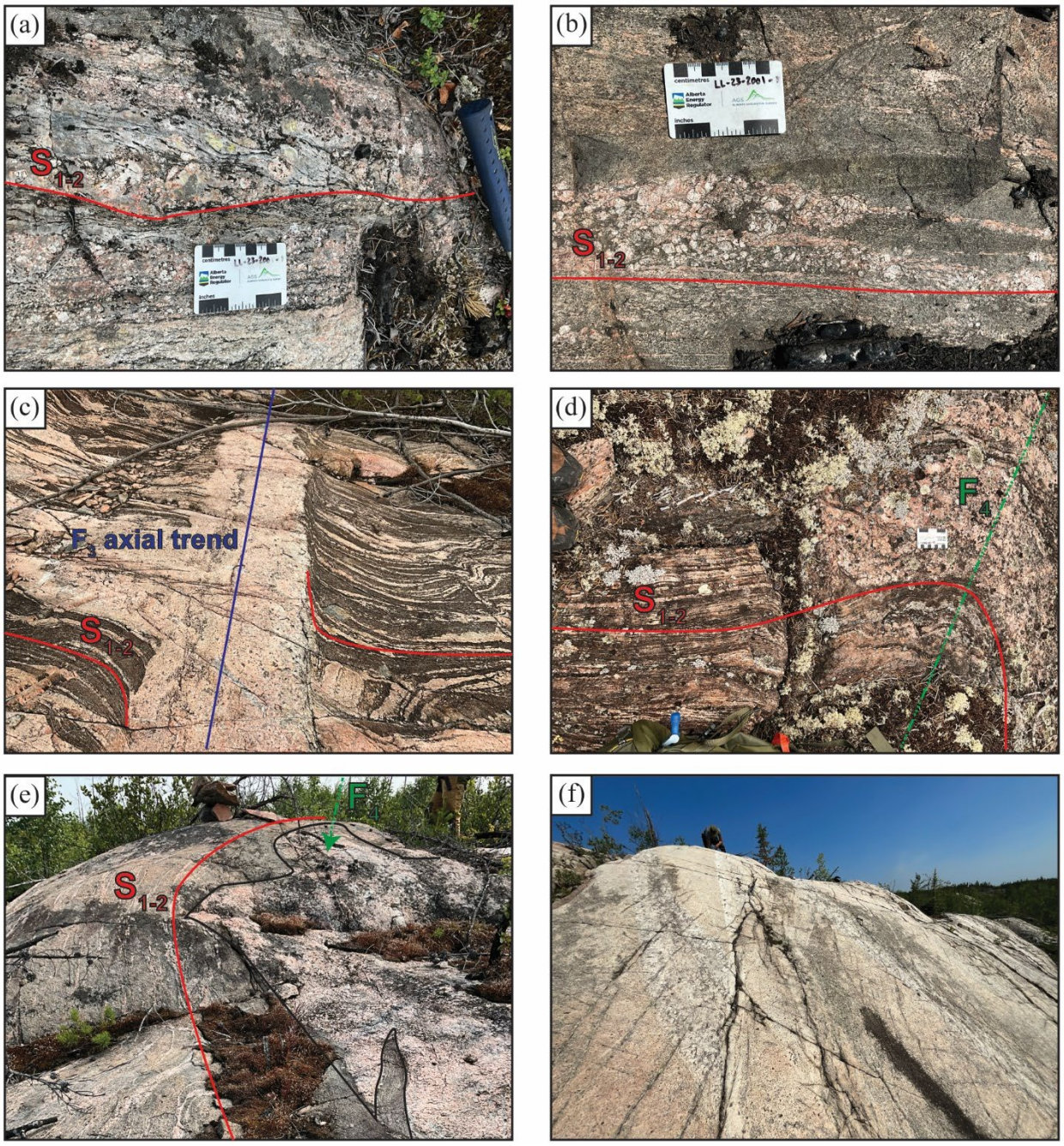

Figure 19. Representative outcrop photographs of structurally controlled pegmatites, northeastern Alberta: (a) sheared, radioactive pegmatite pods aligned parallel to the S_{1-2} composite fabric at Spider Lake, Andrew Lake study area (station AL-23-2175); (b) partially melted biotite-pegmatite selvage within the Bayonet Lake shear zone, Andrew Lake study area (station AL-23-2142); (c) pegmatite entrained along S_{1-2} composite fabric, and intruded along a northwesterly F_3 axial trend, Andrew Lake study area (station AL-23-1197); (d) pod of granitic cumulate refolded by F_4 folds, Andrew Lake study area (station AL-23-2153); (e) zone of granitic pegmatite emplaced into hinge of major F_4 fold, Andrew Lake study area (station AL-23-2167); (f) north-northwest-striking, steeply dipping, in situ pegmatites, which injected into the Slave granitoid near McLelland Lake, Leland Lakes study area (station LL-23-2054).

Subsequent ductile deformation is prominent proximal to the northwest-southeast-trending structural corridor that transects much of the Andrew Lake study area, notably running parallel to the Bonny Fault (Figure 15). Here, the composite south-southwest-striking $S_{1\text{-}2}$ fabric was reoriented by northwest–southeast-striking, upright, close to tight, steeply southeast-plunging F_3 folds with a mean attitude of 157°/86° (Figure 16). Related discrete, metasomatic, greenschist- to amphibolite-facies shear zones (Figure 17d and f) provided new pathways for later stage magmatic intrusions and pegmatite emplacement (Figure 19c), and which are notably absent from the Leland Lakes study area. In such zones, an early generation of xenomorphic garnet and biotite were replaced with a second generation of biotite, along with muscovite and chlorite, which together define a well-foliated schistosity. These F_3 folds were observed locally exhibiting right-lateral slip along their axial planes and dextral fold asymmetry.

Thereafter, the composite $S_{1\text{-}2}$ foliation underwent further deformation by east-west-striking, subvertical, doubly plunging, open to close F_4 crossfolds (Figures 17e and 18e), which were observed at both study areas. An associated F_4 axial planar cleavage was locally developed and is associated with further greenschist-facies and metamorphic overprinting. Pegmatitic intrusions were observed emplaced into the hinges of major F_4 folds, in addition to exhibiting cross-cutting phases that are oriented parallel to the F_4 axial planes (Figure 19d and e). Alternating westerly and easterly plunging F_4 fold hinges, perpendicular to the strike of the $S_{1\text{-}2}$ gneissosity, were commonly observed, confirming F_4 as noncylindrical folding. The timing relationship between D_3 and D_4 remains ambiguous, as the interaction between F_3 and F_4 folds, and their associated cleavages, was not observed. Based on interlimb angles, it is inferred that the close to tight F_3 folds preceded the open to close F_4 crossfolds.

Collectively, the greenschist-facies overprint observed along shear zones, axial planes, and late fractures is referred to as M_3. This metamorphism may be coeval with F_3 and F_4 folding (and may in part represent the tail end of D_2 retrograde processes). Diagnostic M_3 minerals (chlorite, epidote, muscovite, secondary biotite) replace or overprint higher grade assemblages from the M_2 peak. In both study areas, greenschist-facies shear zones overprint earlier granulite-facies shear zones, highlighting the role of reactivated anisotropies from D_2 in focusing fluid flow and deformation during later metamorphic events. Although limited geochronological data hamper precise assignment of M_3 to discrete time intervals, it is conceivable that M_3 reflects multiple pulses of low- to medium-grade metamorphism associated with final exhumation and postcollisional adjustments of the Taltson Orogen. Some of this greenschist-facies overprint could have begun late in D_2 as localized retrogression, then intensified or recurred during D_3 and D_4. Future targeted isotopic dating and microstructural studies will be essential for disentangling the timing and extent of these metamorphic pulses.

5.1.1 Leland Lakes Shear Zone

The LLSZ contains granulite-grade, strike- and dip-lineated mylonite composed of heterogeneous TBC gneisses that span the length of Leland Lakes. The TBC gneisses in this area have been interpreted as an allochthonous slice of Rae crust and termed the Leland Lakes block (McNicoll et al., 2000). The RRC supracrustal gneisses are structurally intermixed with the older basement in the LLSZ. Original linear fabrics in the LLSZ mylonites are sparse due to pervasive younger deformation, recrystallization (McDonough et al., 2000e), and greenschist-grade retrogression. However, a moderately developed, gently south-plunging, mineral-stretching lineation is locally prominent close to the LLSZ.

The LLSZ is well defined on aeromagnetic maps as a continuous highly magnetic feature along a narrow zone of high gradient between the Slave granitoid and Arch Lake granitoid (Figure 15). The geometry of the shear zone and its asymmetry indicates the shear zone dips to the west for depths of up to 5 km; similarly, a detailed three-dimensional (3D) voxel model across the northern shield confirms the dip of the Arch Lake granitoid to the west (Lopez et al., 2024), which contradicts the proposed geometries of McDonough et al. (2000e).

The dominant S_{1-2} gneissosity rotates counterclockwise and clockwise in the northern and southern areas of the Leland Lakes study area, respectively, reflecting the geometry of the LLSZ. The gneissosity variably developed into a series of mylonites, which record both sinistral and dextral kinematic indicators. To the west of the LLSZ, the mylonitic fabric develops into a thin interval of ultramylonite (Figure 18f), which separates the paragneiss from an ~260 m wide zone of spotted migmatite. This unit is in contact with another interval of mylonitized paragneiss on its western margin, which extends for up to 500 m westwards and marks the western extent of the LLSZ. The latter was variably intruded by dikes and sills of the Slave granitoid. The Slave granitoid pluton truncated and obliterated much of the LLSZ, leaving only the easternmost 50–500 m of the shear zone intact. The LLSZ is moderately to strongly foliated and comprises lower amphibolite- to greenschist-grade mylonites, which form both dip-lineated and sinistral-strike–lineated tectonites derived from high-grade mylonites and Slave granitoid (McDonough et al., 2000e). To the west of this dominant high-grade shear zone, garnets disappear within the Slave granitoid over approximately 200 m. In this area, retrogressed greenschist-facies assemblages define the main S_2 foliation, which dips moderately to steeply southeast.

To the west of the LLSZ, a large elliptical aeromagnetic low was identified within the Slave granitoid; it displays a well-defined elliptical rim of higher aeromagnetic intensity (Figure 15). Lopez et al. (2024) posited that this elliptical feature represents an internal domain of the Slave granitoid based on differing magnetic textures. As the Slave granitoid was affected initially by north-northeast–south-southwest-trending F_2 folds and subsequently reoriented by near perpendicular, east-west-trending, steeply plunging F_4 folds, it is possible this feature may represent a domal structure formed via fold interference processes, however, it may be strictly intrusion related.

To the east of the Leland Lakes study area, strain was concentrated into a series of shear zones that variably affected the Arch Lake granitoid and increasingly encompassed aspects of pure shear. Southwest of Leland Lakes, in the McLelland Lake area, the Slave granitoid is weakly foliated and injected by south-southeast-striking, in situ pegmatite dikes (Figure 19f), which are cut by fine-grained, aplitic dikes of similar origin.

5.1.2 Andrew Lake Shear Zone

McDonough et al. (2000e) describe the ALSZ as a 200–800 m wide zone that gently to moderately dips westward. They interpret the ALSZ as a thrust that displaced TBC and RRC gneisses onto the Andrew Lake granodiorite. However, structural data collected in 2023 did not confirm these findings. Despite comprehensive field mapping (Figure 20a–c) and automated structural detection as reported in Lopez et al. (2024), detailed kinematic information remains scarce. Approximately 3 km west of Andrew Lake, a moderately northwest-dipping, greenschist-facies, dip-lineated shear zone approximately 150 m in width records dextral, west-side up movement. However, this is a reactivated structure and does not demonstrate continuity with the zone of high-strain mylonite observed across Andrew Lake (Figure 15).

The ALSZ was defined by Lopez et al. (2024) as a continuous linear feature, enriched in magnetite, that marks the boundary between the TBC and the RRC to the west and the Andrew Lake granodiorite to the east. Near the southern shore of Andrew Lake, the ALSZ splays to the southwest and south-southwest. Approximately 7 km southwest of Andrew Lake, the southwestern splay transects Spider Lake. Here, migmatitic mylonitized paragneiss of the RRC is in sheared contact with the basement GG unit on the lake's western and eastern margins, where the paragneiss develops into diatexite. Garnet-bearing, quartzofeldspathic, predominantly in situ (lesser in-source) leucosome of the Colin Lake white granite is enshrouded in biotite- garnet- and sillimanite-bearing melanosome and folded with the remnant paleosome by northeast-striking F_2 folds. Subsequently, all components of the migmatite were mylonitized parallel to F_2 axial planes, prior to deformation by east-west-striking, open, upright F_4 folds (Figure 17e). Within the basement orthogneisses to the west of the interpreted contact with the migmatitic paragneiss, F_4 interlimb angles are close to tight, suggesting this western basement block was at a lower crustal level during local D_4.

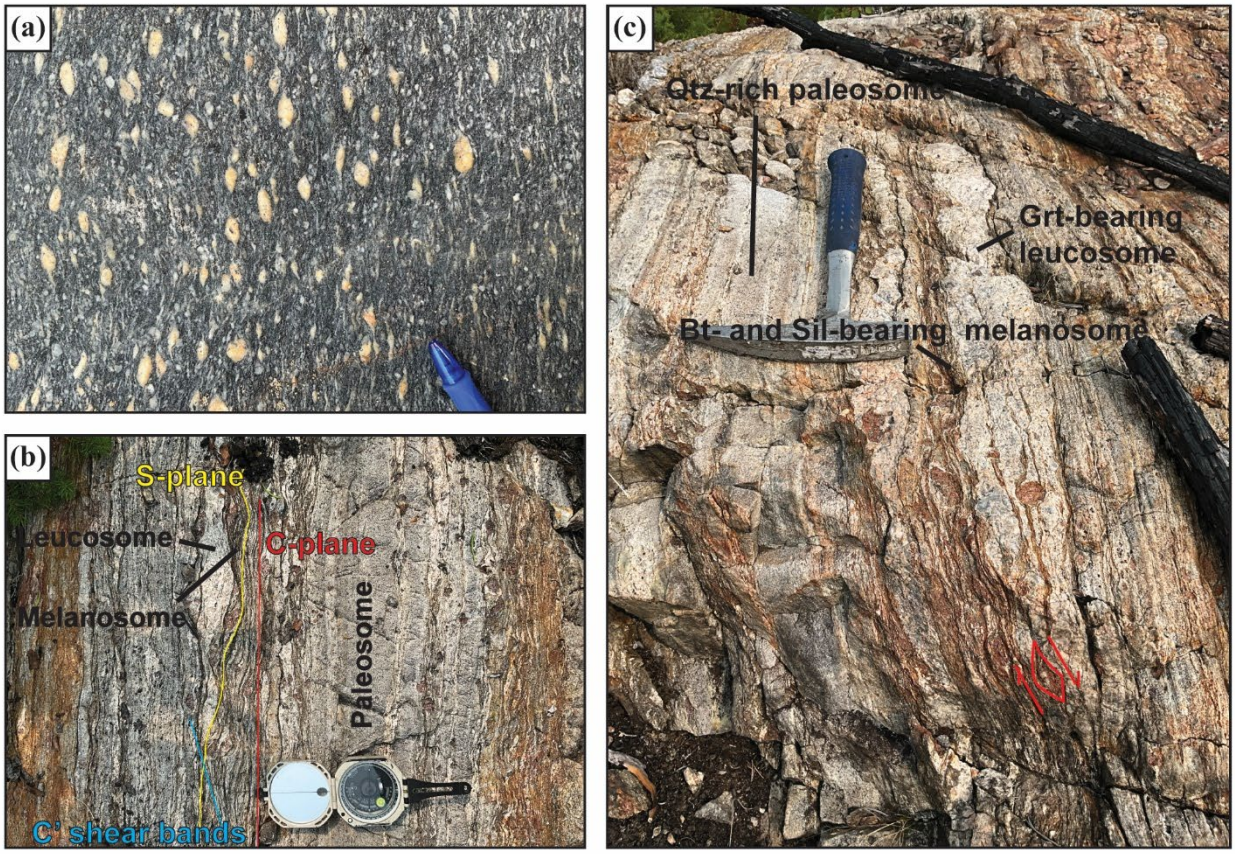

Figure 20. Representative outcrop photographs of structural features of the Andrew Lake shear zone, northeastern Alberta: (a) grey feldspar-porphyroclastic mylonite from the Andrew Lake shear zone, the protolith of this mylonite is difficult to determine but is likely metasedimentary rock, based on mineralogy and structural setting (station AL-23-1202); (b) pervasive strike-lineated, sinistral shear affecting a migmatitic paragneiss in the Spider Lake area, evidenced by C-S-C' fabrics (station AL-23-2172); (c) migmatitic paragneiss of the Rutledge River complex, northeast of Spider Lake, exhibiting dip-lineated, dextral shear (red arrows) along the steeply dipping S_{1-2} composite fabric when viewed from the x, y plane, the leucosomal component represents garnetiferous (Grt) Colin Lake white granite, typically enveloped in melanosome that is rich in biotite (Bt) and sillimanite (Sil; station AL-23-2172). Abbreviation: Qtz, quartz.

The composite S_{1-2} mylonitic fabric is strongly developed within the paragneiss of the RRC and pervasive sinistral shear was preserved, evidenced by C-S-C' fabrics and pre- to syntectonic rotated σ-type garnet porphyroclasts (Figure 20b). This translates to left-lateral, strike-lineated movement, which, when coupled with right-lateral dip-lineated movement observed from the x, y plane, indicates a component of normal oblique slip (Figure 20c). However, 3D geophysical modelling by Lopez et al. (2024) suggests a sharp, east-dipping boundary for the ALSZ, projecting continuously at depth. Conversely, the magnetic vector inversion (MVI) model indicates a moderate dip and lacks subsurface continuity beneath a high magnetic anomaly, contradicting the expected easterly thrust orientation. Furthermore, magnetic signatures within the Swinnerton window—a proposed tectonic window located roughly 5 km northeast of the Bonny Fault—differ significantly from those observed in the Andrew Lake granodiorite. A tectonic window is an erosional or structural feature through which deeper or older basement rocks are exposed (the overlying or more recently formed units have been eroded or shifted), providing a glimpse into deeper crustal levels. This difference in magnetic signatures challenges previous interpretations that the

Andrew Lake granodiorite underlies the Taltson basement complex in this area (Figure 15). As a result, evidence of a major-scale tectonic boundary within the Andrew Lake study area remains enigmatic.

5.1.3 Bayonet Lake Shear Zone

The BLSZ (Figure 15) encompasses gneisses of the TBC and RRC and has been interpreted to represent a major splay of the CLSZ; it formed a 1–3 km wide braided system of high-grade, strike-lineated heteroclastic mylonites with both sinistral and dextral kinematic indicators (McDonough et al., 2000e). McDonough posited a westerly dip direction whereby the BLSZ merged with the CLSZ to form a positive flower structure along with the LLSZ and ALSZ. However, analysis of new aeromagnetic data indicates that the BLSZ extends approximately 18 km north from Pans Lake to the Bonny Fault where it is truncated (Figure 15). According to Lopez et al. (2024), a prominent, narrow, north- to northwest-trending, and east-dipping aeromagnetic feature coincides with the mapped BLSZ, with the caveat that it is a discontinuous feature that does not merge with the CLSZ to the southwest. The 3D MVI model shows a narrow low magnetic zone also dipping in an easterly direction, which extends at depth for up to 5 km, contradicting aspects of the proposed model for the Taltson orogenic assembly after McDonough et al. (2000e).

Within the BLSZ, field relationships suggest that strain was initially accommodated by F_2 folding, before being taken up by a complicated series of shearing and subsequent reactivation along F_2 axial planes (Figure 21a). From east to west, cataclasites of the TBC locally contain lenses of quartzofeldspathic metasedimentary rocks, which gradationally transition westwards through protomylonite into mylonite. Local partial melting was abundant, often forming diatexites of variable parentage. Where the BLSZ intersects with the Bonny Fault, and west of the E-W arm, mylonites transition into spotted diatexite, containing variable concentrations of Th-rich pegmatitic rock. A traverse of the BLSZ eastwards from the southeastern boundary of Bayonet Lake (Figure 6) revealed a complex history of mylonitization, whereby cataclastic to protomylonitic granite to monzogranite and lenses of the RRC metasedimentary rocks define a highly strained, west-northwest-dipping, dip-lineated fabric, which envelopes metre-scale lenses of prefoliated gabbroic bodies (Figure 21b). A pervasive dextral shear fabric seen in thin section AL-23-2145-1 (Appendix 1) translates to west-side down shearing along the dominant $S_{1\text{-}2}$ foliation (215°/70°), which is defined by quartz ribbons and cataclastic, flattened, highly sericitized feldspars. This fabric is accentuated by the preferred orientation of biotite, associated with greenschist-facies retrogression. This, coupled with common observations of Z-fold asymmetries, suggests shearing occurred in an oblique, dextral fashion. Further, a series of locally calcite-bearing quartz-microcline veins were entrained into the dominant fabric, and were coeval to a greenschist-facies, metasomatic event, which would have introduced significant fluids into the system. The locus of opaque, magnetic minerals is concentrated within layers of chlorite and epidote, suggesting greenschist-facies metasomatism associated with reactivation of the BLSZ may have been at least partly responsible for its prominent magnetic signature (Figure 15).

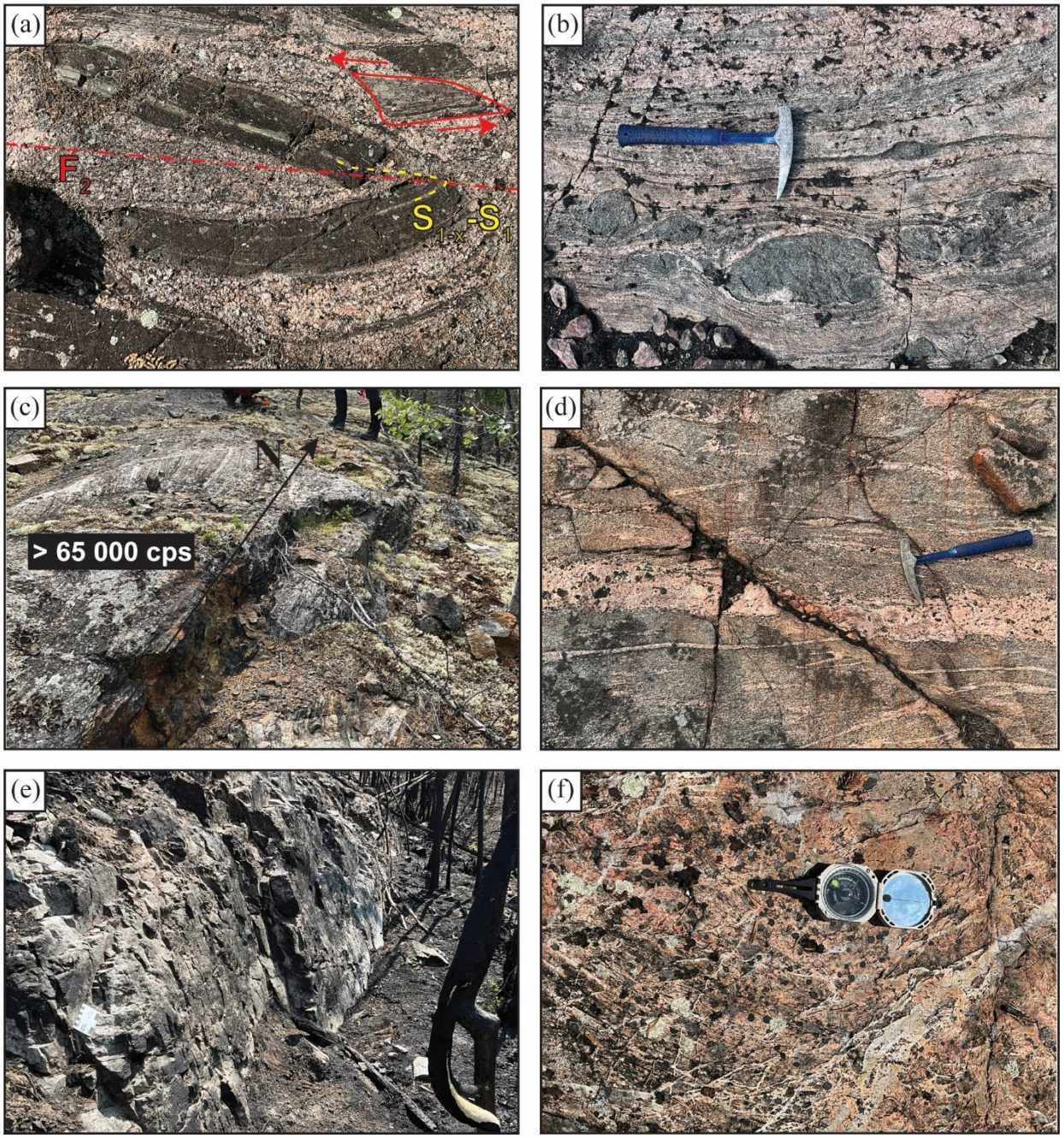

Figure 21. Representative outcrop photographs of the structural features of the Bayonet Lake shear zone (BLSZ), northeastern Alberta: (a) diatexites of the southern BLSZ, exhibiting evidence of folding (F_2-D_2) and subsequent sinistral shearing (red arrows) during the late D_2 (station AL-23-2080); (b) gabbroic clasts suspended in cataclastic to mylonitic $S_{1\text{-}2}$ fabric, central BLSZ (station AL-23-2141); (c) U-rich fault (>65 000 counts per second [cps] on a handheld gamma-ray spectrometer) oriented along a major $S_{1\text{-}2}$ trend (station AL-23-1152); (d) east-west-trending brittle fault with dextral offset (station AL-23-2164); (e) Bonny Fault scarp west of Sedgwick lake (unofficial geographic name, see Figure 6) exposed in a normal fashion, oriented 155°/70° (station AL-23-2093); (f) quartz-matrix crackle breccia on the northeastern side of the Bonny Fault (station AL-23-2094).

5.1.4 Brittle Structures

Brittle faults in the TMZ and TBC (outside the CLSZ) are separated into five groups based on their orientation. From oldest to youngest, the groups have strike orientations of (a) north-northeast, (b) north-northwest, (c) east-northeast, (d) west-northwest, and (e) east-west (Figure 15; Lopez et al., 2024). In the Leland Lakes and Andrew Lake study areas, there is significant parallelism between dominant faulting arrangements and the orientations of shear zones and fold structures (Figure 21c and d), suggesting that late-stage brittle deformation processes were influenced by similar imposed stress fields that shaped the earlier ductile structures.

In the Andrew Lake study area, the orientations of the observed brittle structures (faults, fractures) predominantly mirror the orientation of the north-northeast-trending and northwest-trending shear zones. One notable example of late-stage brittle deformation is a known uranium occurrence located south of the western extent of the E-W arm (Pană and Prior, 2010, location 1), where Taltson basement gneiss was observed sheared and faulted parallel to the dominant $S_{1\text{-}2}$ composite fabric (Figure 21c). A 20–30 cm wide zone of increased radioactivity is exposed for approximately 20 m, and exhibits partial retrogression, with chloritization and limonite alteration (Pană and Prior, 2010). Taken together, these observations suggest that reactivation of pre-existing structural trends and mechanical anisotropies facilitated hydrothermal activity and uranium mobilization along these weaknesses.

Northwest-trending orientations are especially pronounced west of Sedgwick lake, where the Bonny Fault is exposed at surface (Figure 21e). Automated structure detection has delineated a deep-seated, northwest-striking magnetic structure interpreted as a shear zone, which is truncated to the southeast along the western boundary of Andrew Lake, and is visible to depths of 1600 m (Lopez et al., 2024). This structure truncates biotite-bearing, migmatitic gneiss containing quartzitic lenses of the RRC and is interpreted to have offset a zone, associated with increased magnetite destruction, by several kilometres in a dextral fashion (Lopez et al., 2024). At the outcrop scale, this feature was observed as northwest-southeast-trending D_3 shears, defined by a preferred orientation of retrogressed, biotite-chlorite assemblages, which are parallel to flattened quartz and feldspars. This fabric was identified as far southeast as Cherry Lake, and contrasts with the orientation of the exposed fault scarp located west of Sedgwick lake (155°/70°), and a pervasive conjugate fault set that strikes 265°/85°, which acted as conduits for silica-rich hydrothermal fluids that generated quartz-matrix crackle breccia (Figure 21f). Such relationships suggest reactivation of pre-existing ductile structures, further complicated by late-stage brittle deformation. The Bonny Fault, in particular, appears to have resulted from a complex transition from ductile to brittle conditions, allowing for significant hydrothermal fluid input and metasomatic alteration. This reactivation facilitated the development of conjugate fault sets and quartz-matrix crackle breccia, indicating substantial tectonic and hydrothermal activity.

Lineaments trending in various orientations in the Leland Lakes and Andrew Lake study areas represent late-stage brittle-ductile and brittle fault zones, characterized by uncertain displacements. Many of these faults run parallel and may be linked to the reactivation of significant shear zones under greenschist-facies conditions during the overlapping Hudsonian and Wopmay orogenies (Ashton et al., 2009; Card et al., 2014).

5.1.5 Structural Controls on Pegmatite Emplacement

Pegmatites in the Andrew Lake study area manifest as zones, boudins, and pods (Figure 19a–f). This suggests a dynamic emplacement environment influenced by both the local stress field and the rheological properties of the host rocks. These pegmatites are intrinsically linked with the region's polyphase structural framework, established through a complex deformation history spanning from ductile to brittle conditions. Pegmatites are both cross-cutting and parallel to the dominant $S_{1\text{-}2}$ fabric, indicating multiple phases of pegmatitic melt generation and intrusion that correspond to varying tectonic and thermal conditions (Figure 19a–d). Pegmatites that parallel this fabric suggest pre- to synchroneity or late-stage crystallization relative to the formation of the foliation, as the development of the $S_{1\text{-}2}$ composite

gneissosity provided anisotropic media conducive to the migration and crystallization of pegmatitic melts. Importantly, some pegmatites are folded by F_2 structures, suggesting that their generation likely occurred between D_1 and D_2, with emplacement preceding or coinciding with the onset of F_2 folding. This relationship highlights a complex pegmatite emplacement history where melts were generated during the waning stages of D_1 deformation, persisted into D_2, and were later deformed by F_2 folding. Subsequent D_2 shearing, along with the development of D_3 and D_4 structures, would have introduced significant pathways and fold geometries for pegmatitic melts to exploit (Figure 19c and e). In the Leland Lakes study area, pegmatites are particularly concentrated within the Slave granitoid. Near McLelland Lake, the Slave granitoid experienced in situ injections of pegmatite melts, with the pegmatites striking north-northwest and dipping steeply (Figure 19f).

5.1.6 Tectonic Evolution of the TMZ: Insights from Polyphase Deformation

The structural evidence from the Leland Lakes and Andrew Lake study areas suggests a complex, polydeformational history that clarifies the evolving tectonic architecture of the southern TMZ. Field relationships demonstrate that D_1 deformation, characterized by early isoclinal F_1 folds and an associated, composite $S_{1\text{-}x}$-S_1 fabric, preceded the dominant north-northeast–south-southwest-plunging F_2 folds that they were folded about. The presence of D_1 deformation observed in paragneisses of the 2.13–2.09 Ga RRC indicates that early folding postdates ca. 2.13 Ga. Furthermore, the Andrew Lake granodiorite (ca. 1.959 ±0.003 Ga) does not show evidence of F_1 folding, constraining the upper limit for D_1 in this area to pre-1.959 Ga. The timing of D_1, therefore, corresponds to the inversion and closure of Paleoproterozoic sedimentary basins evidenced throughout the TMZ and western Rae craton—a precursor to the peak arc magmatism during D_2 (Cutts et al., 2024; Thiessen et al., 2024). The occurrence of basin closure–related deformation at this stage aligns with both the Andean-type subduction model (McDonough et al., 2000e) and the TTZ and TMZ separation model (Card et al., 2014; Whalen et al., 2018; Davis et al., 2021). The subduction model predicts sediment accretion along a retreating arc, whereas the TTZ and TMZ separation model suggests the evolution of distinct sedimentary basins within a rifted terrane prior to 2.0 Ga. The identification of juvenile and reworked older crust (Cutts et al., 2024) further supports the hypothesis that D_1 deformation occurred amid the progressive inversion of Paleoproterozoic basins prior to ca. 1.97 Ga, a process that facilitated later arc magmatism during the Taltson orogeny.

Similarly, Montenegro (work in progress, 2026) documents an early phase of isoclinal F_1 folding—particularly within the Martyn Lake formation turbidites of the Waugh Lake group and their northern counterparts in the Hill Island Lake assemblage—preceding emplacement of the main body of ca. 1.97 Ga Colin Lake granitoid. Recent geochronology (Thiessen et al., 2024; J.M.K. Deane, K.M. Bethune, K.E. Ashton, N.O. Montenegro, J.L. Crowley and K.P. Larson, work in progress, 2026) refines the maximum depositional ages of the Martyn Lake formation and Hill Island Lake assemblage to ca. 2.02 and 2.1 Ga, respectively, supporting the notion that these early folds (associated with D_1) preceded major arc-related magmatism. If the TMZ developed as part of a subduction-related system, as suggested by McDonough et al. (2000e), this early deformation stage could correspond to a continental back-arc or foreland basin closure rather than simple intraplate thickening (N.O. Montenegro, work in progress, 2026). Moreover, in the Waugh Lake group, F_1 structures were coaxially refolded by north-northeast–south-southwest-striking, steeply and doubly plunging F_2 folds, which developed under amphibolite- to greenschist-facies metamorphism (N.O. Montenegro, work in progress, 2026). The resulting type 3 fold interference patterns mirror those observed in the Leland Lakes and Andrew Lake study areas, supporting a regionally consistent tectonic regime throughout the southern TMZ during D_2. The presence of high-grade metamorphic mineral assemblages west of the ALSZ, whereas greenschist-facies assemblages persist to the east, corroborates a major boundary accommodating significant vertical displacement (N.O. Montenegro, work in progress, 2026).

The D_2 phase, therefore, is interpreted as the peak of orogenesis in the TMZ, coinciding with the emplacement of voluminous continental arc granitoids and the development of doubly plunging F_2 folds under high-grade conditions at ca. 1.94–1.93 Ga (Stern et al., 2003; Card et al., 2014). In the Waugh Lake group, the results of a U-Pb geochronological analysis of titanite aligned with the S_2 foliation directly date D_2 fabric development at ca. 1.93 Ga (N.O. Montenegro, work in progress, 2026). This deformation is closely tied to the interpretation of the TMZ as a continental arc system, as proposed by McDonough et al. (2000e) and Cutts et al. (2024). Evidence from isotopic and geochemical studies supports the derivation of early plutons (e.g., Colin Lake granitoid, Andrew Lake granodiorite) from partial melting of subducted oceanic crust (McDonough et al., 2000e). The progressive crustal thickening associated with D_2 deformation would have facilitated anatexis of accreted sedimentary rocks (e.g., Rutledge River basin rocks), generating S-type granitoids such as the Slave and Chipewyan suites (McDonough et al., 2000e). Continual subsequent deformation involved a transition from a compressional to transpressional structural regime, resulting in the development and reactivation of significant shear zones along the axial planes of major D_2 structures. The locus of strain would manifest as major, deep-seated vertical shear zones, which transect the southern TMZ (i.e., LLSZ, ALSZ, BLSZ, etc.). Subsequent titanite cooling ages (1.917–1.913 Ga) and hornblende Ar-Ar ages (1.904–1.899 Ga) confirm a prolonged retrogression into lower-amphibolite–facies conditions, whereas muscovite Ar-Ar ages (ca. 1.803 Ga) record a late greenschist-facies overprint (McDonough et al., 2000e), indicating that shear zone reactivation and associated deformation persisted well beyond the 1.93 Ga peak of metamorphism. The resulting M_3 metamorphism—expressed in both amphibolite- and greenschist-facies assemblages—is represented by a vague and complex overprint that encompasses late D_2, D_3, and D_4 events, including progressive retrogression of earlier high-grade fabrics.

Numerous lines of evidence indicate that crustal thickening and high-grade metamorphism in the Taltson Orogen peaked ca. 1.94–1.93 Ga, but debate remains as to whether this interval represents ongoing subduction under an Andean-type arc, a purely intraplate mechanism, or the final docking of major cratonic blocks. From a polymetamorphic perspective, the protracted D_2–D_3–D_4 evolution could correspond to a terminal collision, in which final suturing effectively ended the arc system, catalyzed deeper level transpression, and drove localized retrogression. If correct, this culminating event explains why high-grade metamorphism persisted through most of D_2 (while subduction continued) but yielded to lower grade reactivation along shear zones, folds, and faults once subduction effectively ceased. Although direct evidence for a discrete ‘final collision’ remains incomplete, the structural, metamorphic, and geochronological data presented here best fit a subduction-collision history rather than a purely intraplate scenario—highlighting how peak orogenesis and subsequent late-stage reworking fit into a broader series of convergent processes that ultimately shaped the southern Rae craton.

Furthermore, geophysical studies have delineated deep-seated structures that highlight the complexity of the area and the need for further investigation to fully elucidate the tectonic complexity and related mineral potential of the region (Lopez et al., 2024).

6 Summary of Bulk Geochemistry Results

Five hundred and twenty-three of the samples collected during the 2023 field season were submitted for whole-rock lithogeochemical analyses. Three hundred and thirty-four of these samples, representing five main lithological categories, were selected for additional detailed geochemical examination and analysis:

- intrusive igneous rocks of the TMZ (n = 67)
- granitoid gneisses of the TBC (n = 134)
- pegmatites (n = 47)
- mafic metamorphic rocks, including amphibolite, metagabbro, and mafic schist (n = 45)
- metasedimentary rocks of the assumed RRC (n = 41)

6.1 Element Mobility

Bedrock samples collected from the Leland Lakes and Andrew Lake study areas were all exposed to high-grade metamorphism, ranging from upper-amphibolite to granulite facies. In addition, most samples were exposed to varying degrees of structural modification, especially those collected from within major shear zones. The degree of element mobility (Rollinson, 1993) was evaluated using standard approaches (e.g., Harker variation diagrams, Harker, 1909).

Mafic rocks were also tested for element mobility, which included the plotting of major element abundances against trace elements, such as Zr, that are typically immobile in ocean-floor hydrothermal systems (Cann, 1970). However, mafic rocks in this study may have come from diverse sources, so samples were generally not rejected unless the percentage of SiO_2 fell outside the range of intermediate to ultrabasic rocks (<66% SiO_2) or had other obvious signs of significant alteration.

Samples were grouped and compared against others of the same lithology. Those samples with significant scatter in the major elements (SiO_2, Al_2O_3, Fe_2O_3, etc.) were generally excluded from further geochemical analysis and discrimination.

6.2 Geochemistry of Granitoids of the TMZ

Geochemical analysis of rocks from the TMZ can provide valuable insights into the tectonic settings and magmatic evolution of these regions. The granitoid suites from the Leland Lakes and Andrew Lake study areas exhibit a range of geochemical signatures that reflect complex tectonic origins and potential for mineralization. Granitoid complexes that are part of the TMZ and analyzed in this study include the Arch Lake, Slave, Andrew Lake, and Colin Lake suites. Discrimination diagrams by Pearce et al. (1984) and Harris et al. (1986) were employed to classify these granitoids and better understand their emplacement setting. The geochemistry of these suites is compared with the granitoid gneisses of the TBC.

6.2.1 Leland Lakes Study Area

The Arch Lake granitoid suite (1938 ±3 Ma; McDonough et al., 2000e) is a lithologically diverse suite of granite, granodiorite, and quartz monzonite, and exhibits calcalkalic geochemical affinities typical of subduction zone environments (Figure 22a, b, and d). At Leland Lakes, near the LLSZ, the weakly peraluminous nature of the Arch Lake granitoids, with aluminum saturation index (ASI) values ranging on average from 1.0 to 1.1 (Figure 22c), coupled with relatively elevated Sr/Y and Zr/Hf ratios (Figure 23a), suggests an I-type granite origin. Moreover, the steep increase in chondrite-normalized La/Yb ratios (La^{ch}/Yb^{ch}) with decreasing Yb^{ch} concentrations (Figure 24a), combined with strongly fractionated REE patterns, suggests high-pressure melting where garnet remained stable, indicating a garnet-rich source such as deep continental crust or subducting slabs (Moyen and Martin, 2012). This along with chondrite-normalized trace-element patterns showing significant REE fractionation, with weak positive and negative europium (Eu) anomalies, reflects limited plagioclase fractionation during magmatic evolution (Figure 25a). The dominance of K-feldspar as a major phase and the enrichment in large-ion lithophile elements (LILE), over high-field-strength elements (HFSE), further underscores their evolved nature. Most samples classify as volcanic-arc granite on tectonic discrimination diagrams (Figure 26a), further reflecting a subduction-related environment of formation.

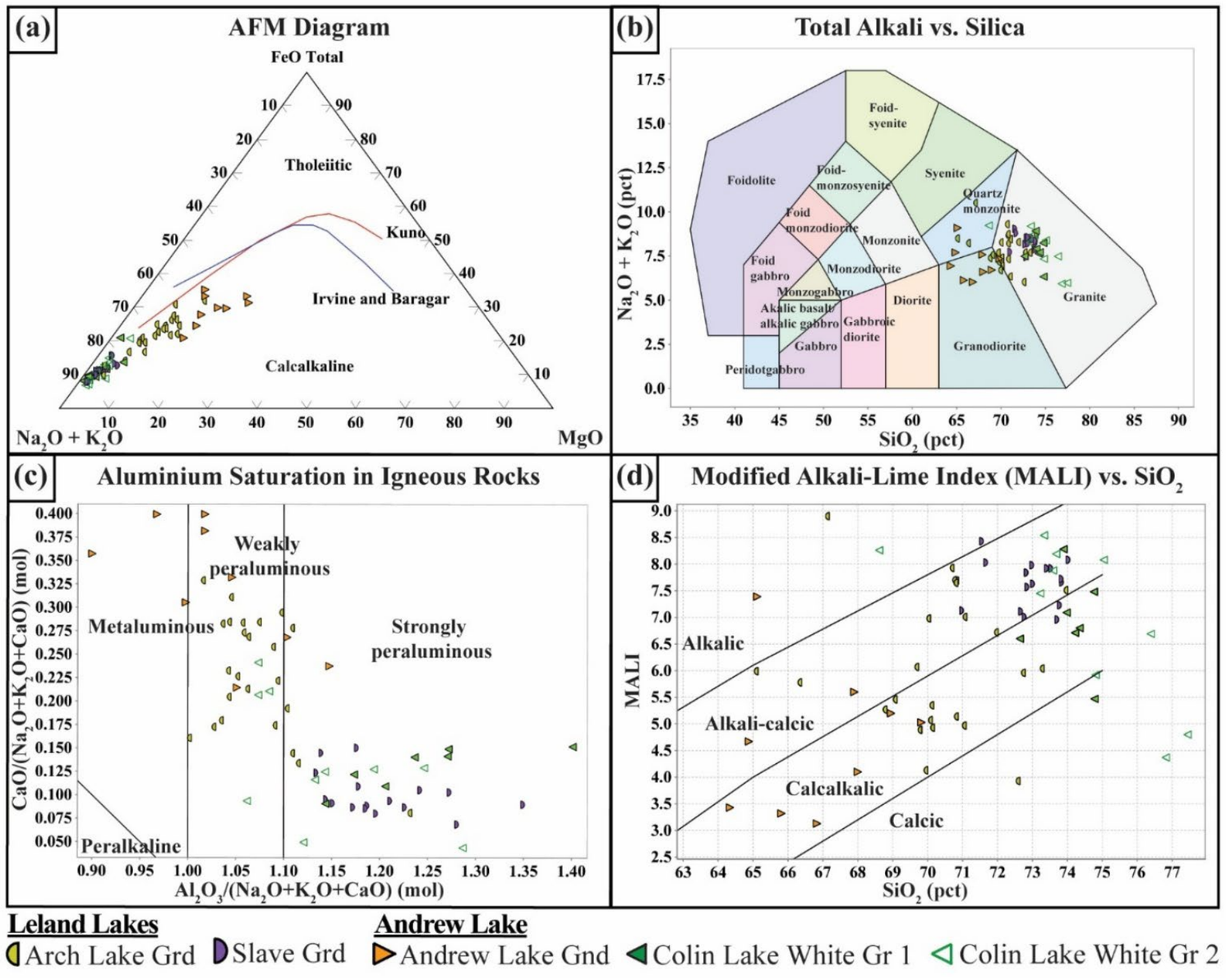

Figure 22. Geochemical discrimination diagrams for selected samples from the Taltson magmatic zone (TMZ) in the Leland Lakes and Andrew Lake study areas, northeastern Alberta: (a) alkalis-iron-magnesium (AFM) diagram, blue curve after Irvine and Baragar (1971) and red curve after Kuno (1968); (b) plutonic total alkali versus silica (TAS) diagram (after Middlemost, 1994); (c) aluminum saturation index for igneous rocks (after Barton and Young, 2002); (d) modified alkali-lime index (MALI) versus SiO_2 diagram (after Frost et al., 2001; Frost and Frost, 2008). Abbreviations: Gnd, granodiorite; Gr, granite; Grd, granitoid; mol, mole; pct, per cent.

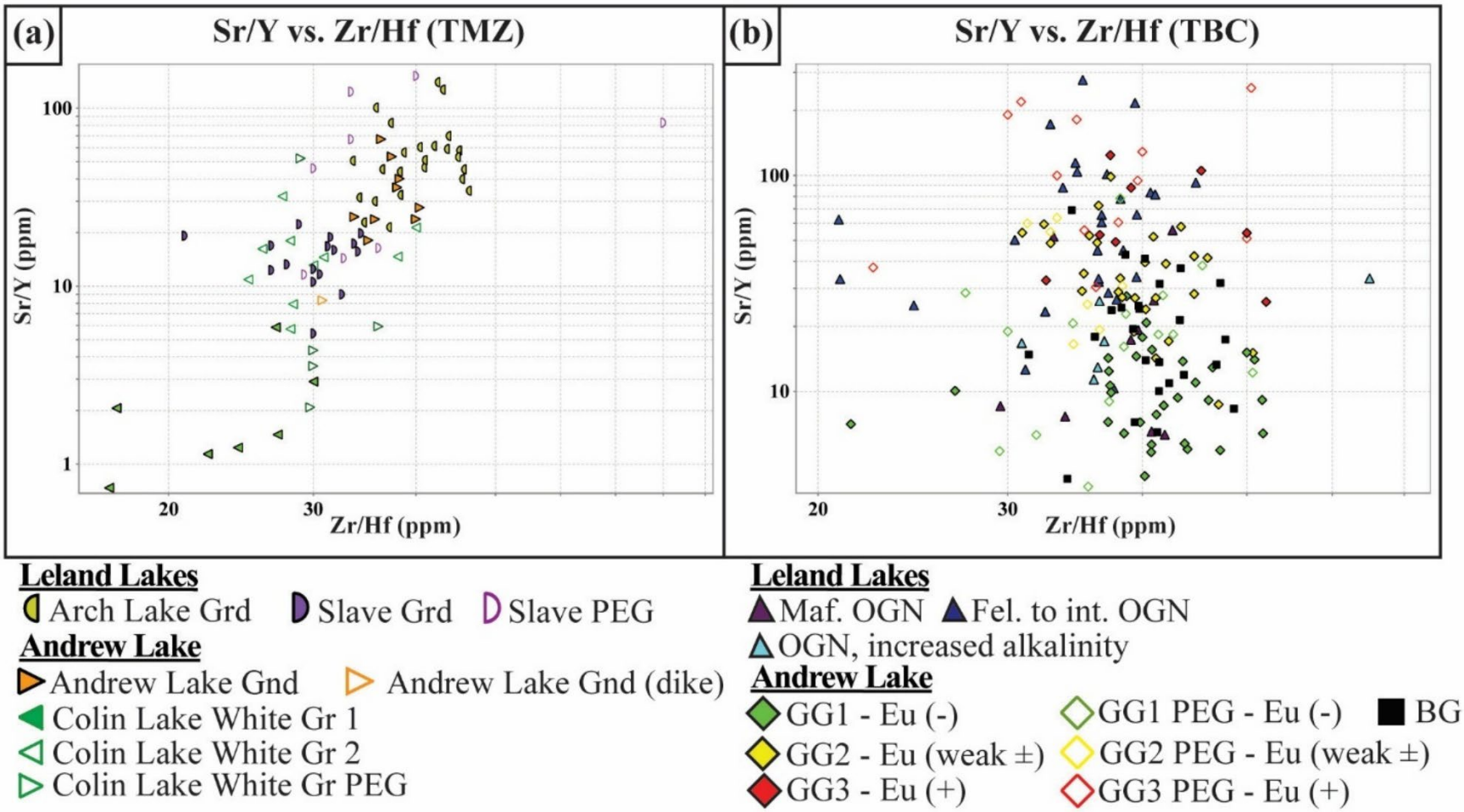

Figure 23. The Sr/Y versus Zr/Hf discrimination diagrams for selected samples from the Leland Lakes and Andrew Lake study areas: (a) Taltson magmatic zone (TMZ) samples; (b) Taltson basement complex (TBC) samples. Abbreviations: BG, Taltson basement gneiss; Fel., felsic; GG, granite gneiss; Gnd, granodiorite; Gr, granite; Grd, granitoid; int., intermediate; Maf., mafic; OGN, biotite-hornblende heterogeneous gneiss; PEG, pegmatite.

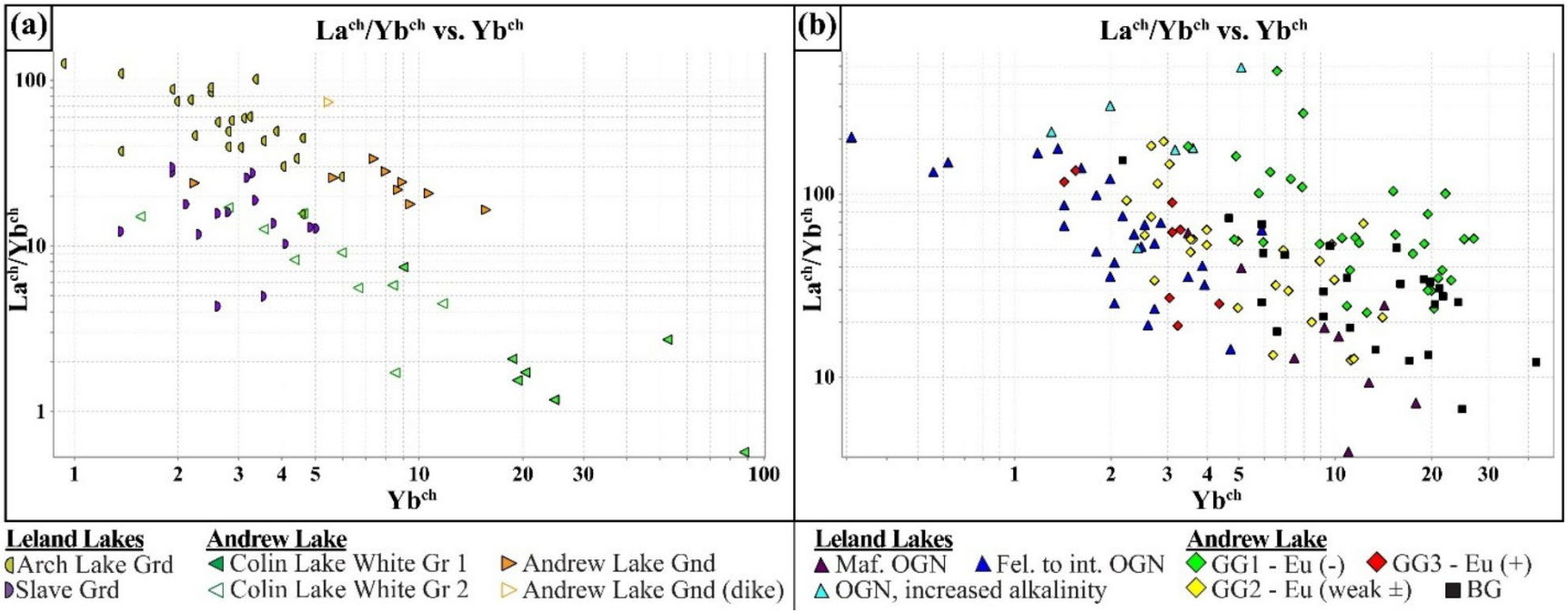

Figure 24. Chondrite-normalized La^{ch}/Yb^{ch} versus Yb^{ch} diagram for selected samples from the Leland Lakes and Andrew Lake study areas, northeastern Alberta (normalizing values from McDonough and Sun, 1995): (a) Taltson magmatic zone (TMZ) samples; (b) Taltson basement complex (TBC) samples. Abbreviations: BG, Taltson basement gneiss; Fel., felsic; GG, granite gneiss; Gnd, granodiorite; Gr, granite; Grd, granitoid; int., intermediate; Maf., mafic; OGN, biotite-hornblende heterogeneous gneiss.

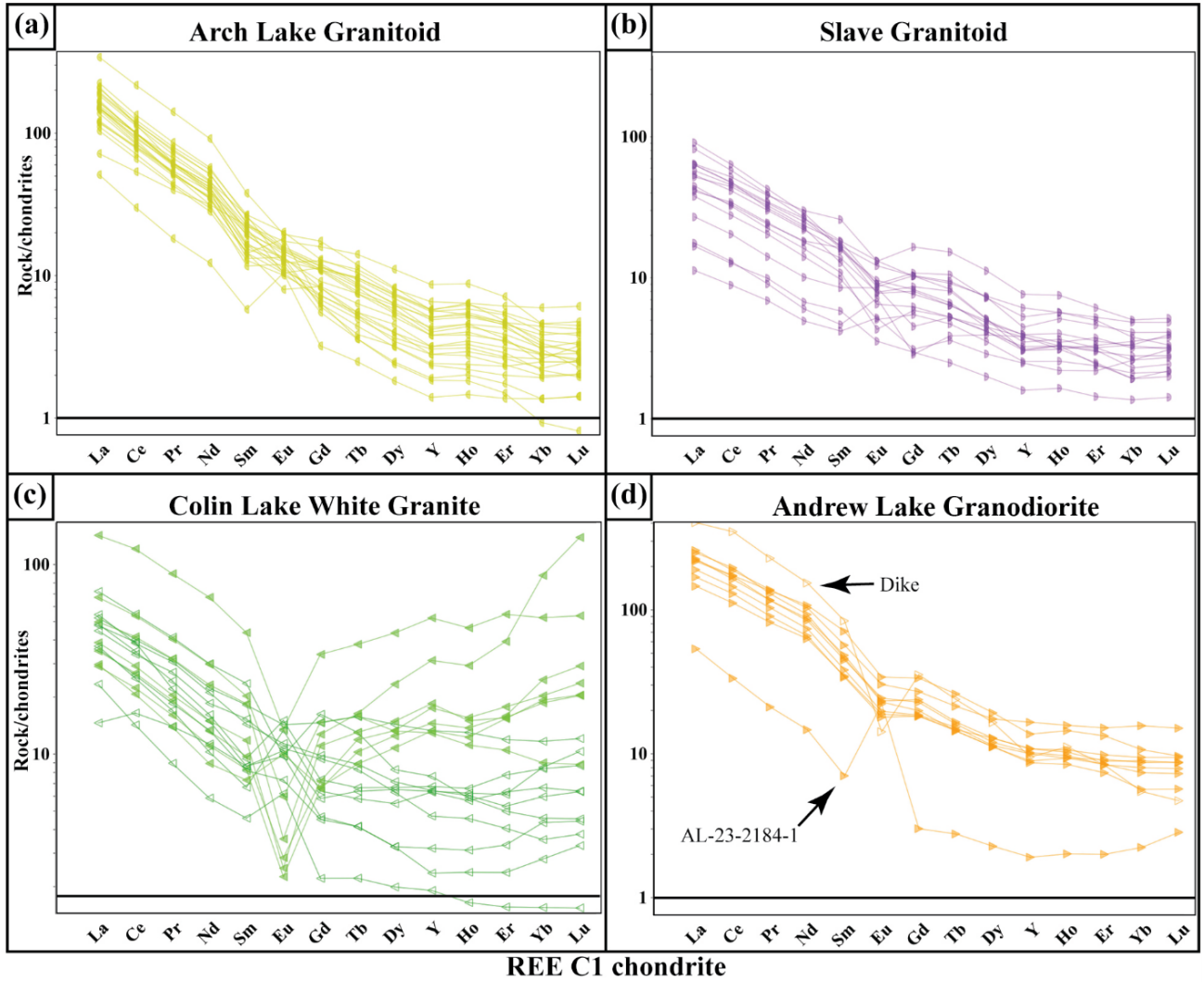

Figure 25. Chondrite-normalized rare-earth-element (REE) plots for selected Taltson magmatic zone samples from the Leland Lakes and Andrew Lake study areas, northeastern Alberta (normalizing values from McDonough and Sun, 1995): (a) Arch Lake granitoid; (b) Slave granitoid; (c) Colin Lake white granite, filled triangles represent relatively heavy rare-earth-element (HREE)–enriched samples (Colin Lake white granite 1) and unfilled triangles represent relatively HREE-depleted samples (Colin Lake white granite 2); (d) Andrew Lake granodiorite, sample AL-23-2184-1 is labelled and unfilled triangles represent a dike sample.

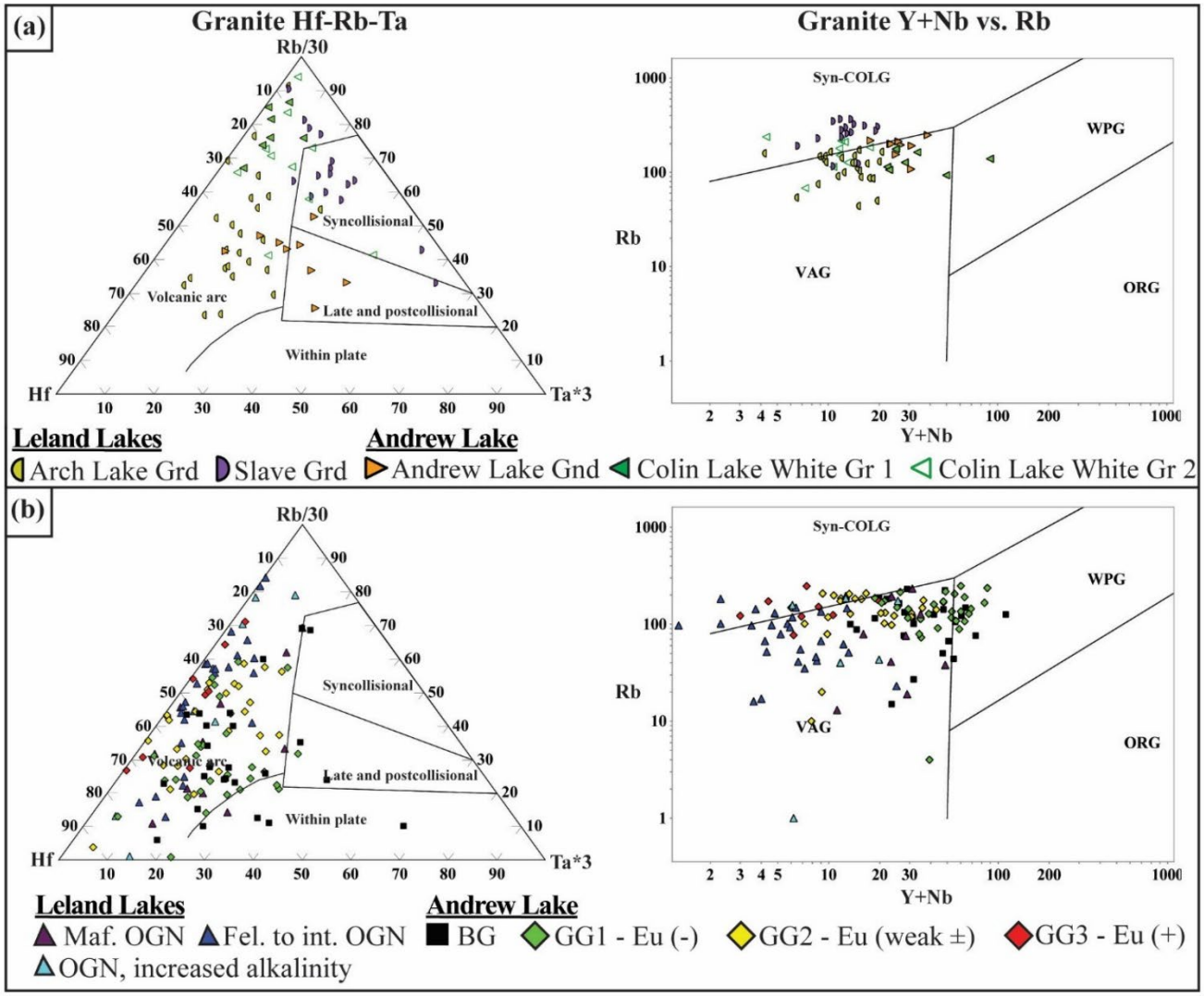

Figure 26. Granite Hf-Rb-Ta and Y+Nb versus Rb tectonic discrimination diagrams (after Harris et al., 1986 and Pearce et al., 1984) for selected samples from the Leland Lakes and Andrew Lake study areas, northeastern Alberta: (a) Taltson magmatic zone (TMZ) samples; (b) Taltson basement complex (TBC) samples. Abbreviations: BG, Taltson basement gneiss; Fel., felsic; GG, granite gneiss; Gnd, granodiorite; Gr, granite; Grd, granitoid; int., intermediate; Maf., mafic; OGN, biotite-hornblende heterogeneous gneiss; ORG, ocean-ridge granite; syn-COLG, syncollisional granite; VAG, volcanic-arc granite; WPG, within-plate granite.

In contrast, the Slave granitoid suite (1934 ±2 Ma; McDonough et al., 2000e) is more homogenous, uniformly classifying as granite with increased modified alkali–lime index (MALI) and ASI values (1.13–1.35) indicative of strongly peraluminous, dominantly alkali-calcic compositions (Figure 22a–d). Furthermore, Sr/Y and Zr/Hf ratios are significantly lower than Arch Lake suite results (Figure 23a), suggesting less plagioclase fractionation and a higher degree of crustal involvement in their genesis. This is further evidenced by significantly lower La^{ch}/Yb^{ch} ratios and similar values of Yb^{ch} relative to the Arch Lake suite (Figure 24a), indicating the Slave granitoid suite is less evolved, yet still records a significantly differentiated magmatic history. Such a gradual change in La^{ch}/Yb^{ch} ratios with relatively constant Yb^{ch} concentrations is characteristic of shallower melting conditions, where plagioclase dominates over garnet (Rollinson, 1993). However, despite these differences, chondrite-normalized trace-element patterns of the Slave granitoid suite exhibit similar characteristics to the Arch Lake granitoids, showing significant REE fractionation and weak negative and positive Eu anomalies (Figure 25b). The geochemical signatures of the Slave granitoids, along with lower REE fractionation, suggest shallower depths of formation conducive to the generation of syncollisional granite (Winter, 2010), with some overlap with volcanic-arc granite (Figure 26a). This indicates they formed during a period of tectonic compression and crustal thickening, typical of orogenic settings (Pearce et al., 1984).

6.2.2 Andrew Lake Study Area

The Andrew Lake granodiorite suite (1962 ±2.5 Ma; McDonough et al., 2000e) consists primarily of alkali-calcic to calcalkalic granodiorite and quartz monzonite with more variable ASI values than the Arch Lake granitoid, ranging from 0.9 to 1.15 (Figure 22a–d). However, these samples bear slightly lower ratios of Sr/Y and Zr/Hf, with lower La^{ch}/Yb^{ch} ratios and higher concentrations of Yb^{ch}, suggesting there was more crustal influence in their genesis (Figures 23a and 24a). Chondrite-normalized trace-element patterns reveal substantial REE fractionation, coupled with negative Eu anomalies, indicating significant magmatic evolution and plagioclase fractionation (Figure 25d). Amphibole fractionation may also have contributed to the REE profiles, particularly in heavy rare-earth-element (HREE) partitioning during midcrustal crystallization. The distinct enrichment in HFSE, attributable to higher concentrations of Zr-, Ti-, and P-bearing minerals, marks a notable compositional divergence from the Colin Lake white granite. Samples classify as a mix of volcanic-arc and postcollisional granite (Figure 26a). A representative sample collected from a younger phase of leucogranitic dikes exhibits a pronounced negative Eu anomaly and is significantly more fractionated in HREEs (Figure 25d), recording a Th/U ratio of 21. These dikes increase in abundance westwards, correlating with increasing strain towards the ALSZ. Moreover, a sample (AL-23-2184-1) collected from the western margin of Cherry Lake fits the composition of a granodiorite but exhibits geochemical affinities to the Colin Lake granitoid. In this area, the Colin Lake white granite is the dominant plutonic phase and exhibits localized uranium enrichment. Petrographic analysis shows that this sample is dominated by plagioclase, biotite, and lesser quartz, consistent with a granodioritic composition. However, sample AL-23-2184-1 displays similar trace-element patterns to the Colin Lake white granite 2, particularly in REE profiles, with a pronounced positive Eu anomaly (Figure 25c and d), and a low Th/U ratio (0.243). The similarity in REE patterns implies that this sample may represent a mixed or intermediary composition resulting from melt interactions between the Andrew Lake granodiorite and the Colin Lake granitoid. Considering their close temporal and spatial proximity, such melt mixing is plausible.

The Colin Lake white granite (ca. 1923–1921 Ma; McDonough et al., 2000e) is predominantly granitic in composition and displays alkali-calcic to calcalkalic affinities and weakly to strongly peraluminous characteristics, with ASI values ranging from 1.06 to 1.40 (Figure 22a–d). Major element compositions indicate a highly evolved melt, with highly variable fractionation trends consistent with varying degrees of plagioclase stability during partial melting and assimilation of country rock. The REE patterns bifurcate after the variable Eu anomalies, reflecting varying degrees of HREE enrichment or depletion, which correlate directly with the presence of garnet in the rock (Figure 25c). Samples with relatively unfractionated REE patterns invariably contain garnet and correspond to the in situ and insource

leucosomal components of the RRC (Colin Lake white granite 1). These samples also display a pronounced negative Eu anomaly, reflecting substantial plagioclase fractionation, or retention, in the residual source. Notably, they display lower average Sr/Y, Zr/Hf, and La^{ch}/Yb^{ch} ratios, with predominantly elevated Th/U ratios relative to samples that are HREE depleted (e.g., Colin Lake white granite 2; Figures 23a, 24a, and 27b). These geochemical signatures indicate deep crustal partial melting where garnet remained stable in the residue, which is consistent with high-pressure conditions. The garnet-bearing leucosome, therefore, likely formed in situ and is a melt-extracted portion of the neosome, derived from partial melting of the paragneiss during high-grade metamorphism. Conversely, samples of the Colin Lake granitoids that display HREE fractionation generally exhibit increased LILE enrichment (Colin Lake white granite 2), and were observed to have intruded the basement gneisses near Andrew Lake. They commonly exhibit positive Eu anomalies, suggesting that plagioclase was incorporated into the melt. These steeper REE patterns, coupled with higher La^{ch}/Yb^{ch} ratios and lower concentrations of Yb^{ch} (Figure 24a), indicate that these melts were generated at a deeper formation depth, under higher pressure conditions than those of Colin Lake white granite 1. The degree of HREE depletion in these samples suggests that garnet remained stable in the source during partial melting, contributing to the fractionation trend observed in their REE patterns. The elevated LILE contents in these samples suggest late-stage melt differentiation and potential interaction with volatiles during injection. On discrimination diagrams, HREE-enriched samples mainly classify as volcanic-arc granite, with one sample plotting as a within-plate granite, whereas the relatively HREE-depleted samples classify as a mix of volcanic-arc and syncollisional granites (Figure 26a). Consequently, the Colin Lake white granites record polybaric magma evolution with variable assimilation of metasedimentary and basement gneiss country rock.

6.3 Geochemistry of Granitoid Gneisses of the TBC

6.3.1 Leland Lakes Study Area

One hundred thirty-four samples from the TBC were analyzed, 43 of which came from the Leland Lakes study area. The analysis of these orthogneisses derived from the biotite-hornblende heterogeneous gneiss (OGN) basement, which spans the length of the LLSZ, provides critical insights into the geochemical and magmatic characteristics of the region. The granitoid gneisses exhibit strong REE fractionation. They also display predominantly calcic to alkali-calcic affinities (Figure 28a–d). Their Sr/Y, Zr/Hf, and La^{ch}/Yb^{ch} ratios broadly overlap with those observed in samples from the Arch Lake granitoid (Figures 23a, b and 24a, b). These samples similarly follow the same trend of increasing La^{ch}/Yb^{ch} ratios with decreasing Yb^{ch} concentrations, suggesting garnet played a role during partial melting at deeper crustal levels; however, the lack of extreme HREE depletion, characteristic of a purely garnet-stable regime, indicate that garnet's influence was less pronounced in the TBC samples. The data suggest a transitional environment, where melting conditions spanned both garnet- and plagioclase-stable fields. In this regime, garnet influenced the REE budget during deeper partial melting, whereas plagioclase exerted greater control during stages of magma evolution or differentiation at shallower depths.

The major-, minor-, and trace-element data of these gneisses highlight their heterogeneous character, which is consistent with a complex history of emplacement and metamorphism (Figure 29a and b). Furthermore, the samples are metaluminous to strongly peraluminous (Figure 28c) and classify as volcanic-arc granite, apart from a minor subset which plots within the syncollisional field on the Y+Nb vs. Rb diagram (Figure 26b), indicating polyphase magmatism that may have once spanned the transition from active subduction to collisional tectonics. The high Sr/Y and Zr/Hf ratios observed in the OGN align with a volcanic-arc granite origin (Figure 23b), but unlike rocks from deeper arc root environments dominated by garnet-bearing residues, these samples indicate melting at midcrustal levels, where garnet was less stable, and plagioclase fractionation played a stronger role. This is further supported by the moderate to weak Eu anomalies, which indicate some plagioclase retention but not extensive fractionation (Figure 29a).

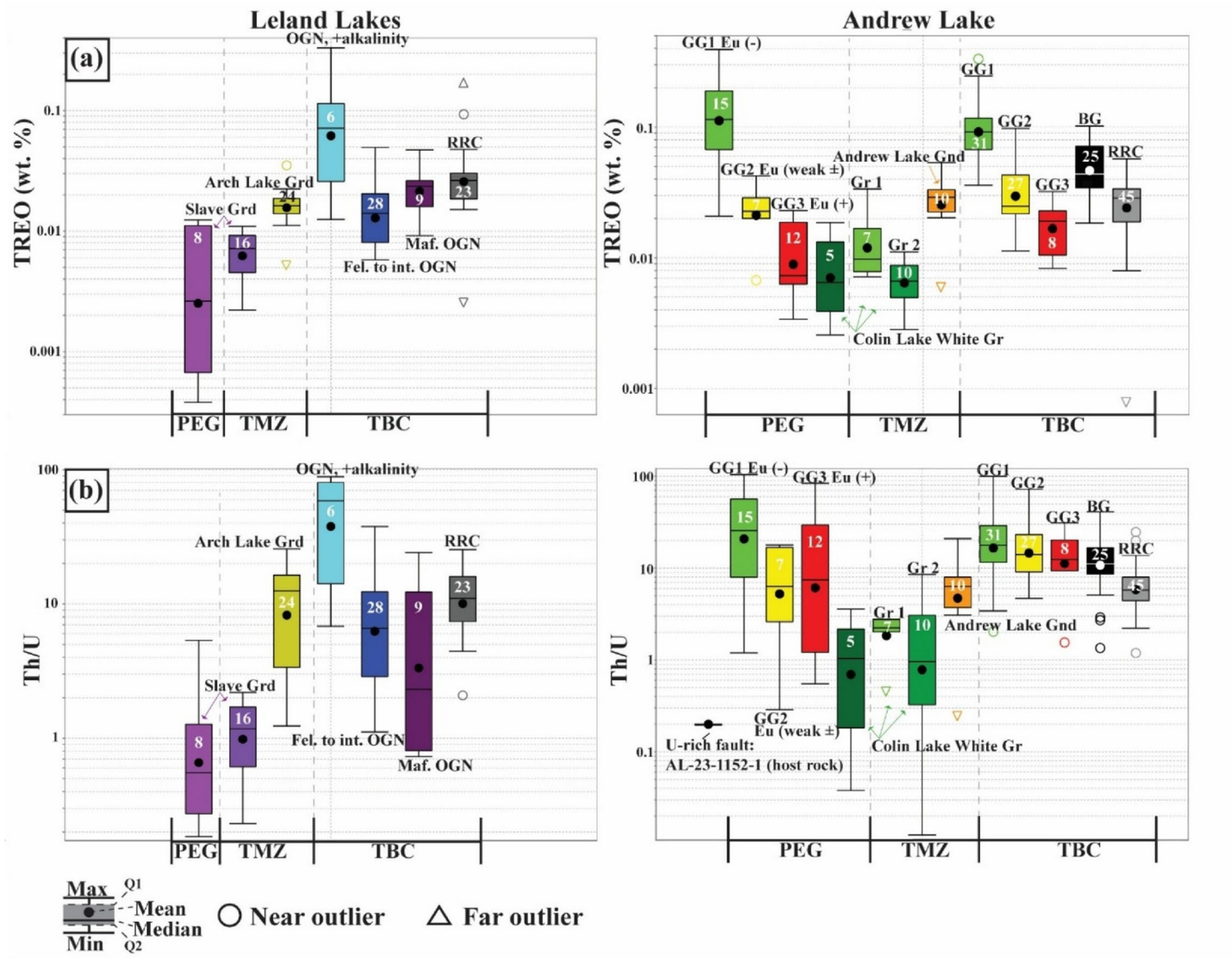

Figure 27. Tukey (1977) analysis of geochemical parameters for selected granitoid, paragneiss, and pegmatite (PEG) samples from the Leland Lakes and Andrew Lake study areas, northeastern Alberta: (a) total rare-earth oxides (TREO); (b) Th/U ratios. Sample count of each unit is listed within the respective boxes. Note, the sample count for the Rutledge River complex (RRC) includes the 41 selected samples and an additional 27 samples that were not submitted for detailed analysis due to evidence of alteration and proximity to shear zones. Abbreviations: BG, Taltson basement gneiss; Eu (-), negative Eu anomaly; Eu (+), positive Eu anomaly; Eu (weak ±), weak negative and positive Eu anomaly; Fel., felsic; Gnd, granodiorite; Gr, granite; Grd, granitoid; int., intermediate; Mafic, mafic; OGN, biotite-hornblende heterogeneous gneiss; TBC, Taltson basement complex; TMZ, Taltson magmatic zone.

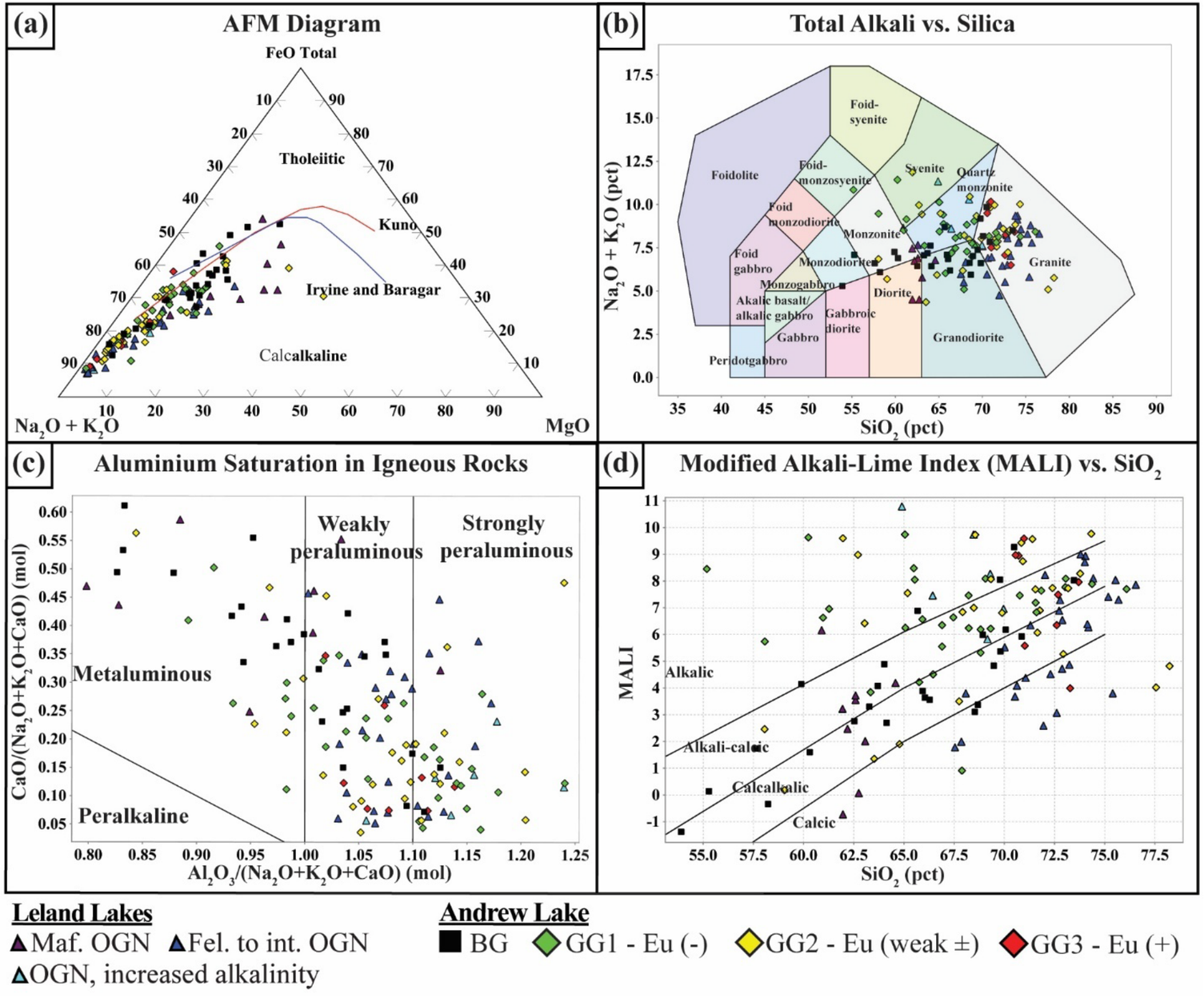

Figure 28. Geochemical discrimination diagrams for selected samples from the Taltson basement complex in the Leland Lakes and Andrew Lake study areas, northeastern Alberta: (a) alkalis-iron-magnesium (AFM) diagram, blue curve after Irvine and Baragar (1971) and red curve after Kuno (1968); (b) plutonic total alkali versus silica (TAS) diagrams (after Middlemost, 1994); (c) aluminum saturation index for igneous rocks (after Barton and Young, 2002); d) modified alkali-lime index (MALI) versus SiO_2 diagram (after Frost et al., 2001; Frost and Frost, 2008). Abbreviations: BG, Taltson basement gneiss; Fel., felsic; GG, granite gneiss; int., intermediate; Maf., mafic; mol, mole; OGN, biotite-hornblende heterogeneous gneiss; pct, per cent.

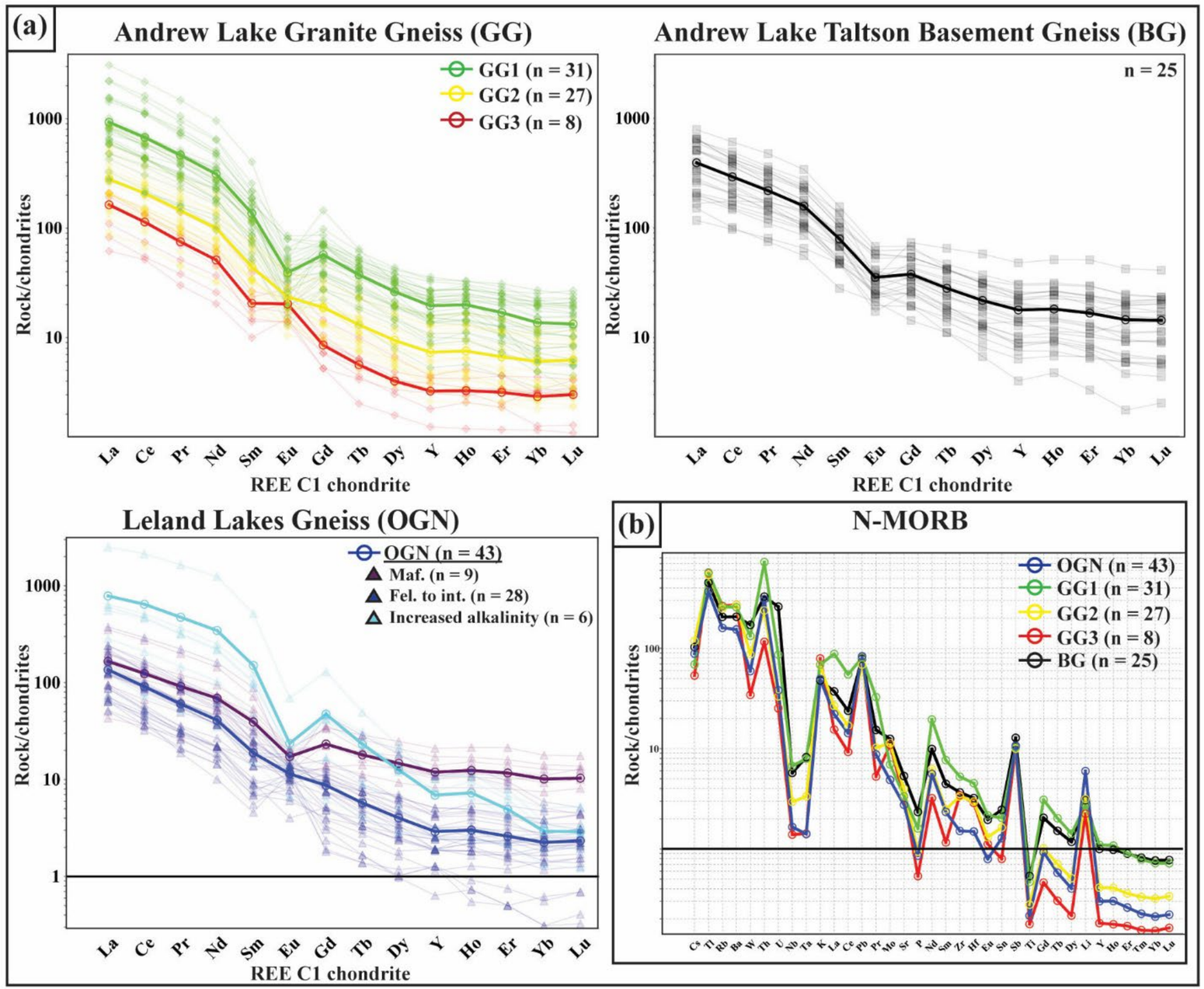

Figure 29. Multi-element geochemical plots for selected Taltson basement complex samples from the Leland Lakes and Andrew Lake study areas, northeastern Alberta: (a) chondrite-normalized rare-earth element (REE) plot (normalizing values from McDonough and Sun, 1995); (b) normal (N-type) mid-ocean ridge basalt (N-MORB) normalized multi-element plot (normalizing values from Sun and McDonough, 1989). Granite gneiss (GG) GG1, GG2, GG3, and Taltson basement gneiss (BG) trends from the Andrew Lake samples, and the biotite-hornblende heterogeneous gneiss (OGN) trend from the Leland Lakes samples are shown.

Notably, several OGN samples with increased alkalinity have SiO_2 concentrations that range from approximately 64–70% and plot near the junction of granodiorite, quartz monzonite, and granite with one outlier with a syenitic composition (Figure 28b). These samples display higher La^{ch}/Yb^{ch} ratios relative to the rest of the suite (Figure 24b). Such elevated ratios often signal fractionation of HREEs by phases like garnet or amphibole, yet they do not necessarily correlate with the highest silica contents. This discrepancy suggests that the processes driving REE fractionation (e.g., residual garnet in the source or distinct fractionation paths at depth) are partially decoupled from the silica evolution in these granitoids. These samples with increased alkalinity record increased LREE contents (Figure 29a). They also exhibit significant negative Eu anomalies, in contrast to the other OGN REE patterns, suggesting significant differentiation and crustal interaction (Figure 29a).

The REE fractionation of the TBC in the Leland Lakes area implies early crystallizing phases (i.e., garnet, amphibole, pyroxene) removed HREE from the melt, leaving a LREE-enriched residue, which formed the protoliths for the granitoids and gneisses that make up the bulk of the TBC in the study area. On normal (N-type) mid-ocean-ridge basalt (N-MORB) normalized multi-element plots, the Leland Lakes orthogneisses exhibit depletion of Nb and Ta relative to the Andrew Lake BG unit, typical of subduction-related settings and arc magmatism (Figure 29b).

The compositional diversity of the Leland Lakes basement granitoid gneisses points to multiple magmatic sources or varying degrees of partial melting and fractional crystallization. The TBC is known to contain a number of different Paleoproterozoic and Archean components, but the Leland Lakes study area has just a single published age. Additional geochronology will be critical for elucidating the geochemical differences identified in this area. Overall, the geochemical characteristics of the Leland Lakes granitoid gneisses reflect a dynamic magmatic environment with significant crustal interaction, fractional crystallization, and contributions from both mantle-derived and crustal sources. Further investigation of trace-element behaviour and isotopic compositions is recommended to provide deeper insights into the petrogenetic evolution of the rock types of the LLSZ.

6.3.2 Andrew Lake Study Area

The geochemical data from the Andrew Lake study area includes 91 granitoid gneisses from the TBC. The two dominant gneissic components, Taltson basement gneiss (BG) and granite gneiss (GG), exhibit distinct compositional and geochemical characteristics that are attributed to unique magmatic histories.

The BG unit, likely reflecting the older Archean component of the basement, contains magnetite, hornblende, and pyroxene, and displays a range of felsic to intermediate compositions, from granite to diorite (Figure 28b). This compositional diversity, punctuated by a predominance of metaluminous to weakly peraluminous and alkali-calcic to calcalkalic classifications (Figure 28c and d), suggests a complex magmatic and metamorphic evolution involving multiple phases of intrusion and varying degrees of magmatic differentiation. Like the Leland Lakes basement orthogneisses, these samples exhibit increasing La^{ch}/Yb^{ch} ratios with decreasing Yb^{ch} concentrations (Figure 24b), indicating HREE depletion during partial melting. However, higher Yb^{ch} concentrations in the Andrew Lake BG unit suggest shallower melting conditions, where garnet was less stable. Instead, amphibole, plagioclase, and pyroxene played significant roles in controlling the REE budget, consistent with lower pressure melting conditions in the middle to upper crust (Rollinson, 1993; Davidson et al., 2007).

The BG samples are enriched in LREE and have average concentrations of HREE relative to chondrite-normalized trace-element signatures (Figure 29a). They primarily plot as volcanic-arc granite, and to a lesser degree, within-plate granite (Figure 26b). They also show enrichment in LILE and HFSE, along with negative Eu anomalies, which indicates fractional crystallization and crustal contamination were important mechanisms during emplacement, prior to multiple metamorphic episodes.

The GG unit of the basement features a narrower range of felsic compositions and reduced mafic mineral content, predominantly classifying as granite, quartz monzonite, and granodiorite (Figure 28a and b). Locally, the GG unit intrudes the BG unit and has a single U-Pb age of ca. 2.3 Ga (McNicoll et al., 2000).

The GG unit exhibits a broader range of ASI values and alkalinity than the BG unit, spanning metaluminous to strongly peraluminous and alkalic to calcic compositions (Figure 28c and d), which indicates a magmatic evolution that involved more extensive fractional crystallization with varying degrees of crustal assimilation.

Three major geochemical trends are discernible from multi-element and REE diagrams within the GG unit, all showing overall enrichment in LREE and relative depletion in HREE (Figure 29a). The most differentiated trend, for GG1 samples, is characterized by elevated REE concentrations, high Th/U ratios, and low Sr/Y ratios (Figures 23b and 27b). Elevated Th/U ratios imply advanced differentiation and possible crustal involvement, whereas low Sr/Y ratios and moderate to pronounced negative Eu anomalies are consistent with significant plagioclase fractionation during crystallization. In general, the La^{ch}/Yb^{ch} ratios among all three GG trends are similarly elevated, indicating a significant depth of formation, where garnet remained in the residue. In contrast with the GG2 and GG3 samples, GG1 samples exhibit the highest concentrations of Yb^{ch}, further evidencing a more evolved melt, formed at shallower depths where feldspar fractionation dominated (Davidson et al., 2007). The trace-element signatures of the GG1 samples are similar (albeit more enriched) to those exhibited by the samples of the BG unit of which the GG unit intrudes, suggesting assimilation of basement gneiss may have been a key factor in generating these geochemical signatures. Furthermore, GG1 samples primarily plot as volcanic-arc granite, and less commonly as within-plate granite, like those of the BG unit, on tectonic discrimination diagrams (Figure 26b). The enrichment in LILEs, such as Rb, Ba, and Th, reflects the dominance of K-feldspar as the primary feldspar phase, particularly in the later stages of crystallization. Moreover, a characteristic of the GG1 component is intense recrystallization and a high degree of metasomatic alteration, evidenced by pervasive greenschist-facies overprinting due to hydrothermal fluid infiltration. Biotite shows partial replacement by muscovite and subsequent chlorite alteration, which is not as pronounced in the other GG samples.

The second geochemical trend, for GG2 samples, displays a range of weak negative and positive Eu anomalies and lower overall enrichment in REEs than GG1 samples (Figure 29a). This trend also shows lower Th/U ratios and concentrations of Yb^{ch}, and higher Sr/Y ratios, suggesting limited crustal interaction and differentiation at lower pressures (Figures 23b, 24b, and 27b). These samples notably lack muscovite, exhibit lower degrees of metasomatic alteration, and are moderately to strongly recrystallized. The lesser extent of feldspar fractionation in the GG2 trend implies a less evolved magmatic history for the GG2 component compared to the GG1. Limited feldspar fractionation suggests that the magma experienced fewer stages of crystal separation, resulting in a composition that retains more characteristics of the primary melt. It may represent an intermediate stage of magmatic evolution, where plagioclase played a role in fractionating Eu, whereas amphibole and, to a lesser extent, garnet influenced the partitioning of heavy REEs. The intermediate nature of the GG2 component suggests that it represents an earlier stage of magmatic evolution.

A less common group, the GG3 component, classifies strictly as granite and exhibits positive Eu anomalies, reflecting lesser degrees of feldspar fractionation and magmatic differentiation. It represents the least evolved melt, where plagioclase accumulation was significant, and amphibole fractionation played a role in reducing Yb^{ch} concentrations (Figure 24b), indicating transitional melting conditions or less differentiation compared to the GG1 and GG2 components. These samples are similarly less altered compared to the dominant trend, GG1 samples, further highlighting their distinct histories. Both the GG2 and GG3 components plot near the border of syncollisional and volcanic-arc granites on tectonic discriminants (Figure 26b), similar to the BG unit, hinting at a shared source or some degree of crustal assimilation from the BG unit. The overall geochemical trends, particularly the progressively higher concentrations of Yb^{ch} from the GG3 to GG1 components, suggest a shift from less evolved, deeper derived melts in the GG3 component to highly evolved, shallow-derived melts in the GG1 component. This progression suggests a shift from garnet- and plagioclase-influenced fractionation at greater depths to amphibole- and plagioclase-dominated fractionation at shallower levels (Pearce and Peate, 1995; Foley et al., 2000); however, without reliable U-Pb geochronology, this remains speculative.

6.4 Geochemistry of Pegmatites

In the Leland Lakes study area, the bulk of analyzed pegmatites (n = 8) are spatially and geochemically related to late-stage magmatic evolution of the Slave granitoid. Similar to their parent granites, these pegmatites have abundant perthite and lesser plagioclase feldspar, along with minor biotite and white mica related to feldspar alteration. They are predominantly strongly peraluminous and classify mainly as syncollisional granite, apart from a subset of samples which classify as volcanic-arc granite on a Hf-Rb-Ta discrimination diagram (Figure 30a and b). Furthermore, they exhibit the lowest Th/U (Figure 27b) and Nb/Ta ratios (Figure 31) and display highly variable Eu anomalies (Figure 30c).

The pegmatites in the Andrew Lake study area (n = 39) typically exhibit fractionated REE patterns, with enrichment in LREE and relative depletion in HREE when normalized to chondritic values (Figure 30c). A small subset of samples related to the anatectic phase of the Colin Lake white granite exhibit some enrichment in HREEs and very low Th/U ratios (Figures 27b and 30c). The calculated ASI values for the sampled pegmatites are predominantly peraluminous, with four samples plotting as metaluminous (Figure 30b). The bulk of pegmatites in the Andrew Lake study area derive from the younger component of the granite gneiss and can similarly be broken into three discernible trends, which mimic those of their parental granites and derived gneisses. Pegmatites with the highest Th/U ratios and elevated concentrations of La and Ce, display evidence of pervasive hydrothermal and greenschist-facies metasomatic alteration. They also exhibit pronounced negative Eu anomalies, whereas those with weak negative and positive Eu anomalies are significantly less enriched in REEs (Figures 27a, b and 30c).

Both anatectic and cross-cutting pegmatites have elevated REE concentrations, low Sr/Y ratios (Figure 23b), and classify primarily as volcanic-arc granite or within-plate granite, with a few samples plotting as syn- and postcollisional granites (Figure 30a). In thin section, the observed mineral assemblage, including abundant K-feldspar and biotite, minor muscovite, and trace amounts of monazite, allanite, titanite, and zircon, reflects the elevated REE concentrations in these samples. Those with weak negative and positive Eu anomalies plot as a mix of volcanic-arc granite and syncollisional granite and exhibit less alteration.

6.4.1 Partial Melting and REE Enrichment in the Andrew Lake Study Area

The geochemical analysis of the Andrew Lake study area rocks, particularly focusing on total rare-earth oxide (TREO) concentrations, provides crucial insights into the potential for critical mineral resources, specifically REEs. The distinct geochemical trends observed in the GG components, namely GG1, GG2, and GG3, along with their relationship to the BG unit and associated pegmatites, are significant in assessing the REE potential of the region (Figure 27a). Of these, the GG1 trend exhibits the highest enrichment in REEs, reflected by elevated TREO values of up to 0.3 wt. %. This enrichment is marked by high LREE concentrations such as La and Ce (Figure 29a), high Th/U ratios (Figure 27b), and low Sr/Y ratios (Figure 23b), all of which signal significant plagioclase fractionation and advanced magmatic differentiation and crustal interaction. Additionally, the high La^{ch}/Yb^{ch} ratios in the GG1 component indicate a degree of garnet involvement at deeper crustal levels, retaining HREEs like Yb (Figure 24b) and enabling LREEs to concentrate in the evolving melt. As the magma ascended, crystallizing plagioclase continued to partition out Eu, accentuating negative Eu anomalies.

Moreover, the similarity in trace-element concentrations between the GG1 component and the BG unit, which the GG1 component intrudes, indicates that the GG1 magmas inherited REE-enriched characteristics from the BG unit, contributing to the observed high TREO concentrations. The REEs in the GG1 samples are dominantly hosted in monazite-, allanite-, and zircon±titanite–bearing radiogenic assemblages (Figure 32a), evidenced by petrographic observations and a positive correlation between La, Ce, Zr, and Ti concentrations and TREO concentrations. Importantly, the REE enrichment in the GG1 component has been further enhanced by postemplacement metasomatic alteration. The intense recrystallization and metasomatic overprinting, primarily driven by hydrothermal fluids, concentrated REE-bearing minerals in zones of magnetite destruction such as the BLSZ (Figure 32b).

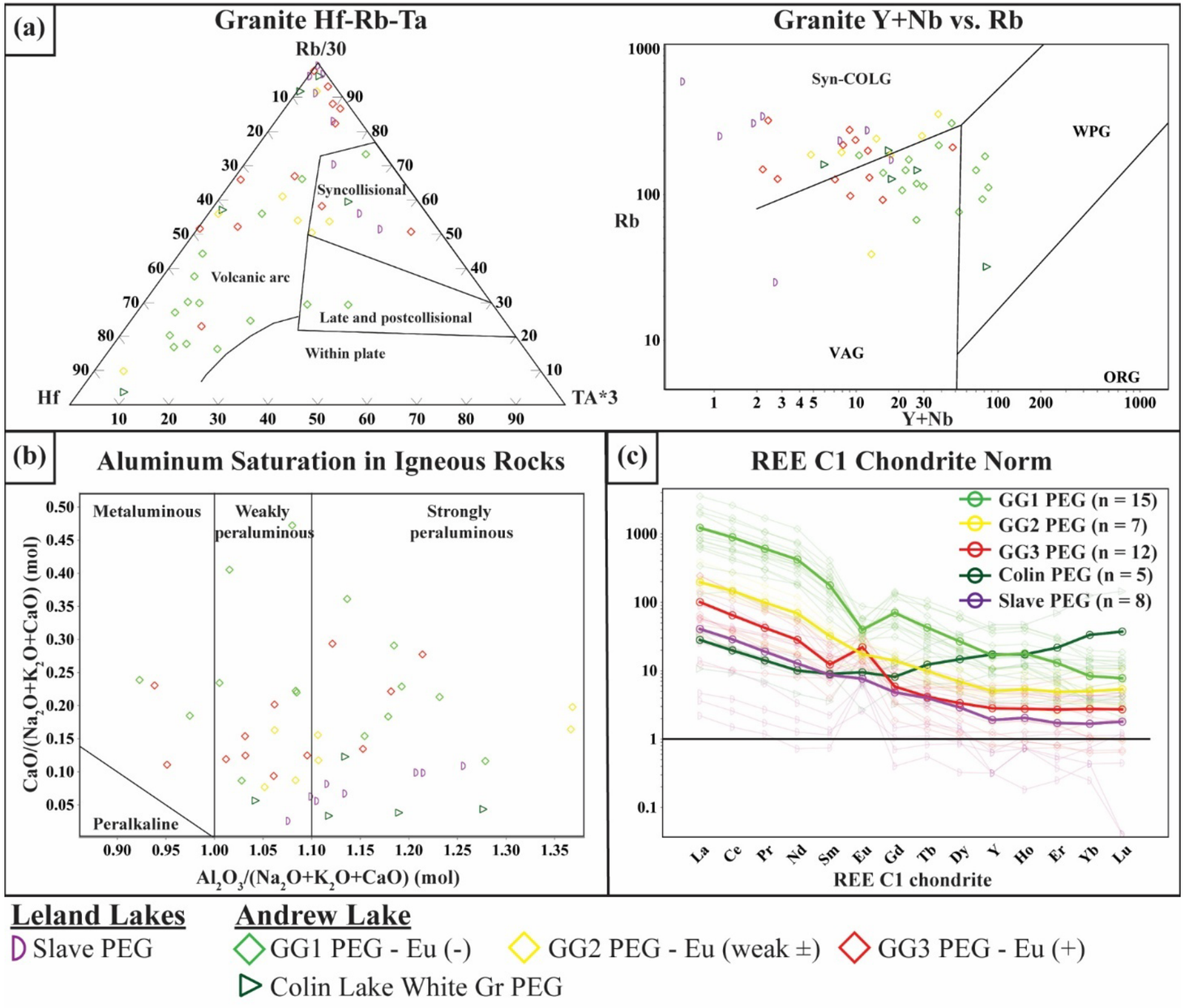

Figure 30. Geochemical and trace-element plots for selected pegmatite (PEG) samples from the Leland Lakes and Andrew Lake study areas, northeastern Alberta: (a) granite Hf-Rb-Ta and Y+Nb versus Rb tectonic discrimination diagrams (after Harris et al., 1986; Pearce et al., 1984); (b) aluminum saturation index for igneous rocks (after Barton and Young, 2002); (c) chondrite-normalized trace-element (rare-earth elements [REEs]) plot (normalizing values from McDonough and Sun, 1995). Abbreviations: Eu (-), negative Eu anomaly; Eu (+), positive Eu anomaly; Eu (weak ±), weak negative and positive Eu anomaly; GG, granite gneiss; Gr, granite; mol, mole; ORG, ocean-ridge granite; Slave, Slave granitoid; Syn-COLG, syncollisional granite; VAG, volcanic-arc granite; WPG, within-plate granite.

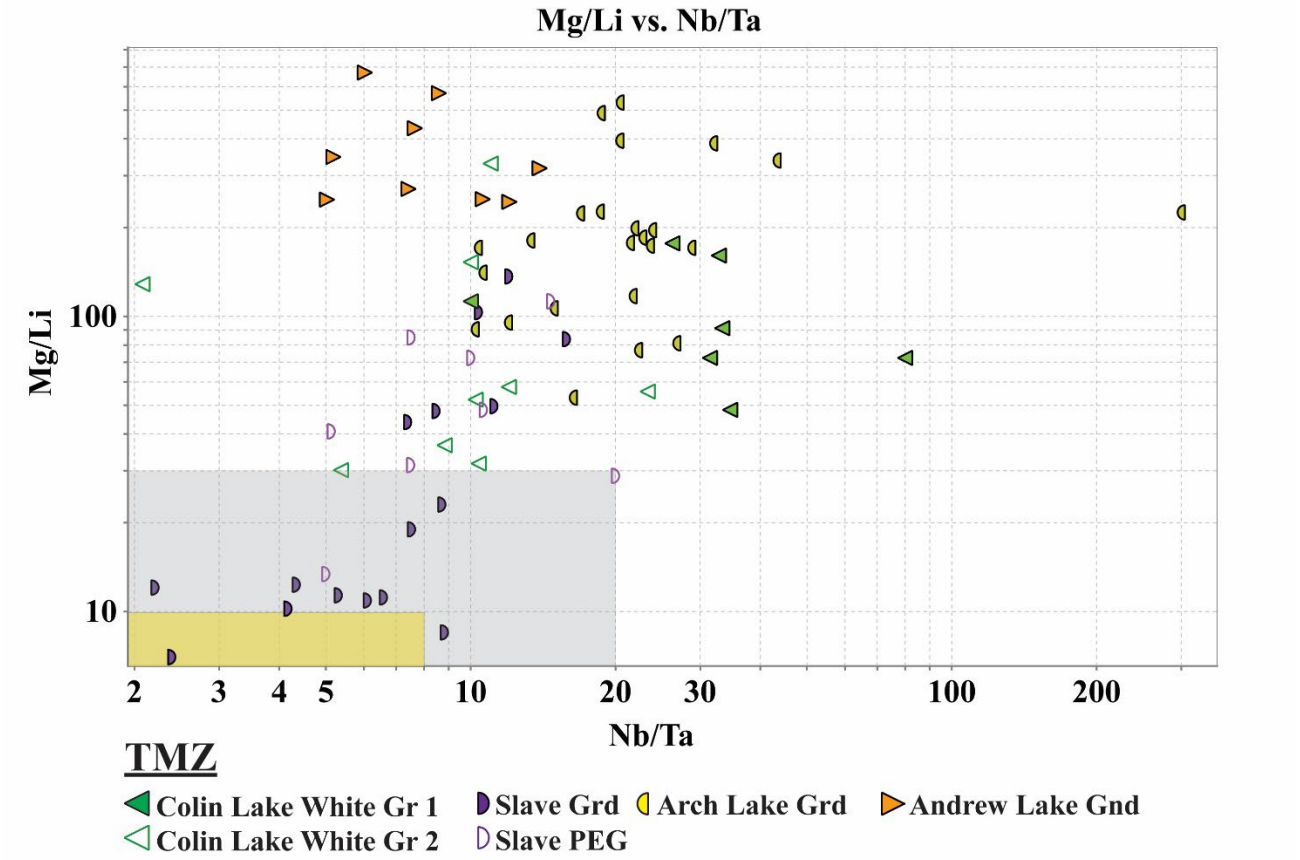

Figure 31. A Mg/Li versus Nb/Ta plot of selected Taltson magmatic zone (TMZ) samples from the Leland Lakes and Andrew Lake study areas, northeastern Alberta. The Mg/Li and Nb/Ta ratios of <10 and <8, respectively, indicate fertility for lithium-cesium-tantalum (LCT) pegmatites (yellow rectangle; Selway et al., 2005). The Mg/Li ratios <30 signify significant fractionation, whereas Nb/Ta ratios >20 may indicate magmas derived from a depleted mantle source or extensive fractional crystallization, which may not have favoured LCT pegmatite formation (Rudnick and Gao, 2003). Abbreviations: Gnd, granodiorite; Gr, granite; Grd, granitoid; PEG, pegmatite.

Additionally, pegmatites associated with the GG1 component feature analogous, radiogenic mineral assemblages (Figure 32c and d), and display similarly elevated REE concentrations. These pegmatites, derived from the GG1 component by partial melting, parallel the geochemical signatures of the GG1 component and are significant contributors to REE mineralization. They exhibit pronounced negative Eu anomalies and elevated concentrations of La and Ce, further enhancing the overall REE potential of the system.

The GG2 samples, although less enriched in REEs compared to GG1 samples, still exhibit notable TREO values (Figure 27a). The weak negative and positive Eu anomalies, lower Th/U ratios (Figure 27b), and higher Sr/Y ratios (Figure 23b) suggest less extensive magmatic differentiation and limited crustal interaction. The La^{ch}/Yb^{ch} ratios in GG2 samples reflect a transitional environment, where plagioclase fractionation dominated REE behaviour at shallower crustal levels, with amphibole partitioning HREEs at midcrustal depths. Garnet exerted only a minor influence, reflecting its decreasing stability under shallower melting conditions. Moderate recrystallization and limited metasomatic alteration further distinguishes the GG2 component from the GG1 component, reflecting its exposure to fewer hydrothermal or fluid-related processes. Despite this, localized REE enrichment still occurred due to

some degree of fractionation and postemplacement fluid activity. However, pegmatites associated with the GG2 component also contributed to localized REE enrichment. These pegmatites, although less enriched in REEs than those related to the GG1 component, still show some degree of fractionation and REE concentration, particularly in areas with enhanced plagioclase fractionation.

The GG3 component, with positive Eu anomalies and low TREO values (Figure 27a), represents a less evolved, primitive magma where plagioclase accumulation dominated over fractionation. The lower alteration levels and minimal REE concentrations in the GG3 component suggest limited potential for significant REE enrichment, although the presence of REE-enriched pegmatites derived from the other GG components emphasizes the broader REE potential of the Andrew Lake study area.

The REE concentrations in the Andrew Lake study area were therefore heavily influenced by the magmatic evolution of the GG1 and GG2 components and the associated pegmatites. The advanced magmatic differentiation of the GG1 component, coupled with high La^{ch}/Yb^{ch} ratios and strong REE enrichment, reflects significant crustal evolution; later metasomatic alteration and pegmatite intrusion enhanced REE concentrations. The GG2 component shows moderate REE enrichment, benefiting from both magmatic differentiation and localized fluid-driven alteration, with pegmatites also contributing to the REE budget. The GG3 component, although less evolved, exhibits minimal REE enrichment, though pegmatitic intrusions may still have played a role in localized REE mineralization across the area.

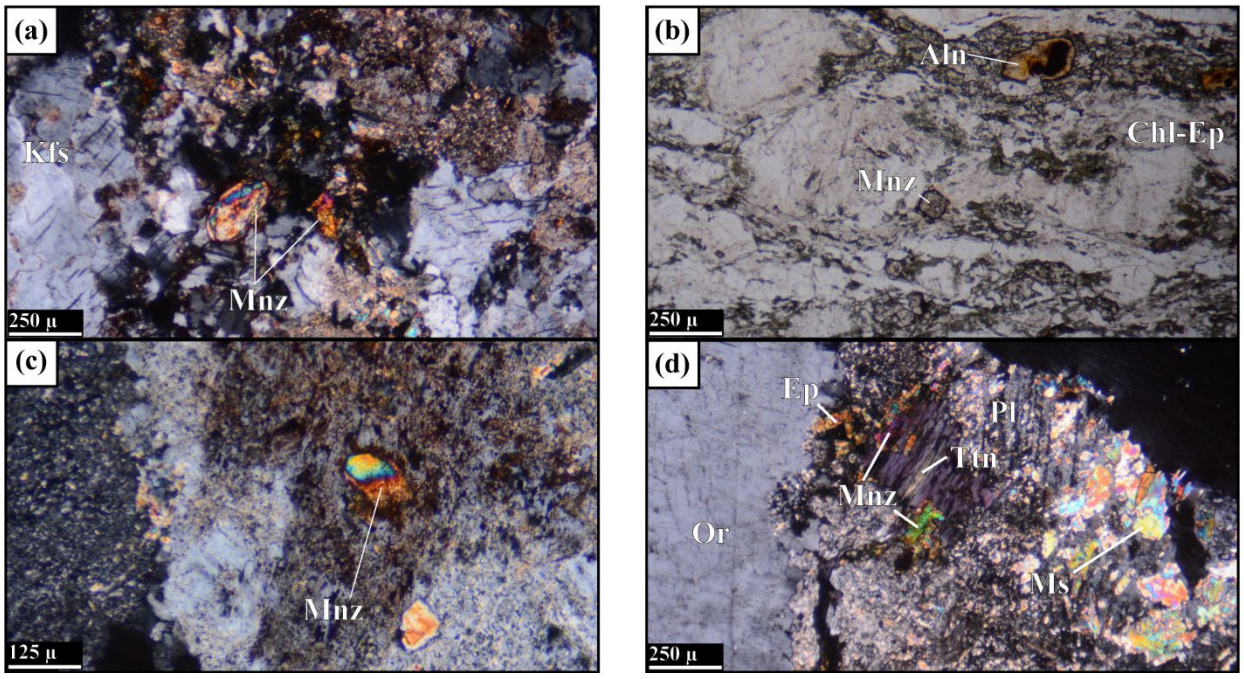

Figure 32. Photomicrographs of thin sections, Andrew Lake study area, northeastern Alberta: (a) monazite (Mnz) hosted within derived granite gneiss (GG) of the GG1 component (sample AL-23-2128-1; cross-polarized light [XPL]); (b) metamict allanite (Aln) hosted within granitic cataclasite of the Bayonet Lake shear zone, aligned parallel to fabric elements (sample AL-23-2145-1; plane-polarized light [PPL]); (c) monazite hosted within feldspar in light rare-earth-element (LREE)–enriched pegmatite with a significant negative Eu anomaly, note the immense degree of alteration (sample AL-23-1117-1; XPL); (d) monazite and titanite (Ttn) in LREE-enriched pegmatite with a significant negative Eu anomaly, concentrated with chlorite and minor epidote (Ep) within an extremely altered grain of plagioclase (Pl), replaced with muscovite (Ms), sericite, and chlorite, adjacent orthoclase (Or), minor talc is present in the matrix (sample AL-23-2126-1; XPL). Abbreviation: Kfs, K-feldspar.

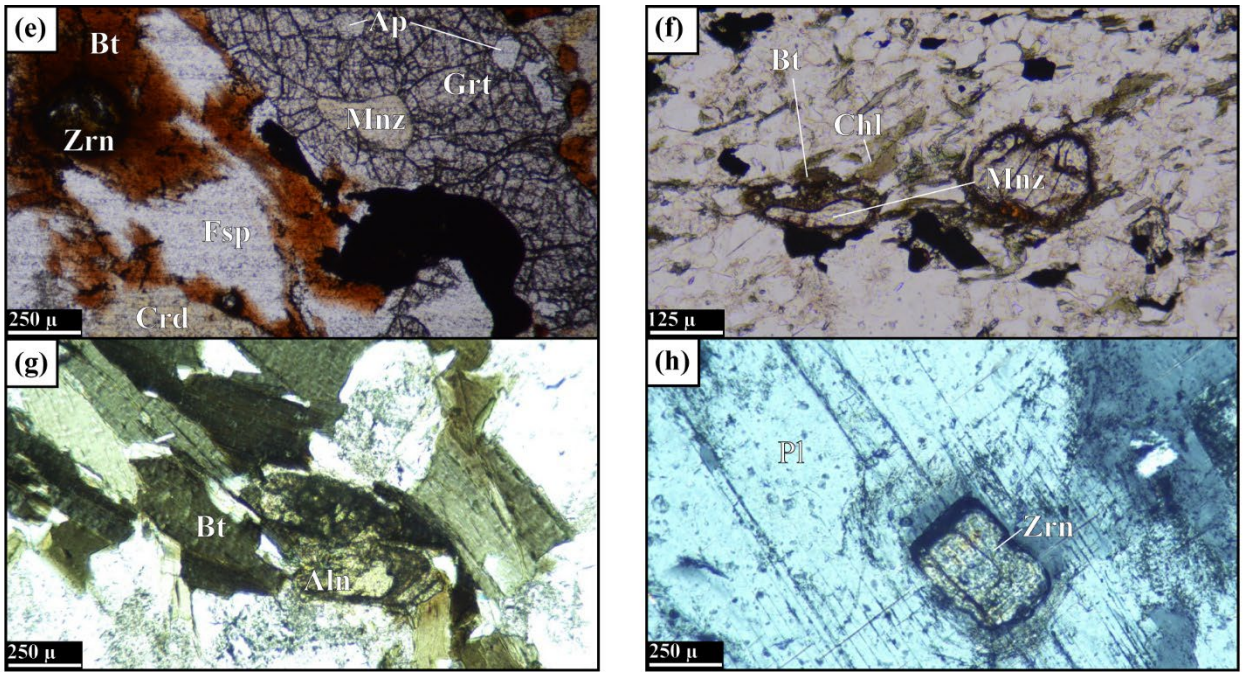

Figure 32 (continued). Photomicrographs of thin sections, Andrew Lake study area, northeastern Alberta: (e) metasedimentary rocks of the Rutledge River complex (RRC), exhibiting monazite (Mnz) and apatite (Ap) hosted within garnet (Grt), adjacent zircon (Zrn)-bearing biotite (Bt), feldspar (Fsp), and cordierite (Crd; sample AL-23-2076-2; PPL); (f) monazite concentrated with biotite and chlorite (Chl) in metasedimentary rocks of the RRC (sample AL-23-2151-1; PPL); (g) yellow zoned allanite (Aln) crystals (centre) with a metamict nature and radiation damage to the surrounding biotite (sample AL-23-1130-2; PPL); (h) zircon with internal zonation imbedded in plagioclase (Pl) with notable radiation damage, exhibited by distinctive anastomosing radiation cracks (sample AL-23-1130-2; XPL).

Beyond the granite gneiss units, the metasedimentary paragneiss of the RRC hosts significant radiogenic mineral assemblages, including monazite and allanite, which indicate an additional source of REEs in the Andrew Lake area (Figure 32e and f). Petrographic observations reveal monazite grains intimately associated with garnet, biotite, and feldspar, suggesting that regional metamorphism and partial melting processes liberated and subsequently concentrated REEs within these metasedimentary sequences. The presence of monazite, in particular, underscores the potential for REE enrichment during both the prograde and retrograde stages of metamorphism, as fluids and melts remobilized incompatible elements into discrete radiogenic phases. Notably, similar monazite-rich assemblages have not been observed in the metasedimentary rocks of the RRC in the Leland Lakes area, suggesting that REE redistribution processes were either localized to the Andrew Lake region, or the sedimentary protolith of these rocks derived its materials from REE-enriched sources during basin development.

6.5 Geochemistry of Mafic Metamorphic Rocks

Mafic metamorphic rocks are chemically complex and variable due, in part, to the wide abundance of protoliths that they may represent, including volcanic rocks, from basalt to andesite, gabbro, diorite, and mafic greywacke. Mafic rocks from the Leland Lakes and Andrew Lake study areas were mapped in the field and categorized lithologically as amphibolite (AMP), metagabbro (GB), metadiorite (DI), and mafic schist (MSCH). Discontinuous bands and fragments of mafic material were categorized in the field, based

on mineralogy and texture, as amphibolite enclave (AMPE), amphibolite phyllonite (AMPPH), amphibolite schlieren (AMPS), and gabbro enclave (GBE). The primary focus of geochemical sample collection and analysis was on larger units of amphibolite, metagabbro, metadiorite, and mafic schist. Sampling of small inclusions and enclaves of mafic rock was generally avoided due to the increased potential for contamination.

Note that mafic metamorphic rocks typically contain 45–60 wt. % SiO_2 and are relatively rich in MgO, FeO, CaO, and Al_2O_3 (Bucher and Frey, 2002). Any samples identified in the field as mafic but subsequently returned concentrations of >66 wt. % SiO_2 were excluded from this analysis. A typical set of Harker diagrams (Figure 33a–c) indicates that mafic rocks from the Andrew Lake study area have a much larger range of chemical compositions than those at Leland Lakes. Samples from the Andrew Lake study area have a much larger range of SiO_2 concentrations and generally have higher Al_2O_3 and Na_2O concentrations and lower Fe_2O_3, MgO, and CaO concentrations. These geochemical differences can also be seen in box plots from the two areas (Figure 34). The geochemical differences between the two study areas can be further explored by examining the trace-element geochemistry

Rock classification through geochemical discrimination was done exclusively using trace-element plots that included elements generally considered to be resistant to mobilization during metamorphic and hydrothermal processes (Cann, 1970). The Nb/Y versus Zr/Ti volcanic rock plot of Pearce (1996), modified after Winchester and Floyd (1977), indicates that most samples from the Leland Lakes study area have a geochemical character most similar to typical basalts (Figure 35). The Andrew Lake study area samples have a larger spread on this chart with numerous samples plotting in the basalt and intermediate field of andesite and basaltic andesite. A small number of samples from both areas plot in the alkali basalt field. Sample LL-23-1069-2, a magnetite-rich mafic schist that was identified in the field (Leland Lakes study area) as being a sheared amphibolite, has an anomalously low Zr/Ti ratio and plots at the bottom of the alkali basalt field (Figure 35). Sample AL-23-2125-2 from the Andrew Lake study area is an amphibolite with an anomalously high Zr/Ti ratio and elevated SiO_2 and Na concentrations, and an exceptionally low Fe_2O_3 concentration; it plots in the trachyte field (Figure 35).

Trace-element diagrams were employed to examine the potential tectonic setting of selected mafic rocks from the Leland Lakes and Andrew Lake study areas. Leland Lakes amphibolite samples (n = 22) plot within the ocean-floor basalt field on the Ti-Zr-Y diagram (Figure 36) of Pearce and Cann (1973). This field encompasses mid-ocean ridge basalt, island-arc tholeiite, and calcalkali basalt. Chondrite normalized REE patterns for the amphibolite samples are displayed in Figure 37a. A generally negative slope is consistent with LREE enrichment. The N-MORB normalized REE pattern (Figure 37b) also displays this LREE enrichment, along with a generally flat MORB-like HREE trend. A portion of samples display a clear negative Eu anomaly that typically indicates fractional crystallization of plagioclase from the magma. These samples could potentially represent a separate mafic source from the majority of the sample population from the Leland Lakes study area.

.

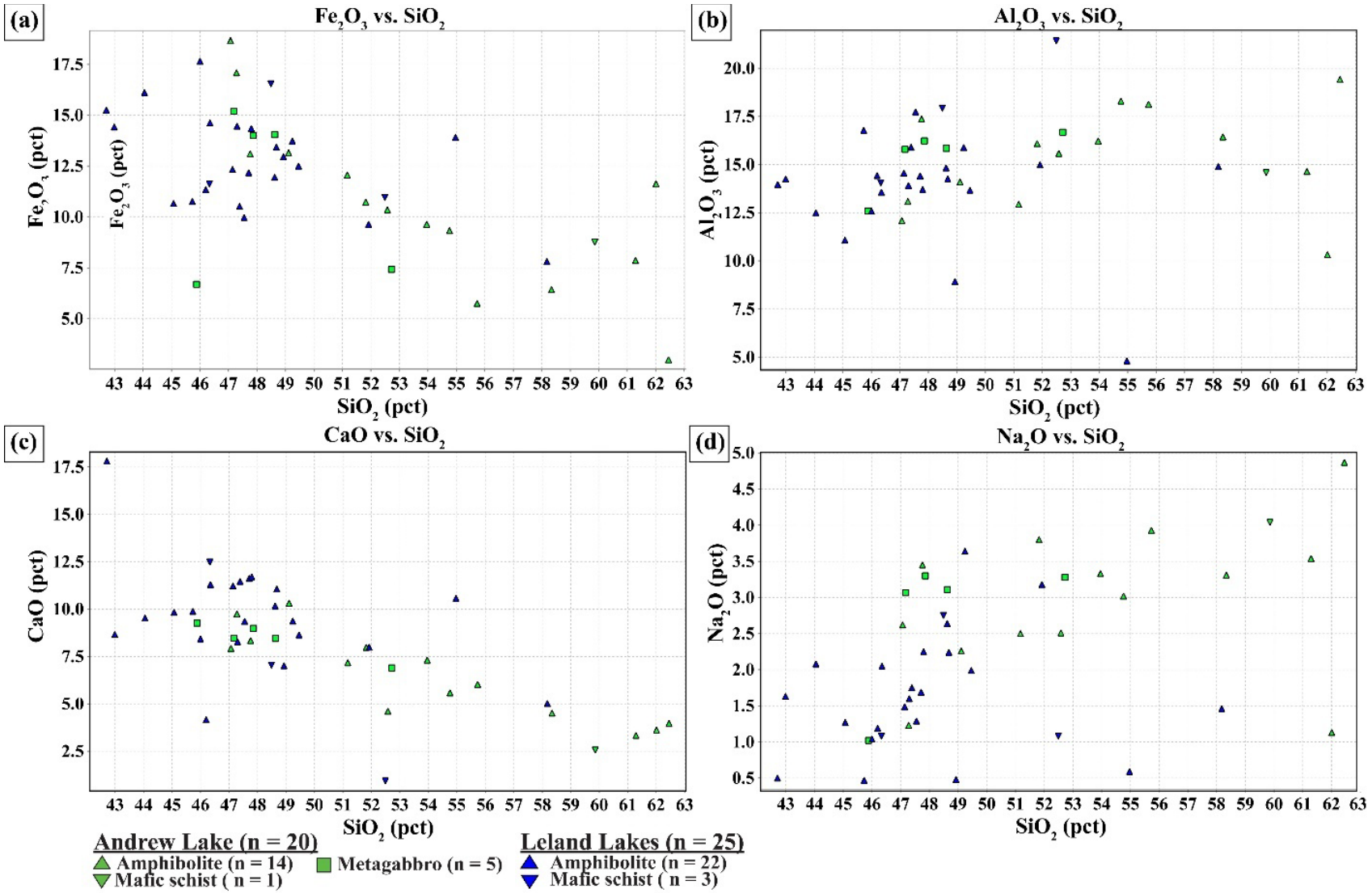

Figure 33. Binary plots displaying SiO_2 versus major elements for selected mafic rock samples from the Leland Lakes and Andrew Lake study areas, northeastern Alberta: (a) Fe_2O_3 versus SiO_2; (b) Al_2O_3 versus SiO_2; (c) CaO versus SiO_2; (d) Na_2O versus SiO_2. The Andrew Lake study area samples have a clear trend towards higher SiO_2, Al_2O_3, and Na_2O concentrations, with lower Fe_2O_3 and CaO concentrations than the Leland Lakes study area samples. Abbreviation: pct, per cent.

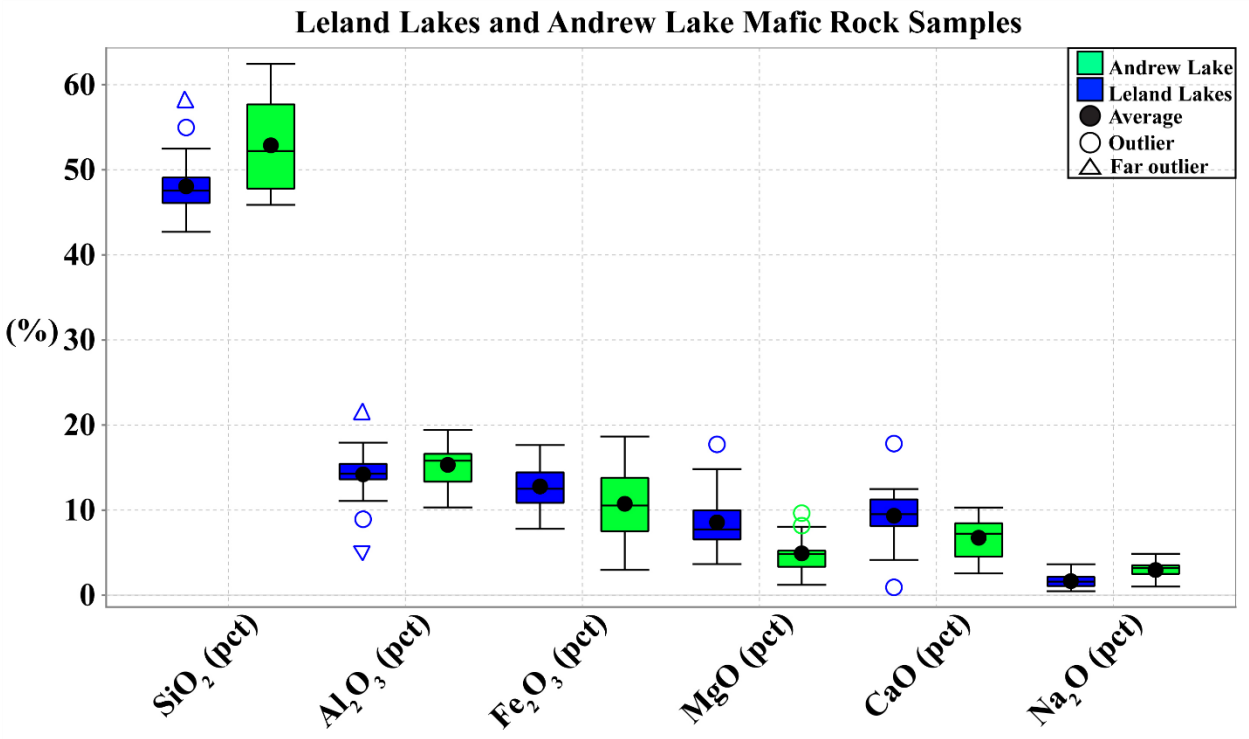

Figure 34. Box and whisker plots displaying the percentage of major elements (SiO_2, Al_2O_3, Fe_2O_3, MgO, CaO, and Na_2O) in selected mafic rock samples from the Leland Lakes (blue, n = 25) and Andrew Lake (green, n = 20) study areas, northeastern Alberta. Note that Andrew Lake samples have higher SiO_2, Al_2O_3, and Na_2O concentrations and lower Fe_2O_3, MgO, and CaO concentrations than those from Leland Lakes. Abbreviation: pct, per cent.

The mafic samples collected in the Andrew Lake study area have a much larger range of geochemical compositions compared to those at Leland Lakes (Figure 35). This diversity likely represents multiple periods of mafic magmatism in this area. Three of these samples (AL-23-1181-1, AL-23-1185-1, and AL-23-1185-2) were collected from a single large distinctive gabbroic body that extends for several hundred metres south of Andrew Lake, within the Taltson basement gneiss. These samples have a well-defined pattern of LREE enrichment (Figure 38) that is matched by a subset of amphibolite samples (LL-23-1025-1, LL-23-1055-1, LL-23-2041-2, and LL-23-2059-2) collected from within the Taltson basement gneiss in the Leland Lakes study area. The near-identical REE patterns, combined with similar Zr/Ti and Nb/Y ratios, suggests that there was a similar period of mafic magmatism in the Taltson basement in both the Leland Lakes and Andrew Lake study areas.

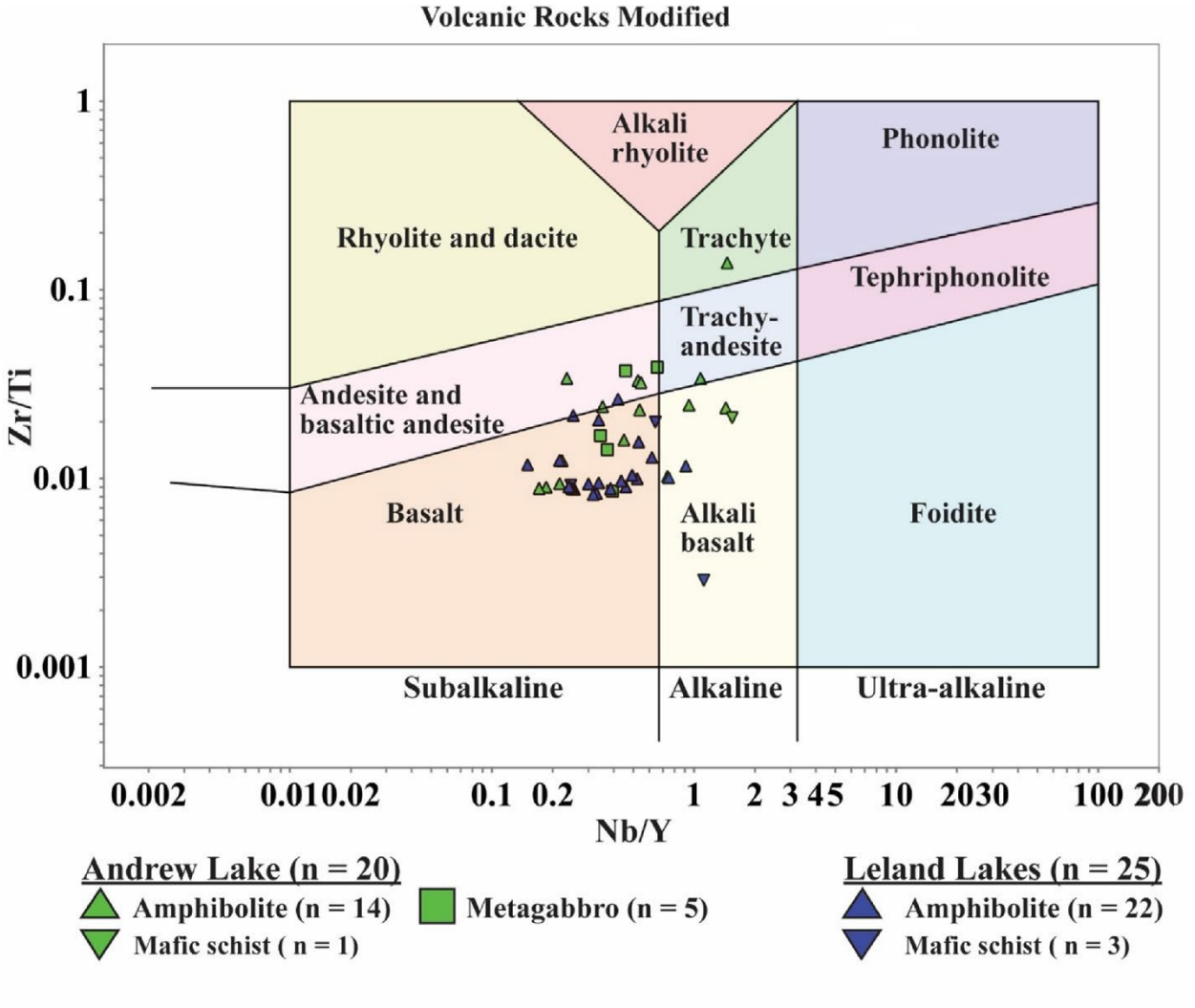

Figure 35. A Zr/Ti versus Nb/Y trace-element rock classification diagram (Pearce, 1996, modified after Winchester and Floyd, 1977) for selected mafic rock samples from the Leland Lakes (blue, n = 25) and Andrew Lake study areas (green, n = 20), northeastern Alberta.

6.6 Geochemistry of Metasedimentary Rocks

Metasedimentary rocks in the study area are primarily represented by quartz-rich schists and gneisses with variable amounts of feldspar, biotite, muscovite, garnet, sillimanite, and graphite. Sixty-eight samples collected as part of field studies were ascribed to the Rutledge River complex. Many of these samples are mylonitic, tectonized, or significantly altered. Only 41 samples were selected for detailed geochemical analysis since they were identified as paragneisses and lack probable contamination. Field and petrographic examination of the metasedimentary rocks in the Leland Lakes study area indicated that they have a higher proportion of garnet and mica, and a lower proportion of quartz and feldspar, than those in the Andrew Lake study area. The mineralogical discrimination methods for metamorphosed clastic sedimentary rocks (Maxeiner et al., 1999) indicate that there is a predominance of pelite in the Leland Lakes study area and psammite and psammopelite in the Andrew Lake study area. Major-element geochemistry reflects these mineralogical differences (Figure 39), with metasedimentary rock samples from the Leland Lakes study area having overall lower SiO_2 and higher Al_2O_3 and Fe_2O_3 concentrations.

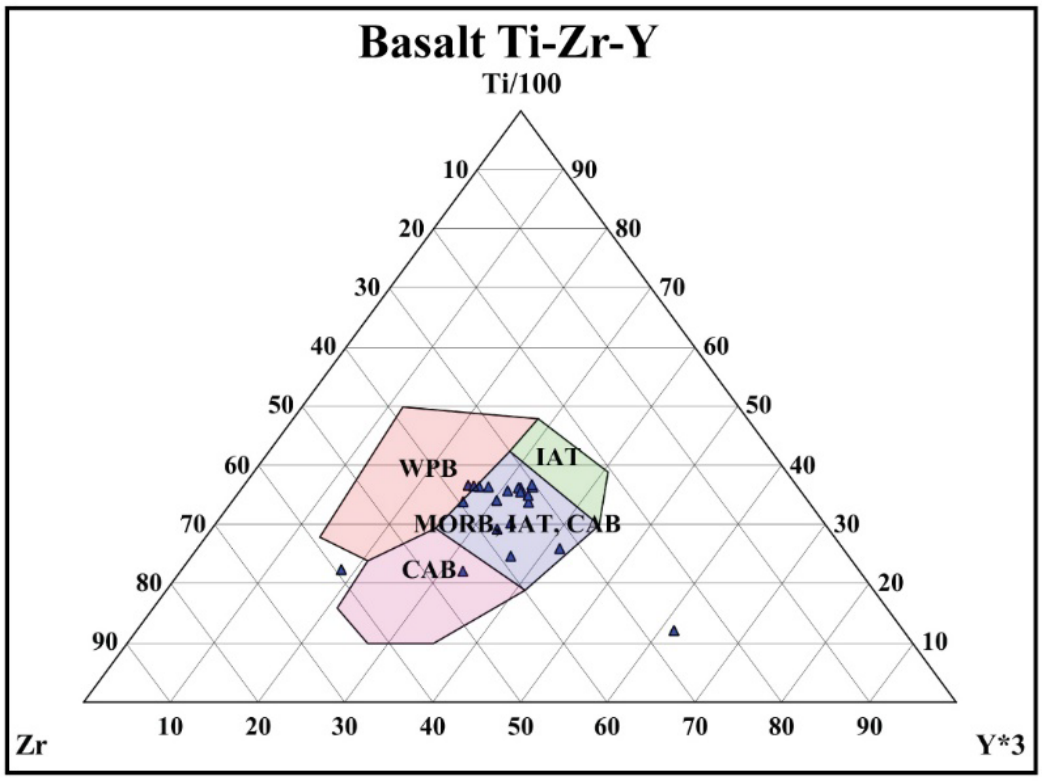

Figure 36. A Zr versus Ti/100 versus Y*3 ternary trace-element rock classification diagram (after Pearce and Cann, 1973) showing the majority of selected amphibolite samples (n = 22) from the Leland Lakes study area (northeastern Alberta) plot within the ocean-floor basalt field, labelled here as MORB (mid-ocean ridge basalt), IAT (island-arc tholeiite), and CAB (calcalkali basalt). Abbreviation: WPB, within-plate basalt.

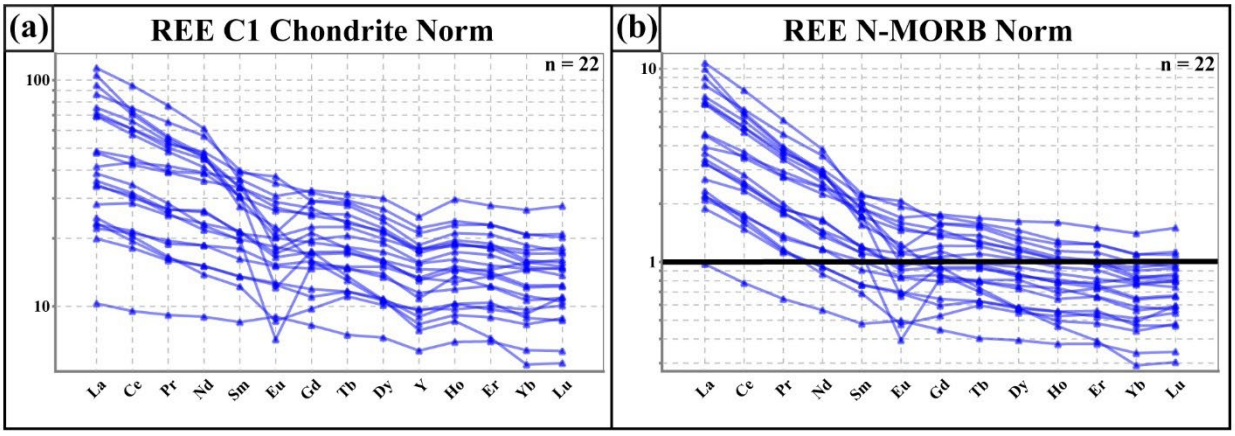

Figure 37. Chondrite-normalized (Norm) and normal (N-type) mid-ocean ridge basalt (N-MORB)–normalized plots of selected trace elements (rare-earth elements [REEs]) for selected amphibolite samples from the Leland Lakes study area, northeastern Alberta: (a) chondrite-normalized plot (normalizing values from McDonough and Sun, 1995); (b) N-MORB–normalized plot (normalizing values from Sun and McDonough, 1989).

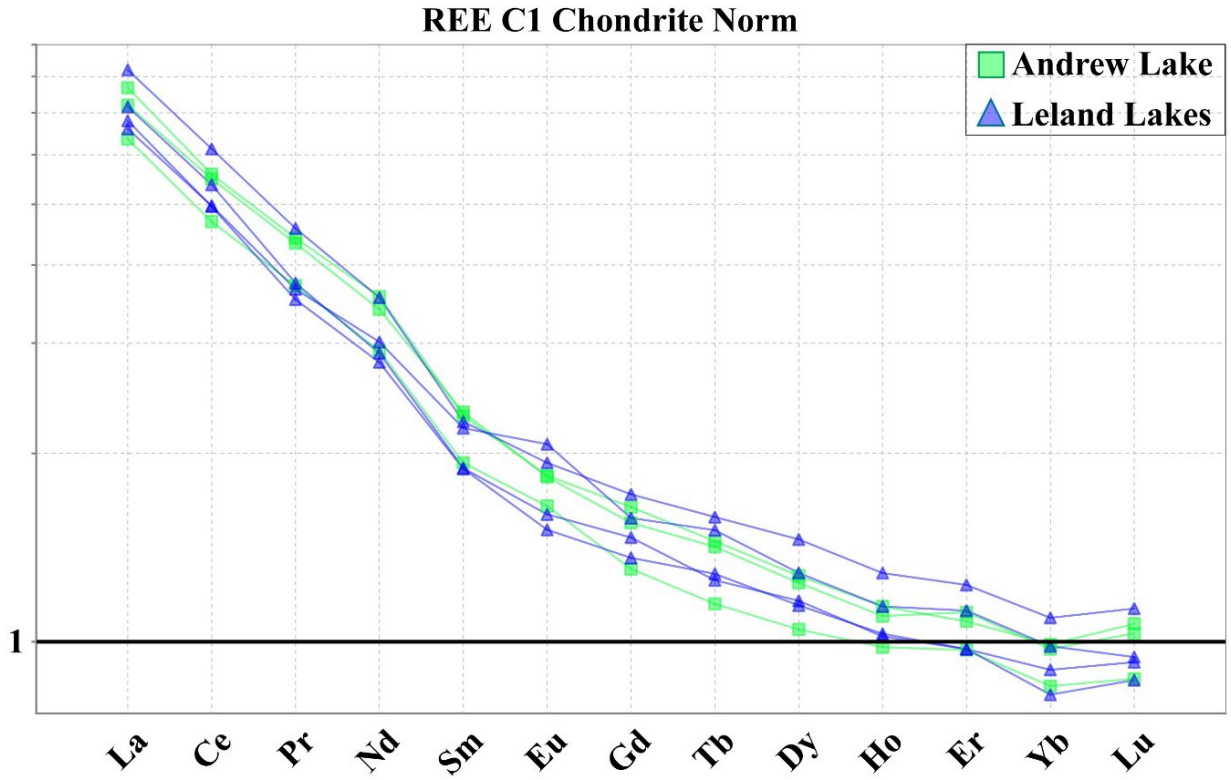

Figure 38. A C1 chondrite-normalized (Norm) plot of selected trace elements (rare-earth elements) for three samples from a large gabbroic body within the Taltson basement gneiss in the Andrew Lake study area (green squares) as well as four mafic amphibolite samples found within the quartzofeldspathic basement gneiss in the Leland Lakes study area (blue triangles), northeastern Alberta. Normalizing values from Sun and McDonough (1989).

The chondrite-normalized REE plot (Figure 40a) for the metasedimentary rocks displays typical LREE enrichments and negative Eu anomalies consistent with derivation from upper continental crust. Samples roughly lie within the REE geochemical field of post-Archean average Australian sedimentary rocks identified by Taylor and McLennan (1981; Figure 40a). Normalizing sample REEs to the North American shale composite of Gromet et al. (1984) yields a relatively flat pattern for the majority of samples (Figure 40b). This pattern highlights the similarity of the Leland Lakes and Andrew Lake metasedimentary rocks to more modern continental-derived sedimentary rocks, which tend to have an average geochemistry similar to granodiorite (Gromet et al., 1984).

Two Leland Lakes channel samples (LL-23-1064-C1 and -C2), which were collected at an outcrop of garnet-rich paragneiss, yielded high gamma-ray readings and possessed much higher LREE values compared to the other paragneiss samples from the study areas (Figure 40a and b). Petrographic analysis of a sample from this outcrop indicates that the paragneiss at this location contains 50–60% garnet and 35–50% quartz, minor biotite, and trace zircon.

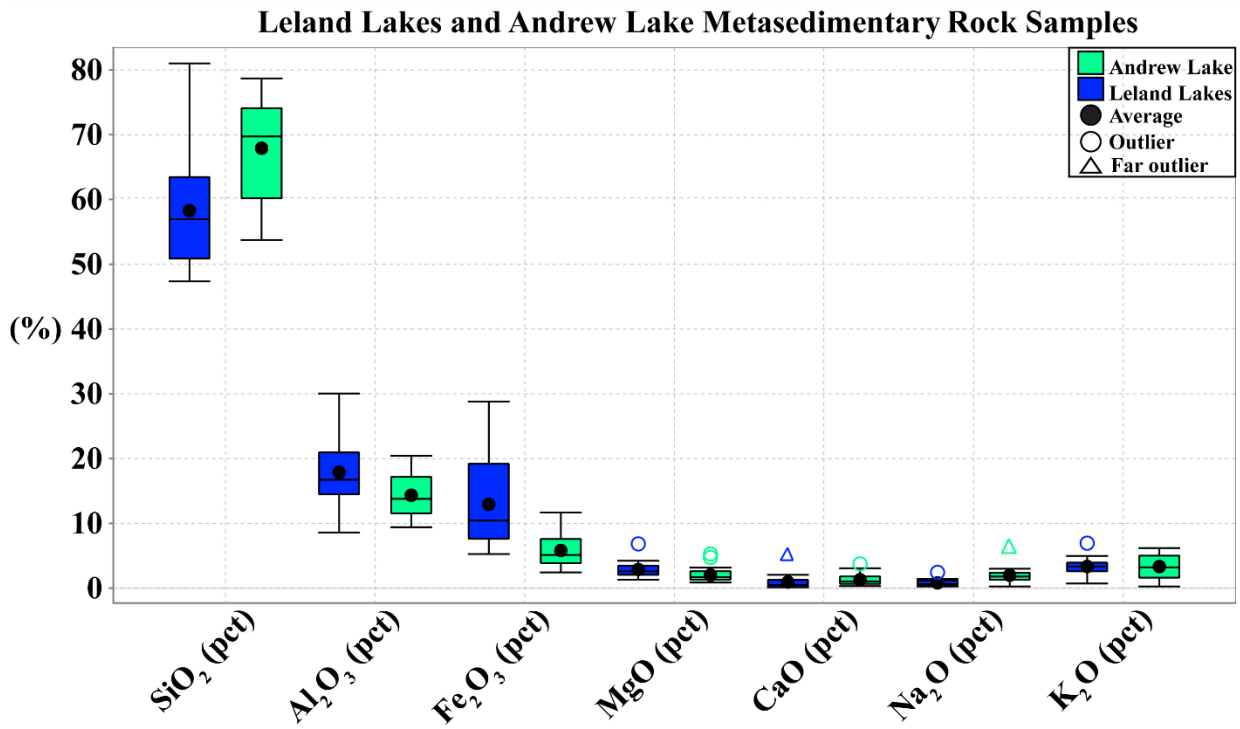

Figure 39. Box and whisker plots displaying the percentage of major elements (SiO_2, Al_2O_3, Fe_2O_3, MgO, CaO, Na_2O, and K_2O) in selected metasedimentary rock samples from the Leland Lakes (blue, n = 17) and Andrew Lake (green, n = 24) study areas, northeastern Alberta. Abbreviation: pct, per cent.

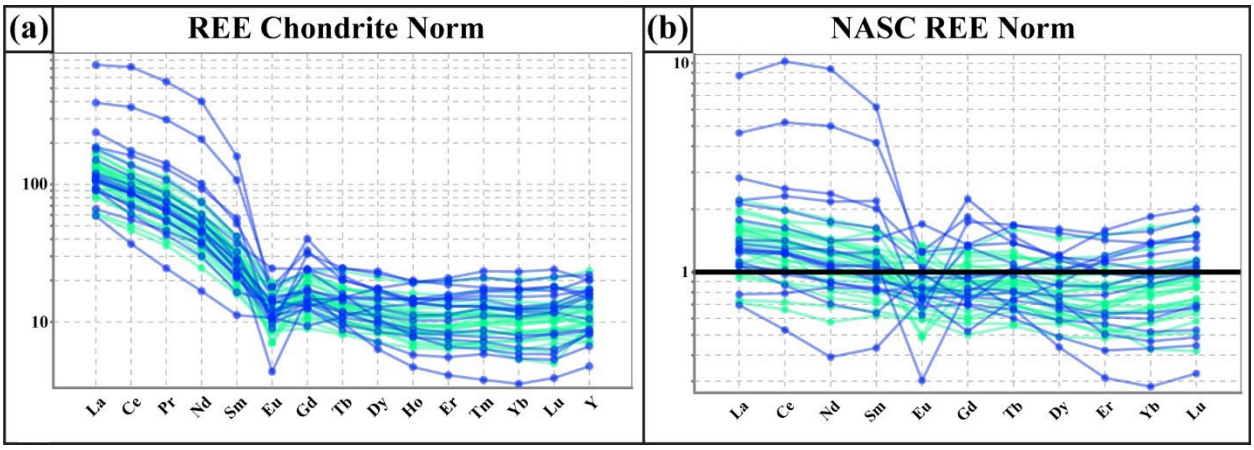

Figure 40. Rare-earth-element (REE) normalization plots for selected metasedimentary rock samples from the Leland Lakes (blue, n = 17) and Andrew Lake (green, n = 24) study areas, northeastern Alberta: (a) chondrite-normalized (Norm) REE plot (normalizing values from Taylor and McLennan, 1985); (b) North American shale composite (NASC)–normalized REE plot (normalizing values from Gromet et al., 1984).

7 Discussion of Critical Mineral Potential

As highlighted in Section 2.4.2, historical exploration work in the region has primarily focused on uranium and precious metals exploration. The current global focus on critical minerals, exemplified by initiatives in Alberta and Canada, has raised awareness of these important commodities and triggered an increase in mineral exploration.

The Leland Lakes and Andrew Lake study areas offer excellent exploration potential due to the large extent of exposed Canadian Shield and presence of numerous critical mineral occurrences. Although the critical mineral potential of the exposed Canadian Shield in Alberta includes an array of critical minerals and metals, this report is focused on three major suites deemed to be significant: (1) granite- and pegmatite-hosted REE and lithium, (2) structurally controlled / fluid-related uranium and minor REE, and (3) mafic-associated critical metals, including copper, nickel, chromium, and cobalt.

7.1 Granitoid- and Pegmatite-Hosted REEs and Lithium

Granitoids and pegmatites are typically enriched in rare elements, though the degree of enrichment is dependent on a wide variety of factors including the source melt and emplacement setting. Rare-earth-element contents that are at least three times that of the average upper continental crust are of interest for REE exploration (McLennan, 2001). One of the major goals of this field program was to assess the pegmatite-hosted critical mineral potential in the region.

Pegmatites are defined as a texturally distinct subdivision of much more voluminous igneous rocks (London and Kontak, 2012). They represent the final stages of crystallization of granitic magmas and are important sources of rare elements, including lithium (Li), cesium (Cs), tantalum (Ta), and REEs. The remarkable texture of pegmatites is thought to be a product of processes that concentrate a rich variety of elements to values thousands of times higher than average crustal abundances (London and Kontak, 2012). The high concentration and purity of rare elements, combined with a large grain size, make pegmatites an excellent exploration target (Černý, 1991). Rare-element pegmatites in the Superior Province, noted by Selway et al. (2005), occur along large regional-scale fault structures in greenschist- and amphibolite-facies metamorphic terranes. However, Linnen et al. (2012) indicated that field relationships, mineral chemistry, and experimental constraints suggest that the critical elements are predominantly concentrated by magmatic processes. Pegmatitic rocks in the study areas can be subdivided into three types based on structural setting: (1) cross-cutting pegmatitic granite dikes, (2) narrow pegmatitic granite sheets that are parallel to the main foliation, and (3) pegmatitic phases of larger intrusions.

Moreover, pegmatites can be classified based on their mineralogical and geochemical characteristics. In the context of critical mineral exploration, certain important classes are recognized:

1) LCT (lithium-cesium-tantalum) pegmatites: these pegmatites are enriched in Li, Cs, Ta, and commonly contain significant concentrations of other rare elements such as beryllium (Be), rubidium (Rb), and tin (Sn). They are typically associated with S-type granites derived from the partial melting of sedimentary rocks and are often found in orogenic belts related to continental collision zones (Černý, 1991; Selway et al., 2005). The LCT pegmatites are important sources of lithium minerals such as spodumene, petalite, and lepidolite, as well as tantalum minerals such as tantalite and microlite. A prime example of an LCT pegmatite is at the Tanco mine in Manitoba, Canada, which is one of the world's largest producers of cesium-, tantalum-, and lithium-bearing minerals (Černý et al., 1981).
2) NYF (niobium-yttrium-fluorine) pegmatites: these pegmatites are enriched in elements such as Nb, Y, F, U, Th, and HREEs. They are typically associated with A-type granites formed in anorogenic settings and are less common than LCT pegmatites (Černý and Ercit, 2005). For example, the Rutherford pegmatite in Virginia, United States, is a well-known NYF-type pegmatite enriched in Nb, Ta, and REEs (Wise and Brown, 2010).

3) Abyssal pegmatites: although abyssal pegmatites are generally not considered economically viable due to their typically low concentrations of rare elements, there are notable exceptions where these deep-crustal formations exhibit significant enrichment in REEs. In the context of the Leland Lakes and Andrew Lake study areas, the Alces Lake REE project, located approximately 120 km east of the Andrew Lake area in northwestern Saskatchewan, is a remarkable example of abyssal pegmatites enriched in REEs. The mineralized zones at this project exhibit exceptionally high concentrations of REEs, particularly neodymium and praseodymium, compared to global REE occurrences (Workman, 2023).

7.1.1 Regional REE Deposits and Projects

7.1.1.1 Alces Lake REE Project

The Alces Lake REE-Th-U mineralization zones exhibit notable rare-earth concentrations relative to global occurrences. Of the prospects discovered so far, 19 are considered high grade compared to other global REE occurrences (Workman, 2023). These zones are located within the Beaverlodge domain, a polydeformed terrane within the Rae craton, which was overprinted by mid- to high-pressure amphibolite- and granulite-facies metamorphism (Bethune et al., 2013). Recent exploration has revealed multiple mineralization zones with TREO concentrations exceeding 30% over significant widths (Workman, 2023). The Alces Lake mineralization is structurally controlled, with REEs associated with polyphase anatectic processes linked to major orogenic events that led to the mobilization and concentration of REE-bearing minerals such as monazite and allanite. The mineralized pegmatites were emplaced within or near the Archean–Paleoproterozoic transition zone, which marks a boundary between crustal terranes of different ages dating to ca. 2.5 Ga. This zone, where Archean and Paleoproterozoic rocks interacted, provided a favourable structural and rheological environment for the emplacement of REE-enriched pegmatites. These pegmatites formed under midcrustal pressure-temperature (P-T) conditions and occur as polyphase anatectic pods, boudins, and zones near this transition (Poliakovska et al., 2022). The mineralized pegmatites represent the final stages of crystallization of the granitic- to residual-melt / cumulate magma and are very strongly enriched (>>10000x chondrites) in LREE and relatively fractionated in HREE with significant negative Eu anomalies. Their emplacement and associated distribution of monazite were controlled by shear zones, faults, and folds in combination with lithological contacts and rheological contrasts (Poliakovska et al., 2023).

7.1.1.2 Nechalacho REE Deposit

Another significant REE deposit in Canada is the Nechalacho (previously known as Thor Lake) REE deposit, located in the Northwest Territories. The Nechalacho deposit is one of the largest undeveloped REE resources globally and is hosted within peralkaline syenite and nepheline syenite intrusions of the Blatchford Lake complex (Sheard et al., 2012). The deposit is enriched in both light and heavy REEs, with significant concentrations of neodymium (Nd), praseodymium (Pr), dysprosium (Dy), and terbium (Tb).

The mineralization at the Nechalacho deposit is associated with multiple phases of magmatic intrusion and hydrothermal alteration. Rare-earth-element minerals such as bastnäsite, monazite, allanite, and xenotime are present, often associated with zircon, fergusonite, and other Nb-Ta minerals. The deposit is subdivided into several zones, with the Upper Zone being enriched in LREEs and the Basal Zone being enriched in HREEs (Sheard et al., 2012).

7.1.2 REE-Enriched Pegmatite Potential in the Andrew Lake Study Area

Pegmatites in the Andrew Lake study area show many similarities to those in the Alces Lake area, including emplacement into an Archean and Paleoproterozoic basement that has undergone mid- to high-grade metamorphism. In addition, the sampled pegmatites with the most REE-enrichment at Andrew Lake exhibit strong enrichment in LREE, relative depletion in HREE, and significant negative Eu anomalies. Field relationships, spectrometer readings, petrography, and geochemical data indicate that the

REEs in these rocks are associated with elevated concentrations of Th, U, and Zr that are hosted in monazite, allanite, zircon, and titanite within pegmatites that crystallized from granitic to residual melt / cumulates (Figure 32c and d), classifying these pegmatites as within the abyssal-LREE (U, Th, Ti) subclass after Černý and Ercit (2005). Furthermore, these pegmatites represent polyphase anatectic melt/cumulates that were emplaced both parallel to, and cross-cutting, the dominant fabric ($S_{1\text{-}2}$). Locally, pegmatites in the Andrew Lake study area were emplaced along, or near, fold axial planes, shear zones, and faults, which exhibit transitions from ductile to brittle behaviour, exploiting planes of anisotropy linked to regional polyphase deformation.

The trace-element patterns of these pegmatites are remarkably similar to the enriched trend of granite gneisses (GG1 samples, in particular), as well as the older basement gneisses. The most likely origin of these pegmatites involved partial melting of the TBC, augmented by anatectic contributions from metasedimentary rocks of the RRC, followed by migration of the melt to structurally favourable zones, and subsequent fractional crystallization. As the GG unit of the TBC in the Andrew Lake area yielded a single U-Pb date of 2.3 Ga (McNicoll et al., 2000), derived pegmatites could be linked to multiple phases of partial melting, beginning with the Arrowsmith orogeny (~2.3 Ga), followed by remobilization during the subsequent Taltson orogeny (~2.0–1.9 Ga). Such successive orogenic phases may have enhanced REE concentrations through progressive partial melting. These LREE-enriched pegmatites appear as dikes, layers, and locally boudinaged lenses and pods. Observations of zoned and feldspar-hosted monazites suggest metasomatic processes may have played a significant role in remobilizing REEs, similar to what happened at Alces Lake (Normand, 2014; Poliakovska et al., 2022).

However, despite these similarities, the Andrew Lake pegmatites exhibit significantly lower REE concentrations than those at Alces Lake. This difference may be attributed to a combination of factors. The pegmatites at Andrew Lake likely formed from partial melting of the TBC and metasedimentary rocks, which may have been less enriched in REEs compared to the source material at Alces Lake. Additionally, monazite-rich restite may have remained in the source region during partial melting, limiting the amount of REEs incorporated into the melt. There are a number of reasons similar occurrences have not been noted in Alberta. Firstly, economic REE-bearing restite zones are small and potentially topographically recessive. Given the lack of detailed REE-targeted exploration in northeastern Alberta, these zones could remain undiscovered. Additionally, these zones may be under cover in topographic lows or were emplaced deeper in the subsurface in favourable structures. Secondly, metasomatic processes that may have played a significant role in concentrating REEs at Alces Lake seem to have been less efficient at Andrew Lake, which could contribute to lower concentrations of REEs in the Andrew Lake pegmatites. Lastly, the structural environment at Alces Lake, with its extensive faulting and shearing along the limbs of a major, regional-scale fold structure, may also have been more conducive to concentrating REE-rich melts (Poliakovska et al., 2023).

7.1.3 Newly Identified REE Occurrences in the Study Areas

Previous geochemical investigations by Godfrey (1986) identified several REE anomalies in the study areas. To build upon Godfrey's work, his samples were reanalyzed to verify and enhance the existing geochemical data (Meek et al., 2023). During fieldwork, efforts were made to visit as many of these anomalies as possible, however, due to logistical challenges, such as difficult terrain and limited accessibility, only a small subset of the anomalies could be examined directly in the field.

In general, the bedrock west of the LLSZ had few samples with elevated REEs (Figure 41a). However, areas containing surface expressions of the TBC hosted abundant REE anomalies. Within the Andrew Lake study area, the highest REE values were recorded in samples along the north-south-trending BLSZ, along the northwest-southeast-trending Bonny Fault, and along the E-W arm (Figure 41b).

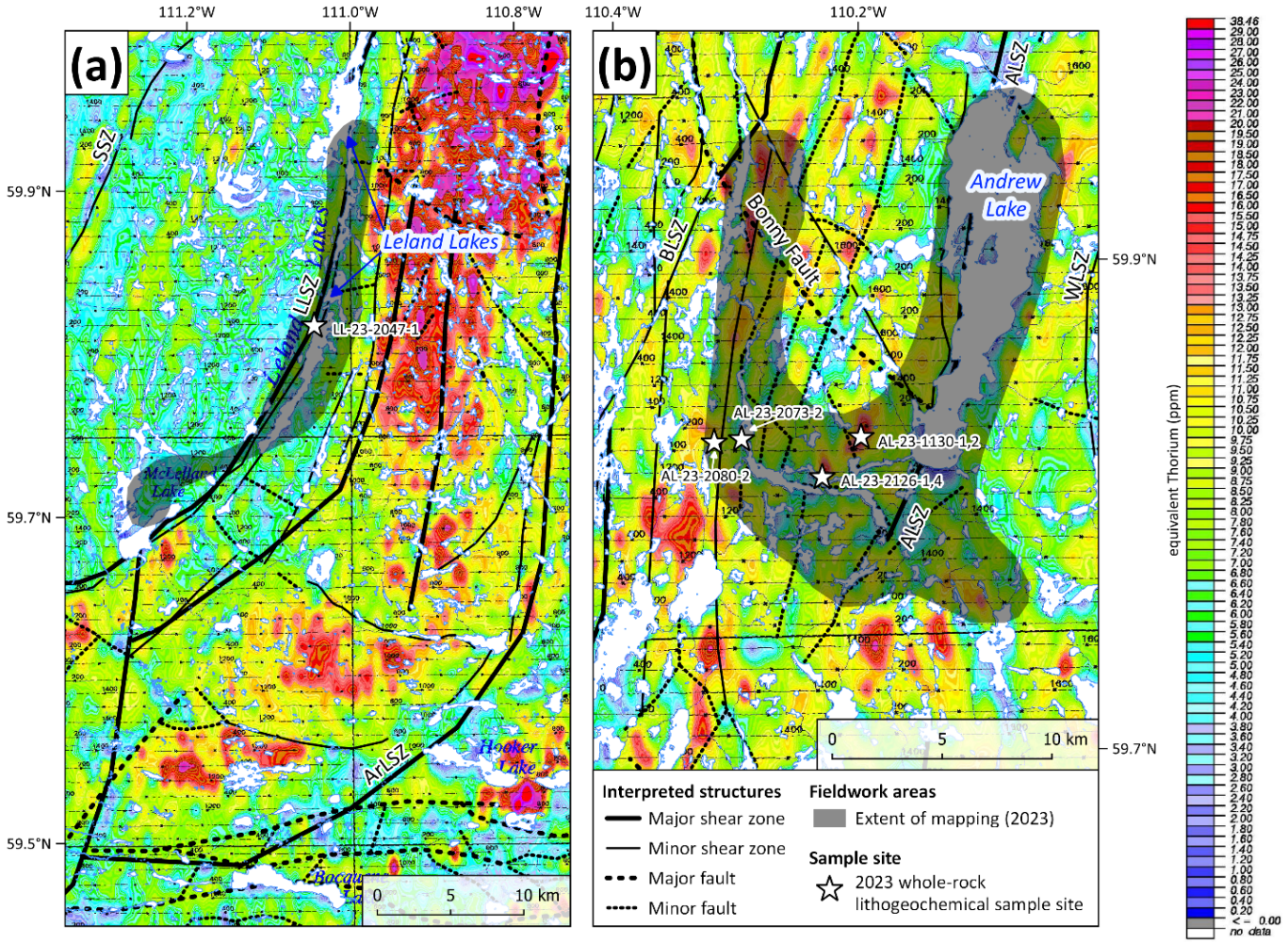

Figure 41. Equivalent thorium (eTh) radiometric maps of northeastern Alberta (adapted from Charbonneau et al., 1994): (a) Leland Lakes study area, note the concentration of elevated values in the northern portion of the study area where the Arch Lake granitoid is flanked by the Leland Lakes shear zone (LLSZ) on the west and the Arch Lake shear zone (ArLSZ) to the east; (b) Andrew Lake study area. Structural interpretations after Lopez et al. (2024). White stars indicate sites with the highest recorded rare-earth-element values. Abbreviations: ALSZ, Andrew Lake shear zone; BLSZ, Bayonet Lake shear zone; SSZ, Slave shear zone; WLSZ, Waugh Lake shear zone.

7.1.3.1 Andrew Lake Study Area

The E-W arm is of particular interest because there are exposures of the TBC where several REE mineral occurrences have been reported (Langenberg et al., 1993; Pană and Prior, 2010; Lopez et al., 2020). Notably, this area hosts five intrusion-related REE occurrences originally discovered by North American Gem Inc. (Smith and Griffith, 2007). Three of these occurrences were recorded as pegmatite hosted and two of them were indicated to be gneiss hosted. A thorium-rich, uranium-poor, pegmatite zone exposed in two trenches on the north shore of the E-W arm yielded high REE values (Pană and Prior, 2010, location 6, samples 6607 and 6608); values of 1010 ppm La and 1850 ppm Ce were recorded from a sample near the centre of the zone. At this location, the exposed outcrop comprises migmatitic-banded gneiss variably intruded by white, homogenous, and locally pegmatitic granodiorite. The host gneiss comprises metaluminous gabbroic diorite pertaining to the BG unit. The pegmatite zone yielded high magnetic susceptibility values as well as gamma-ray values of up to 10 000 counts per second (cps), relative to background values of 200–400 cps recorded within the banded gneiss and the granodiorite components, which are oriented near parallel to the dominant $S_{1\text{-}2}$ composite fabric.

A syenitic pegmatite sample (AL-23-2126-1; Figure 41b) collected from the eastern trench yielded values of 844 ppm La, 1600 ppm Ce, and 1190 ppm Th (Figure 42a). An additional syenitic pegmatite sample (AL-23-2126-4; Figure 41b) collected from the western trench yielded 589 ppm La, 1050 ppm Ce, 732 ppm Th, and elevated values of Pr, Nd, Sm, and Pb. This pegmatitic zone is located on the southern margin of a major equivalent thorium (eTh) high (Charbonneau et al., 1994), which correlates with an aeromagnetic high. A biotite-rich banded gneiss, identified on a traverse 2 km northeast of the zone, returned gamma-ray spectrometer readings above 4000 cps. Two samples (AL-23-1130-1 and -2; Figure 41b) collected from these mafic bands were silica poor, Th rich, and had zoned, metamict allanite, visible in petrographic thin section (Figure 32g and h). Although allanite is an important host mineral for Th and REEs, the main rare-earth-element–bearing minerals extracted and processed are bastnäsite, xenotime, and monazite (Haque et al., 2014). An assay of sample AL-23-1130-2 yielded 732 ppm La, 1330 ppm Ce, 137 ppm Pr, 437 ppm Nd, 60 ppm Sm, and 481 ppm Th. Notably, this gneiss exhibits strong LREE enrichment, with significant negative Eu anomalies, comparable to the relatively LREE-enriched trend of the GG1 component.

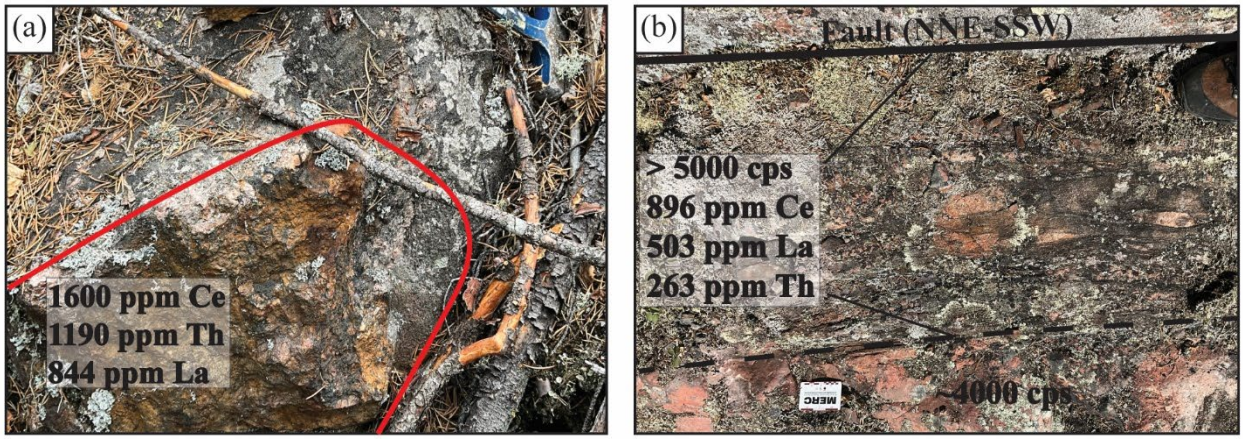

Figure 42. Outcrop photographs of select newly identified rare-earth-element occurrences west of Andrew Lake, northeastern Alberta: (a) biotite-pegmatite selvage contained 844 ppm La, 1600 ppm Ce, and 1190 ppm Th (sample AL-23-2126-1); (b) sheared contact (dashed line) between raft of metasedimentary rocks and granitic gneiss. A handheld gamma-ray spectrometer recorded >5000 counts per second (cps) within the metasedimentary rocks localized along a north-northeast–south-southwest (NNE-SSW)-trending vertical fault, recordings decreased to 4000 cps in the adjacent gneiss, and to background values of ~400–800 cps within a metre of the contact. Sample AL-23-2073-2 of the gneiss contained 503 ppm La, 896 ppm Ce, and 263 ppm Th.

The western reaches of the E-W arm, near the BLSZ, provided further insights into the REE potential of the area. Approximately 70 m west of the shoreline, discontinuous and sheared rafts, over several metres in length, of magnetic metasedimentary rocks were identified within banded granitic gneiss and gamma-ray spectrometer readings of up to 5000 cps were recorded along a north-northeast-trending vertical fault. A sample (AL-23-2073-2; Figure 41b) collected from this component yielded 503 ppm La, 896 ppm Ce, 263 ppm Th, and elevated values of Pr, Nd, Hf, Sb, Y, Nb, Ag, Dy, and Ho relative to the bulk of samples. At this sample site, gamma-ray readings of up to 4000 cps were recorded at the contact between a raft and the adjacent granitic gneiss. Within a metre of this contact, the readings decreased to background values of 400–800 cps (Figure 42b). Similarly, readings decreased to background values across the northwestern contact of the fault.

These metasedimentary rafts decrease in abundance westwards until the enveloping granitic gneiss transitions to migmatitic paragneiss over a north-northeast–south-southwest-trending gradational contact ~40 m wide. The extent of the paragneiss correlates spatially to a gradual increase in aeromagnetic intensity. Another north-northeast–south-southwest-trending gradational contact farther to the west is blanketed by Quaternary sediments in an area of lowland and divides metatexitic paragneiss from variably mylonitized diatexites of the BLSZ and parallels the dominant $S_{1\text{-}2}$ gneissosity. Westwards, mafic schlieren of uncertain parentages are suspended within rocks that crystallized within a leucosomal pegmatitic melt. A sample (AL-23-2080-2; Figure 41b) of pegmatite selvage yielded gamma-ray readings of up to 2300 cps, and values of 56 ppm Nb, 572 ppm La, 1050 ppm Ce, 103 ppm Pr, 343 ppm Nd, 39.9 ppm Sm, and 280 ppm Th.

7.1.3.2 Leland Lakes Study Area

A thorium-rich, uranium-poor granitoid sample (LL-23-2047-1; Figure 41b) enriched in LREEs was collected from a 1–2 m thick layer of buff-weathering, sheared granite near the gradational contact with a garnetiferous, migmatitic paragneiss. This sample yielded anomalous values of 593 ppm La, 1310 ppm Ce, 152 ppm Pr, 569 ppm Nd, 76.3 ppm Sm, 3.91 ppm Eu, 25.7 ppm Gd, and 473 ppm Th. This layer is one of several foliation-parallel granitic interlayers that likely are the product of the melting of the basement gneiss and overlying supracrustal rock during peak regional metamorphism. These melt sheets locally yielded gamma-ray spectrometer readings of over 1000 cps compared to background values of ~200–600 cps. The sampled layer yielded gamma-ray values of 1000–2000 cps and was traced for 100 m south to the shore of Leland Lakes (Figure 43). The REE profile of this granite gneiss sample, exhibiting relative LREE enrichment and HREE depletion, closely matches that of two garnet-rich, partially melted samples of paragneiss from Leland Lakes metasedimentary rocks (LL-23-1064-C1 and -C2; Figure 44). In turn, this is consistent with the concentration of LREEs in granitic melt during the partial melting of metasedimentary rocks.

The Arch Lake granitoid exhibits similar TREO contents to the basement gneisses in the region. Geochemical and petrographic analyses indicate an I-type granite origin, contrary to previous interpretations that proposed an S-type granitoid origin (Goff et al., 1986). The samples collected for this study are from the southwestern margin of the Arch Lake granitoid and may not represent the entire pluton. In the northern part of the study area, the Arch Lake granitoid shows a significant Th anomaly, identified by regional radiometric analysis (Charbonneau et al., 1994), confined by the LLSZ to the west and the newly recognized Arch Lake shear zone (ArLSZ) to the east (Lopez et al., 2024; Figure 41a). This suggests an increased contribution of crust northward, possibly explaining its previous classification as an S-type granitoid origin. No samples were collected from this northern region due to field access limitations, but it presents a promising target for REE exploration.

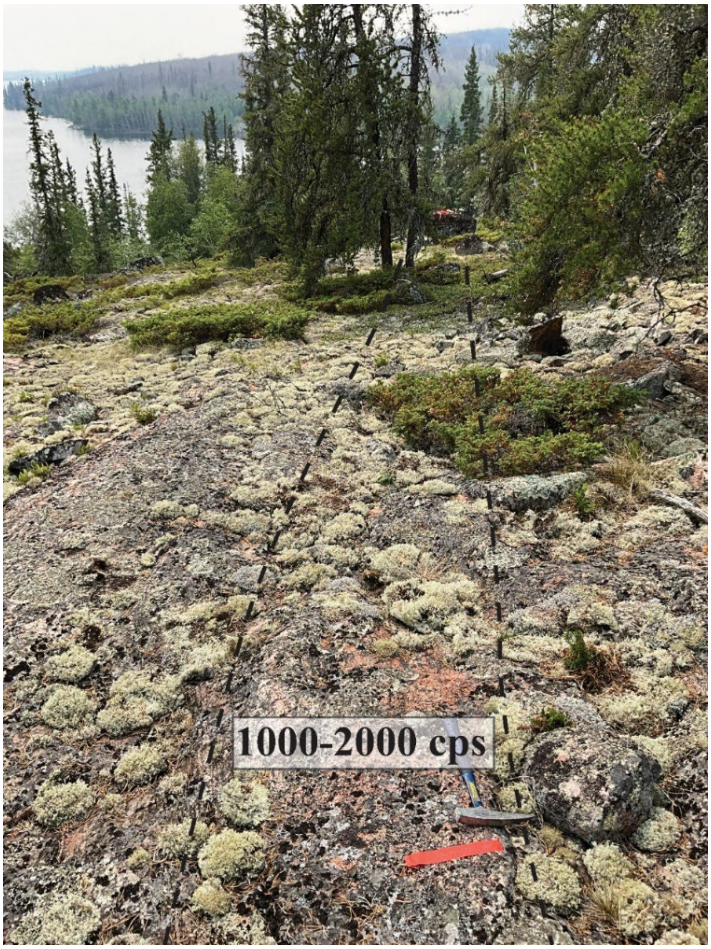

Figure 43. A multitude of 1–2 m thick interlayers of granite, within the biotite-hornblende heterogeneous basement gneiss unit along the Leland Lakes shear zone (northeastern Alberta), are marked by elevated gamma-ray readings relative to background values, and exhibit increased alkalinity and relative enrichment in light rare-earth-element concentrations. These interlayers are most prominent in proximity to the western margin of the biotite-hornblende heterogeneous basement gneiss, where it is in sheared contact with Leland Lakes metasedimentary rocks of the Rutledge River complex. They often extend for dozens of metres or more, much like the one pictured, which extends southwest to the lakeshore (station LL-23-2047). Abbreviation: cps, counts per second.

7.1.4 Pegmatite-Hosted Lithium Potential—Slave Granitoid

The voluminous Slave granitoid is located west of the LLSZ and exhibits numerous pegmatitic phases. The potential for LCT pegmatites, which are important sources of lithium and tantalum, is particularly associated with the Slave granitoid in the Leland Lakes area. Lithium-cesium-tantalum pegmatites are typically formed from highly evolved granitic melts that have undergone extensive fractional crystallization. For LCT mineralization, key characteristics of fertile granites and pegmatites include a peraluminous composition, high degree of fractionation, and a favourable structural setting (proximity to large-scale shear zones and faults).

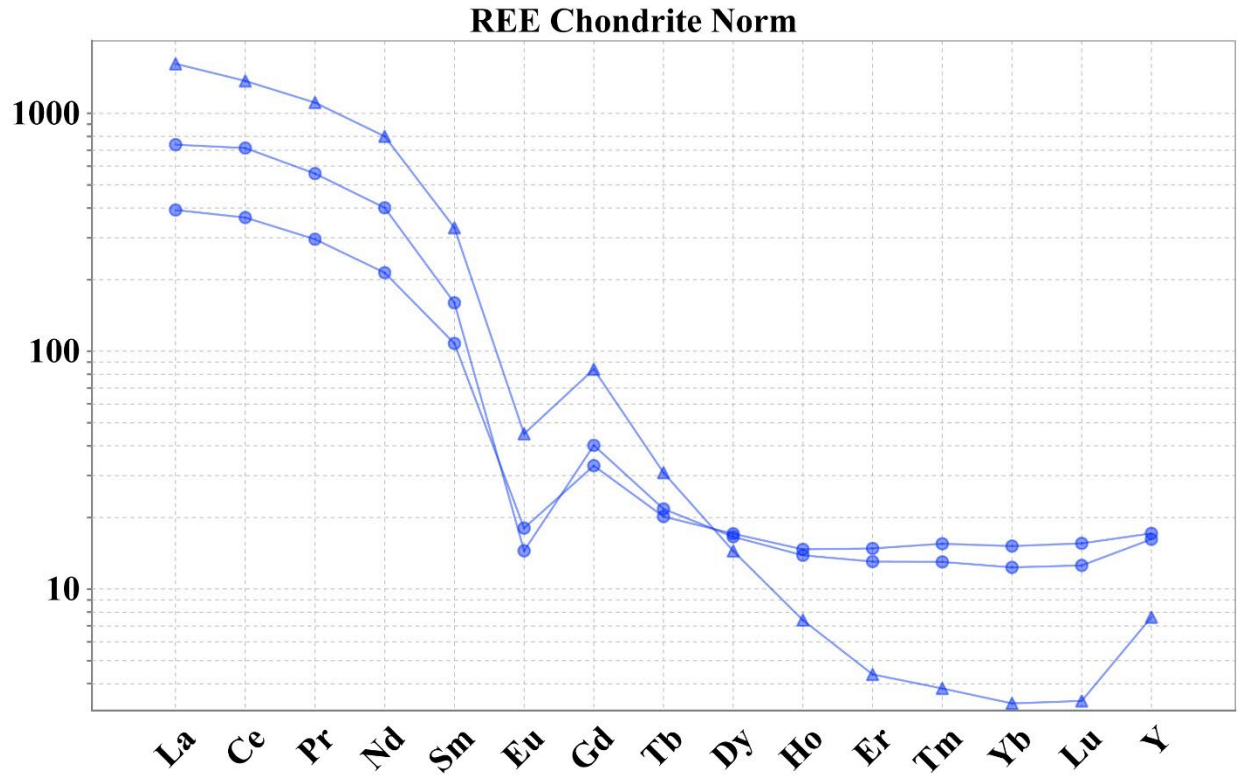

Figure 44. Chondrite-normalized (NORM) rare-earth-element (REE) plot for selected light REE-enriched, garnet-rich, metasedimentary paragneiss samples (blue circles, samples LL-23-1064-C1 and -C2) and an adjacent mylonitic granite gneiss sample (blue triangle, sample LL-23-2047-1) from the Leland Lakes study area, northeastern Alberta (normalizing values from Taylor and McLennan, 1985). These patterns are consistent with LREE enrichment via partial melting of the metasedimentary rocks.

Among the studied rock units, the Slave granitoid has the greatest potential for LCT pegmatite genesis, with average Li concentrations of 128 ppm, and one sample recording 434 ppm. The Mg/Li ratio from bulk whole-rock lithogeochemical analysis serves as a crucial indicator of the extent of fractionation in granites and pegmatites. Research by Černý (1989a) suggests that Mg/Li ratios of <30 signify significant fractionation. Higher Mg/Li ratios, such as Mg/Li = 50, indicate a predominance of Mg in primitive rocks like barren granite, whereas low ratios, such as Mg/Li <10, suggest higher Li concentrations in evolved rocks such as fertile granite. Additionally, low Nb/Ta ratios (typically <10) may indicate magmas derived from a more enriched source or were influenced by crustal contamination, enhancing the potential for Ta enrichment (Selway et al., 2005). Values of <8 are considered indicative of fertile granite with the potential to generate LCT pegmatites. Conversely, elevated Nb/Ta ratios (usually >20) may suggest magmas were derived from a depleted mantle source or extensive fractional crystallization, which may not have favoured LCT pegmatite formation (Rudnick and Gao, 2003). Many sampled Slave granitoids fall within a favourable range, with one notable sample (LL-23-1012-1) exhibiting Mg/Li and Nb/Ta ratios of 7.0 and 2.4, respectively (Figure 44). Furthermore, the classification of these granitoids as syncollisional—formed during periods of tectonic compression and crustal thickening—is consistent with Černý's (1991) survey, which found that the majority of LCT pegmatites form during late syntectonic to early post tectonic stages. This tectonic context further reinforces the potential for LCT pegmatite formation within the Slave granitoid suite.

Meek et al.'s (2023) geochemical reanalysis of historical whole-rock samples (Godfrey, 1986) from the Leland Lakes area revealed strong indicators of advanced fractionation, particularly along the eastern margin of the pluton adjacent to the LLSZ. The Nb/Ta ratios in samples collected along this shear zone are notably low, typically <5 (Figure 45a), suggesting a highly fractionated and fertile environment conducive to LCT pegmatite genesis (Selway et al., 2005). The K/Rb ratio also serves as an important indicator of the degree of fractionation. Low K/Rb ratios are characteristic of evolved granitic systems and are often linked to LCT mineralization potential (Černý, 1991). The distribution of K/Rb values shows that most samples near the LLSZ are below 150, indicative of significant fractionation (Figure 45b). Additionally, the Zr/Hf ratios across the Leland Lakes area reflect advanced fractionation, with most values near the shear zone falling below 35 (Meek et al., 2023). Lower Zr/Hf ratios suggest increased levels of differentiation and are commonly associated with granitic melts capable of producing LCT pegmatites (Černý, 1989b).

Moreover, the peraluminous nature of the Slave granitoid, combined with its proximity to lithium-rich metasedimentary rocks of the RRC, makes it a strong candidate for having hosted or generated LCT pegmatite melt. The eastern margin adjacent to the LLSZ exhibits strong geochemical indicators for LCT pegmatite potential and the western margin also presents significant exploration opportunities. Radiometric surveys (Charbonneau et al., 1994) identified notable anomalies along this western boundary. The highest K values, identified from radiometric surveys (Charbonneau et al., 1994), occur along the western margin of the Slave granitoid, localized on the eastern margin of a newly recognized, north-northeast-trending shear zone, the Slave shear zone (SSZ; Figure 46a; Lopez et al., 2024). These high K radiometric anomalies could reflect differences in mineralogy of the granitoid and/or significant hydrothermal alteration related to the intrusion, however, their proximity to the SSZ highlights the potential for mineralization. Interestingly, equivalent U concentrations are elevated along the western flank of this shear zone (Figure 46b). The juxtaposition of high K and equivalent U anomalies across the SSZ suggests a complex geochemical environment that may enhance the potential for mineralization along this structure (Lopez et al., 2024).

Furthermore, there is potential for Slave granite dikes and pegmatites to appear up to 10 km from the parent granite along fractures and faults. Pegmatites with the greatest economic potential may occur within this range, as they are more likely to contain abundant volatiles and other refractory phases (Selway et al., 2005).

The Leland Lakes region also demonstrates geochemical evidence for LCT pegmatite potential based on GSC lake sediment data, which revealed significant anomalies of key tracer elements, such as Cs, Rb, and Ta (Friske et al., 1994). Interpolation of these lake sediment anomalies defines the margins of the ellipsoidal Slave granitoid pluton, with large bodies of RRC situated at its periphery and with smaller lenses smattered throughout. These findings suggest a highly prospective environment for LCT mineralization along the edges of the Slave granitoid and within associated pegmatitic bodies.

Given the voluminous character of the Slave granitoid, its geochemically evolved nature, and significant crustal assimilation, this pluton is worthy of future investigation, particularly towards the margins of the intrusion. The eastern margin adjacent to the LLSZ exhibits strong geochemical indicators for LCT pegmatite potential and the western margin of the Slave granitoid also presents significant exploration opportunities.

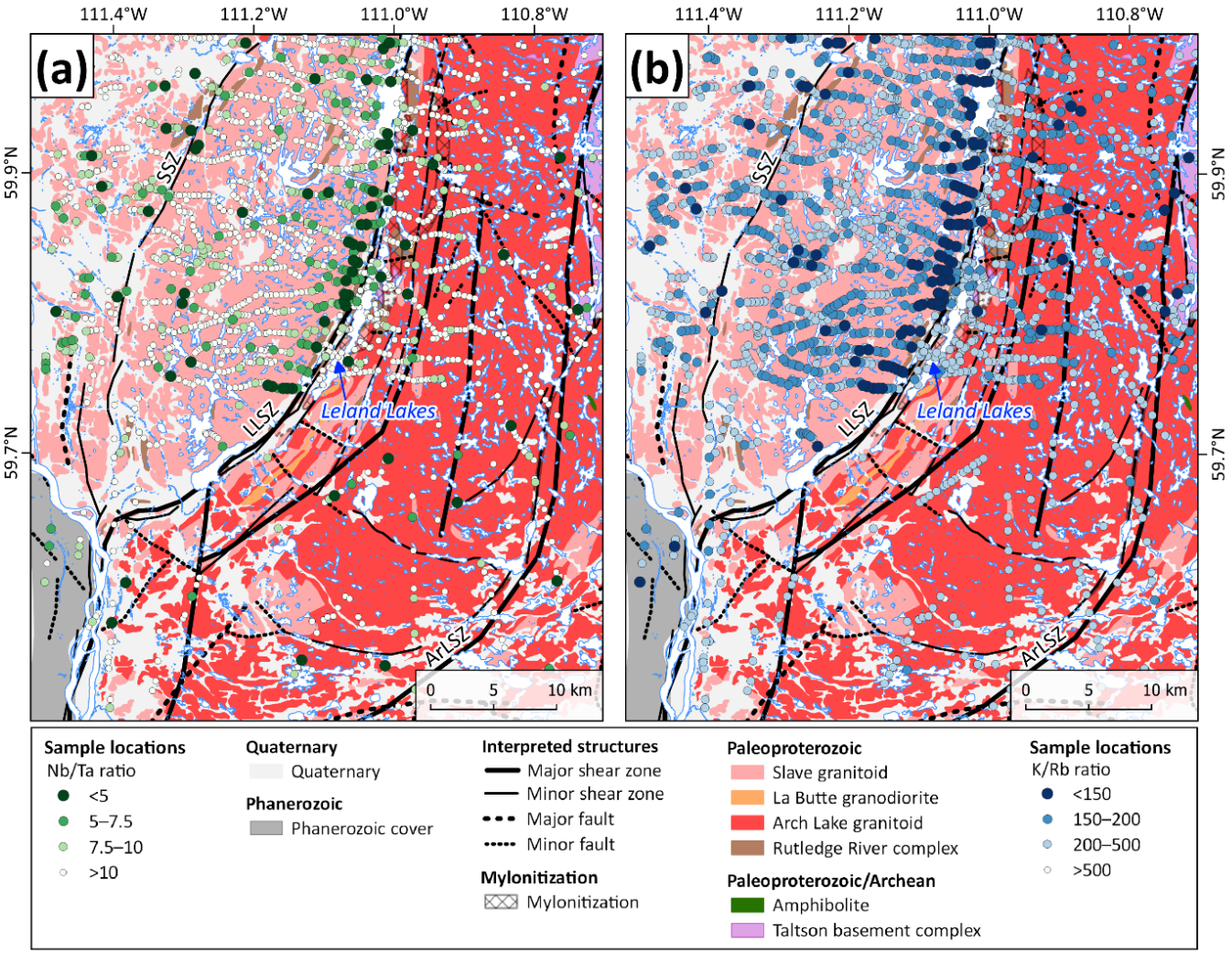

Figure 45. Granite fertility fractionation indicators in the Slave granitoid, Leland Lakes study area, northeastern Alberta, based on the geochemical reanalysis of historical whole-rock samples (Meek et al., 2023, 2026): (a) Nb/Ta ratios, with notably low values localized along the eastern margin of the pluton, along the Leland Lakes shear zone (LLSZ); (b) K/Rb ratios, with a concentration of values of <150 similarly localized along the LLSZ. Background geology from Pană (2010b) with interpreted structures modified from Lopez et al. (2024). Abbreviations: ArLSZ, Arch Lake shear zone; SSZ, Slave shear zone.

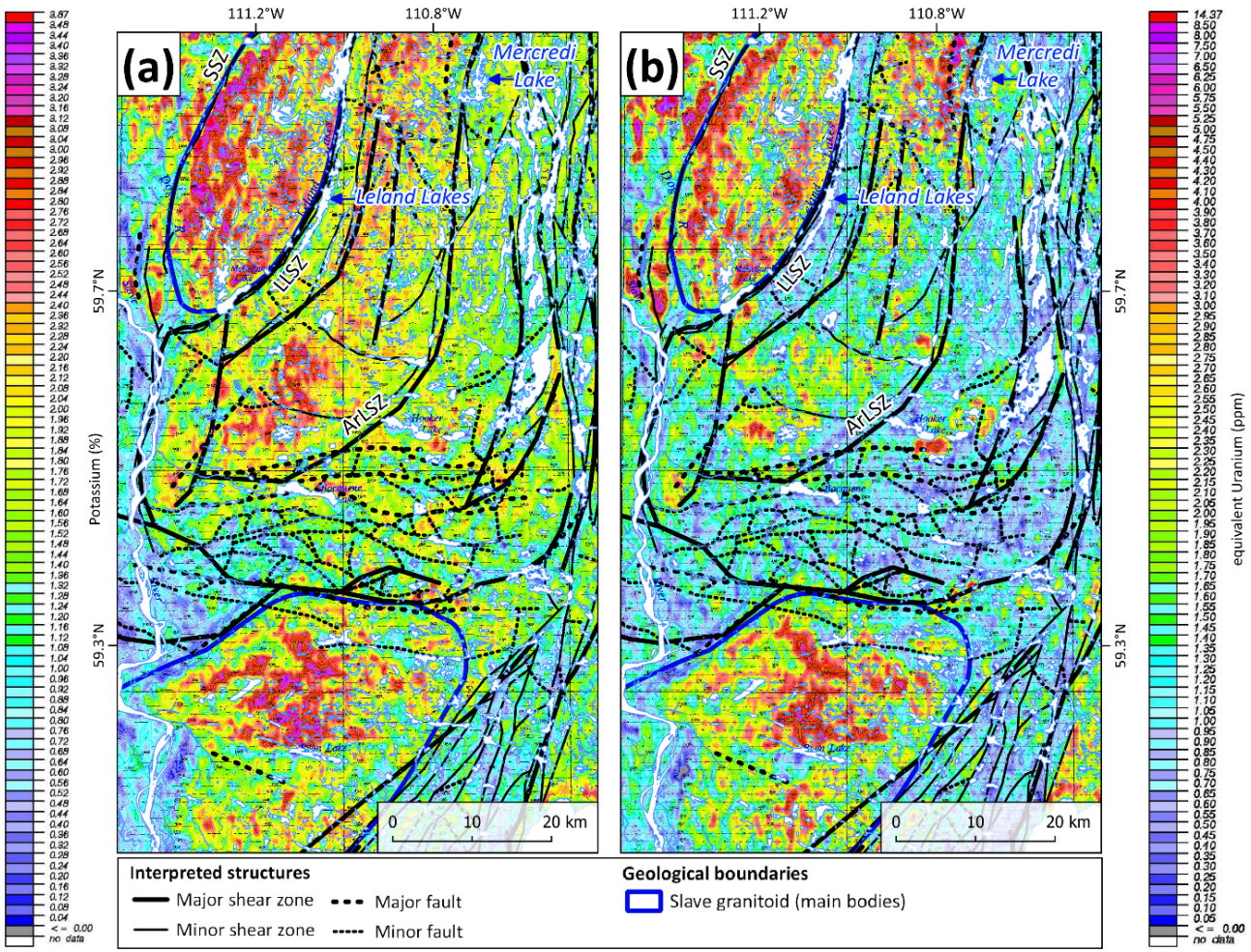

Figure 46. Geological Survey of Canada radiometric maps (adapted from Charbonneau et al., 1994) showing (a) potassium values in the Leland Lakes region (northeastern Alberta), note the elevated values (pink-purple) along the western flank of the northern Slave granitoid body and along the eastern margin of a regional north-northeast-trending shear zone (Slave shear zone [SSZ]) recently identified by aeromagnetic interpretation and automatic structure detection (Lopez et al., 2024) and (b) equivalent U concentrations in the Leland Lakes region (northeastern Alberta), note the concentration of elevated values along the western flank of the SSZ. Moreover, another newly identified shear zone, Arch Lake shear zone (ArLSZ; Lopez et al., 2024), transects Mercredi Lake, where anomalous U concentrations are reported.

7.2 Structurally Controlled / Fluid-Related Uranium and Minor REEs

7.2.1 Assessing Uranium Potential—Spider Lake and Cherry Lake Areas

The Spider Lake and Cherry Lake areas have a significant history of uranium exploration as highlighted in Section 2.4. Radioactivity in the area was first reported by Godfrey (1963). After uranium mineralization near Cherry Lake was confirmed, a helicopter-borne scintillometer survey conducted for McIntyre Porcupine Mines Ltd. confirmed the presence of radioactive anomalies on the northern shore of Spider Lake (Lipsett and Trigg, 1968). A series of trenches blasted across the radioactive belt (Langenberg et al., 1994, M.O. 64, 65, and 66) and two subsequent drillholes failed to intersect economic mineralization (Thorpe, 1969). In 2023, these areas were re-examined as a secondary objective of a regional hyperspectral reconnaissance project (Rivard and Feng, 2024).

In the Spider Lake area, metatexitic basement gneisses of the TBC lie on the western shore, in sheared contact with high-grade, mylonitized RRC paragneiss along a northeast-trending fault zone. The three mineralized zones identified in 1968 by scintillometer survey (Lipsett and Trigg, 1968) are located along this contact, where large homogenous pegmatites associated with the Colin Lake white granite exhibit elevated uranium concentrations. Based on geophysical analysis, this contact represents a southwest-trending splay of the ALSZ (Figure 47a and b). The proximity of mineralized zones to this sheared contact is critical, as it suggests that the ALSZ could have acted as a conduit for mineralizing fluids and pegmatitic intrusions, further enhancing the uranium potential in the area.

Moreover, a separate northeast-trending fault zone extending from the northeastern shore of Spider Lake forms a gradational boundary between the metatexitic paragneiss and diatexite, where pegmatitic intrusions associated with the Colin Lake white granite similarly exhibit elevated uranium concentrations. Although pegmatites are found in both the metatexitic paragneiss and diatexite, those which occur in the former generally exhibit lower uranium concentrations and less pervasive mineral staining. These structurally controlled pegmatites display pronounced yellow mineral staining (Figure 48a) and host uranium-bearing phases such as carnotite. These observations highlight the structural control on mineralization and the significant uranium potential along this corridor. The western sheared contact indicates that polyphase deformation influenced uranium concentration in this region. Shear zones, such as the ALSZ, are effective at channelling fluids, which can mobilize and deposit uranium in structural traps. The faulting and shearing at this site likely facilitated postemplacement metasomatism, leading to the remobilization and enrichment of uranium in the pegmatitic intrusions. The structural framework provided by these shear zones likely acted as conduits for fluid migration during and after pegmatite emplacement, making these structural zones strong candidates for further uranium exploration.

Through 1968–1969, the Cherry Lake area was the site of a helicopter-borne scintillometer survey, rock trenching (11 trenches), and the drilling of six diamond drillholes totalling 575 m (Lipsett and Trigg, 1968; Thorpe, 1969). The geology of the Cherry Lake area was significantly controlled by structural processes, characterized by northwest-southeast-trending, steeply dipping shear zones, along with northern- and southwestern-striking shears and brittle-ductile faulting. These shear zones create a structurally complex environment that played a key role in localizing uranium mineralization.

A sample (AL-23-2189-1) collected during the 2023 field season from an old trench (Langenberg et al., 1994, M.O. 25) on the northern shore revealed significant uranium mineralization, with gamma-ray readings of approximately 40 000 cps and samples yielding up to 930 ppm uranium but no enrichment in other metals. Based on petrographic observations and geochemical analysis, the 2023 sample is from a component of the Colin Lake white granite 2, which was sheared along a northerly trend.

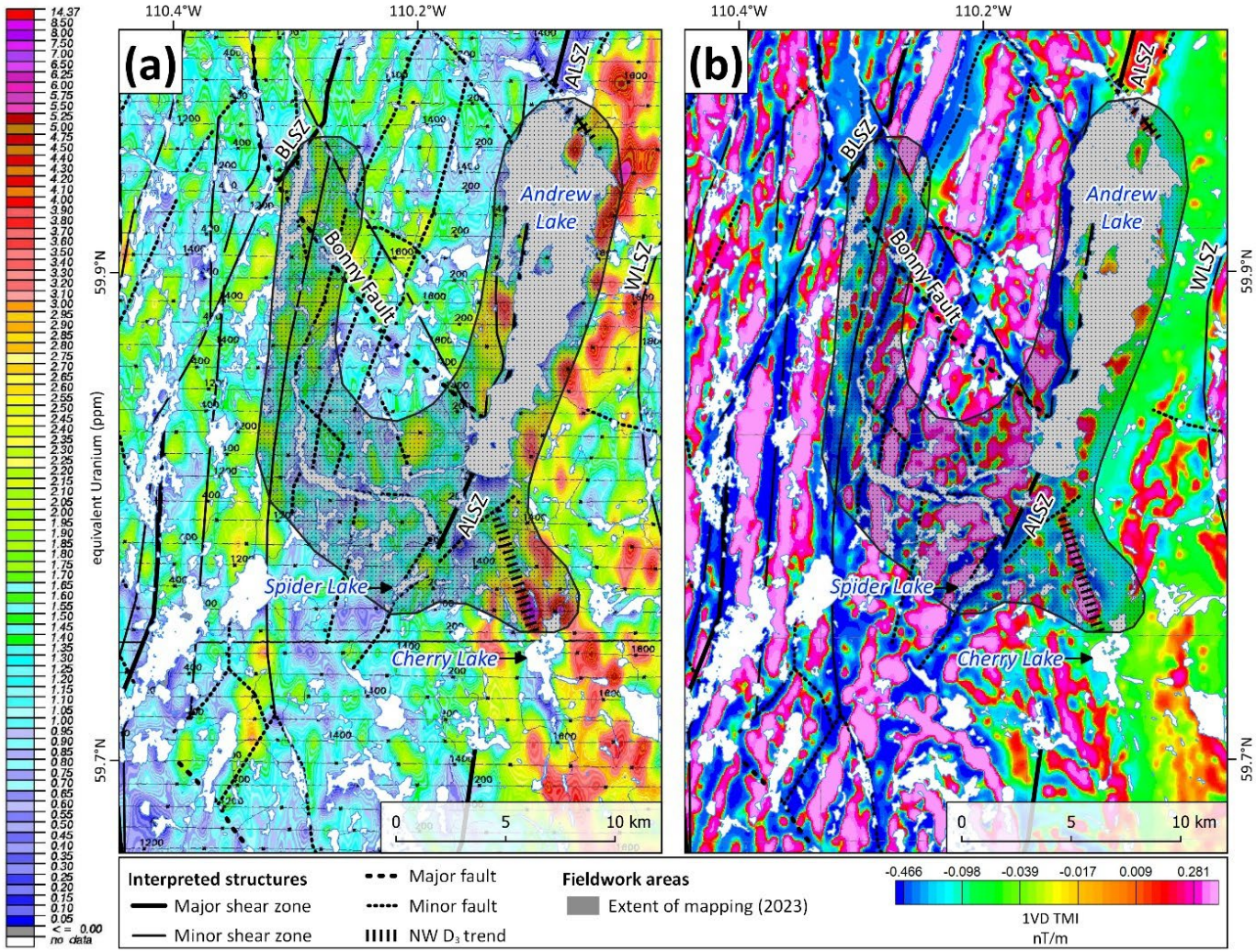

Figure 47. (a) Geological Survey of Canada radiometric map (modified from Charbonneau et al., 1994) exhibiting equivalent uranium anomalies in the Cherry Lake and Andrew Lake area, northeastern Alberta. Structural interpretations from Lopez et al. (2024). Northwest (NW)-trending brittle-ductile and brittle deformation (D_3) is prominent in both locales. (b) Structural first vertical derivative (1VD) aeromagnetic map (Lopez et al., 2024), showing total magnetic intensity (TMI) in the Cherry Lake and Andrew Lake area, northeastern Alberta. Abbreviations: ALSZ, Andrew Lake shear zone; BLSZ, Bayonet Lake shear zone; nT, nanoTesla; WLSZ, Waugh Lake shear zone.

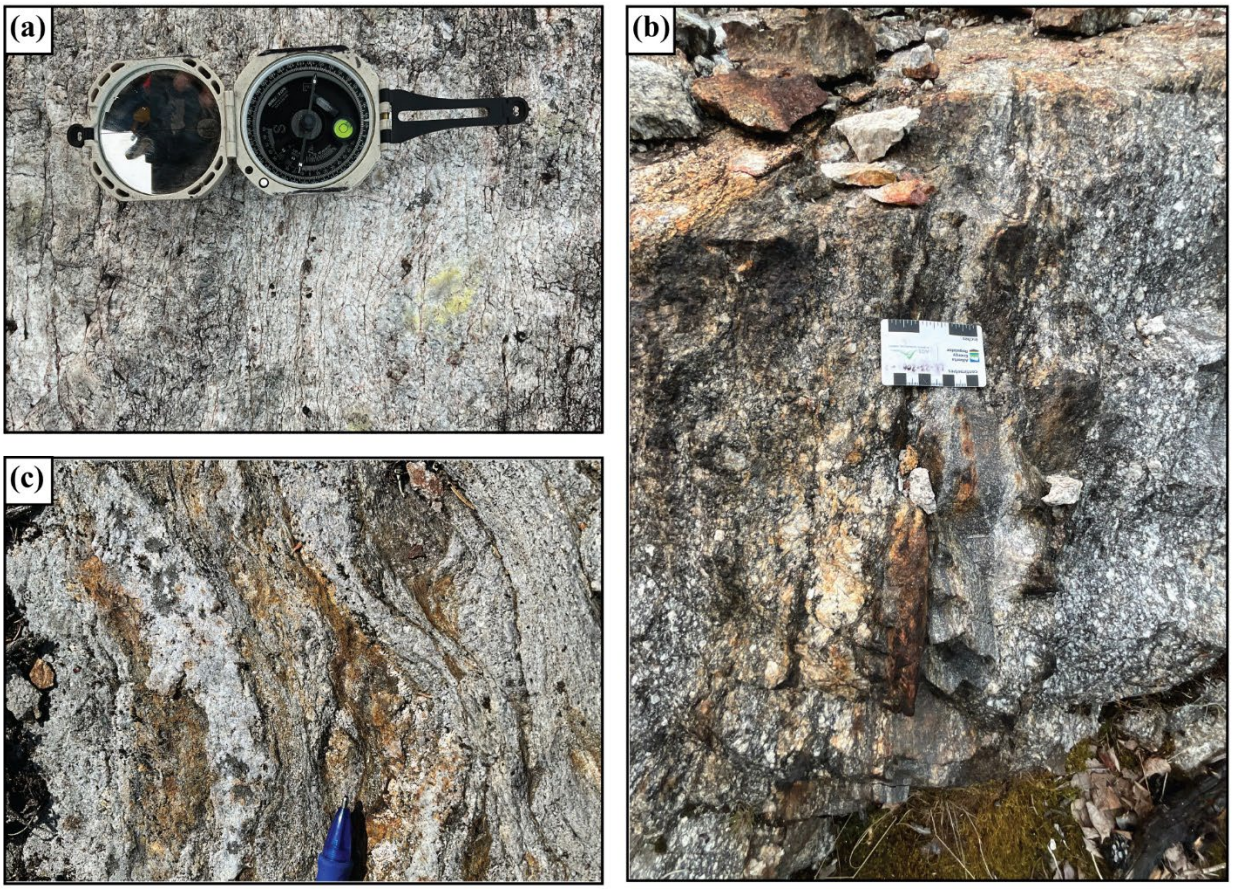

Figure 48. Representative photographs of outcrops in the Andrew Lake study area, northeastern Alberta: (a) garnet-bearing Colin Lake white granite 1, which originated as a partial melt of the Rutledge River complex and exhibits yellow mineral staining; (b) quartzofeldspathic leucosome with affinities to the Colin Lake granitoid and Andrew Lake granodiorite, which exhibits pervasive mineral staining and high uranium concentrations; (c) northwest-southeast-trending discrete shear zones in the northern reaches of Andrew Lake, which bear similar characteristics to those observed at Cherry Lake.

On the western shore of Cherry Lake, garnetiferous granite to granodiorite is in contact with migmatitic paragneiss over an area of lowland. Both of these units dip steeply to the southwest and record an associated S_3 foliation, which is retrogressed and sericitized along a northwesterly trend. The structural overprinting observed here suggests that deformation and fluid migration through these shear zones syn- to post-D_3 played a critical role in the development of uranium-bearing phases. The presence of a northwest-southeast-trending boudinaged leucosome that exhibits yellow mineral staining points to localized uranium enrichment along these shear planes. Such deformation likely enhanced fluid flow and the remobilization of uranium, leading to concentrated mineralization along structural weaknesses.

Farther northwest, a sample of quartzofeldspathic leucosome, with petrographic and geochemical affinities to both the Colin Lake white granite and the Andrew Lake granodiorite, showed pervasive yellow mineral staining, interlayering with remnants of paleosome, and elevated uranium concentrations and U/Th ratios (Figure 48b). The deformation associated with these shear zones facilitated fluid movement, which likely mobilized uranium, concentrating it within the leucosome and associated structures.

Approximately 500 m to the northwest of Cherry Lake, an elliptical structure, which extends at depth for roughly 400–800 m, was identified by automatic structure detection (Lopez et al., 2024) and overlaps

with an elliptical uranium anomaly identified by radiometric surveying (Charbonneau et al., 1994; Figure 47a). This correlation between structural features and uranium enrichment suggests that the elliptical structure acted as a conduit for uranium-bearing fluids, channelling them into favourable zones.

Roughly 2 km farther northwest of this structure, west of a small lake informally named Carrot lake, historical exploration blasting exposed lenses of pegmatites with increased radioactivity relative to the enveloping granitic gneiss. Historical sampling of the trenches west of Carrot lake returned values of up to 0.18% U_3O_8 (Burgan, 1971), and subsequent government sampling of a fault gouge zone exposed in one of the trenches yielded 17 957 ppm U (Langenberg et al., 1993). The presence of uranium within these pegmatites and fault gouge zones highlights the direct role of structural features in controlling mineralization. Faulting and shearing facilitated fluid migration and created zones where uranium-bearing fluids were concentrated, resulting in localized uranium deposits within these structurally complex areas.

Additional northwest-southeast-striking D_3 fault zones are also present in the northern reaches of Andrew Lake, identified by field mapping (Figure 48c) and automatic structure detection (Lopez et al., 2024; Figure 47a and b). At one such locale, significant uranium anomalies were identified by radiometric surveying (Charbonneau et al., 1994) on both sides of the fault (Figure 47a). These data suggest that significant deformation along these northwest-southeast-trending fault zones contributed to the development of polyphase structural corridors, which facilitated fluid flow, partial melting, and the emplacement of uranium-bearing pegmatites. These areas exhibit some of the most elevated equivalent uranium radiometric signatures of the Precambrian shield in Alberta.

In the Leland Lakes region, regional radiometric analysis (Charbonneau et al., 1994) identified the highest equivalent uranium concentrations along the western flank of the SSZ, which transects the western margin of the Slave granitoid (Lopez et al., 2024; Figure 46b). Additionally, along the northern portion of the ArLSZ, there are elevated equivalent uranium concentrations, indicating the shear zone could have introduced and concentrated uranium-bearing fluids, making it a potentially prospective target for uranium exploration (Figure 46b). The association of elevated equivalent uranium concentrations with these shear zones highlights their potential role in localizing uranium mineralization.

7.3 Critical Metals (Cu, Ni, Cr, Co) Potential

7.3.1 Mafic-Associated Critical Metals

In addition to REEs, the 2023 field campaign targeted several other commodities from Canada's critical minerals list (Natural Resources Canada, 2023), including Cu, Ni, Cr, and Co. One of the most prospective areas for these metals was along the LLSZ. This structural zone hosts exposures of Archean basement gneiss, amphibolite, and paragneiss of the RRC (Bostock and van Breemen, 1994). The spatial correlation of historical mineral occurrences (Langenberg et al., 1994) with a prominent aeromagnetic break suggests that some of the mineralization is structurally controlled, consistent with models where shear zones and tectonic boundaries act as conduits for mineralizing fluids (Alsop and Holdsworth, 2004). This is supported by previous work indicating that Cu and Au mineral showings in this area are structurally controlled (Langenberg et al., 1994). One such occurrence, described as gossanous zones in mylonitic metasedimentary rocks, particularly garnetiferous quartzites and gneisses, returned an assay value of 215 ppm Cu (Langenberg et al., 1994, M.O. 13, sample 14-03).

A recent forest fire in this area improved bedrock exposure, allowing for a more detailed examination in 2023. A sample (LL-23-1103-1) of gossanous pyrite-rich metasedimentary rock with thin quartz veins was collected from the area and yielded 556 ppm Cu. A green fuchsitic vein sample (LL-23-1102-3), 30 m northeast of sample LL-23-1103-1, yielded 408 ppm Cu, 444 ppm Ni, 1250 ppm Cr, 91 ppm Co, and 619 ppm As (Figure 49a). Both occurrences lie adjacent to a mafic amphibolite with elevated Co and As values (sample LL-23-1102-2). Approximately 170 m northeast of this area, a mafic sample (LL-23-1002-1) taken from an enclave within the basement gneiss returned values of 700 ppm Cr, 228 ppm Ni, and 14.1 ppm Cs. Additionally, 2 km to the northeast of these sites, on the eastern shore of Leland Lakes,

a sample (LL-23-2044-1) taken from another mafic enclave interlayered with gossanous metasedimentary rock returned values of 1730 ppm Cr, 658 ppm Ni, 71 ppm Co, 79 ppm Cu, and 0.157% S (Figure 49b). To the south-southeast, a similar sample (LL-23-2010-2) taken from a gabbroic amphibolite enclave within the basement gneiss returned assay values of 1790 ppm Cr, 69 ppm Co, 433 ppm Ni, 237 ppm Zn, and elevated Cu, Ge, Sn, and Cs values. The combination of historical Cu occurrences and newly discovered Cu-polymetallic occurrences stretches for more than 14 km along the length of Leland Lakes.

The association of Au, Cu, Cr, Ni, and Co mineralization with a significant structural zone and mafic igneous rocks indicates that this area may be prospective for a variety of mineral deposit types, including orogenic gold (Goldfarb et al., 2001) and magmatic sulphides (Naldrett, 2004). The polymetallic nature of the occurrences, with elevated Cr, Ni, and Co values, indicates significant ancient magmatic contributions to metal enrichment. These characteristics certainly warrant further detailed mapping, geophysical surveys, and geochemical analyses to refine the deposit model prospectivity and guide future exploration efforts.

The Andrew Lake area hosts numerous gabbroic and amphibolite units within the TBC. These mafic units also hold potential for magmatic Cu-Ni-Co–platinum-group element deposits but lack the elevated metal contents that are seen in grab samples from the Leland Lakes area.

8 Conclusions

The combination of new field studies, geophysical and structural analyses, petrographic work, and geochemical analysis resulted in several important findings, as well as highlighted several avenues for future study. A primary conclusion is that the Archean to Paleoproterozoic gneisses of the Taltson basement complex (TBC) have significant potential to host anatectic rare-earth-element (REE) mineralization. The basement granitoid suite at the Leland Lakes study area contains metre-scale bands with elevated values of Th, La, and Ce, but the largest region of exposed Taltson basement gneiss (BG) investigated in this study is found in the south-central portion of the Andrew Lake study area. In this area, the trend of derived granite gneiss (GG) with significant negative Eu anomalies (GG1 samples) exhibits the most REE enrichment and may be the source of the enriched pegmatites (Th, Ce, La). Allanite, zircon, titanite, and monazite are all locally abundant in the basement gneiss. The metasedimentary gneiss of the Rutledge River complex (RRC) in the Leland Lakes study area is locally enriched in light rare-earth elements (LREEs) and may represent a significant source rock for REE-enriched partial melts.

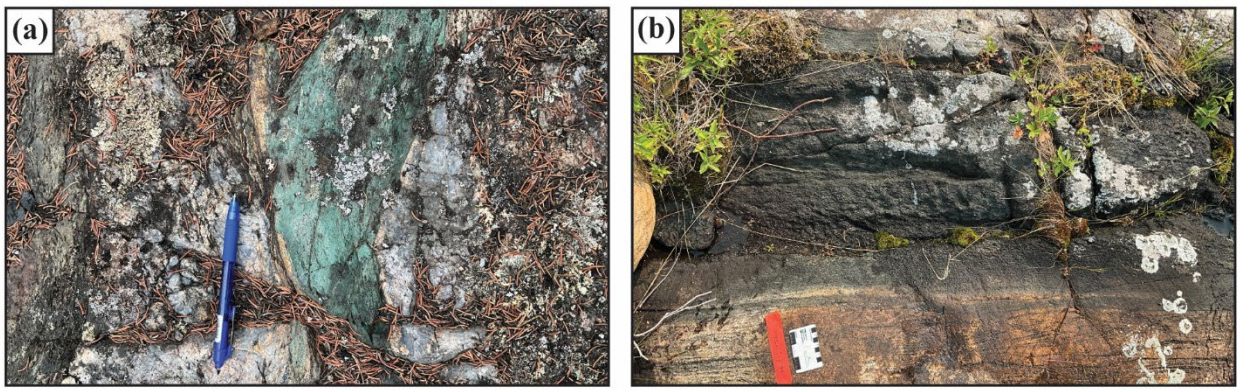

Figure 49. Representative outcrop photographs, Leland Lakes study area, northeastern Alberta: (a) a green fuchsitic vein, which yielded 408 ppm Cu, 444 ppm Ni, 1250 ppm Cr, 91 ppm Co, and 619 ppm As (sample LL-23-1102-3), is parallel to paragneiss of the Rutledge River complex; (b) a mafic enclave interlayered with metasedimentary rock yielded 1730 ppm Cr, 658 ppm Ni, 71 ppm Co, 79 ppm Cu, and 0.157% S (sample LL-23-2044-1).

The enriched pegmatites in the Andrew Lake study area exhibit significant LREE enrichment and relative heavy rare-earth element (HREE) depletion with strong negative Eu anomalies and classify as the abyssal-LREE (U, Th, Ti) subclass of pegmatites. Similar to those observed in the Alces Lake region of northwestern Saskatchewan, pegmatites at Andrew Lake were formed under mid- to high-grade metamorphic conditions, occur as dikes, pods, and boudins, and are commonly situated in structurally controlled zones. The REE mineralization is primarily hosted in monazite-, allanite-, zircon-, and titanite-bearing pegmatites, which represent granitic- to residual-melt / cumulate magmas. The pegmatites have undergone significant magmatic differentiation and subsequent metasomatic alteration. Trace-element patterns suggest that these pegmatites may have resulted from the fractional crystallization of partially melted granite and paragneiss of the TBC. Metasomatic processes played a crucial role in remobilizing REEs, leading to the formation of LREE-enriched pegmatites.

The Slave granitoid suite in the Leland Lakes study area shows promising potential for lithium-cesium-tantalum (LCT) pegmatite emplacement. This granitoid suite is characterized by syncollisional, strongly peraluminous and alkali-calcic compositions, indicating a high degree of crustal involvement and minimal plagioclase fractionation. Key geochemical indicators, such as low Sr/Y and Zr/Hf ratios, as well as favourable Mg/Li and Nb/Ta ratios, suggest fractionation and enrichment in lithium and tantalum, which are encouraging geochemical markers for LCT pegmatite genesis. The chondrite-normalized trace-element patterns exhibit LREE enrichment and HREE depletion, with weak negative and positive Eu anomalies, indicating a differentiated magmatic history conducive to LCT pegmatite formation. Moreover, the syncollisional nature of these granitoids, formed during tectonic compression and crustal thickening, emphasizes the favourable structural and magmatic conditions for LCT pegmatite genesis.

Beyond their petrogenetic significance, selected samples of the leucogranitic phase of the Colin Lake white granite and associated pegmatites reveal low Th/U ratios and variable REE fractionation, indicating significant potential for uranium mineralization. The spatial association of these granites and pegmatites with north-northeast to south-southwest-trending and northwest-southeast-trending deformation corridors was crucial to the mineralization observed in the Andrew Lake area. The structural complexity, including steeply dipping shear zones, mylonitization, and faulting, provided pathways for uranium-bearing hydrothermal fluids, facilitating remobilization and concentration of uranium within these shear-hosted systems. High gamma-ray spectrometer readings and elevated uranium concentrations in samples, particularly near Spider and Cherry lakes, underscore the area's exploration potential. These findings suggest that these deformation corridors played a significant role in enhancing uranium mineralization, making them promising targets for future exploration.

The 2023 fieldwork in the Leland Lakes study area confirmed the presence of mineral occurrences and the potential for precious metals and other critical metals, including Cu, Ni, Cr, and Co. Mineralization appears to be structurally controlled along the Leland Lakes shear zone (LLSZ) with mineral occurrences found just east of a major magnetic break in aeromagnetic data and well-exposed by recent forest fires. New assay results from sulphide-rich metasedimentary rocks, green fuchsitic veins, and mafic enclaves within the biotite-hornblende heterogeneous gneiss (OGN) unit demonstrate elevated concentrations of critical metals, affirming the area's potential for undiscovered mineralization.

The bulk geochemical analysis of samples from the granitoid suites within the Taltson magmatic zone (TMZ) in the Leland Lakes and Andrew Lake study areas reveals significant differences in tectonic setting, magmatic evolution, and melt generation processes. The Leland Lakes study area preserves a transition from deeper, subduction-related melting to syncollisional granitic magmatism. Although the Arch Lake granitoid suite was initially classified as an S-type granitoid (Goff et al., 1986), analytical results from this study suggest an I-type granite origin for the Arch Lake granitoid in the Leland Lakes region. However, the analyzed samples represent a limited spatial extent and may not fully capture the heterogeneity of the entire pluton. This suite exhibits diverse lithologies with calcalkalic affinities typical of subduction zone environments, weak peraluminous characteristics, elevated Sr/Y and Zr/Hf ratios, and LREE enrichment coupled with relative HREE depletion—all supporting a mantle-derived source with

some crustal assimilation. Chondrite-normalized trace-element patterns suggest significant magmatic differentiation, and tectonic discrimination diagrams classify it as volcanic-arc granite, consistent with subduction-related magmatism rather than the previously inferred S-type origin. By contrast, the Slave granitoid in the same region, though still syncollisional and locally garnet bearing, exhibits more homogeneous geochemical signatures, with lower La^{ch}/Yb^{ch} ratios, and decreased Sr/Y ratios, pointing to shallower melting conditions and a greater proportion of crustal involvement. Pegmatitic phases associated with the Slave granitoid show evidence of late-stage differentiation, with strongly peraluminous signatures and variable Eu anomalies reflective of fluid-rich conditions during final crystallization.

In the Andrew Lake area, the Andrew Lake granodiorite suite likewise shows pronounced LREE enrichment and negative Eu anomalies, but its moderate Sr/Y ratio, relatively higher Yb concentrations, and abundant minerals rich in high-field-strength elements suggest a more hybrid tectonic setting, where mantle and crustal contributions were mixed. This unit was intruded by the Colin Lake white granite, which exhibits geochemical signatures typical of more evolved magmas and is compositionally and texturally heterogeneous. It consists of two distinct phases: (1) garnet-bearing phase, enriched in HREEs, with strong negative Eu anomalies, lower La^{ch}/Yb^{ch} ratios, and higher Yb^{ch} concentrations; and (2) a garnet-absent phase, which is weakly to strongly peraluminous, displays higher La^{ch}/Yb^{ch} ratios and lower Yb^{ch} content, and is enriched in large-ion lithophile elements. These features, coupled with fractionated REE patterns and positive Eu anomalies in some samples, suggest melt generation under higher pressure conditions. These distinctions are reflected in structural relationships—in situ leucosomes within the RRC are aligned with metamorphic fabrics, whereas later leucogranitic injections are discordant, cutting across the host units. The coexistence of high-pressure leucosomes and later garnet-absent injections underscores a polybaric evolution, where multiple melt pulses migrated through the crust during progressive metamorphism and deformation along the Andrew Lake shear zone (ALSZ), variably assimilating basement gneiss and/or metasedimentary country rock. The presence of both structurally controlled leucosomes and intrusive cross-cutting phases reflects the transition from in-source partial melting to mobilization and emplacement in higher crustal levels. This complexity highlights the interplay of partial melting, melt extraction, structural overprinting, and syn- to postcollisional magmatism, demonstrating that traditional geochemical classification alone cannot fully capture the heterogeneity of these granitoids or their tectonometamorphic history.

The TBC at Leland Lakes is primarily represented by the OGN unit, which exhibits volcanic-arc granite signatures, calcalkalic affinities, and pronounced Nb and Ta depletion, hallmarks of a subduction-related magmatic origin. Elevated Sr/Y and Zr/Hf ratios, pronounced LREE enrichment, and the negative correlation between La^{ch}/Yb^{ch} and Yb^{ch} point to partial melting at mid- to lower crustal depths where garnet was present but not fully dominant. Moderate Eu anomalies suggest plagioclase retention, consistent with fractionation at mid- to lower crustal levels where garnet was present but not dominant. By comparison, the Andrew Lake TBC consists of the BG and GG units. The BG unit, likely reflecting older Archean basement, contains magnetite, hornblende, and pyroxene, and ranges from granite to diorite compositions. Higher Yb^{ch} concentrations and lower La^{ch}/Yb^{ch} ratios than in the Leland Lakes OGN suggest a shallower melt source where garnet was less stable, and amphibole, plagioclase, plus pyroxene played a greater role in REE partitioning. The GG unit, which is more felsic and can be strongly peraluminous, exhibits three distinct geochemical trends (GG1, GG2, GG3) that point to progressive differentiation and varying depths of melting. Both regions share volcanic-arc granite affinities, but the Leland Lakes TBC preserves deeper, partially garnet-influenced melting, whereas the Andrew Lake TBC reflects lower pressure conditions where amphibole, plagioclase, and pyroxene were the dominant fractionating phases. These differences underscore distinct crustal evolution pathways within the Taltson basement, likely controlled by variations in subduction geometry, crustal thickness, and regional thermal gradients.

The mafic rocks in the Leland Lakes and Andrew Lake study areas reveal distinct geochemical trends, with Andrew Lake samples showing greater compositional diversity, including higher SiO_2, Al_2O_3, and Na_2O, reflecting multiple magmatic events, whereas Leland Lakes samples exhibit more uniform compositions consistent with ocean-floor basalts (mid-ocean–ridge basalt/island-arc tholeiite/calcalkali basalt). Importantly, amphibolite samples from the Leland Lakes study area exhibit geochemical and REE patterns closely matching gabbroic samples from the Andrew Lake study area, suggesting a shared period of mafic magmatism within the BG unit. The metasedimentary rocks in both areas display upper continental crustal signatures, including LREE enrichment and negative Eu anomalies, indicating a felsic sedimentary provenance. However, Leland Lakes metasedimentary rocks, richer in pelitic material, show lower SiO_2 and higher Al_2O_3 and Fe_2O_3 concentrations, whereas Andrew Lake metasedimentary rocks are more quartz and feldspar rich. These differences reflect variations in sedimentary input, metamorphic conditions, and tectonic reworking.

The Leland Lakes and Andrew Lake region records a polyphase deformation history that culminated in significant crustal thickening, arc-related magmatism, and the development and reactivation of late-stage transpressional shear zones. Although some authors invoke intraplate crustal thickening to explain these events, structural observations and geochemical data from this study are more consistent with an orogenic setting, in which crustal shortening was driven by subduction at the western margin of the Rae craton. The earliest deformation (D_1) involved isoclinal folding (F_1) of a cryptic, steeply dipping foliation ($S_{1\text{-}x}$) in the TBC and RRC, resulting in the formation of a composite $S_{1\text{-}x}$-S_1 foliation fabric. This phase, constrained in the study areas between ca. 2.13–1.96 Ga, is linked to major crustal shortening and possibly partial inversion of Paleoproterozoic basins in the region. In establishing a structural framework for subsequent deformation, D_1 facilitated anatexis of REE-enriched metasedimentary rocks, contributing to the generation of early granitoids and enriched pegmatites. The primary orogenic episode (D_2) at ca. 1.94–1.93 Ga corresponds to the peak of deformation and metamorphism in the TMZ. Coaxial refolding of F_1 structures by steeply, doubly plunging, upright F_2 folds produced a subvertical, anastomosing $S_{1\text{–}2}$ composite fabric through pervasive transposition, under upper-amphibolite- to granulite-facies conditions, synchronous with the intrusion of voluminous arc-related melts. A spectrum from strongly arc-type to more syncollisional signatures reflects multiple intrusive phases during D_2. For example, the Arch Lake granitoid (ca. 1.938 Ga) preserves classic arc geochemistry, whereas the slightly younger Slave granitoid (ca. 1.934 Ga) exhibits a more peraluminous, syncollisional affinity, suggesting partial melting of increasingly thickened crust. High-grade conditions persisted from D_1, or were locally reestablished during progressive deformation, as indicated by the retention of granulite-facies mineral assemblages in $S_{1\text{–}2}$ fabrics. Ongoing crustal shortening evolved into transpression, with minor and major deep-seated shear zones (e.g., LLSZ, ALSZ, Bayonet Lake shear zone) nucleating along F_2 axial planes and persisting well beyond the ca. 1.93 Ga magmatic climax. Such relationships highlight how peak thermal conditions enabled partial melting, syntectonic pegmatite emplacement, and localized mineralization. Subsequent deformation phases (D_3 and D_4) imposed additional upright, steeply plunging folds on older fabrics, along with a broad greenschist-facies overprint (M_3). Although the metamorphic details of M_3 remain vague, it encompassed late-D_2 retrogression plus discrete pulses of lower grade metamorphism, commonly concentrating along shear zones, fault planes, and fold axial surfaces, suggesting that reactivated anisotropies focused both deformation and fluid flow as the orogen cooled and underwent exhumation. Taken together, these observations support a subduction-to-collision continuum in the southern TMZ. This multistage evolution shaped the high-grade crustal architecture and imparted notable critical mineral potential, especially through repeated partial melting and deformation that produced REE-bearing pegmatites in structurally favourable sites.

9 Recommendations and Future Work

The recommendations in this section aim to build on the significant findings of the 2023 fieldwork and provide a roadmap for future exploration and research in the Canadian Shield of northeastern Alberta. The

Taltson basement complex has excellent potential for critical elements, but detailed mapping and geochronological analysis to differentiate the primary units and the structural boundaries that may separate them is currently lacking. Of particular interest is separating components of the basement that may be related to the ca. 2.5–2.3 Ga Arrowsmith orogeny from those that may represent older Archean basement. Once a better geochronological framework is established, the petrological and geochemical differences can be further explored. The only known basement U-Pb age in the Leland Lakes study area is a 3.2 Ga age that is older than most other basement ages in Alberta. It is unclear if this age is representative of the entire assumed basement in the Leland Lakes study area, or if it is just a small fragment of ancient basement within younger basement rocks. In the Andrew Lake study area, there is a single 2.3 Ga U-Pb age for a basement granitoid, but the basement in this area has significant heterogeneity and likely contains much older components.

The crystallization age of mafic rocks in the Taltson basement complex is currently unknown, but some of these are likely ca. 2.3 Ga. It is recommended that the larger gabbroic bodies from the Andrew Lake region be targeted for igneous zircon analysis. The age of metasedimentary rocks of the Rutledge River complex in the Leland Lakes and Andrew Lake study areas is also poorly constrained, despite the abundance of base and precious metal occurrences in the region. A detrital zircon study is recommended to help elucidate their depositional age, tectonic setting, and potential for economic mineralization. Analyzing these metasedimentary rocks for monazite and metamorphic zircon would also help to place a minimum age constraint on the timing of deposition as well as determine if any relict of ca. 2.3 Ga Arrowsmith orogeny–related metamorphism can be detected.

The total rare-element oxides geochemical signatures and associated geochemical trends in the Andrew Lake study area highlight its substantial potential for critical mineral resources, particularly REEs. Additional mapping along with the integration of U-Pb geochronological analysis, Sm-Nd and Lu-Hf isotopic analyses, and detailed mineralogical studies of existing geochemical data will provide a more comprehensive understanding of the magmatic processes and enhance the assessment of the critical mineral potential in the Andrew Lake study area, and the Taltson Orogen as a whole. Targeting deeper shear zones and areas with signs of metasomatic alteration, such as the Bayonet Lake, the Arch Lake, and the Charles Lake shear zones could reveal additional REE-rich zones. Moreover, the recent identification of numerous unexplored shear zones across Alberta's exposed Precambrian shield highlights its major map-scale structural features (Lopez et al., 2024) and presents numerous opportunities for REE exploration. Integration of this geophysical data with available geochemical and radiometric datasets would further assist in identifying potential REE-rich zones throughout the southern Taltson Orogen. Further mineral exploration activities to refine targets could include airborne electromagnetic surveys to discover potentially mineralized structures and subsurface conductors, tighter spaced radiometric and aeromagnetic surveys to better define plutons and structures, and stream and soil sampling to identify geochemical anomalies.

To fully assess the potential of the Arch Lake granitoid for REE mineralization, detailed geochemical and petrographic surveys in the northern region is recommended. This should involve comprehensive sampling, particularly around the identified Th anomaly, along with detailed geochemical assays to determine REE concentrations. Thorough petrographic analyses should be performed to confirm the granitoid's origin and understand the mineralogical variations. Extending radiometric surveys to cover the entire Arch Lake granitoid and adjacent areas at a higher resolution would help identify any further anomalies, providing a clearer understanding of the area's REE potential and guiding future exploration efforts.

Further investigation into the Colin Lake white granite is warranted to clarify its genesis, especially given its complex REE patterns and localized uranium enrichment. Geothermobarometry should be applied to resolve the pressure-temperature conditions of formation and to further distinguish the two distinct magmatic phases. Additionally, understanding the inheritance of the REE signature from the metasedimentary source is crucial for interpreting the petrogenesis of the in situ leucogranite phase. The

uranium mineralization potential of the area is significant, particularly within the deformation corridors that facilitated the intrusion of the Colin Lake white granite and movement of uranium-bearing fluids. Future exploration should focus on these structural features, as they likely played a key role in enhancing mineralization.

In addition, the Leland Lakes shear zone (LLSZ) stands out as a distinct structural feature hosting promising occurrences of precious and critical metals. Future exploration should therefore pursue both targets through detailed structural mapping, high-resolution geophysical surveys, systematic sampling in the northwest-southeast corridors to delineate uranium mineralization, and focused investigations along the LLSZ to further define its critical metal endowment and clarify the tectonomagmatic controls driving enrichment.

The peraluminous Slave granitoid provides a large Li-Cs-Ta exploration target, but given the large spatial extent, only a limited area was examined on a few select field traverses in 2023. Re-examination of available historical geochemical samples from this granitoid and its pegmatitic components, could help identify trends and anomalies. Important fractionation indicators may include the occurrence of tourmaline, beryl, and ferrocolumbite, Mn concentrations within garnet, Rb concentrations within K-feldspar, and Mg/Li and Nb/Ta ratios, all obtained from bulk whole-rock geochemical analysis. This could be considered in combination with a regional analysis of aeromagnetic, radiometric, and spectral data west of the LLSZ.

Further structural analysis is recommended to understand the complicated network of ductile and brittle structures that characterize the Taltson Orogen, particularly their role in accommodating polyphase deformation and facilitating magmatic and metamorphic processes. These structural studies could also help decode how the major structures relate to the Archean and Paleoproterozoic blocks of the area. Importantly, the observed geometries of fundamental shear zones of the Precambrian shield in Alberta differ significantly from previous interpretations and therefore require structural re-evaluation. Integrating field-based structural mapping with geophysical data, such as aeromagnetic and gravity surveys, could provide new insights into how these shear zones partitioned deformation and controlled the emplacement of REE-enriched pegmatites and granitoids, as well as insights into the subsurface architecture and structural continuity. Gravity surveys, in particular, could help delineate density contrasts between lithological units, define buried shear zones, and locate concealed magmatic bodies such as granites and pegmatites. Structural lineament mapping using remote sensing could further refine surface expressions of regional trends, whereas detailed petrochronological and fluid-inclusion analysis would provide temporal and chemical constraints on REE-enrichment processes. Finally, geothermal gradient modelling could help link magmatic and metasomatic events to tectonic processes, offering a more holistic understanding of the tectonic evolution and related REE potential of the Andrew Lake area.

10 References

Alberta Geological Survey (2023): High quality regional airborne geophysical surveys in Alberta, version 2 (data, multiple formats); Alberta Energy Regulator / Alberta Geological Survey, URL <https://ags.aer.ca/publication/iam-013> [January 2024].

Alberta Ministry of Energy (2021): Renewing Alberta's mineral future: a strategy to re-energize Alberta's minerals sector; Government of Alberta, 24 p., URL <https://open.alberta.ca/publications/renewing-albertas-mineral-future> [February 2024].

Alcock, F.J. (1915): Geology of the north shore of Lake Athabaska, Alberta and Saskatchewan; Geological Survey of Canada, Summary Report, 1914, p. 60–61, doi:10.4095/103796.

Alcock, F.J. (1917): Black Bay and Beaverlodge Lake areas, Saskatchewan; Geological Survey of Canada, Summary Report, 1916, p. 152–156, doi:10.4095/103744.

Allan, J.R. (1976a): Progress report on Aquarius Resources Ltd. quartz mineral exploration permits 182, 183, 184 and the Cherry Lake property (permit pending) northeastern Alberta for Tachyon Venture Management Ltd.; Alberta Energy and Minerals, Mineral Assessment Report 19760002, 2 p., URL <https://content.energy.alberta.ca/xdata/MARS/MAR_19760002.pdf> [January 2024].

Allan, J.R. (1976b): Progress report on quartz mineral exploration permits 182, 183, 184 and 247 Andrew Lake project, Alberta for Tachyon Venture Management Ltd.; Alberta Energy and Minerals, Mineral Assessment Report 19760003, 2 p., URL <https://content.energy.alberta.ca/xdata/MARS/MAR_19760003.pdf> [January 2024].

Allan, J.R. (1976c): Geological and exploration report, Andrew Lake project, northeastern Alberta, Dec. 31, 1976 for Tachyon Venture Management Ltd.; Alberta Energy and Minerals, Mineral Assessment Report 19760004, 41 p., URL <https://content.energy.alberta.ca/xdata/MARS/MAR_19760004.pdf> [January 2024].

Allan, J.R. (1977): Geological and exploration report, Andrew Lake project, northeastern Alberta, quartz mineral exploration permits 182 and 247, July 15, 1977 for Tachyon Venture Management Ltd.; Alberta Energy and Minerals, Mineral Assessment Report 19770001, 9 p., URL <https://content.energy.alberta.ca/xdata/MARS/MAR_19770001.pdf> [January 2024].

Alsop, G.I. and Holdsworth, R.E. (2004): Shear zones – an introduction and overview; *in* Flow processes in faults and shear zones, G.I. Alsop, R.E. Holdsworth, K.J.W. McCaffrey and M. Hand (ed.), Geological Society, Special Publication 224, p. 1–16, doi:10.1144/GSL.SP.2004.224.01.01.

Ashton, K.E., Hartlaub, R.P., Heaman, L.M., Morelli, R.M., Card, C.D., Bethune, K. and Hunter, R.C. (2009): Post-Taltson sedimentary and intrusive history of the southern Rae Province along the northern margin of the Athabasca Basin, western Canadian Shield; Precambrian Research, v. 175, p. 16–34.

Baadsgaard, H. and Godfrey, J.D. (1967): Geochronology of the Canadian Shield in northeastern Alberta: I. Andrew Lake area; Canadian Journal of Earth Sciences, v. 4, no. 3, p. 541–563, doi:10.1139/e67-029.

Baadsgaard, H. and Godfrey, J.D. (1972): Geochronology of the Canadian Shield in northeastern Alberta II. Charles-Andrew-Colin lakes area; Canadian Journal of Earth Sciences, v. 9, no. 7, p. 863–881, doi:10.1139/e72-070.

Babcock, E.A., Hartley, E.A. and Morton, R.D. (1971): Summary of geological exploration permits 111 and 112, Myers Lake, Alberta for Vestor Explorations Ltd.; Alberta Energy and Minerals, Mineral Assessment Report 19710004, 16 p., URL <https://content.energy.alberta.ca/xdata/MARS/MAR_19710004.pdf> [January 2024].

Barton, M.D. and Young, S. (2002): Non-pegmatitic deposits of beryllium: mineralogy, geology, phase equilibria and origin; Reviews in Mineralogy and Geochemistry, v. 50, no. 1, p. 591–691, doi:10.2138/rmg.2002.50.14.

Bednarski, J.M. (1996): Geochemistry of surficial deposits of northeastern Alberta; Geological Survey of Canada, Open File 3348, 63 p., URL <https://ostrnrcan-dostrncan.canada.ca/handle/1845/187928> [April 2023].

Bednarski, J.M. (1999): Quaternary geology of northeastern Alberta; Geological Survey of Canada, Bulletin 535, 29 p., URL <https://ostrnrcan-dostrncan.canada.ca/handle/1845/189564> [April 2023].

Belosevic, M.B.K., Meek, D.M. and Reimert, C. (2024): Summary of 2023 field activities: Leland Lakes and Andrew Lake areas, Canadian Shield, northeastern Alberta; Alberta Energy Regulator / Alberta Geological Survey, AER/AGS Open File Report 2024-01, 15 p., URL <https://ags.aer.ca/publication/ofr-2024-01> [January 2014].

Berman, R.G. and Bostock, H.H. (1997): Metamorphism in the northern Taltson magmatic zone, Northwest Territories; The Canadian Mineralogist, v. 35, no. 5, p. 1069–1091.

Berman, R.G., Sanborn-Barrie, M., Stern, R.A. and Carson, C.J. (2005): Tectonometamorphism at ca. 2.35 and 1.85 Ga in the Rae domain, western Churchill Province, Nunavut, Canada: insights from structural, metamorphic and in situ geochronological analysis of the southwestern Committee Bay belt; Canadian Mineralogist, v. 43, no. 1, p. 409–442, doi:10.2113/gscanmin.43.1.409.

Berman, R.G., Pehrsson, S., Davis, W.J., Ryan, J.J., Qui, H. and Ashton, K.E. (2013): The Arrowsmith orogeny: geochronological and thermobarometric constraints on its extent and tectonic setting in the Rae craton, with implications for pre-Nuna supercontinent reconstruction; Precambrian Research, v. 232, p. 44–69, doi:10.1016/j.precamres.2012.10.015.

Berman, R.G., Cutts, J.A., Davis, W.J., Camacho, A., Sanborn-Barrie, M. and Smit, M.A. (2023): The tectonic evolution of Thelon tectonic zone, Canada: a new model based on petrological modeling linked with Lu-Hf garnet and U-Pb accessory mineral geochronology; Canadian Journal of Earth Sciences, v. 60, no. 5, p. 550–582, doi:10.1139/cjes-2022-0147.

Berman, R.G., Taylor, B.E., Davis, W.J., Sanborn-Barrie, M. and Whalen, J.B. (2024): Crustal architecture and evolution of the central Thelon tectonic zone, Nunavut: insights from Sm-Nd and O isotope analysis, U-Pb zircon geochronology, and targeted bedrock mapping; Geological Survey of Canada, Bulletin 612, p. 115–158, doi:10.4095/332497.

Bethune, K.M., Berman, R.G., Rayner, N. and Ashton, K.E. (2013): Structural, petrological and U–Pb SHRIMP geochronological study of the western Beaverlodge Domain: implications for crustal architecture, multi-stage orogenesis and the extent of the Taltson Orogen in the SW Rae craton, Canadian Shield; Precambrian Research, v. 232, p. 89–118, doi:10.1016/j.precamres.2013.01.001.

Bostock, H.H. and van Breemen, O. (1992): The timing of emplacement and distribution of the Sparrow diabase dyke swarm, District of Mackenzie, Northwest Territories; *in* Radiogenic age and isotopic studies report 6, Geological Survey of Canada, Paper 92-2, p. 49–55, doi:10.4095/134164.

Bostock, H.H. and van Breemen, O. (1994): Ages of detrital and metamorphic zircons and monazites from a pre-Taltson magmatic zone basin at the western margin of Rae Province; Canadian Journal of Earth Sciences, v. 31, no. 8, p. 1353–1364, doi:10.1139/e94-118.

Bostock, H.H., van Breemen, O. and Loveridge, W.D. (1991): Further geochronology of plutonic rocks in northern Taltson magmatic zone, District of Mackenzie, N.W.T.; *in* Radiogenic age and isotopic studies report 4, Geological Survey of Canada, Paper 90-2, p. 67–78, doi:10.4095/131938.

Bucher, K. and Frey, M. (2002): Petrogenesis of metamorphic rocks (7th edition); Springer Berlin, Heidelberg, Germany, 341 p., doi:10.1007/978-3-662-04914-3.

Burgan, E.C. (1971): Report of work, quartz mineral exploration permit #158, Hudson's Bay Oil and Gas Company Limited; Alberta Energy and Minerals, Mineral Assessment Report 19710009, 6 p., URL <https://content.energy.alberta.ca/xdata/MARS/MAR_19710009.pdf> [January 2024].

Cameron, A.E. (1930): Report of progress on mineral explorations in the Precambrian; Scientific and Industrial Research Council of Alberta, Tenth Annual Report, p. 34–39.

Cameron, A.E. and Hicks, H.S. (1931): The Precambrian area of northeastern Alberta; Research Council of Alberta, Eleventh Annual Report, p. 32–40.

Cann, J.R. (1970): Rb, Sr, Y, Zr, and Nb in some ocean floor basaltic rocks; Earth and Planetary Science Letters, v. 10, p. 7–11, doi:10.1016/0012-821X(70)90058-0.

Cantin, R.G. (1996): Waugh Lake assessment report, permit 9393100018; Alberta Energy and Minerals, Mineral Assessment Report 19960007, 26 p., URL <https://content.energy.alberta.ca/xdata/MARS/MAR_19960007.pdf> [January 2024].

Card, C.D., Bethune, K.M., Davies, W.J., Rayner, N. and Ashton, K.E. (2014): The case for a distinct Taltson orogeny: evidence from northwest Saskatchewan, Canada; Precambrian Research, v. 255, no. 1, p. 245–265, doi:10.1016/j.precamres.2014.09.022.

Černý, P. (1989a): Exploration strategy and methods for pegmatite deposits of tantalum; *in* Lanthanides, tantalum and niobium, P. Möller, P. Černý and F. Saupé (ed.), Society for Geology Applied to Mineral Deposits, Special Publication 7, p. 271–299.

Černý, P. (1989b): Characteristics of pegmatite deposits of tantalum; *in* Lanthanides, tantalum and niobium, P. Möller, P. Černý and F. Saupé (ed.), Society for Geology Applied to Mineral Deposits, Special Publication 7, p. 192–236.

Černý, P. (1991): Rare-element granitic pegmatites. Part 1: anatomy and internal evolution of pegmatitic deposits; Geoscience Canada, v. 18, no. 2, p. 49–67.

Černý, P. and Ercit, T.S. (2005): The classification of granitic pegmatites revisited; The Canadian Mineralogist, v. 43, no. 6, p. 2005–2026, doi:10.2113/gscanmin.43.6.2005.

Černý, P., Meintzer, R.E. and Anderson, A.J. (1981): The Tanco pegmatite at Bernic Lake, Manitoba: V. fractionation trends, evolution, and petrogenetic considerations; Economic Geology, v. 76, no. 5, p. 1513–1533.

Chacko, T., De, S.K., Creaser, R.A. and Muehlenbachs, K. (2000): Tectonic setting of the Taltson magmatic zone at 1.9-2.0 Ga: a granitoid-based perspective; Canadian Journal of Earth Sciences, v. 37, no. 11, p. 1597–1609, doi:10.1139/e00-029.

Charbonneau, B.W., Holman, P.B. and Hetu, R.J. (1994): Airborne geophysical survey, northeast Alberta; Geological Survey of Canada, Open File 2807, 13 maps, 1:250 000 scale, URL <https://ostrnrcan-dostrncan.canada.ca/handle/1845/193546> [April 2023].

Cook, J.T. (1969a): A report on a helicopter borne gamma ray spectrometer survey, quartz mineral permits 77, 78, 79, 80, 81, and 57, northeastern Alberta for Citizens Pipeline Limited; Alberta Energy and Minerals, Mineral Assessment Report 19690013, 16 p., URL <https://content.energy.alberta.ca/xdata/MARS/MAR_19690013.pdf> [January 2024].

Cook, J.T. (1969b): Gamma ray spectrometer survey, quartz mineral permit no. 60, northeastern Alberta for Souvenir Mines Ltd.; Alberta Energy and Minerals, Mineral Assessment Report 19690014, 10 p., URL <https://content.energy.alberta.ca/xdata/MARS/MAR_19690014.pdf> [January 2024].

Cutts, J.A., Dyck, B.V., Perrot, M.G., Davies, J.H.F.L., Osinchuk, A.M., Šilerová, D., Stern, R.A., Chiaradia, M. and Canam, R. (2024): A contiguous Taltson-Thelon margin revisited; Geochemistry, Geophysics, Geosystems, v. 25, issue 7, art. e2024GC011527, 20 p., doi:10.1029/2024GC011527.

Davidson, J., Turner, S., Handley, H., Macpherson, C. and Dosseto, A. (2007): Amphibole "sponge" in arc crust?; Geology, v. 35, no. 9, p. 787–790, doi:10.1130/G23637A.1.

Davis, W.J., Sanborn-Barrie, M., Berman, R.G. and Pehrsson, S. (2021): Timing and provenance of Paleoproterozoic supracrustal rocks in the central Thelon tectonic zone, Canada: implications for the tectonic evolution of western Laurentia from ca. 2.1 to 1.9 Ga; Canadian Journal of Earth Sciences, v. 58, no. 4, p. 378–395, doi:10.1139/cjes-2020-0046.

Day, W. (1975): Zircon geochronology in northeastern Alberta; M.Sc. thesis, University of Alberta, 72 p.

De, S.K., Chacko, T., Creaser, R.A. and Muehlenbachs, K. (2000): Geochemical and Nd-Pb-O isotope systematics of granites from the Taltson magmatic zone, NE Alberta: implications for early Proterozoic tectonics in western Laurentia; Precambrian Research, v. 102, p. 221–249, doi:10.1016/S0301-9268(00)00068-1.

Esri (2023): World Imagery basemap; Esri, image, URL <https://www.arcgis.com/home/item.html?id=10df2279f9684e4a9f6a7f08febac2a9> [April 2023].

Foley, S.F., Barth, M.G. and Jenner, G.A. (2000): Rutile/melt partition coefficients for trace elements and an assessment of the influence of rutile on the trace element characteristics of subduction zone magmas; Geochimica et Cosmochimica Acta, v. 64, issue 5, p. 933–938, doi:10.1016/S0016-7037(99)00355-5.

Friesen, E.J. (1998): Geological report on Dog River mineral permit number 9392060003, 9392060004, 9392070001, 9392070004 for GRQ Mining Inc.; Alberta Energy and Minerals, Mineral Assessment Report 19980020, 13 p., URL <https://content.energy.alberta.ca/xdata/MARS/MAR_19980020.pdf> [January 2024].

Friske, P.W.B., McCurdy, M.W., Day, S.J., Gross, H., Balma, R.G., Lynch, J.J. and Durham, C.C. (1994): National Geochemical Reconnaissance lake sediment and water data, northeastern Alberta (parts of NTS 74E, 74L, and 74M); Geological Survey of Canada, Open File 2856, 150 p., URL <https://ostrnrcan-dostrncan.canada.ca/handle/1845/190532> [January 2024].

Frost, C.D. and Frost, B.R. (2008): A geochemical classification for feldspathic igneous rocks; Journal of Petrology, v. 49, p. 1955–1969, doi:10.1093/petrology/egn054.

Frost, B.R., Barnes, C.G., Collins, W.J., Arculus, R.J., Ellis, D.J. and Frost, C.D. (2001): A geochemical classification for granitic rocks; Journal of Petrology, v. 42, p. 2033–2048, doi:10.1093/petrology/42.11.2033.

Gayfer, E.R. (1968): Summary report of 1968 exploration activity on quartz mineral permits number 49 and 50, Giant Explorations Limited; Alberta Energy and Minerals, Mineral Assessment Report 19680018, 2 p., URL <https://content.energy.alberta.ca/xdata/MARS/MAR_19680018.pdf> [January 2024].

Godfrey, J.D. (1958a): Mineralization in the Andrew, Waugh, and Johnson lakes area, northeastern Alberta; Research Council of Alberta, RCA/AGS Earth Sciences Report 1958-04, 24 p., URL <https://ags.aer.ca/publication/esr-1958-04> [April 2023].

Godfrey, J.D. (1958b): Aerial photographic interpretation of Precambrian structures north of Lake Athabasca; Alberta Research Council, Alberta Geological Survey, Bulletin 1, 19 p., URL <https://ags.aer.ca/publication/bul-001> [April 2023].

Godfrey, J.D. (1961): Geology of the Andrew Lake, North District; Research Council of Alberta, Alberta Geological Survey, Earth Sciences Report 1958-03, 35 p., URL <https://ags.aer.ca/publication/esr-1958-03> [April 2023].

Godfrey, J.D. (1963): Geology of the Andrew Lake, South District, Alberta; Research Council of Alberta, Alberta Geological Survey, Earth Sciences Report 1961-02, 35 p., URL <https://ags.aer.ca/publication/esr-1961-02> [April 2023].

Godfrey, J.D. (1966): Geology of the Bayonet, Ashton, Potts and Charles Lakes districts, Alberta; Research Council of Alberta, RCA/AGS Earth Sciences Report 1965-06, 52 p., URL <https://ags.aer.ca/publication/esr-1965-06> [April 2023].

Godfrey, J.D. (1986): Geology of the Precambrian Shield in northeastern Alberta (NTS 74M and 74L N1/2); Alberta Research Council, Alberta Geological Survey, Map 180, scale 1:250 000, URL <https://ags.aer.ca/publication/map-180> [April 2023].

Godfrey, J.D. and Langenberg, C.W. (1986): Geology of the Fitzgerald, Tulip-Mercredi-Charles Lakes District, Alberta; Alberta Research Council, Alberta Geological Survey, Earth Sciences Report 1984-07, 43 p., URL <https://ags.aer.ca/publication/esr-1984-07> [April 2023].

Goff, S.P., Godfrey, J.D. and Holland, J.G. (1986): Petrology and geochemistry of the Canadian Shield of northeastern Alberta; Alberta Research Council, Alberta Geological Survey, Bulletin 51, 65 p., URL <https://ags.aer.ca/publication/bul-051> [April 2023].

Goldfarb, R.J., Baker, T., Dubé, B., Groves, D.I., Hart, C.J. and Gosselin, P. (2001): Orogenic gold and geologic time: a global synthesis; Ore Geology Reviews, v. 18, issues 1–2, p. 1–75, doi:10.1016/S0169-1368(01)00016-6.

Grant, M. and Smith, D. (2007): North American Gem Inc. 2005 to 2007 exploration of the Bonny Fault property, northeast Alberta; Alberta Energy and Minerals, Mineral Assessment Report 20070018, 8 p., URL <https://content.energy.alberta.ca/xdata/MARS/MAR_20070018.pdf> [January 2024].

Greig, J.A. (1970): Permit termination report quartz mineral exploration permit 139 in the province of Alberta; Alberta Energy and Minerals, Mineral Assessment Report 19700015, 4 p., URL <https://content.energy.alberta.ca/xdata/MARS/MAR_19700015.pdf> [January 2024].

Gromet, L.P., Haskin, L.A., Korotev, R.L. and Dymek, R.F. (1984): The "North American shale composite": its compilation, major and trace element characteristics; Geochimica et Cosmochimica Acta, v. 48, issue 12, p. 2469–2482, doi:10.1016/0016-7037(84)90298-9.

Grover, T.W., McDonough, M.R. and McNicoll, V. (1993): Preliminary report on the metamorphic geology of Taltson magmatic zone, Canadian Shield, northeastern Alberta; *in* Current research, pt. C, Geological Survey of Canada, Paper 93-1C, p. 233–238, doi:10.4095/134249.

Grover, T.W., Pattison, D.R.M., McDonough, M.R. and McNicoll, V. (1997): Tectonometamorphic evolution of the southern Taltson magmatic zone and associated shear zones, northeastern Alberta; Canadian Mineralogist, v. 35, p. 1051–1067.

Haque, N., Hughes, A., Lim, S. and Vernon, C. (2014): Rare earth elements: overview of mining, mineralogy, uses, sustainability and environmental impact; Resources, v. 3, no. 4, p. 614–635, doi:10.3390/resources3040614.

Harker, A. (1909): The natural history of igneous rocks; Methuen & Co., London, United Kingdom, 384 p.

Harris, N.B.W., Pearce, J.A. and Tindle, A.G. (1986): Geochemical characteristics of collision-zone magmatism; *in* Collision tectonics, M.P. Coward and A.C. Ries (ed.), Geological Society, Special Publication 19, p. 67–81, doi:10.1144/GSL.SP.1986.019.01.04.

Hart, E.A. (1967): Report on Alberta concessions for 1967, New Senator-Rouyn Limited; Alberta Energy and Minerals, Mineral Assessment Report 19670002, 10 p., URL <https://content.energy.alberta.ca/xdata/MARS/MAR_19670002.pdf> [January 2024].

Hartlaub, R.P. (2004): Archean and Proterozoic evolution of the Beaverlodge Belt, Churchill Craton, Canada; Ph.D. thesis, University of Alberta, 189 p.

Hartlaub, R.P., Heaman, L.M., Chacko, T. and Ashton, K.E. (2007): Circa 2.3-Ga magmatism of the Arrowsmith orogeny, Uranium City Region, Western Churchill craton, Canada; The Journal of Geology, v. 115, no. 2, p. 181–195, doi:10.1086/510641.

Hicks, H.S. (1930): A petrographic study of Precambrian rocks in northeastern Alberta; M.Sc. thesis, University of Alberta, 47 p.

Hicks, H.S. (1932): The geology of the Fitzgerald and northern portion of the Chipewyan map areas, northern Alberta, Canada; Ph.D. thesis, University of Minnesota, 82 p.

Hoffman, P.F. (1988): United plates of America, the birth of a craton: early Proterozoic assembly and growth of Laurentia; Annual Review of Earth and Planetary Sciences, v. 16, p. 543–603, doi:10.1146/annurev.ea.16.050188.002551.

Hoffman, P.F. (1989): Precambrian geology and tectonic history of North America; *in* The geology of North America—an overview, A.W. Bally and A.R. Palmer (ed.), The Geological Society of America, p. 447–512, doi:10.1130/DNAG-GNA-A.447.

Iannelli, T.R., Langenberg, C.W. and Eccles, D.R. (1995): Stratigraphy, structure and mineral occurrences of the Aphebian Waugh Lake Group, northeastern Alberta; Alberta Energy, Alberta Geological Survey, Open File Report 1995-05, 52 p., URL <https://ags.aer.ca/publication/ofr-1995-05> [April 2023].

Irvine, T.N. and Baragar, W.R.A. (1971): A guide to the chemical classification of the common volcanic rocks; Canadian Journal of Earth Sciences, v. 8, no. 5, p. 523–548, doi:10.1139/e71-055.

Klewchuk, P. (1972): Mineralogy and petrology of some granitic rocks in the Canadian Shield north of Fort Chipewyan, Alberta; M.Sc. thesis, University of Calgary, 134 p.

Kovesi, P. (2015): Good colour maps: how to design them; arXiv, preprint, 42 p., URL <https://arxiv.org/abs/1509.03700> [March 2025].

Kuno, H. (1968): Differentiation of basalt magmas; *in* Basalts: the Poldervaart treatise on rocks of basaltic composition, H.H. Hess and A. Poldervaart (ed.), Interscience, New York, New York, p. 623–688.

Kuo, S.L. (1972): Uranium-lead geochronology in the Charles Lake area; M.Sc. thesis, University of Alberta, 126 p.

Langenberg, C.W. (1983): Polyphase deformation in the Canadian Shield of northeastern Alberta; Alberta Research Council, Alberta Geological Survey, Bulletin 45, 33 p., URL <https://ags.aer.ca/publication/bul-045> [January 2024].

Langenberg, C.W. and Nielsen, P.A. (1982): Polyphase metamorphism in the Canadian Shield of northeastern Alberta; Alberta Research Council, Alberta Geological Survey, Bulletin 42, 80 p., URL <https://ags.aer.ca/publication/bul-042> [January 2024].

Langenberg, C.W., Salat, H., Turner, A. and Eccles, D.R. (1993): Evaluation of the economic mineral potential in the Andrew Lake-Charles Lake area of northeast Alberta; Alberta Research Council, Alberta Geological Survey, Open File Report 1993-08, 100 p., URL <https://ags.aer.ca/publication/ofr-1993-08> [April 2023].

Langenberg, C.W., Salat, H.P. and Eccles, D.R. (1994): Mineral occurrences of the Selwyn and Leland Lakes areas, northeast Alberta; Alberta Research Council, Alberta Geological Survey, Open File Report 1994-05, 28 p., URL <https://ags.aer.ca/publication/ofr-1994-05> [April 2023].

LeCheminant, A.N. and Heaman, L.M. (1989): Mackenzie igneous events, Canada: Middle Proterozoic hotspot magmatism associated with ocean opening; Earth and Planetary Science Letters, v. 96, issues 1–2, p. 38–48, doi:10.1016/0012-821X(89)90122-2.

Linnen, R.L., Van Lichtervelde, M. and Černý, P. (2012): Granitic pegmatites as sources of strategic metals; Elements, v. 8, no. 4, p. 275–280, doi:10.2113/gselements.8.4.275.

Lipsett, E. and Trigg, C.M. (1968): Airborne scintillometer survey of the New Senator option, northeast Alberta, McIntyre Porcupine Mines Limited; Alberta Energy and Minerals, Mineral Assessment Report 19680004, 4 p., URL <https://content.energy.alberta.ca/xdata/MARS/MAR_19680004.pdf> [January 2024].

London, D. and Kontak, D.J. (2012): Granitic pegmatites: scientific wonders and economic bonanzas; Elements, v. 8, no. 4, p. 257–261, doi:10.2113/gselements.8.4.257.

Lopez, G.P., Pawlowicz, J.G., Weiss, J.A. and Jean, G.M. (2020): Metallic mineral occurrences of Alberta (tabular data, tab-delimited format); Alberta Energy Regulator / Alberta Geological Survey, AER/AGS Digital Data 2019-0026, URL <https://ags.aer.ca/publication/dig-2019-0026> [January 2024].

Lopez, G.P., McGill, D. and McKenzie, J. (2024): Airborne geophysics data analysis and interpretation, Canadian Shield, northeastern Alberta; Alberta Energy Regulator / Alberta Geological Survey, AER/AGS Special Report 119, 111 p., URL <https://ags.aer.ca/publication/spe-119> [May 2024].

Lyatsky, H.V. and Pană, D.I. (2003): Catalogue of selected regional gravity and magnetic maps of northern Alberta; Alberta Energy and Utilities Board, EUB/AGS Special Report 56, 43 p., URL <https://ags.aer.ca/publication/spe-056> [April 2023].

Mann, A.G. (1991): Assessment report, Alberta, metallic mineral exploration permit number 6890090002, Andrew Lake, northeast Alberta for E.J. Friesen & Associates Inc.; Alberta Energy and Minerals, Mineral Assessment Report 19910001, 35 p., URL <https://content.energy.alberta.ca/xdata/MARS/MAR_19910001.pdf> [January 2024].

Mann, A.G. (1995): Geological report on Fort Smith and Fort Fitzgerald area exploration project in northeastern Alberta for E.J. Friesen & Associates Inc.; Alberta Energy and Minerals, Mineral Assessment Report 19950011, 20 p., URL <https://content.energy.alberta.ca/xdata/MARS/MAR_19950011.pdf> [January 2024].

Mann, A.G. (1996): Geological report on Dog River industrial mineral permit number 9392060004 for GRQ Mining Inc.; Alberta Energy and Minerals, Mineral Assessment Report 19960020, 9 p., URL <https://content.energy.alberta.ca/xdata/MARS/MAR_19960020.pdf> [January 2024].

Maxeiner, R.O., Gilboy, C.F. and Yeo, G.M. (1999): Classification of metamorphosed clastic sedimentary rocks: a proposal; *in* Summary of investigations 1999, v. 1, Saskatchewan Geological Survey, Saskatchewan Energy and Mines, Miscellaneous Report 99-4.1, p. 89–91, URL <https://publications.saskatchewan.ca/#/products/81621> [January 2024].

McDonough, M.R. (1997): Structural controls and age constraints on sulphide mineralization, southern Taltson magmatic zone, northeastern Alberta; *in* Exploring for minerals in Alberta: Geological Survey of Canada geoscience contributions, Canada-Alberta Agreement on Mineral Development (1992–1995), R.W. Macqueen (ed.), Geological Survey of Canada, Bulletin 500, p. 13–30, doi:10.4095/209206.

McDonough, M.R. and McNicoll, V.J. (1997): U-Pb age constraints on the timing of deposition of Waugh Lake and Burntwood (Athabasca) groups, southern Taltson magmatic zone, northeastern Alberta; *in* Radiogenic age and isotopic studies report 10, Geological Survey of Canada, Current Research 1997-F, p. 101–111, doi:10.4095/209096.

McDonough, M.R., Grover, T.W., McNicoll, V.J. and Lindsay, D.D. (1993a): Preliminary report of the geology of the southern Taltson magmatic zone, northeastern Alberta; *in* Current research, pt. C, Geological Survey of Canada, Paper 93-1C, p. 221–232, doi:10.4095/134248.

McDonough, M.R., Grover, T.W., McNicoll, V.J., Lindsay, D.D., Kelly, K.L. and Guerstein, P.G. (1993b): Geology, Andrew Lake, Alberta-Saskatchewan-Northwest Territories; Geological Survey of Canada, Open File 2664, scale 1:50 000, URL <https://ostrnrcan-dostrncan.canada.ca/handle/1845/194689> [April 2023].

McDonough, M.R., Grover, T.W., McNicoll, V.J., Lindsay, D.D., Kelly, K.L. and Guerstein, P.G. (1993c): Geology, Mercredi Lake, Alberta-Northwest Territories; Geological Survey of Canada, Open File 2629, scale 1:50 000, URL <https://ostrnrcan-dostrncan.canada.ca/handle/1845/194661> [April 2023].

McDonough, M.R., Cooley, M.A. and Schetselaar, E.M. (1994a): Geology, Hay Camp, Alberta (NTS 74 M/11); Geological Survey of Canada, Open File 2832, scale 1:50 000, URL <https://ostrnrcan-dostrncan.canada.ca/handle/1845/190529> [April 2023].

McDonough, M.R., Grover, T.W., McNicoll, V.J., Cooley, M.A., Schetselaar, E.M. and Robinson, N.N. (1994b): Geology, Cornwall Lake (74M/10); Geological Survey of Canada, Open File 2896, scale 1:50 000, URL <https://ostrnrcan-dostrncan.canada.ca/handle/1845/190657> [April 2023].

McDonough, M.R., Grover, T.W., McNicoll, V.J., Lindsay, D.D., Kelly, K.L. and Guerstein, P.G. (1994c): Geology, Tulip Lake (NTS 74 M/14) east-half, Alberta-NWT; Geological Survey of Canada, Open File 2820, scale 1:50 000, URL <https://ostrnrcan-dostrncan.canada.ca/handle/1845/190447> [April 2023].

McDonough, M.R., Grover, T.W., McNicoll, V.J., Lindsay, D.D., Kelly, K.L. and Guerstein, P.G. (1994d): Revised geology, Andrew Lake (NTS 74 M/16), Alberta–Saskatchewan–NWT; Geological Survey of Canada, Open File 2905, scale 1:50 000, URL <https://ostrnrcan-dostrncan.canada.ca/handle/1845/190658> [April 2023].

McDonough, M.R., Grover, T.W., McNicoll, V.J., Lindsay, D.D., Kelly, K.L. and Guerstein, P.G. (1994e): Revised geology, Mercredi Lake (74 M/15), Alberta-Northwest Territories; Geological Survey of Canada, Open File 2904, scale 1:50 000, URL <https://ostrnrcan-dostrncan.canada.ca/handle/1845/191079> [April 2023].

McDonough, M.R., McNicoll, V.J. and Grover, T.W. (1994f): Whole rock major trace element analyses of selected mineral occurrences, Taltson magmatic zone, Canadian Shield, northeastern Alberta (NTS 74M and 74L); Geological Survey of Canada, Open File 2893, 6 p., URL <https://ostrnrcan-dostrncan.canada.ca/handle/1845/190656> [April 2023].

McDonough, M.R., Plint, H.E., McNicoll, V.J. and Grover, T.W. (1994g): $^{40}Ar/^{39}Ar$ and K–Ar age constraints on shear zone evolution, southern Taltson magmatic zone, northeastern Alberta; *in* 1994 LITHOPROBE Alberta basement transects workshop, G.M. Ross (ed.), LITHOPROBE Secretariat, University of British Columbia, LITHOPROBE Report 37, p. 267–269.

McDonough, M.R., Grover, T.W., McNicoll, V.J., Cooley, M.A., Schetselaar, E.M., Robinson, N.N. and Bednarski, J.M. (1995a): Geology, Colin Lake (74M/9), Alberta-Saskatchewan; Geological Survey of Canada, Open File 3047, scale 1:50 000, URL <https://ostrnrcan-dostrncan.canada.ca/handle/1845/192179> [April 2023].

McDonough, M.R., McNicoll, V.J. and Thériault, R.J. (1995b): Taltson basement complex: basement to a Paleoproterozoic continental collisional and magmatic orogen; Geological Association of Canada–Mineralogical Association of Canada, Victoria, British Columbia, May 17–19, 1995, Program with Abstracts, p. 20.

McDonough, M.R., Grover, T.W., McNicoll, V.J., Cooley, M.A., Schetselaar, E.M., Robinson, N.M. and Bednarski, J. (2000a): Geology, Colin Lake, Alberta-Saskatchewan; Geological Survey of Canada, Map 1952A, scale 1:50 000, URL <https://ostrnrcan-dostrncan.canada.ca/handle/1845/184931> [April 2023].

McDonough, M.R., Grover, T.W., McNicoll, V.J., Lindsay, D.D., Kelly, K.L., Guerstein, P.G. and Bednarski, J. (2000b): Geology, Andrew Lake, Alberta–Saskatchewan–Northwest Territories; Geological Survey of Canada, Map 1953A, scale 1:50 000, URL <https://ostrnrcan-dostrncan.canada.ca/handle/1845/184932> [April 2023].

McDonough, M.R., Grover, T.W., McNicoll, V.J., Schetselaar, E.M., Cooley, M.A., Robinson, N.M., Van Ham, J.A. and Bednarski, J.M. (2000c): Geology, Turtle Lake, Alberta; Geological Survey of Canada, Map 1958A, scale 1:50 000, URL <https://ostrnrcan-dostrncan.canada.ca/handle/1845/184935> [April 2023].

McDonough, M.R., Grover, T.W., McNicoll, V.J., Schetselaar, E.M., Cooley, M.A., Robinson, N.M., Van Ham, J.A. and Bednarski, J.M. (2000d): Geology, Wylie Lake, Alberta-Saskatchewan; Geological Survey of Canada, Map 1951A, scale 1:50 000, URL <https://ostrnrcan-dostrncan.canada.ca/handle/1845/184930> [April 2023].

McDonough, M.R., McNicoll, V.J., Schetselaar, E.M. and Grover, T.W. (2000e): Geochronological and kinematic constraints on crustal shortening and escape in a two-sided oblique-slip collisional and magmatic orogen, Paleoproterozoic Taltson magmatic zone, northeastern Alberta; Canadian Journal of Earth Sciences, v. 37, no. 11, p. 1549–1573, doi:10.1139/e00-089.

McDonough, M.R., Van Ham, J.A. and Bednarski, J.M. (2000f): Geology, Fletcher Lake, Alberta; Geological Survey of Canada, Map 1957A, scale 1:50 000, URL <https://ostrnrcan-dostrncan.canada.ca/handle/1845/184934> [April 2023].

McDonough, M.R., Van Ham, J.A. and Bednarski, J.M. (2000g): Geology, Winnifred Lake, Alberta-Saskatchewan; Geological Survey of Canada, Map 1956A, scale 1:50 000, URL <https://ostrnrcan-dostrncan.canada.ca/handle/1845/184933> [April 2023].

McDonough, W.F. and Sun, S.-s. (1995): The composition of the Earth; Chemical Geology, v. 120, issues 3–4, p. 223–253, doi:10.1016/0009-2541(94)00140-4.

McLennan, S.M. (2001): Relationships between the trace element composition of sedimentary rocks and upper continental crust; Geochemistry, Geophysics, Geosystems, v. 2, paper no. 2000GC000109, 24 p., doi:10.1029/2000GC000109.

McNicoll, V.J., Thériault, R.J. and McDonough, M.R. (2000): Taltson basement gneissic rocks: U-Pb and Nd isotopic constraints on the basement to the Paleoproterozoic Taltson magmatic zone, northeastern Alberta; Canadian Journal of Earth Sciences, v. 37, no. 11, p. 1575–1596, doi:10.1139/e00-034.

Meek, D.M., Lopez, G.P. and Knudson, C. (2023): Geochemistry of plutonic and metamorphic rock samples from the Canadian Shield, northeastern Alberta (74L, 74M), version 2 (tabular data, tab-delimited format); Alberta Energy Regulator / Alberta Geological Survey, AER/AGS Digital Data 2023-0015, URL <https://ags.aer.ca/publication/dig-2023-0015> [April 2023].

Meek, D.M., Montenegro, N. and Hartlaub, R.P. (2026): Station observations and whole-rock lithogeochemistry data from 2023 fieldwork on the Canadian Shield in northeastern Alberta (tabular data, tab-delimited format); Alberta Energy Regulator / Alberta Geological Survey, AER/AGS Digital Data 2025-0001, URL <https://ags.aer.ca/publication/dig-2025-0001>.

Middlemost, E.A.K. (1994): Naming materials in the magma/igneous rock system; Earth-Science Reviews, v. 37, issues 3–4, p. 215–224, doi:10.1016/0012-8252(94)90029-9.

Moyen, J.F. and Martin, H. (2012): Forty years of TTG research; Lithos, v. 148, p. 312–336, doi:10.1016/j.lithos.2012.06.010.

Naldrett, A.J. (2004): Magmatic sulfide deposits: geology, geochemistry and exploration (1st edition); Springer, Berlin, Germany, 728 p., doi:10.1007/978-3-662-08444-1.

NASA JPL (2013): NASA Shuttle Radar Topography Mission Global 1 arc second; NASA EOSDIS Land Processes Distributed Active Archive Center, zipped HGT format, doi:10.5067/MEaSUREs/SRTM/SRTMGL1.003.

Natural Resources Canada (2023): The Canadian critical minerals strategy, from exploration to recycling: powering the green and digital economy for Canada and the world; Natural Resources Canada, 52 p., URL <https://www.canada.ca/en/campaign/critical-minerals-in-canada/canadian-critical-minerals-strategy.html> [January 2023].

Neil, B.J.C., Tersmette, D.B., Chacko, T., Heaman, L.M., Kjarsgaard, B.A., Martel, E., Creaser, R.A., Pearson, D.G., Stern, R.A., Dufrane, S.A. and Luo, Y. (2023): Discovery of a giant 3.3–3.1 Ga terrane in the Rae craton, Canada: implications for the timing and extent of ancient continental growth; Geology, v. 51, no. 6, p. 597–601, doi:10.1130/G51110.1.

Normand, C. (2014): Rare earths in Saskatchewan: mineralization types, settings, and distributions; Saskatchewan Ministry of the Economy, Saskatchewan Geological Survey, Report 264, 105 p., URL <https://publications.saskatchewan.ca/#/products/79893> [January 2024].

Pană, D.I. (2010a): Overview of the geological evolution of the Canadian Shield in the Andrew Lake area based on new field and isotope data, northeastern Alberta (NTS 74M/16); Energy Resources Conservation Board, ERCB/AGS Open File Report 2009-22, 76 p., URL <https://ags.aer.ca/publication/ofr-2009-22> [April 2023].

Pană, D.I. (2010b): Precambrian geology of northeastern Alberta (NTS 74M, 74L and part of 74E); Energy Resources Conservation Board, ERCB/AGS Map 537, scale 1:250 000, URL <https://ags.aer.ca/publication/map-537> [April 2023].

Pană, D.I. and Olson, R.A. (2009): Overview of uranium exploration work along the northern rim of the Athabasca Basin, northeastern Alberta; Energy Resources Conservation Board, ERCB/AGS Open File Report 2009-19, 228 p., URL <https://ags.aer.ca/publication/ofr-2009-19> [April 2023].

Pană, D.I. and Prior, G. J. (2010): Geology of uranium and other mineral occurrences in the Andrew Lake area, Canadian Shield, northeastern Alberta (NTS 74M/16); Energy Resources Conservation Board, ERC/AGS Open File Report 2010-08, 32 p., URL <https://ags.aer.ca/publication/ofr-2010-08> [April 2023].

Pană, D.I., Olson, R.A. and Byron, S.J. (2006): Geological reconnaissance work in the Andrew Lake area of northeastern Alberta; Alberta Energy and Utilities Board, EUB/AGS Earth Sciences Report 2006-02, 22 p., URL <https://ags.aer.ca/publication/esr-2006-02> [January 2024].

Pearce, J.A. (1996): A user's guide to basalt discrimination diagrams; *in* Trace element geochemistry of volcanic rocks: applications for massive sulphide exploration, D.A. Wyman (ed.), Geological Association of Canada, Short Course Notes 12, p. 79–113.

Pearce, J.A. and Cann, J.R. (1973): Tectonic setting of basic volcanic rocks determined using trace element analyses; Earth and Planetary Science Letters, v. 19, issue 2, p. 290–300, doi:10.1016/0012-821X(73)90129-5.

Pearce, J.A. and Peate, D.W. (1995): Tectonic implications of the composition of volcanic ARC magmas; Annual Review of Earth and Planetary Sciences, v. 23, p. 251–285, doi:10.1146/annurev.ea.23.050195.001343.

Pearce, J.A., Harris, N.B.W. and Tindle, A.G. (1984): Trace element discrimination diagrams for the tectonic interpretation of granitic rocks; Journal of Petrology, v. 25, issue 4, p. 956–983, doi:10.1093/petrology/25.4.956.

Peikert, E.W. (1961): Petrological study of a group of porphyroblastic rocks in the Precambrian of northeastern Alberta; Ph.D. thesis, University of Illinois, 151 p.

Peikert, E.W. (1963): Biotite variation as a guide to petrogenesis of granitic rocks in the Precambrian of northeastern Alberta; Journal of Petrology, v. 4, issue 3, p. 432–459, doi:10.1093/petrology/4.3.432.

Plint, H.E. and McDonough, M.R. (1995): $^{40}Ar/^{39}Ar$ and K-Ar age constraints on shear zone evolution, southern Taltson magmatic zone, northeastern Alberta; Canadian Journal of Earth Sciences, v. 32, no. 3, p. 281–291, doi:10.1139/e95-023.

Poliakovska, K., Annesley, I.R., Ivanik, O., Sykes, J., Guest, N. and Otsuki, I. (2022): Geological setting, geochemistry and petrology of the granitic pegmatites hosting REE-Th-U mineralization at the Alces Lake area, northern Saskatchewan, Canada; *in* Proceedings of the 16th SGA Biennial Meeting, virtual, March 28–31, 2022, v. 1, p. 325–328.

Poliakovska, K., Annesley, I.R. and Hajnal, Z. (2023): Geophysical constraints to the geological evolution and genesis of rare earth element–thorium–uranium mineralization in pegmatites at Alces Lake, SK, Canada; Minerals, v. 14, no. 1, art. 25, 33 p., doi:10.3390/min14010025.

Pollock, D.W., Mitchell, D.C. and Burgan, E.C. (1971): Andrew Lake project, Alberta quartz mineral permits 24, 25 & 26, NTS 74M, review of work completed during 3-year permit period; Alberta Energy and Minerals, Mineral Assessment Report 19710001, 18 p., URL <https://content.energy.alberta.ca/xdata/MARS/MAR_19710001.pdf> [January 2024].

Prior, G.J., Hathway, B., Glombick, P.M., Pană, D.I., Banks, C.J., Hay, D.C., Schneider, C.L., Grobe, M., Elgr, R. and Weiss, J.A. (2013): Bedrock geology of Alberta; Alberta Energy Regulator, AER/AGS Map 600, scale 1:1 000 000, URL <https://ags.aer.ca/publication/map-600> [April 2023].

Ramsay, J.G. and Huber, M.I. (1987): The techniques of modern structural geology, vol. 2: folds and fractures; Academic Press, London, United Kingdom, 697 p.

Riley, G.C. (1960): Fort Fitzgerald, west of Fourth Meridian, Alberta; Geological Survey of Canada, Preliminary Map 12-1960, scale 1:253 440, URL <https://ostrnrcan-dostrncan.canada.ca/handle/1845/111809> [January 2024].

Rivard, B. and Feng, J. (2025): Analysis of WorldView-3 satellite imagery for the Andrew Lake area, northeastern Alberta; Alberta Energy Regulator / Alberta Geological Survey, AER/AGS Special Report 123, 19 p., URL <https://ags.aer.ca/publications/all-publications/spe-123> [February 2025].

Rollinson, H.R. (1993): Using geochemical data: evaluation, presentation, interpretation (1st edition); Routledge, Abingdon, United Kingdom, 384 p., doi:10.4324/9781315845548.

Ross, G.M., Parrish, R.R., Villeneuve, M.E. and Bowring, S.A. (1991): Geophysics and geochronology of the crystalline basement of the Alberta Basin, western Canada; Canadian Journal of Earth Sciences, v. 28, no. 4, p. 512–522, doi:10.1139/e91-045.

Rudnick, R.L. and Gao, S. (2003): Composition of the continental crust; Treatise on Geochemistry, v. 3, p. 1–64, doi:10.1016/B0-08-043751-6/03016-4.

Rukhlov, A.S. (2011): Review of metallic mineralization in Alberta with emphasis on gold potential; Energy Resources Conservation Board, ERCB/AGS Open File Report 2011-01, 93 p., URL <https://ags.aer.ca/publication/ofr-2011-01> [April 2023].

Salat, H.P., Eccles, D.R. and Langenberg, C.W. (1994): Geology and mineral occurrences of the Aphebian Waugh Lake Group, northeastern Alberta; Alberta Research Council, Alberta Geological

Survey, Open File Report 1994-04, 38 p., URL <https://ags.aer.ca/publication/ofr-1994-04> [April 2023].

Schultz, M.E.J., Chacko, T., Heaman, L.M., Sandeman, H.A., Simonetti, A. and Creaser, R.A. (2007): Queen Maud block: a newly recognized Paleoproterozoic (2.4-2.5 Ga) terrane in northwest Laurentia; Geology, v. 35, no. 8, p. 707–710, doi:10.1130/G23629A.1.

Selway, J.B., Breaks, F.W. and Tindle, A.G. (2005): A review of rare-element (Li-Cs-Ta) pegmatite exploration techniques for the Superior Province, Canada, and large worldwide tantalum deposits; Exploration and Mining Geology, v. 14, no. 1–4, p. 1–30, doi:10.2113/gsemg.14.1-4.1.

Sheard, E.R., Williams-Jones, A.E., Heiligmann, M., Pederson, C. and Trueman, D.L. (2012): Controls on the mineralogy and geochemistry of the rare earth element deposit at Nechalacho, Thor Lake, Northwest Territories, Canada; Economic Geology, v. 107, no. 1, p. 81–100.

Smith, D. and Griffith, F. (2007): North American Gem Inc. 2007 summer exploration of the Bonny Fault property, northeast Alberta; Alberta Energy and Minerals, Mineral Assessment Report 20070025, 6 p., URL <https://content.energy.alberta.ca/xdata/MARS/MAR_20070025.pdf> [January 2024].

Sprenke, K.F., Wavra, C.S. and Godfrey, J.D. (1986): Geophysical expression of the Canadian Shield of northeastern Alberta; Alberta Research Council, Alberta Geological Survey, Bulletin 52, 60 p., URL <https://ags.aer.ca/publication/bul-052> [January 2024].

Stemp, R.W. (1969): Report on airborne geophysical survey in the Andrew Lake area of Alberta for Hudson's Bay Oil and Gas Company Limited by Canadian Aero Mineral Surveys Limited, project no. 9543; Alberta Energy and Minerals, Mineral Assessment Report 19690005, 5 p., URL <https://content.energy.alberta.ca/xdata/MARS/MAR_19690005.pdf> [January 2024].

Stern, R.A., Card, C.D., Pană, D. and Rayner, N. (2003): SHRIMP U-Pb ages of granitoid basement rocks of the southwestern part of the Athabasca Basin, Saskatchewan and Alberta; Geological Survey of Canada, Current Research 2003-F3, 20 p., doi:10.4095/214595.

Sullivan, J. (1974): Report on the northeast Alberta project of Aquarius Mines Ltd.; Alberta Energy and Minerals, Mineral Assessment Report 19740005, 14 p., URL <https://content.energy.alberta.ca/xdata/MARS/MAR_19740005.pdf> [January 2024].

Sun, S.-s. and McDonough, W.F. (1989): Chemical and isotopic systematics of oceanic basalts: implications for mantle composition and processes; *in* Magmatism in the ocean basins, A.D. Saunders and M.J. Norry (ed.), Geological Society, Special Publication 42, p. 313–345, doi:10.1144/GSL.SP.1989.042.01.19.

Sutton, D., Cerne, J. and Dowds, N. (1969): Economic minerals, file report no. U-AF-069 (1) and U-AF-070 (1); Alberta Energy and Minerals, Mineral Assessment Report 19690035, 9 p., URL <https://content.energy.alberta.ca/xdata/MARS/MAR_19690035.pdf> [January 2024].

Taylor, S.R. and McLennan, S.M. (1981): The composition and evolution of the continental crust: rare earth element evidence from sedimentary rocks; Philosophical Transactions of the Royal Society of London, Series A, Mathematical and Physical Sciences, v. 301, no. 1461, p. 381–399.

Taylor, S.R. and McLennan, S.M. (1985): The continental crust: its composition and evolution; Blackwell Scientific Publications, Oxford, United Kingdom, 312 p.

Thériault, R.J. (1992): Nd isotopic evolution of the Taltson magmatic zone, Northwest Territories, Canada: insights into early Proterozoic accretion along the western margin of the Churchill Province; The Journal of Geology, v. 100, no. 4, p. 465–475, doi:10.1086/629598.

Thiessen, E.J., Davies, J., Dyck, B., Perrot, M.G. and Martel, E. (2024): Detrital zircon U-Pb + Hf data supports 2.1 Ga extensional and 2.0 Ga syn-orogenic basin in southwest Rae Province during early Nuna assembly; Precambrian Research, v. 410, art. 107455, doi:10.1016/j.precamres.2024.107455.

Thompson, P.H. (1989): An empirical model for metamorphic evolution of the Archaean Slave Province and adjacent Thelon tectonic zone, north-western Canadian Shield; *in* Evolution of metamorphic belts, J.S. Daly, R.A. Cliff and B.W.D. Yardley (ed.), Geological Society, Special Publication 43, p. 245–263, doi:10.1144/GSL.SP.1989.043.01.17.

Thorpe, W.H. (1968): McIntyre Porcupine Mines Limited report on New Senator-Rouyn option northeast Alberta concession; Alberta Energy and Minerals, Mineral Assessment Report 19680005, 4 p., URL <https://content.energy.alberta.ca/xdata/MARS/MAR_19680005.pdf> [January 2024].

Thorpe, W.H. (1969): McIntyre Porcupine Mines Limited, New Senator-Rouyn option, N.E. Alberta; Alberta Energy and Minerals, Mineral Assessment Report 19690002, 7 p., URL <https://content.energy.alberta.ca/xdata/MARS/MAR_19690002.pdf> [January 2024].

Tukey, J.W. (1977): Exploratory data analysis; Addison-Wesley, Reading, Massachusetts, 688 p.

Tyrrell, J.B. (1896): Report on country between Athabasca Lake and Churchill River, with notes on two routes travelled between the Churchill and Saskatchewan rivers; Geological Survey of Canada, Annual Report, v. 8, 120 p., doi:10.4095/247595.

van Breemen, O. and Bostock, H.H. (1994): Age of emplacement of the Thoa metagabbro, western margin of the Rae Province, Northwest Territories: initiation of rifting prior to Taltson magmatism?; *in* Radiogenic age and isotopic studies report 8, Geological Survey of Canada, Current Research 1994-F, p. 61–68, doi:10.4095/195171.

van Breemen, O., Bostock, H.H. and Loveridge, W.D. (1992): Geochronology of granites along the margin of the northern Taltson magmatic zone and western Rae Province, Northwest Territories; *in* Radiogenic age and isotopic studies report 5, Geological Survey of Canada, Paper 91–2, p. 17–24, doi:10.4095/132904.

Watanabe, R.Y. (1961): Geology of the Waugh Lake metasedimentary complex, northeastern Alberta; M.Sc. thesis, University of Alberta, 89 p.

Watanabe, R.Y. (1965): Petrology of cataclastic rocks of northeastern Alberta; Ph.D. thesis, University of Alberta, 219 p.

Whalen, J.B., Berman, R.G., Davis, W.J., Sanborn-Barrie, M. and Nadeau, L. (2018): Bedrock geochemistry of the central Thelon tectonic zone, Nunavut; Geological Survey of Canada, Open File 8234, 49 p., doi:10.4095/306385.

Williams, H.M. (1970): Geological report exploration permits 111 and 112, northeastern Alberta; Alberta Energy and Minerals, Mineral Assessment Report 19700007, 11 p., URL <https://content.energy.alberta.ca/xdata/MARS/MAR_19700007.pdf> [January 2024].

Winchester, J.A. and Floyd, P.A. (1977): Geochemical discrimination of different magma series and their differentiation products using immobile elements; Chemical Geology, v. 20, p. 325–343, doi:10.1016/0009-2541(77)90057-2.

Winter, J.D. (2010): An introduction to igneous and metamorphic petrology (2nd edition); Pearson Prentice Hall, Upper Saddle River, New Jersey, 720 p.

Wise, M.A. and Brown, C. M. (2010): Chemical evolution of the Rutherford No. 2 pegmatite, Amelia County, Virginia: evidence for multiple NYF-type pegmatite emplacement; The Canadian Mineralogist, v. 48, no. 4, p. 815–832.

Wiskel, B.N. (1999): Preliminary geological assessment of the Waugh Lake mineral property for Esmeralda Exploration International Inc.; Alberta Energy and Minerals, Mineral Assessment Report 19990014, 14 p., URL <https://content.energy.alberta.ca/xdata/MARS/MAR_19990014.pdf> [January 2024].

Workman, A.W. (2023): A technical review of the Alces Lake rare earth mineral exploration project, Beaverlodge domain, Saskatchewan, Canada; prepared for Appia Rare Earths & Uranium Corporation, Canadian Securities Administrators, SEDAR public securities filings, NI43-101 technical report, filed January 31, 2023, 170 p., URL <https://www.sedarplus.ca/csa-party/records/document.html?id=f0c412816f5890a3f2d9c57f20fe602526f67bdb8d55f9f3dce7f761a7eef6aa> [June 2024].